CFD ANALYSIS OF THE COMBUSTION OF HYDROGEN FUEL ON A CFM56-3 COMBUSTOR

Rafael Silva Domingues

Dissertação para obtenção do Grau de Mestre em
Engenharia Aeronáutica
(mestrado integrado)

Orientador: Prof. Doutor Francisco Miguel Ribeiro Proença Brójo

outubro de 2022

Declaração de Integridade

Eu, Rafael Silva Domingues, que abaixo assino, estudante com o número de inscrição a37853 de Engenharia Aeronáutica da Faculdade de Engenharia, declaro ter desenvolvido o presente trabalho e elaborado o presente texto em total consonância com o **Código de Integridades da Universidade da Beira Interior**.

Mais concretamente afirmo não ter incorrido em qualquer das variedades de Fraude Académica, e que aqui declaro conhecer, que em particular atendi à exigida referenciação de frases, extratos, imagens e outras formas de trabalho intelectual, e assumindo assim na íntegra as responsabilidades da autoria.

Universidade da Beira Interior, Covilhã 10/10/2022

Rafael Domingues

Dedication

This dissertation is dedicated to my parents, sister, and all the people who supported me during this chapter of my life.

Acknowledgments

As with any other book, on the cover of a dissertation, there should be not only the name of the author, but also the names of all those people who, for some reason, provided assistance, encouragement, and guidance and without whom I would never have succeeded in this task. I am very grateful to all those people who gave me so much of their time, joy, and energy to face what can be my last academic challenge. However, I would like to express my gratitude in particular:

To my family, for the tremendous support and hope they gave me in the hardest times of this difficult path and for all the efforts they made to provide me with what I needed to accomplish this huge objective of my life. I will be forever thankful to you.

A big appreciation goes also to my supervisor, Professor Dr. Francisco Brójo, for the amazing supervision, guidance, and encouragement. My thanks are extended to all the knowledge transmitted, constructive feedback, support, advice, and availability demonstrated during the course of this dissertation. There are not enough words to express my gratitude for the patience you have always demonstrated during this study. Thank you very much.

Last, but not least, to all the great friends I made during this path and with whom I shared this journey. I am sure without them I would not have finished this chapter of my life. Thank you for all the support and special moments you provided me throughout these more than six years.

Thank you all!

Resumo

Neste trabalho é apresentada uma visão geral do uso do hidrogénio no setor aeronáutico, das modificações necessárias para adaptar uma turbina de gás existente para o uso de hidrogénio e uma simulação em CFD da queima deste combustível numa turbina de gás existente. O estudo em CFD foi feito num modelo de combustor de um CFM56-3 enquanto queimava hidrogénio e Jet A (como padrão de referência). Com isto pretendia-se avaliar a viabilidade de conversão de turbinas de gás existentes para hidrogénio, do ponto de vista da combustão, através da análise das emissões durante a queima deste combustível através do ciclo LTO da ICAO. O software ANSYS Fluent 2020R2 foi utilizado para realizar o estudo numérico e os modelos viscosos e de radiação utilizados foram o RSM e o P-1, respetivamente. Somente as emissões de NOx foram avaliadas como poluentes, uma vez que os produtos de combustão do hidrogénio são reduzidos a vapor de água e NOx. Estas emissões foram avaliadas através de um mecanismo detalhado e do modelo de NOx disponível no ANSYS Fluent 2020R2, de modo a obter uma melhor concordância com os valores da ICAO. Para esta avaliação, também foram efetuados vários estudos de sensibilidade para analisar a influência de alguns parâmetros nas emissões de poluentes durante a queima de hidrogénio, como por exemplo, a análise do escoamento de ar com e sem efeito de *swirl* na zona primária e diferentes temperaturas e pressões de injeção do combustível. No final, concluiu-se que teoricamente o combustor do CFM56-3 pode ser convertido para operar com hidrogénio com pequenas alterações (relacionadas com sistema de injeção). No entanto, é expectável que a quantidade de NOx produzida para cada percentagem de acelerador ao queimar hidrogénio seja quase o dobro dos valores obtidos para o Jet A. Em relação aos testes de sensibilidade, apenas as alterações no efeito de *swirl* e na temperatura do combustível produziram mudanças relevantes nos resultados.

Palavras-chave

CFM56-3; Camara de Combustão; Emissões de Poluentes; Combustível de aviação; Hidrogénio.

Resumo Alargado

Nos últimos anos o setor da aviação tem vindo a ganhar cada vez mais importância em áreas como o comércio, intercâmbio cultural, crescimento económico, desenvolvimento, entre muitas outras.

De acordo com alguns relatórios recentes, em 2015 a aviação internacional consumiu aproximadamente 160 megatoneladas (Mt) de combustível e, devido à crescente relevância da aviação, espera-se (segundo alguns especialistas) o crescimento deste setor de tal forma que, até 2045, o tráfego aéreo internacional deverá aumentar 3,3 vezes em relação a 2015. Assim, dependendo dos avanços na tecnologia e no cenário de Gerenciamento de Tráfego Aéreo, é expectável que, até 2045, o consumo de combustível deva aumentar 2,2 a 3,1 vezes em relação a 2015.

Nos dias de hoje, as emissões decorrentes da queima de combustíveis fósseis são geralmente apontadas como as principais emissões de Gases de Efeito Estufa (GEE), considerados como o principal fator que leva ao aquecimento global. Para as alterações climáticas, as principais preocupações estão relacionadas com as emissões de CO, CO_2, NOx e nvPM. Para mitigar os problemas com essas emissões, no setor da aviação existem várias soluções possíveis que podem ser agrupadas em duas opções principais. Por um lado, a redução do consumo de combustível através da atualização da tecnologia empregada nas aeronaves atuais, como por exemplo nas fuselagens (aerodinâmica e massa) e nos motores, ambos com o objetivo de obter maior eficiência; por outro lado, existe também a possibilidade do uso de combustíveis alternativos (SAFs, hidrogénio, etc.).

Neste contexto, o presente trabalho inicia-se com uma visão geral do uso do hidrogénio no setor aeronáutico, seguida de uma breve descrição dos componentes das turbinas de gás atuais, bem como as modificações necessárias para adaptar esses motores ao uso de hidrogénio como combustível. Em seguida, é feita uma introdução aos mecanismos de formação de poluentes, com foco nas espécies mais prováveis de serem formadas nestes motores aquando da queima dos combustíveis considerados neste estudo.

Ainda neste trabalho, a avaliação da viabilidade da conversão de turbinas de gás existentes, de Jet A para hidrogénio, do ponto de vista da combustão, é feita com recurso a uma análise das emissões durante a queima destes combustíveis através das configurações de potência específicas representadas no ciclo LTO da ICAO. Para isso, foram realizadas simulações em CFD num modelo do combustor de um CFM56-3 enquanto este queimava hidrogénio e Jet A (como padrão de referência).

Sendo este um estudo de continuidade, foi utilizado o modelo CAD do combustor do CFM56-3 desenvolvido por J. Oliveira, porém foram efetuadas algumas alterações para obter um modelo mais realista do combustor em análise. Estas alterações (realizadas no CATIA V5) foram baseadas em dados/desenhos técnicos recolhidos, bem como em resultados de simulações preliminares feitas durante as primeiras fases deste trabalho. Além disso, também foi necessário adaptar o sistema de injeção de combustível para hidrogénio (por este ser um combustível gasoso) e recalcular as condições de fronteira, nomeadamente os caudais de ar e combustível a usar nas simulações.

Vários softwares foram testados para criar uma malha de boa qualidade para essa geometria complexa. No entanto, apenas um deles (*Fluent Meshing*) foi capaz de criar uma malha independente suficientemente boa para as simulações, onde todos os detalhes da geometria ficaram representados corretamente com os recursos computacionais disponíveis. Em seguida, foi utilizado o software comercial *ANSYS Fluent 2020R2* para realizar o estudo numérico. O modelo de radiação utilizado foi o P-1, uma vez que funciona razoavelmente bem para aplicações de combustão em geometrias complexas com custos computacionais reduzidos. O modelo viscoso utilizado foi o RSM. Este modelo é mais eficiente do que outros modelos RANS para fornecer previsões quantitativas de velocidade, temperatura e distribuição das espécies. Além disso, é o melhor para prever com precisão os comprimentos das zonas de recirculação e oferecer uma previsão razoável sobre a distribuição da energia cinética turbulenta no combustor.

Para a análise das emissões resultantes da combustão do hidrogénio somente as emissões de NOx foram avaliadas como poluentes, uma vez que os produtos de combustão do hidrogénio são reduzidos a vapor de água e NOx. Estas emissões foram avaliadas, num primeiro momento, por meio de um mecanismo detalhado e depois através do modelo de NOx disponível no *ANSYS Fluent 2020R2* de modo a obter uma melhor concordância entre os resultados finais e os valores do banco de dados da ICAO. Durante esta avaliação, foram ainda feitos vários estudos de sensibilidade para a queima de hidrogénio com o intuito de analisar a influência de alguns parâmetros nas emissões de poluentes, como por exemplo a análise do escoamento de ar com e sem efeito de *swirl* na zona primária e diferentes temperaturas e pressões de injeção do combustível.

Ressalta-se que como o objetivo principal deste trabalho era a análise da emissão de poluentes durante a queima de hidrogénio, a atomização do combustível líquido (Jet A) não foi considerada nas simulações para simplificar o trabalho.

Em relação aos resultados, começando pelas simulações de controlo com o Jet A (padrão de referência), embora os resultados obtidos através do estudo numérico sejam aceitáveis quando comparados com os apresentados pela ICAO, ainda existe uma pequena margem de erro nas condições estudadas (mais evidente nas condições de maior acelerador). No entanto, existem várias razões possíveis que podem ser apontadas para justificar as diferenças entre os valores das simulações e os valores do banco de dados da ICAO. Por exemplo, o facto de ter sido considerado que o Jet A estava no estado gasoso quando injetado na câmara de combustão simula uma atomização "perfeita", aumentando a eficiência da combustão e criando uma temperatura mais elevada no interior da câmara. Outra razão pode ser o facto do mecanismo/sub-mecanismo escolhido não representar da melhor forma a combustão do Jet A ou a produção de NOx, respetivamente. A escolha do modelo de radiação também pode influenciar este resultado, uma vez que a representação da radiação é mais importante ao simular a queima do Jet A do que a queima do hidrogénio. Outra possível razão pode ser o modelo químico utilizado. No entanto, devido aos recursos computacionais limitados, não foi possível utilizar modelos mais complexos.

Em relação aos restantes resultados, foi demonstrado que teoricamente o CFM56-3 pode ser convertido para operar com hidrogénio como combustível através de pequenas alterações (relacionadas com o sistema de injeção). Com os resultados obtidos para o hidrogénio foi também demonstrado que com o aumento da percentagem de acelerador é produzida maior massa de NOx por massa de hidrogénio, devido ao aumento da temperatura dentro da câmara. Comparando as emissões de NOx obtidas para as simulações (tanto para Jet A quanto para hidrogénio) mostrou-se que para as geometrias de combustor e injetor utilizadas, é esperado que ao usar hidrogénio como combustível, a quantidade de NOx produzida seja quase o dobro da quantidade de NOx produzida aquando da utilização de Jet A para cada percentagem de acelerador. Este comportamento está de acordo com outros trabalhos disponíveis na literatura.

Em relação aos testes de sensibilidade (alteração do efeito de *swirl*, pressão de injeção do combustível e temperatura do combustível), apenas as mudanças no efeito *swirl* e na temperatura do combustível produziram alterações relevantes nos resultados. O facto de as alterações na pressão de injeção de combustível não influenciarem os resultados pode ser explicado como uma consequência dos caudais mássicos de combustível e da geometria do injetor serem fixos para cada condição de operação e pelo fato de as mudanças na densidade do combustível, devido à modificação da pressão de injeção, serem irrelevantes. Assim, é possível concluir que as mudanças de pressão não afetarão de forma significativa o comportamento do jato de combustível nem os perfis de velocidade dentro da câmara. Consequentemente, o efeito sobre as emissões de NOx também é irrelevante. Ainda assim, para este teste específico, deve-se notar que este comportamento pode ainda ter ocorrido devido a algum problema relacionado com os valores escolhidos para os testes, ou à forma como foram introduzidos no Fluent.

Em relação aos testes do efeito de *swirl*, verificou-se que sem o efeito de *swirl*, a qualidade da zona de recirculação foi reduzida e a temperatura na câmara de combustão aumentou ligeiramente. Consequentemente, as emissões de NOx também aumentaram. Assim, concluiu-se que a presença do efeito de *swirl* aumenta a rotação do escoamento de ar, melhorando a intensidade de mistura entre o combustível e o ar, estabilizando e retendo a chama na zona primária, o que por sua vez ajuda a reduzir o pico de temperatura na camara e, consequentemente, as emissões de NOx.

Sobre a influência da temperatura do combustível, esperava-se que um aumento exponencial neste valor pudesse afetar a temperatura na saída da camara em grande medida, devido ao aumento da eficiência da combustão. No entanto, isso não aconteceu, e não só a temperatura de saída da câmara mudou apenas ligeiramente (1% a 2%) para o dobro da temperatura inicial do combustível, como também causou situações de mau funcionamento um pouco por toda a câmara. Este mau funcionamento tem maior evidência nas condições de maior potência, onde a análise da chama (obtida no estudo numérico) mostra uma grande deterioração da zona de recirculação e a presença de um fenómeno que parece ser a ocorrência de autoignição ou *flashback* dentro dos *swirlers*. Este mau funcionamento foi associado à velocidade do caudal de hidrogénio, que quase duplicou aquando do aumento da temperatura. A razão mais credível para esta ocorrência consiste na redução da densidade do hidrogénio devido à mudança de temperatura do mesmo.

Deve-se notar que ao longo da secção dos resultados são ainda apontados os motivos para possível mau funcionamento do combustor aquando do uso de hidrogénio como combustível.

Em suma, durante este trabalho todos os objetivos foram cumpridos e pode-se concluir que o hidrogénio tem potencial para substituir o Jet A como combustível no CFM56-3. Para além disso, previa-se uma redução significativa nas emissões de poluentes (que ocorreu efetivamente), porém, para a mesma condição de operação, verificou-se que o NOx produzido aquando da queima de hidrogénio é quase o dobro do NOx produzido aquando da queima de Jet A. Isto já considerando que menos hidrogénio deve ser queimado (em massa) para produzir a mesma quantidade de tração que com o Jet A.

Abstract

In this work is presented an overview of the use of hydrogen in aviation, the modifications needed to adapt an existing gas turbine to use hydrogen, and a CFD simulation of an existing gas turbine burning this fuel. The CFD simulation was done in a CFM56-3 combustor model burning hydrogen and Jet A (as a reference standard). It was intended to evaluate the viability of conversion of existing gas turbines to hydrogen, from a combustion point of view, by analyzing the emissions while burning this fuel through ICAO's LTO cycle. The software ANSYS Fluent 2020R2 was used to perform the numerical study and the viscous and radiation models used were the RSM and P-1, respectively. Only the NOx emissions were assessed as pollutant once the hydrogen combustion products are reduced to water vapor and NOx. These emissions were evaluated through a detailed mechanism and the NOx model available on ANSYS Fluent 2020R2 to get a better agreement with the ICAO’s values. For this assessment, several sensibility studies were also made for hydrogen burn to analyze the influence of some parameters in the pollutant emissions, for example, the analysis of the airflow with or without swirl effect in the primary zone and different inlet temperature and pressure for fuel. In the end, it was concluded that theoretically the CFM56-3 combustor can be converted to operate with hydrogen fuel with minor changes (related with the injection system). However, the quantity of NOx produced for each power setting when burning hydrogen is expected to be almost twice the values obtained for Jet A. Regarding the sensibility tests, only the changes in the swirl effect and the fuel temperature produced relevant changes in the results.

Keywords

CFM56-3, Combustion Chamber, Pollutant Emissions, Jet Fuel, Hydrogen Fuel.

Contents

List of Figures

List of Tables

List of Acronyms

AFR	Air to Fuel Ratio
AGB	Accessory Gearbox
AIT	Autoignition Temperature
APU	Auxiliary Power Unit
ASTM	American Society for Testing and Materials
ATM	Air Traffic Management
BC	Boundary Conditions
BTU	British Thermal Unit
CAD	Computer Aided Design
CAEP	Committee on Aviation Environmental Protection
CCS	Carbon Capture and Storage
CFD	Computational Fluid Dynamics
CORSIA	Carbon Offsetting and Reduction Scheme for International Aviation
COT	Combustor Outlet Temperature
CPU	Central Processing Unit
DLE	Dry Low-Emissions
DLN	Dry Low-Oxides of Nitrogen
DNS	Direct Numerical Simulation
DOM	Discrete Ordinates Method
ECAC	European Civil Aviation Conference
EFTA	European Free Trade Association
ERF	Explicit Relaxation Factor
ETS	Emissions Trading System
EU	European Union
FAR	Fuel to Air Ratio
GH_2	Gaseous Hydrogen
GHG	Greenhouse Gas
GTE	Gas Turbine Engine
HC	Hydrocarbons
HE	Heat Exchanger
HHV	Higher Heating Value
HPC	High-Pressure Compressor
HPT	High-Pressure Turbine

ICAO	International Civil Aviation Organization
IGB	Inlet Gear Box
IGV	Inlet Guide Vane
IRENA	International Renewable Energy Agency
LBO	Lean Blowout
LCAF	Lower Carbon Aviation Fuel
LDI	Lean Direct Injection
LES	Large Eddy Simulation
LH_2	Liquid Hydrogen
LHV	Lower Heating Value
LPC	Low-Pressure Compressor
LPG	Liquefied Petroleum Gas
LPP	Lean Premixed Prevaporized
LPT	Low-Pressure Turbine
LTO	Landing and Take-Off
MTOW	Maximum Take-Off Weight
NASA	National Aeronautics and Space Administration
NMVOCs	Non-Methane Volatile Organic Compounds
NOx	Nitrogen Oxides
nvPM	non-volatile Particulate Matter
OGV	Outlet Guide Vane
PDF	Probability Density Function
PLF	Pressure Loss Factor
PM	Particulate Matter
PMC	Photon Monte Carlo
Ppmv	Parts per million by volume
PRESTO!	PREssure STaggering Option
R&D	Research and Development
RAM	Random Access Memory
RANS	Reynolds Averaged Navier–Stokes
RNG	Renormalization group
RQL	Rich-Quench-Lean
RSM	Reynolds Stress Model
RTE	Radiative Transfer Equation
SAF	Sustainable Aviation Fuel
SFC	Specific Fuel Consumption
SHM	Spherical Harmonics Method

SIT	Self-Ignition Temperature
SMD	Sauter Mean Diameter
SRM	Steam Reforming of Methane
SRS	Scale-Resolving Simulations
SST	Shear-Stress Transport
STL	Stereo Lithography
STOL	Short Take-Off and Landing
TAP	Transportes Aéreos Portugueses
TBC	Thermal Barrier Coating
TET	Turbine Entry Temperature
TGB	Transfer Gearbox
TIM	Time-In-Mode
TTQ	Temperature Traverse Quality
UHC	Unburned Hydrocarbons
URF	Under Relaxation Factor
US	United States
USA	United States of America
VBV	Variable Bleed Valve
VSV	Variable Stator Vanes

Nomenclature

A	Area	$[m^2]$
AFR	Air to fuel Ratio	$[---]$
a_s	Strain rate	$[s^{-1}]$
C	Heat capacity	$[J/K]$
C_D	Discharge coefficient	$[---]$
CN	Cetane Number	$[---]$
c_p	Specific heat at constant pressure	$[J/kg.K]$
C_μ	k-ε model constant in Equation (4.5)	[0.09]
c_v	Specific heat at constant volume	$[J/kg.K]$
CV	Calorific value	[MJ/kg]
D_a	Damköhler number	$[---]$
D_p	Mass of gaseous pollutant emitted	$[g]$
d_r	Relative density	$[---]$
D_{sw}	Outer swirler diameter	$[m]$
EI	Emission Index	$[g/kg]$
F	Engine thrust	$[kN]$
F_{00}	Engine take-off thrust (or rated thrust)	$[kN]$
F_S	Specific thrust	$[kN/(kg/s)]$
G_m	Axial flux of angular momentum	$[(kg \cdot m^2)/s^2]$
G_t	Axial thrust	$[(kg \cdot m)/s^2]$
h	Enthalpy	$[J/kmole]$
$\Delta h_{f,i}^0$	Enthalpy of formation (or heat of formation) for specie i	$[J/kmole]$
$\Delta h_{s,i}$	Sensible enthalpy change for specie i	$[J/kmole]$
$\Delta \mathrm{H_R}$	Enthalpy of combustion	$[J/kmole]$
$\bar{h}_i$	Absolute enthalpy for specie i	$[J/kmole]$
$\mathrm{H_{mix}}$	Mixture calorific value	$[MJ/m^3]$
k	Turbulence kinetic energy	$[m^2/s^2]$
K_1, K_2	Constants in Equation (2.14)	$[---]$
L	Characteristic length	$[m]$
LHV	Lower Heating Value	$[MJ/kg]$

m	Mass	$[kg]$
$\dot{m}$	Mass flow rate	$[kg/s]$
M	Molecular weight	$[kg/kmol]$
MN	Methane Number	$[---]$
MON	Motor Octane Number	$[---]$
n	Number of moles	$[kmol]$
p	Pressure	$[Pa]$
$\dot{Q}$	Heat release rate	$[W]$
Q	Heat transfer	$[J]$
RON	Research Octane Number	$[---]$
r_p	Pressure ratio (p_3/p_2)	$[---]$
RSN	Regulatory Smoke Number	$[---]$
s	Specific Entropy	$[kJ/kg.K]$
SN	Smoke Number	$[---]$
S_N	Swirl number	$[---]$
$sp.gr$	Specific gravity with respect to air	$[---]$
t	Time	$[s]$
T	Temperature	$[K]$
T_{ad}	Adiabatic flame temperature	$[K]$
TP	Thrust power	$[kN \cdot m/s]$
$TSFC$	Thrust specific fuel consumption	$[(kg/hr)/N]$
U	Characteristic mean flow velocity	$[m/s]$
u, v, w	Velocity magnitude	$[m/s]$
$\dot{V}$	Volumetric flow rate	$[m^3/s]$
V	Volume	$[m^3]$
W_o	Wobbe number	$[MJ/Nm^3]$

Greek letters

α	Azimuthal Start Angle	$[deg]$
γ	Ratio of specific heats	$[---]$
η	Efficiency	$[---]$
η_0	Overall efficiency	$[---]$
η_b	Combustion efficiency	$[---]$
η_e	Energy conversion efficiency	$[---]$
η_{joule}	Joule-Brayton cycle efficiency	$[---]$

η_p	Propulsive efficiency	$[---]$
μ_T	Turbulent viscosity	$[Pa \cdot s]$
π_{00}	Reference pressure ratio at take-off	$[---]$
Δ	Change in variable (final-initial)	$[---]$
$\mathrm{f}(\xi)$	Combustion intensity	$[\mathrm{kW/m}^3 atm]$
ν	Kinematic viscosity	$[m^2/s]$
δ	Delta function	$[---]$
ε	Turbulence dissipation rate	$[m^2/s^3]$
λ	Excess air coefficient	$[---]$
μ	Dynamic Viscosity	$[Pa \cdot s]$
ξ	Mixture fraction	$[---]$
ρ	Density	$[kg/m^3]$
τ	Time Scale	$[s]$
ω	Specific dissipation rate	$[s^{-1}]$
∂	Partial differential	$[---]$
ϕ	Equivalence ratio	$[---]$

Subscripts

0	Values related to the standard state
01	Combustor's entry conditions
02	Combustor's exit conditions
1	Engine inlet stage
2	Compressor inlet stage
3	Combustion chamber inlet stage
4	Combustion chamber outlet stage
1/4	Values for a quarter of the combustor
a, air	Air
actual	Current value for the parameter
eq	Equilibrium value
f	Value for formation of compound
f, fuel	Fuel
i, j	Coordinate directions
Ideal	Ideal value for the parameter
max	Maximum value for the parameter
o	Outlet

prod	Products
reac	Reactants
ref	Reference state/data
s	Value related to the sensible enthalpy
stoich	Stoichiometric value
x, y, z	Cartesian components

Chapter 1 – Introduction

1.1 Motivation

In the last years the aviation sector is being increasingly important for areas such as the commerce, cultural exchange, economic growth, development, among many others.

According to some recent reports, in 2015 international aviation used approximately 160 megatons (Mt) of fuel and due to the increasing relevance of the aviation in the current days, it is expected (according to some experts) the growth of this sector in such a way that, by 2045, the international air traffic (expressed in revenue ton kilometers) should increase 3.3 times in relation to 2015. Accordingly, by 2045, the fuel consumption is projected to increase by 2.2 to 3.1 times compared to 2015, depending on the advances in technology and the Air Traffic Management (ATM) scenario [1].

In Europe, the latest ICAO CAEP Environmental Trends Assessment [2] shows that in the most likely scenario, the number of flights departing from airports in the European Civil Aviation Conference (ECAC) region is expected to grow from 5.2 million in 2016 to 8.4 million in 2040, whilst fuel consumption is expected to increase from 46.2 Mt in 2016 to 67.5 Mt in 2040.

Nowadays, the emissions resulting from the combustion of fossil fuels are usually considered as the main responsible for the global Greenhouse Gas (GHG) emissions, which are pointed as the primary factor that leads to global warming. Generally, the overall impact of the emissions on global surface temperature over a given timescale is determined by the combination of a number of factors which consist mainly in: quantities emitted, residence time, radiative forcing, and the temperature response profile of a particular pollutant [3]. For climate change, the primary concerns are related with the emissions of CO, CO_2, NOx and nvPM [3]. Also of concern are persistent contrails which lead to cirrus clouds (when the atmosphere is ice-supersaturated) [3].

The CO_2 emissions are of particular concern because of its exceptionally long residence time (thousands of years) [3]. Aviation today accounts for 2% to 3% of the global CO_2 emissions and, while at the global level, CO_2 emissions are increasing by around 3% per year, the emissions from aviation covered by the EU ETS increased by an average of 5% year over year between 2013 and 2018. According to some experts, by 2040, it is expected that the international aviation emissions could rise by up to 150% when compared to 2020. This growth forecast takes into account the incremental technology improvements that may reduce fuel consumption and emissions by 1% to 1.5% annually [4].

Regarding the NOx emissions, they can be evaluated in two possible scenarios, which are the landing and take-off (LTO) NOx emissions, which primarily affect the local air quality, and the full-flight NOx emissions, which have more effect on the global climate. In 2015, the LTO NOx emissions (of international aviation) were approximately 0.18 Mt, by 2045, they are projected to range from 0.44 to 0.80 Mt depending on the technology and ATM scenario (which represents a growth between 2.4 and 4.4 times over the period) [1]. While, in 2015, the full-flight NOx emissions of international aviation were 2.50 Mt, by 2045, the projected full-flight NOx emissions range from 5.53 Mt to 8.16 Mt, which represents a growth of 2.2 to 3.3 times compared to 2015 [1].

Considering what was mentioned before, the continued rise of aviation emissions represents an increasing challenge in terms of reaching the GHG reduction target and commitments under the Paris Agreement [4].

A solution is being tried to reduce the international aviation emissions since 2016, when governments meeting at ICAO agreed to establish the world's first climate pricing mechanism for any single global sector. For the aviation sector, the CORSIA (Carbon Offsetting and Reduction Scheme for International Aviation) had the objective of offset about 80% of the growth in international aviation CO_2 emissions from the end of 2020. This mechanism is intended to offset the growth in emissions from international aviation, which is not covered under the Paris Agreement. Like the Paris Agreement, CORSIA is initially a voluntary scheme, with States deciding if their country will be included. In later years, it is mandatory for all but small and developing countries. CORSIA does not cover domestic air transport services, as these are subject to national action under the 'nationally determined contributions' outlined in the Paris Agreement [5].

In practice, to mitigate the problems with the emissions in the aviation sector, there are several possible solutions which can be grouped into two main options. On the one hand, the fuel burn reductions through the upgrade of the technology employed in the actual aircrafts like the airframes (aerodynamics and mass) and the engines, both with the aim of achieve higher efficiency [3]; on the other hand, the use of alternative fuels and power sources [5, 6]. According to the ICAO 2016 trends assessment, a 100 per cent substitution of aviation fuel with SAFs[1] could reduce 63 percent of the baseline CO_2 emissions from international flights in 2050 [6]. As referred by ATAG [5][2], it is possible that aviation meets net-zero CO_2 emissions by 2050, however it would take an enormous effort to make it a reality. This would mean a rapid and massive transformation on aviation's

---

[1] According to CORSIA's definition, "sustainable aviation fuels" are not restricted to liquid fuels.

[2] This reference has Covid-19 into account.

energy supply through the use of SAFs and it would require an acceleration in aircraft and engine technology development, mainly: electric-, hybrid- and hydrogen- powered aircrafts.

Within this context, the conversion of the current gas turbine engines to new sustainable fuels can also be a solution. To date, several factors still hinder a possible use of hydrogen in commercial flights, such as on-board storage, safety concerns, the high cost of producing the fuel and the need for dedicated infrastructure at airports. However, research projects are ongoing to demonstrate the feasibility of hydrogen propulsion and to overcome these challenges, in support of longer-term environmental objectives for civil aviation [7]. Some of the results of these researches will be presented in CAEP/12 (from 2019 to 2022) where will be also presented an evaluation of SAFs and LCAFs (where is included the hydrogen) availability through 2035 [8].

1.2 Objectives

The objectives of this work can be divided in two groups, the general (or main) objectives and the specific objectives which, if completed, can help to improve the results of the main objectives.

1.2.1 General objectives

Within the context of the previous section, the main objectives of the work presented in this dissertation are:

- Study the feasibility of the use of gaseous hydrogen as substitute of the conventional jet fuel in a CFM56-3 combustor.
- Analyze and compare the results obtained for hydrogen and Jet A fuel.

For these purposes, it was necessary to simulate the combustion and pollutant emissions resulting from the burning of gaseous hydrogen and Jet A in the combustor while completing the ICAO’s LTO cycle.

1.2.2 Specific objectives

To achieve and improve the results of the previous objectives, it was necessary to:

- Understand the process of combustion and pollutant formation in annular chambers while burning gaseous fuels.
- Change the geometry of the injector to improve the use of a gaseous fuel;

- Define and adjust the air mass flow rates for the inlets of the chamber;
- Analyze the influence of several operating parameters such as swirl effect, temperature and pressure of fuel in the pollutant emissions while burning hydrogen;
- Compare and choose the best injection parameters while burning gaseous hydrogen;
- Simulate the gaseous hydrogen combustion at the considered points;
- Perform a comparative study of the combustor performance through the results obtained for hydrogen and conventional jet fuel;
- Analyze the characteristics of the flow and justify possible malfunctions.

1.3 Dissertation Structure

The work developed and presented in this dissertation is divided into six chapters.

The present chapter is constituted by the motivation that leads the author to the development of this dissertation's theme, the objectives of the work developed and also a brief historical review, where some uses of the hydrogen in the aeronautical sector (until our days) are mentioned. Some works (numerical and experimental) are still introduced once they were used as basis for the development of the present work.

The chapter two introduces the fundamentals, components (with greater focus on the combustor), systems and performance parameters associated to the gas turbine engines. Then, the configuration of the CFM56-3 engine, to which the combustor in study belongs is presented. In the end of this chapter, a close-up on the fuel injection parameters and techniques used for liquid and gaseous fuels will also be introduced.

In the chapter three, a brief introduction will be made about the current aviation fuels and the ones that are more likely to be used in a closer future. Then, some of the properties and characteristics of the fuels used in this work are introduced, as well as the mechanisms of oxidation (detailed chemical mechanisms) and mechanisms of pollutant formation for both analysis (Jet A and hydrogen combustion).

The fourth chapter presents all the followed methodology (including the objectives and the data used in each step taken) and still a detailed description of the processes and approaches that allowed to obtain the final geometry, mesh and numerical setup used to get the final results through the CFD simulation process.

In the fifth chapter, the results are presented and discussed. In the beginning of this chapter, some of the choices made in the chapter four, for the models and procedures, are justified using the results obtained in the initial simulations. Then, the most relevant results about the performance of the combustor in the tests carried out are also analyzed, being explained which of the results were expected, which were not and the reasons why those unexcepted results occurred.

The sixth chapter is the last one and it presents the main conclusions of the research made in this dissertation. There are also some suggestions for future studies with the aim of improve the work presented.

1.4 Historical Review

To date, the largest users of hydrogen in aeronautics are the space applications where it is used as fuel for the rocket engines of launch vehicles. The first successful launch of a space vehicle propelled by a liquid hydrogen/liquid oxygen rocket engine took place at Cape Kennedy on November 27, 1963. The launch vehicle was an Atlas-Centaur built by the General Dynamics Corporation Convair Division. In this case, the RP-1 kerosine/liquid oxygen-fueled Atlas stage boosted the Centaur upper stage which employed two RL-10 hydrogen-fueled rocket engines developed by Pratt & Whitney Aircraft.

Several other rocket engine manufacturers in the U.S. were involved in development of designs using LH_2, e.g., General Electric Company, Rocketdyne Division of North American Aviation (now Rockwell Collins, Corp.) and Aerojet General Corporation were among the leaders. Of the designs developed by these companies, the Rocketdyne J2 engine is an example which has been eminently successful. It was used in both the second and third stages of the Saturn V launch vehicle, used in the Apollo program which landed U.S. astronauts on the moon. In all of the launches of the Apollo program there has never been a failure of one of the hydrogen-fueled rocket engines. This remarkable record is at least partly due to the fact that hydrogen is a most tractable fuel [9].

However, the space applications are relatively recent, looking at history, the first reported use of hydrogen in aeronautics was a long time ago. According to Brewer [9], hydrogen was first employed as lifting medium when, in France, a small silk balloon was constructed by the Roberts brothers, under the direction of physicist J.A.C. Charles, and it was flown in Paris on August 27, 1783. This balloon rose to a height of 3000ft (914.4m) and traveled a distance of 15mi (24.14km) despite a pouring rain. In that year, on December 1, a larger hydrogen-filled model which carried two passengers, the physicist Charles and one of the Roberts brothers, was launched. This flight traveled 25mi (40km) from Paris in less than two hours and it occurred just ten days after the historic flight made by the Montgolfier hot-air balloon in which human passengers were first carried aloft [9]. Hydrogen balloons have been used for scientific work, e.g., to study the physics and chemistry of the atmosphere and the stratosphere, to provide meteorological data, and to gather evidence of the effect of high altitude on human performance; for military operations, such as reconnaissance and observation; as well as for sport. The use of hydrogen in balloons has largely been supplanted today by helium because of safety considerations.

Later in history, airships came into being as a result of man's desire to control the direction and speed of flight. Numerous attempts were made to achieve such control with balloons without measurable success until 1852, when a Frenchman, Henri Giffard, constructed an airship on which he mounted a steam engine of his own design. Giffard flew this hydrogen-filled airship from the Hippodrome in Paris on September 24, 1852, attained an estimated speed of 6 mph, and demonstrated the first appreciable control of a "lighter-than-air craft". In 1872, Paul Haenlein (German engineer), developed and flew an airship powered by an internal combustion engine, which was fueled by gaseous hydrogen that was drawn from the lifting cells of the airship envelope [9]. The first airship to possess sufficient control to enable it to return to its point of departure was a French design powered by battery. This hydrogen-filled craft was constructed by Charles Renard and A.C. Krebs and flown on August 9, 1884, completing a circular flight of about 5 miles. A significant step leading to the use of hydrogen in commercial air transportation occurred in 1900, when the first rigid airship designed by Count Ferdinand von Zeppelin, the LZ-1, made a successful flight. In 1911, commercial air operations were started by a German transport company (DELAG) using five Zeppelin airships. In the next years, before the operations were terminated in 1914 by World War I, these hydrogen-filled airships made 1600 flights carrying 37,250 passengers without injury. The Treaty of Versailles prohibited further development in Germany and stopped the manufacture of airships by the Zeppelin company until the U.S. Navy commissioned the construction of the airship LOS ANGELES, designated by Zeppelin as the LZ-126, as a part of wartime reparations. In October 1924, the Zeppelin factory at Lake Constance, in Germany, completed the construction of the LZ-126, inflated it with hydrogen, and delivered it to the U.S. by a transatlantic flight. In the service of the U.S. Navy, the LOS ANGELES was inflated using helium and it had flown a total of 4320 hours, being decommissioned at Lakehurst, New Jersey, in 1932. The next airship built by the Zeppelin Co., the LZ-127, was the original GRAF ZEPPELIN. It was completed in September 1928 and saw 9 years of continuous, successful service using hydrogen as the lifting medium. When decommissioned in 1937, this rigid airship had made 590 flights (including 144 ocean crossings, mostly between Germany and South America) carrying 13,110 passengers and 235,300lb of mail and freight [9].

In 1936, the Zeppelin Co. built the LZ-129, a 200,000 m^3 design christened HINDENBURG. It was 245m long and employed the conventional Zeppelin design with an aluminum framework. The propellers were turned by four 1100hp Mercedes-Benz diesel engines and provided to the HINDENBURG a maximum speed of 135 km/h. At a cruising speed of 125 km/h, the airship had a range of 8750 miles, carrying 50 passengers in spacious accommodations. In 1936, the first commercial air service across the North Atlantic between Germany and the U.S. was initiated with the HINDENBURG carrying 1002 passengers on ten scheduled round-trips. Eastbound crossings averaged 65 hours; westbound, 52 hours. On May 6, at the end of the westbound leg of the first round-trip scheduled for the 1937 season, while approaching its mooring mast at Lakehurst, New Jersey, the HINDENBURG burst into flames and was destroyed. Of the 96 persons on board, 35 lost their lives. These were the first passenger fatalities in the history of commercial airship operations. The destruction of the HINDENBURG signaled the end of the use of hydrogen in commercial airships [9].

In 1955, a report by Silverstein and Hall of the (then) NACA-Lewis Flight Propulsion Laboratory was published in which the potential of liquid hydrogen as a fuel for use in both subsonic and supersonic aircraft was explored. According to it, theoretically, the use of hydrogen fuel could, among other advantages, significantly improve the maximum range [11]. As a result of this study, an experimental program with a U.S. Air Force B-57 twin-engine medium bomber was initiated to demonstrate the feasibility of burning hydrogen in a turbojet engine at high altitude. The modified aircraft first flown in 1956 and the liquid hydrogen (LH_2) was carried in a tank located under the left-wing tip. At the same time, gaseous helium was carried in a tank of similar size and shape under the right-wing tip for use as a pressurant. During this NACA hydrogen flight test program, the converted B-57 aircraft took off and climbed to the altitude and speed specified for the test, typically 50,000ft (15,240m) and Mach 0.75, over Lake Erie, using conventional JP fuel in both engines. Upon reaching test conditions, the flow of hydrocarbon fuel to the convertible J-65 turbojet engine on the left-hand side was reduced and stopped while the flow of gaseous hydrogen (GH_2, converted from LH_2 by a heat exchanger), was initiated and increased to the required rate. The weight flow rates were adjusted to be inversely proportional to the heats of combustion of the two fuels, LH_2 and JP fuel ($HV_{LH2}/HV_{JP}=2.8$). Enough LH_2 was carried in the tank for about 21 minutes of operation. When the LH_2 supply was exhausted, the JP flow to the engine was restored for the flight back to base. Throughout the flight test program, the performance of the engine at altitude was found to be exceptionally smooth, reliable and in conformity with expectations, no operational safety problems were encountered with the hydrogen fuel system [9].

From 1954 to 1955, Lockheed Aircraft Corporation made a series of conceptual design studies of hydrogen-fueled aircrafts in cooperation with Pratt & Whitney Aircraft and the Rex Division of AiResearch Corporation. In 1956, the U.S. Air Force awarded a contract to Lockheed's Advanced Development Projects organization, better known as Kelly Johnson's Skunk Works, to build two prototype aircraft (known as CL-400) which would be capable of cruising at Mach 2.5 at 100,000ft (30,480m) altitude. The CL-400 was to carry a two-man crew, a payload of 1500lb (680kg) of reconnaissance equipment, and to be capable of a range of 2200nmi (4074.4km).

Because of the pioneering nature of the work, Lockheed found it necessary to perform many experiments to verify theory and analyze almost every step of the way.

Also in 1956, at the same time the U.S. Air Force contracted with Lockheed for development of the CL-400 airplane, the Pratt & Whitney Aircraft Division of United Aircraft Corporation was awarded a contract to investigate the feasibility of using LH_2 as a fuel in aircraft engines to use in the CL-400. The entire propulsion package, including engines, inlets, and nozzles, was to be designed and supplied by Pratt & Whitney Aircraft. The inlets were a fixed, double-cone, axisymmetric external compression type. The nozzles were fixed with convergent-divergent configurations.

The work at Pratt & Whitney covered a broad spectrum ranging from applied research efforts such as heat transfer and materials investigations, to development testing of a J57 engine modified to operate on LH_2. It also included the design, construction, and test of a new design of engine (the Model 304).

The conversion of the J57 to operate on LH_2 was accomplished in just 5 months and the first tests were performed in the fall of 1956 [10]. The work with the J57 showed that conventional jet engines could be readily adapted to use LH_2 fuel. However, better performance was desired than the one that could be provided by a modified existing engine. So, in that research, after examining many possible cycles, the Hydrogen Expander cycle (which is well explained by Brewer [9]) was selected for experimental evaluation to create the Model 304 engine [10]. This was a unique cycle developed specifically to take advantage of the properties of hydrogen and to meet the performance requirements of the CL-400 airplane. The first demonstration test of a complete 304 engine was accomplished in September 1957 with a total of 25 hours of sea level engine testing where all performance predictions were confirmed. Each propulsion package weighed 6500lb (2948kg) and delivered 9500lb (4309kg) of installed thrust at sea level static conditions with a specific fuel consumption (SFC) of 1.36lb/h per pound of thrust. At Mach 2.5, 95,000 ft (28956km), the thrust was 6100lb (2767kg) with a SFC of 0.803lb/h per pound of thrust.

In spite of the success in developing practical solutions to the problems encountered with handling the cryogenic liquid fuel, the CL-400 aircraft was never built due to performance and logistics limitations. First, the airplane was marginal in range capability and did not show potential for significant improvement. The second reason for termination of the CL-400 program was the logistic problem posed by the fuel. The aircraft was intended for reconnaissance purposes which would require flights to many different locations around the world. Therefore, LH_2 would have to be available at these locations for the aircraft to be able to fly the return trip. Since concurrent studies at Lockheed had shown that the desired missions could be performed using a more conventional fuel, even with a compromise in cruise altitude, there was little incentive to continue the development of the CL-400. The alternative which was subsequently pursued led to the Skunk Works Blackbird program, the Lockheed SR-71/YF-12 aircraft designs which used the Pratt & Whitney J-58 engine. So, in 1957, the program was terminated by mutual agreement between the Air Force, Lockheed, and Pratt & Whitney. Overall, the CL-400 design and development program showed that it was entirely feasible to build a hydrogen-fueled airplane. LH_2 could be handled, with proper care and procedures, as easily and safely as conventional hydrocarbon fuel. The termination of the CL-400 airplane program resulted in cancellation of the Model 304 engine development and the efforts at Pratt & Whitney relative to hydrogen were redirected to development of the RL-10 hydrogen/oxygen rocket engine for use in the U.S. space program, as referred before. The RL-10 used the same hydrogen expander cycle to drive its turbopumps as was successfully demonstrated with the Model 304 turbojet engine.

In the 1970s, Lockheed performed studies on different liquid hydrogen fueled subsonic cargo and passenger transport jets for NASA Langley Research Center. The results are presented in the NASA-reports NASA CR-132558, NASA CR-132559 and NASA CR-144935. The main conclusions from these and furthers studies have been summarized by Daniel G. Brewer in [9]. The studies showed that hydrogen propulsion is especially beneficial in terms of energy use for long range aircrafts with internal hydrogen tanks. According to the author, the more energy required to perform the mission, the greater the advantage to be gained by using a higher energy fuel. The long range LH_2 aircrafts would be lighter; require smaller wing area and shorter span, but larger, longer fuselages; use smaller engines; can operate from shorter runways; and use 25% less energy to perform the mission. Further, the LH_2 airplane would cost less both to develop and to produce [12].

In the 1980s, Tupolev developed the Tu-155 that was based on the medium range transport aircraft TU-154B. Moreover, the TU-155 was built and successfully tested without any serious incidents and it first flew burning hydrogen in one of its three engines in April 1988. The modified engine was also able to run with natural gas. The TU-155 was followed by the TU-156 that could be run with natural gas or kerosene [12].

At the beginning of the 21st century, the Cryoplane Project comprised 36 European research partners from industry, universities and research institutions. They contributed to this project covering aircraft configuration, systems & components, propulsion, safety, environmental compatibility, fuel sources & infrastructure, transition. The total project time was 26 months and started in April 2000. During this project several conventional and unconventional overall aircraft design studies and detailed investigations of hydrogen fuel systems and components were performed [12, 13, 23]. However, the obtained results were partially contradictory to previous studies such as those of Lockheed and NASA in the 1970s. For example, the "energy consumption would increase by 9% to 14%" for all investigated aircraft designs due to "bigger wetted surface" [12, 13].

More recently, in July 2010, Boeing unveiled its hydrogen powered Phantom Eye UAV that uses two converted Ford Motor Company piston engines [14].

Nowadays, governments and companies are investing again in hydrogen's potential. For instance, the ENABLEH2 (ENABLing cryogEnic Hydrogen based CO_2 free air transport) consortium was given such a hand, almost 20 years after the European Commission's last attempt to ramp up LH_2 research and development under the Cryoplane project [18]. The project's objective is to demonstrate that switching to hydrogen is feasible and must complement research and development into areas like advanced airframes, propulsion systems and air transport operations [22].

Another example is the project named ZEROe, announced by Airbus, in September 2020, that has the ambition to develop the world's first zero-emission commercial aircraft. This project is a flagship of the European Union's multibillion-euro stimulus package (aimed at greening the bloc's economy) and it consists in the development of three concept aircrafts (powered by hydrogen) which Airbus says that could be ready for deployment by 2035 [15, 16]. All three designs are envisaged as hydrogen hybrids, which means they would be powered by gas turbine engines that burn liquid hydrogen as fuel, and also generate electricity via hydrogen fuel-cells to complement the gas turbine engines, resulting in a highly efficient hybrid-electric propulsion system [15, 16].

For the future, according to some studies, the successful development of hypersonic aircrafts can only be expected with the use of hydrogen fuel. The research of this type of aircrafts started in the mid-1960s, when some studies were performed to explore the possibilities of hypersonic aircraft. In 1965 (and later in the 1980s), conceptual design studies led to the realization that the lifting body and the blended wing-body configurations would offer significant advantages for hydrogen-fueled hypersonic aircrafts.

Unfortunately, because of security classification, not much is discussed in the open literature concerning the hypersonic aircrafts performance or intended use. The best that can be done in some instances is merely a listing for reference, as Brewer did in [9], where several of those hypersonic concepts are listed and briefly described.

1.5 Bibliographic Review

Over the last decades, some authors published studies that showed concepts of combustion chambers and injection systems that promised potential for significant pollutant emission reduction in the gas turbine engines. For example, Reid Smith et al. [24] analytically investigated numerous of these combustion chamber concepts applied in high pressure ratio aircraft gas turbine engines that entered (or will enter) in service this century. The objective of this task was to identify the most promising concepts, discover existing technological barriers to implementation, design approaches, and development strategies for low emissions, from which a development program could be structured. In that work, two essentially separate research and development paths were proposed, the rich and the lean combustion, each with its own specific barriers, but also with some common concerns. In the end, Reid Smith et al. [24] concluded that although lean premixed prevaporized and lean catalytic combustion offer the potential for very low NOx, they were deemed to be impractical for aircraft engines. Instead, lean direct injection (LDI) in the form of lean multisource combustion was identified as an approach to be pursued.

More recently, Robinson et al. [25] performed a detailed study on the design and testing of a micro-mix combustor with recuperative wall cooling for hydrogen burning. The investigation used a set of mass and equivalence ratio variations at different temperatures and pressures to perform exhaust gas analysis on combustion efficiency and stability.

Related to performance assessment for the use of hydrogen as fuel in a converted gas turbine engine, the few existing publications focus on the gas path and cycle performance using conventional or unconventional aero engines. According to Boggia et al. [26], who studied and compared four different cycles (preheating the hydrogen fuel with exhaust gases, cooling the compressor air with hydrogen fuel, cooling turbine cooling air with hydrogen fuel, hydrogen topping cycle), the conclusion was that the precooled and high TET cycles (both that use the hydrogen to cool the air) appeared to be the most promising, offering a reduction in operational cost on the order of 3%. Furthermore, they point out that the positive aspect of these two cycles is that the innovations are technically feasible and do not involve any additional turbomachinery. The configuration with fuel preheating was considered the simplest solution and would require only minimum modifications to the original engine.

Payzer and Renninger [27], in their work, concluded that there is a definite thermodynamic benefit in switching from hydrocarbon fuel to hydrogen because of the difference in fuel properties. However, having evaluated eight different unconventional cycles, both in terms of aircraft mission performance and uninstalled engine performance, they stated that the additional complexity associated with these cycles does not appear to be justified.

In this field, Haglind and Singh [28] also conducted a study on the performance and emissions effect of changing the fuel from kerosene to hydrogen on a V2500 aero engine. The main studied changes comprise fuel control system, implementation of facilities to evaporate the hydrogen prior to its entry into the combustion chamber and a possible redesign of the combustion chamber. In order to retrofit a gas turbine engine and adapt the combustion chamber for hydrogen, the authors concluded that, some changes are necessary and some others are desired to utilize the favorable properties of hydrogen in an optimal fashion. The minimum change that has to be done to adapt a conventional combustion chamber for hydrogen is to replace the injection system because when the hydrogen is injected into the chamber it is in the gaseous state while the kerosene is liquid. In addition, there are several other factors that need to be considered to optimally utilize the changed conditions owing to burning hydrogen. For example, when burning hydrogen, the thermal energy radiated to the surroundings is lower than that of kerosene, thereby beneficially affecting the liner durability and cooling requirements (this phenomenon is explained in section 4.2.2). Following Haglind and Singh [28], when changing to hydrogen, either the turbine entry temperature (TET) or the net thrust could be retained. The study showed that a small performance improvement, in the order of a few percent (which depend on the fuel temperature and cycle configuration), may be obtained by changing to hydrogen and retain the TET. In order to obtain a certain performance (the same net thrust), a lower TET could be used, thus requiring less advanced cooling technology as well as having a favorable effect on turbine blade life. According to Boggia and Jackson [33], the performance improvements could be explained by the two fundamental changes when using hydrogen: reduced mass flow and changed composition of the gases expanding through the turbines. These changes will be explained in the section 3.3.1.1.

The study [28] showed reduced emissions and an increase in NOx, which is in line with the works of Lee et al. [29], Svensson et al. [30], and Yildiz et al [31].

In line with Haglind and Singh [28], also Osigwe et al. [32] predicted the turbofan engine's performance using LH_2 and concluded that when compared to jet fuel, LH_2

combustion has a lower mass flow rate (due to the higher LHV of the fuel) to achieve the same net thrust. This also reflects an increase in the enthalpy drop and changes in the gas composition through the turbine. The resulting discussion in [28] and [32] comparing hydrogen with jet fuel is consistent with a similar assessment done for the EU CRYOPLANE project, in collaboration with Cranfield University and Universidad Politecnica, Madrid [34]. It should be noted that in [34] is considered the effect of the fuel temperature on the engine performance and it is referred that if the fuel temperature is considered only just above the liquefaction temperature, instead of a higher value, the TET required to achieve the same thrust would rise by 2-3ºC. So, if the fuel is stored in a liquid/cryogenic state, it is important to vaporize the hydrogen fuel efficiently.

Lastly, in the field of performance comparison, Gunasekar and Manigandan [35] utilized an exergy approach (it is another way to understand and compare the performance) to assess LH_2 and jet fuel performance. Their results showed that the introduction of LH_2 reduced exergy efficiency, due to the high specific exergy of hydrogen fuel compared to jet fuel.

About the fuel control, G. Dahl and F. Suttrop [36] demonstrated safe hydrogen metering and engine control under the conditions of a gaseous fuel in an APU GTCP 36-300 that was converted from kerosene to hydrogen operation. In that work, it was also proved that a substantial reduction of the engine’s NOx emissions could be achieved by the application of micro-mix diffusive combustion of hydrogen. However, if applied only the minimum change configuration of the hydrogen injection nozzles this change would even increase the NOx emissions [36]. The authors also refer that, in the case of study, diffusive burning was inherently safe against flashback reducing the risk of engine failure. The possibility of rapid hydrogen fuel metering according to the quickly changing load conditions of a typical aircraft APU has been considered and showed margins for further development, especially to adapt the system to cryogenic hydrogen supply. In that work, safe ignition and engine start procedures have also been developed and tested in order to avoid the risk of uncontrolled combustor deflagrations and intolerable pressure rises.

About the hydrogen injection methods into the combustion chamber there are some studies that provided precious information to this work. For instance, J. Ziemann et al. [37] evaluated six different fuel injector concepts through steady and transient tests. In those tests, the nozzle designs followed two different strategies. The most advanced low-NOx concept was the lean premix combustion which strives to achieve thorough mixing of the fuel into the airstream, prior to the delivery to the combustor being that two of the injectors tested fall into this category. The second concept was lean combustion without premixing where the lean direct fuel injection strategy injects gaseous hydrogen into a vigorous shear-layer mixing region of the combustor. Four of the tested injectors fall into this category and the NOx levels (for this injectors) depend strongly on the proper injection of the fuel into the mixing shear layer. In general, the authors concluded that the NOx emissions improve when the degree of premixing increases. Based on the test results from this program, practical low-NOx hydrogen gas turbine combustors can be achieved.

In another study, C. J. Marek et al. [38] tested a total of five fuel injector configurations to investigate the combustion performance of gaseous hydrogen using lean direct injection. In their work, one of the designs used was generated inhouse at NASA Glenn (used as reference), while the four remaining designs were generated by major fuel injector manufacturers. The selected manufacturers had previously been testing configurations for either rocket injectors or low emission injectors for Jet A fuel. All of the tested configurations use some variation or combination of lean direct injection (LDI) and lean premixed prevaporized (LPP) schemes. The specifications of each injector used in that study were presented by C. J. Marek et al. [38]. In the end, the authors concluded that all of the LDI configurations performed well and were very stable. Moreover, all of the lean direct injection configurations did result in low levels of NOx and compare well with the LDI Jet A combustors. No flashback or autoignition phenomena were encountered. For the more conservative configuration with a single hole hydrogen injection with counter swirl (as in conventional combustors) the minimum NOx levels were twice than the LDI Jet A values which was poorer, however, the configuration was very durable. That study also showed that the more injection points result in a lower level of NOx, but without advanced manufacturing techniques, the injectors might be more difficult to construct. Cooling can be a problem with hydrogen combustors, and two of the configurations failed during the tests. Other conclusion is that as the pressure is increased, the fuel flow must be increased resulting in more penetration and better mixing (this specifically for the NASA N1 injector). Likewise, at low equivalence ratio and high pressure, the NOx levels are greater than the LDI Jet A values.

Finally, and still related with hydrogen injection methods, Lei and Khandelwal [39] proposed ways in their studies to reduce the combustion temperature in the chamber to reduce the NOx emissions. For this purpose, six cases of injection method and injector position effect were simulated to understand the combustion performance. Their results showed that the angled air inlet increased the airflow rotation, which improved the mixing intensity of hydrogen and air and reduced the chamber's peak temperature.

About the pollutant formation, the use of hydrogen offers the possibility of a significantly reduced number of emission species, resulting only in H_2O and NOx emissions [28]. An excellent discussion on the formation of NOx as related to gas turbine combustors can be found in Kuo [40] and Lefebvre et Ballal [41]. For instance, in [41], the authors summarize the body of work on NOx formation to show clearly that emission levels increase with inlet air temperature and longer combustor residence times. For that reason, when burning hydrogen, the attempts to reduce the NOx emissions are focused on lowering the flame temperature, eliminating hot spots from the reaction zone and reducing the duration and exposure in the flame region [42]. Another conclusion presented by Lefebvre [41] is that fuel injector designs that provide high levels of mixing between the fuel and air have been a key to reduce NOx emissions. Results for pressure increase are inconclusive, in some cases there is an increase in the emissions and in other studies, no effect [38, 41].

Still related to the pollutant formation, NOx emissions from hydrogen rich fuels have been very well correlated to adiabatic flame temperature both in laboratory scale flame, by Ströhle et al. [44], and gas turbine tests, by Todd and Battista [45]. Besides those works, Cocchi et al. [46] were able to model the emissions from a hydrogen fired combustor over a wide range of parameters variation by tuning a model based on the thermal NO mechanism solely. Other works on combustion design and pollutant mitigation for LH_2 are documented in the references [32], [47-51].

Another assessment that must be done is related with the impact of the utilization of LH_2 on the hot section of the aero-engine when compared with jet fuel, since the hot gas path temperature profiles will probably be changed with the retrofit of the system to hydrogen combustion [56]. For that assessment, some of the factors that must be taken into account are the maintenance costs and the engine's life (mainly for the turbine). In this field, Agbadede et al. [52] provided a comparison for hydrogen and natural gas using an industrial gas turbine. The study shows a longer life to rupture for hydrogen against natural gas. In that same study, Agbadede et al. [52] compared the effect of the use of hydrogen and natural gas on the HPT blade's creep life (creep is one of the most common failure mechanisms that reduce component life). The result also shows an improved creep life when hydrogen was used rather than natural gas, which is in line with other literature reviews [53] on the longer engine life and lower maintenance costs for LH_2.

Osigwe et al. [32] also provided an evaluation of LH_2 compared with jet fuel, from a creep life viewpoint, in a turbofan aero engine. In that study, there was a slight decrease in the turbine entry temperature (TET), which would have also contributed to a longer life on the turbine blades as the stress and thermal load values were lower than when the jet fuel was utilized in the turbofan engine, as described by Eshati et al. [54]. The assessment [32] shows a 15% improvement in extended blade life for hydrogen when compared with jet fuel. The effect of TET on creep life for the HPT blades is aligned with the work of

Eshati et al. [55] for a given radial temperature distribution factor, which showed a 70% reduction in creep life for a 3% increase in TET.

Finally, some assessments related to the numerical simulation modelling had been taken into account for a better performance in this study. For example, L. Y. Jiang [57] performed an assessment of the turbulence modeling under gas turbine conditions focusing on the turbulence models most widely used in practical engineering, which are the RANS (Reynolds-averaged Navier-Stokes) models, and concluded that all the turbulence models tested can capture the flow features or patterns. However, for the quantitative predictions of velocity, temperature and species fields, different levels of performance were revealed. The RSM model gave the best performance, and it was the only one that could accurately predict the lengths of the recirculation zones and offer reasonable prediction on the turbulence kinetic energy distribution in the combustor. In addition, the performance of the Rk-ε model was better than that of the other four two-equation models, and it could give similar results as those from the RSM under the same configuration and operating conditions.

In another study, G. Boudier et al [58] studied some specific aspects of an aeronautical gas turbine combustion chamber (multiple inlets, multi-perforated plates and film cooling) using LES and comparing the results with predictions provided by Reynolds Averaged Navier–Stokes (RANS) simulations and experimental measurements. The authors concluded that the application of LES is of great interest for design purposes because of the capacity to predict unsteady turbulent reacting flows and yield information that is not accessible with conventional numerical approaches. Other conclusion is that the mean temperature fields within the chamber, provided by LES, were observed to be sharper and to reach larger values. The assessment of the predictions in terms of the profile of the mean exit temperature heterogeneities seen by the turbine proves LES to be very promising and out-performing RANS. However, currently, the computational capabilities still remain favorable to RANS especially in the industrial context. This is in line with the conclusions taken by A. Benedetto and V. Sarli [59] in their comprehensive study about the theory, modeling and computation of gas explosion phenomena.

Chapter 2 – Turbofan Basic Considerations

2.1 Gas turbine engine

The gas turbine engine is essentially a heat engine that uses air as a working fluid to provide thrust. To achieve this, the air passing through the engine has to be accelerated, which means that the velocity or kinetic energy of the air has to be increased. In order to obtain this increase, the pressure energy is first of all increased, followed by the addition of heat energy, and finally all this pressure and heat energy is converted back to kinetic energy in the form of a high velocity jet efflux [60].

2.1.1 Working Cycle

The Joule–Brayton cycle is a conceptually simple thermodynamic cycle that can fulfill those previous steps and be technically made in operation with a very small set of components. As shown in Figure 2.1, the cycle consists of four processes (associated to induction, compression, combustion and exhaust) that occur continuously in a gas turbine engine [60, 61].

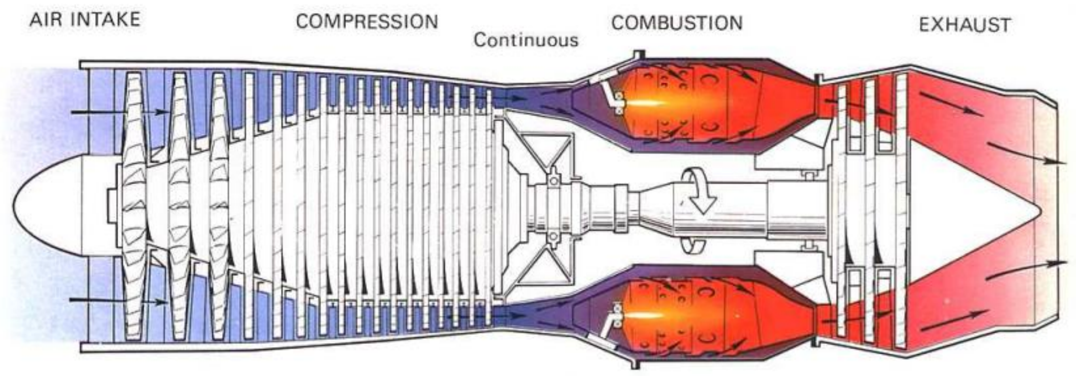

Figure 2.1: Phases of the working cycle of a turbo-jet engine [60]

Due to the continuous action of the turbine engine and the fact that the combustion chamber is not an enclosed space, the pressure of the air does not rise during the combustion process, but its volume does increase. This process is known as heating at constant pressure. Under these conditions, there are no peak or fluctuating pressures to be withstood [60].

2.1.1.1 Variants of the cycle

The Joule-Brayton cycle can be plotted within two types of diagrams, P-V (showed next) or T-s [62], and it can be presented in two basic forms, the ideal and the real cycle, as shows the Figure 2.2. Both these variants can still have an open or closed configuration. In this subsection these terms will be explained in the context of this work.

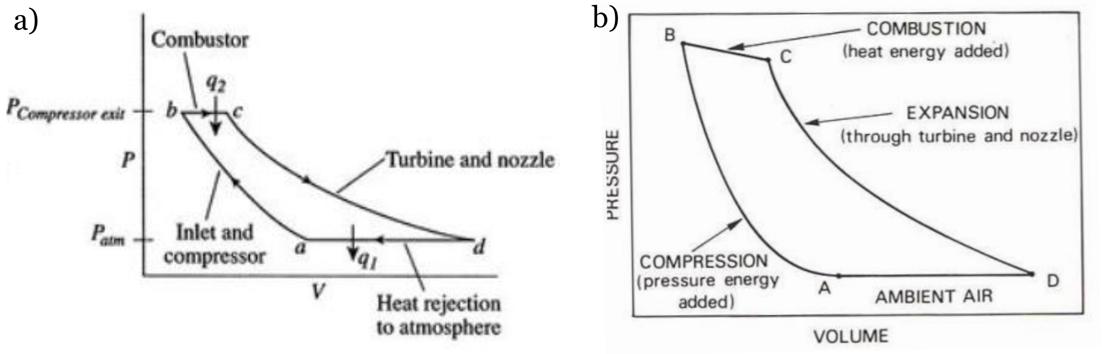

Figure 2.2: Joule-Brayton cycles represented on pressure-volume diagrams: a) ideal cycle [70]; b) real cycle [60].

First, the ideal cycle is based on the assumptions that the working fluid is an ideal gas, with constant composition, flow rate and specific heat at constant pressure in all the cycle processes of heat addition (b-c) and heat rejection (d-a), and that all the transformations occur in ideal machines without any irreversible process: the combustion chamber does not have any heat loss to the environment or any pressure loss in the fluid flow; and the processes of compression (a-b) and expansion (c-d) are assumed as adiabatic and isentropic [61, 62].

The real Joule–Brayton cycle can be described by removing all the simplifying assumptions concerning the working fluid and the components [61]. These assumptions include friction, shock, heat transfer and aerodynamic losses in compressor and turbine, losses in combustion chamber, piping and mechanical losses, etc. However, with such a large number of variables affecting the performance of a gas turbine engine it is really difficult to estimate its performance unless certain other assumptions are made [62]. Thus, if it is considered a closed cycle, the following assumptions can be made:

- The fluid is real and the specific heat at constant pressure is a polynomial function of the temperature.
- The heat exchangers (in the closed cycle, or the combustor in the open cycle) have heat losses, and the passage of the working fluid in them or in any other duct produces friction losses, thereby reducing the pressure from the inlet to the outlet of each component.

- The fluid in the compressor and the expander produces friction losses and the compression and expansion processes are adiabatic but they are not isentropic.
- There is no increase in the mass flow rate due to the addition of the fuel. However, if the cycle is open, there is the additional assumption that the fluid flow rate and composition change when the fuel is added to the air flow and the combustion process transforms the composition from air to flue gases [61].
- Radiation and mechanical losses are neglected.

As mentioned before, the cycle can still be either closed or open. In the open cycle, the air is taken from the atmosphere at ambient pressure and temperature to the engine; and the products of combustion along with the excess air are exhausted into the atmosphere. Thus, in this case, the working fluid is always changed and, for the next cycle, fresh air is taken again from the atmosphere. In a closed cycle, the air is heated in an air heater by burning fuel externally; and, in the end of the cycle, the hot air is cooled in a precooler and supplied back to the compressor to restart the cycle without changing its original composition and thermodynamic conditions. Thus, in this case, the same working fluid is repeatedly circulated in the system [62].

2.1.1.2 Description of the cycle

Considering the closed cycles represented in Figure 2.2, the starting point for the description of the Joule-Brayton cycle is point a that represents the ambient conditions (with the lowest pressure and temperature of the whole cycle). The gas is then compressed in the compressor to reach point b, which is at the maximum pressure of the cycle. The compression of air between the points a and b is accompanied by an increase in the temperature of the air. This air is then mixed with a fuel in the combustor where heat is released in the combustion process, which ends at point c (that represents the maximum temperature of the cycle). Therefore, between the points b and c, the working fluid does not only reach a higher temperature, but its composition also changes from air to the combustion products, thereby considerably increasing the volume of the flow [61]. In the ideal cycle the process b to c is assumed at constant pressure, however, in the real cycle, the pressure losses that occur due to the combustion process in the chamber are indicated by the drop between b and c represented in the Figure 2.2 b) [60]. From c to d the gases resulting from combustion expand through the turbine and jet pipe until they reach the lowest cycle pressure at point d, which lies on the same pressure line as point a. During this part of the cycle, some of the energy in the expanding gases is turned into mechanical power by the turbines (to drive the compressors); the remainder, on its discharge to atmosphere, provides a propulsive jet [60].

The performance of the cycle can be evaluated by using two parameters: the thermal efficiency and the work output [61]. Since the turbofan engine is a heat engine, the higher the temperature of combustion, the greater is the expansion of the gases, and consequently, the efficiency. However, the combustion temperature must not exceed a value that gives a suitable turbine gas entry temperature for the design and materials of the turbine assembly [60].

2.1.1.3 Modifications needed in the cycle for hydrogen fuel

The cycle consisting of the basic components completing the processes described before is generally called the simple Joule–Brayton cycle, to distinguish it from some of the modifications that have been proposed over the years to improve its performance.

For this work, as the main objective is to maintain almost all the same components as the original CFM56-3 engine, the cycle will be considered the same. However, and as referred by several researchers that investigated some of the possible cycle configurations for the use of hydrogen fuel, in a practical solution, the minimum change that needs to be adopted with the engine cycle is the implementation of facilities to evaporate the hydrogen, which is stored in the tanks in a liquid (or cryogenic) state, prior to its entry into the combustion chamber. This fuel heating can be accomplished either by an external heat source (i.e., cooling systems of hydraulic fluids, pumps, electric equipment, etc.) or a heat exchanger located at a suitable engine location. Placing the heat exchanger outside the engine does not affect the engine performance; however, it might cause practical problems when the fuel system is integrated with the other aircraft systems [28].

As for the case of evaporating the hydrogen using a heat exchanger suited within the engine cycle, the cryogenic properties of hydrogen could be exploited to improve the performance through the use of unconventional cycles such as those studied by Boggia et al [26]. Some of these cycles are also proposed for kerosene-powered cycles; however, the main advantage when using hydrogen is the involvement of an additional fluid with favorable properties. According to Boggia et al. [26], considering unconventional designs, there are basically four options, and various combinations of these that could be employed:

- Preheating the hydrogen fuel with exhaust gases (simplest solution);
- Cooling the compressor air with hydrogen fuel;
- Cooling turbine cooling air with hydrogen fuel;
- Hydrogen topping cycle.

A conclusion of the study [26] is that the options that use the hydrogen fuel as cooling fluid are the more promising ones. The detailed information about these cycles is presented by Boggia et al. [26]. Other cycle options for the use of hydrogen fuel are presented by Payzer and Renninger [27].

2.2 Turbofan Engine Components

In this subsection, a brief description will be made about the main components that are typically present in a turbofan, starting with the description of the intake (or inlet), followed by the fan and compressor. Then, the turbine will also be described. Finally, a brief overview will be made on the exhaust system.

It should be noted that the combustor will not be described in this subsection.

2.2.1 Intake (or inlet)

The air intake (or inlet) duct is the first part of all airbreathing propulsion systems and it is usually designed and manufactured by the airframe manufacturer, however both (airframe and engine manufacturers) cooperate in testing the air intakes.

An aircraft will require one or more intakes to capture the atmospheric air (working fluid) at free-stream Mach number, sometimes changing the direction of this flow and supplying it to the engine with as little distortion as possible to ensure smooth running and efficient propulsion. Moreover, the intake has to achieve all this with minimum disturbance to the external flow around the aircraft and thus minimum external drag [60]. So, for a successful operation of the engine within the desired flight envelope, engine-intake compatibility is essential.

The surface of the intake is a continuous smooth curve, whose very front (most upstream portion) is called as intake lip. For a subsonic aircraft, this intake lip is relatively thick and usually the subsonic intakes have fixed geometry.

The most common type of subsonic intake is the pitot intake, which consists of a simple forward entry hole with a cowl lip. This type of intake makes the fullest use of ram pressure due to forward speed, and suffers the minimum loss of ram pressure with changes in the aircraft altitude [60]. However, as sonic speed is approached, the efficiency of this type of air intake begins to fall because of the formation of a shock wave at the intake lip. The three major types of pitot intakes are the podded, integrated and flush types.

In the case of CFM56-3 the intake is of the podded type, as represented in Figure 2.3.

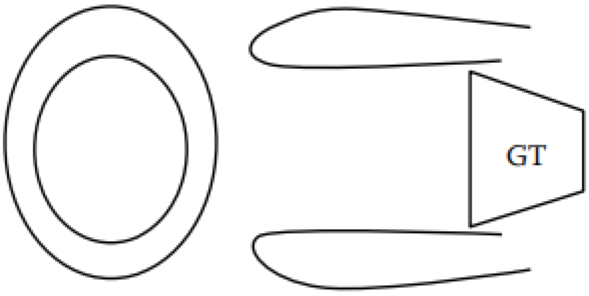

Figure 2.3: Typical layout of a podded pitot subsonic intake: in left, front view; in right, side cut-view [68].

For this type of intake, the friction losses are insignificant while the flow separation is of prime importance. The internal flow has the shortest and most direct route possible to the engine and its pressure recovery is almost 100% [68]. From an aerodynamic point of view, the flow in the intake resembles the flow in a duct. The duct "captures" a certain stream tube of air, thus dividing the air stream into an internal flow and an external flow. The external flow preserves the good aerodynamics of the airframe, while the internal flow feeds the engine.

For more information about the intakes, please consult reference [68].

2.2.2 Fan and Compressors

Gas turbine engines use dynamic or steady flow compressors that utilize momentum charges in the flowing air to cause the desired compression and temperature increase. Generally, these compressors can be of three types: centrifugal (or radial), axial, and mixed flow (combine the two previous types).

In the case of CFM56-3, the compressor employed is of the axial flow type. Thus, in this section, a brief comparison will be made between the types of compressors, putting the focus in the features of the axial compressors.

Considering the flow direction, axial compressors are those in which the air flows mainly in a parallel direction to the rotational axis whereas in a centrifugal compressor the air flows essentially at right angles to the rotational axis of the compressor [62, 68].

About the working principles, in a centrifugal compressor the air is imparted at high velocity and the pressure rise is made by a row of moving blades, i.e., an impeller. The increase in kinetic energy is converted into further pressure rise by a diffuser. On the other hand, a typical axial compressor, as depicted in Figure 2.4, has a series of rotating "rotor" blades followed by a stationary "stator" set of blades that are concentric with the axis of rotation [68]. The moving blades are fixed on a central drum and the fixed blades on the outer casing [62]. Each pair of rotors and stators is referred to as a "stage". The number of stages in an axial compressor is defined according to the desired compression and these several stages are placed concentrically in a row along a common power shaft [68]. The presence of the stator blades is required to guide the airflow to the next row of moving blades to ensure reasonable efficiency [62]; without them the airflow would rotate with the rotor blades resulting in a large drop in efficiency [68].

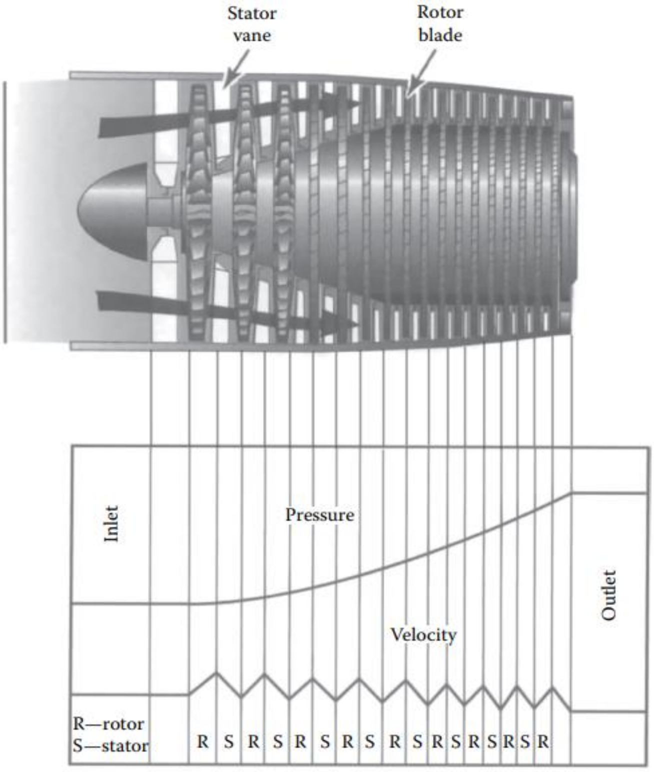

Figure 2.4: Layout of an axial compressor [68].

As it is possible to see in Figure 2.4, the axial compressor compresses the working fluid (air) by first accelerating the air (increasing the kinetic energy) and then diffusing it (convert this kinetic energy into static pressure) to obtain a pressure increase. The air is accelerated in the rotor (absolute velocity increases) and diffused in the stator (absolute velocity decreases) [68]. For successive stages, a saw-teeth pattern is obtained for the velocity, while the static pressure continuously increases in both the rotor and stator rows of all stages [68]. As the pressure increases in the direction of flow, the volume of air decreases, and to keep the same velocities for each stage, the blade height is usually decreased along the axis of the compressor [62].

About the performance, axial flow compressors have a large mass flow capacity, high reliability, and high efficiency, but have a smaller pressure rise per stage (1.1:1–1.4:1) than centrifugal compressors (4:1–5:1). However, it is easy to link together several stages and produce a multistage axial compressor having pressure ratios up to 40:1, as in modern compressors. Integrally bladed rotors permit blade speeds significantly above conventional rotors and hence stage pressure ratios greater than 1.8 [68]. Moreover, axial flow compressors provide constant delivery at variable pressures and generally have a narrower stable operating range than centrifugal compressors [62].

The mixed flow compressor combines the advantages of both centrifugal and axial compressors [62].

The fan in turbofan engines is also an axial compression module, which is treated as an axial compressor having less blades of very large height, wide chord, and large twist. These fans may be single stage (as in CFM56-3), or up to three stages, in low bypass turbofan engines [68]. In the case of CFM56-3, this fan represents the first stage of the compressor and it is followed by some stages of the axial compressor, which represents the first module of the engine core. This module is named as low-pressure compressor (LPC) [68]. The compressor of this engine consists of two modules, the first is the low-pressure compressor (LPC) and the second is the high-pressure compressor (HPC).

A deeper comprehension about the compressor principals and operation modes in a turbofan is made by Mathur and Sharma [62] and EL-Sayed [68].

2.2.3 Turbines

Turbines may be defined as turbomachines that extract energy from the fluid and convert it into mechanical/electrical energy [68]. The principal task of the turbine section in an aero gas turbine engine is to provide the power to drive the compressor and accessories, and in applications that do not require solely the propulsive jet, the turbine can also provide shaft power for a propeller or rotor [41].

Turbines may be classified, based on the direction of the gas flow, in axial, radial, or mixed [62, 68]. In axial turbines, the flow moves parallel to the axis of rotation. In radial turbines, the gas moves perpendicularly to the axis of rotation. In mixed-flow turbines, the gases have a combined radial and axial motion. Virtually, all turbines in aircraft engines are of the axial type, regardless of the type of compressor used. So, in this subsection, only this type of turbines will be presented.

An axial turbine is similar to an axial compressor operating in reverse. So, the analysis of these turbines is very similar to that of the compressors discussed earlier. Like an axial compressor, an axial turbine is composed by a set of stages and each of them has two successive stator (called nozzles or nozzle guide vanes) and rotor blade rows, where airfoil-shaped blades are used. The number of stages depends entirely on the engine type. In these turbines, the stators are used to keep the flow from spiralling around the rotation axis by bringing the flow back parallel to the axis. [62, 68].

Regarding the turbine operation, it is necessary to consider that when the hot gases, resultant from the combustion process, force their way through the combustion chamber discharge nozzle, they are accelerated close to the speed of sound before entering the turbine, due to the convergent shape of the nozzle. So, the gases that enter the turbine have high kinetic energy and static pressure.

When the energy is extracted from the flow, the pressure drops across the turbine. The pressure gradient helps to keep the flow attached to the turbine blades. Therefore, turbines, unlike compressors, are easier to design, since the pressure drop across a single turbine stage can be much greater than the pressure increase across a corresponding compressor stage without the danger of separating the flow [68]. Consequently, higher efficiencies can be achieved in a turbine stage, which can be used to drive multiple compressor stages [68]. However, the turbine blades exist in a much more hostile environment than compressor blades, since for efficient operation, the turbine rotates at very high speed, which makes the turbine drum one of the most highly stressed parts in the engine. Moreover, sitting just downstream of the burner, the turbine inlet blades may be exposed to temperatures of 850°C–1700°C [68]. What defines this turbine inlet temperature is the temperature resultant from the combustion process. In theory, to achieve the best performance, the burning temperature should be as high as can be achieved from the complete combustion of the fuel and oxygen in the air [68].

To overcome the challenge of the high temperature exposure, turbine blades therefore make use of advancements in metallurgy and manufacturing processes and they can be either made of special metals that can withstand better the heat, or be actively cooled, or both [62]. The more recent blades are hollow, and the cooling air (bled off the compressor) is pumped through the blades and exits through the small holes on the surface to keep the blade’s surface cool.

More information about the limiting factors in the turbine design, the materials used, and various cooling methods are discussed by Mathur and Sharma [62] and EL-Sayed [68].

Like the compressor, in the CFM56-3 engine there are two turbine sections, the low-pressure turbine (LPT), which drives the fan and the low-pressure compressor (LPC); and the high-pressure turbine (HPT), which drives the high-pressure compressor (HPC) [66].

2.2.4 Exhaust System

Aero gas turbines have an exhaust system whose objective is to pass the turbine discharge gases into the atmosphere at an appropriate velocity and direction to the flight condition.

Like the CFM56-3, the vast majority of jet-powered aircraft use what are known as axisymmetric nozzles. These nozzles produce direct thrust purely along the axis of the engine, hence the term axisymmetric. In some aircrafts (mainly military), two-dimensional nozzles (which can adjust the direction of the thrust) are used. This concept is explained in detail by EL-Sayed [68].

The main components of the exhaust system for non-afterburning engines are the tail cone (or diffuser), the exhaust duct (which is often referred to as the tail pipe), and the exhaust nozzle. All these components are represented in Figure 2.5 [68].

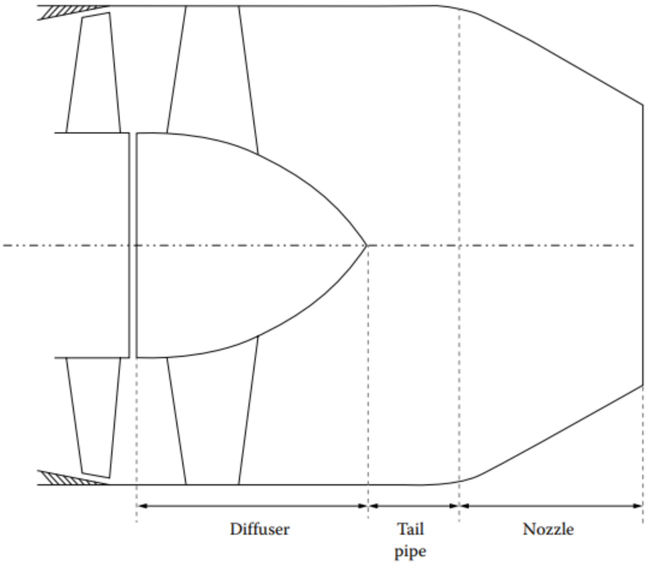

Figure 2.5: Layout of a simple exhaust system of the core (or hot) stream of a turbofan engine [68].

In the case of CFM56-3, which is an unmixed turbofan engine, there are two separate nozzles for exhausting core and fan streams, named as hot and cold (or fan) nozzles, respectively. The hot nozzle is located downstream of the turbine, more specifically after the low-pressure turbine, and the cold nozzle is located downstream of the fan section and it is used to discharge the air that has bypassed the fan. Together, they provide the thrust force required for all flight conditions.

Usually, the gases from the engine turbine enter the exhaust system at velocities from 750 ft/s (229 m/s) to 1200 ft/s (366 m/s) [62]. This high velocity produces high friction losses; thus, these high speeds have to be reduced by diffusion, which is accomplished by increasing the passage area between the exhaust cone and the outer wall as shown in Figure 2.5. The tail cone is fastened to the casing by turbine rear support struts. These struts straighten the flow before the gases pass into the jet pipe. The exhaust gases pass into the atmosphere through the propelling nozzle, which, in the case of study, is a convergent duct, increasing the velocity of the gases and creating thrust. A convergent nozzle consists in a nozzle that starts large and progressively its cross-sectional area decreases. According to the Bernoulli principle, as the fluid (air) enters the smaller cross-section, it must increase its velocity due to the conservation of mass [69].

The design of the exhaust system is of great importance because it exerts a considerable influence on the performance of the engine. This is because the areas that belong to the nozzle affect the turbine entry temperature, the air mass flow, the velocity and pressure of the exhaust jet [69]. In a non-afterburning turbojet engine, the exit velocity of the exhaust gases is subsonic at low-thrust conditions and reaches the speed of sound in the higher operating conditions.

2.3 Combustor

2.3.1 Overview

In a gas turbine engine, the combustor is a component, located between the compressor and turbine, which accepts air from the compressor and delivers the flue gases at a suitable temperature for the turbine inlet [68].

Firstly, it is important to understand the difference between the combustor and the combustion chamber. So, the combustor includes all of the combustion systems, i.e., the diffuser, the combustion chamber, the inner and outer casing, the spark plugs and the fuel injectors whereas the combustion chamber refers only to the exact place where combustion takes place [69].

The main purpose of a gas turbine combustor is to introduce heat energy into the mass of air previously compressed (in the compressor), by burning fuel in it so that the combustion products can be expanded to get useful work output (absorbed by the turbines) and then, on their discharge to atmosphere, provide a propulsive jet [62, 68]. Due to space limitations and requirements of energy and momentum, the volume flow rate and the heat release rate are very high in a gas turbine combustion chamber and the fuel residence time is very small, of the order of a few milli-seconds [62]. In gas turbines, the combustion is a continuous process that takes place at high pressure in a smaller space and usually at a very high temperature [68]. Thus, continuously high combustion temperatures, large continuous flow, and high heat energy release make the design and development of a gas turbine combustor quite difficult [62].

2.3.2 Combustor Performance Requirements

A gas turbine combustor must satisfy a wide range of requirements whose relative importance varies among the engine type and application. According to [41, 62, 68], the main requirements of combustors may be listed as:

1. High combustion efficiency at different operating conditions: (a) altitude ranging from sea level to 11 km for civil transport, and higher for some military aircraft; and (b) Mach numbers ranging from zero during ground run to supersonic for military aircraft;
2. Reliable and smooth ignition both on the ground (especially at very low ambient temperature), or at high altitude; and relighting capability in the case of aircraft engine flameout;
3. Wide stability limits (i.e., the flame should stay alight over wide range of pressures and air to fuel ratios);
4. Minimum pressure losses;
5. An outlet temperature distribution (pattern form) that is tailored to maximize the life of the turbine blades and nozzle guide vanes;
6. Meet the pollutant emission regulations (low emissions of smoke, unburned fuel and gaseous pollutant species);
7. Freedom from pressure pulsations and other manifestations of combustion-induced instabilities;
8. The length and frontal area should remain within the limits set by other engine components, i.e., the size and shape must be compatible with the engine envelope;
9. Design for minimum cost and ease of maintenance;
10. High durability;
11. The formation of carbon deposits (coking) must be avoided, particularly the hard brittle variety, since small particles carried into the turbine in the high-velocity gas stream can erode the blades. Furthermore, aerodynamically excited vibration in the combustion chamber might cause sizeable pieces of carbon to break free, resulting in even worse damage to the turbine.

It must be noted that many of the above requirements are mutually incompatible. For example, a high degree of turbulence necessary for good combustion efficiency results in higher pressure losses and it is also very easy to get a good combustion efficiency and uniform outlet temperature distribution if there is no limit on the length of the combustion chamber [62].

For the aircraft gas turbine combustors, among all of the listed requirements, the priorities are the low fuel consumption, low pollutant emissions, reliability, maintenance costs, engine size and weight [41].

2.3.3 Combustor design fundamentals

2.3.3.1 <u>“Conventional” combustor design</u>

Considering the present work, for a better comprehension of the reader, it is of interest to briefly analyze the considerations that dictate the basic geometry design of the “conventional” gas turbine combustors.

Firstly, the design of a combustor is a process where aerodynamics, chemical kinetics, and mechanical design are linked together [68]. The interweaving of these processes and the hardware geometry is reflected in the empirical nature of much of the design process. However, although the individual processes are well known, their combination into a working combustion system owes much more to experimentation and experience than to mathematical modelling. Recent developments in computational fluid dynamics (CFD) have helped reducing this experimentation [68].

The Figure 2.6 shows the logical evolution of the combustor design, starting with the simplest design, in Figure 2.6 a), and then introducing the modifications that have to be made until obtain the current “conventional” gas turbine combustor design, in Figure 2.6 d), in order to meet the considerations presented in the following.

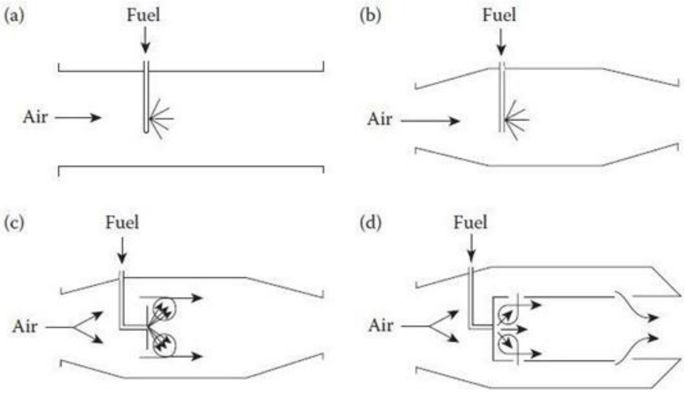

Figure 2.6: Stages in the evolution of the conventional aircraft engine combustors: a) straight walled duct, b) addiction of the diffuser, c) presence of plain baffle, d) basic “conventional” combustor [41].

Before starting with the analysis of Figure 2.6, it is necessary to refer two previous considerations. First, for good combustion efficiency the fuel must be thoroughly mixed with the air and if a liquid fuel is used, it must also be well atomised into small droplets. Second, the inlet temperature and the turbulence required for mixing should be sufficient to reduce ignition delay so that, while passing through the combustion chamber with a moderately low velocity, the fuel-air mixture has enough time for complete burning and uniform the temperature distribution before reaching the exit [62].

The Figure 2.6 a) shows the simplest possible form of combustor, i.e., a straight walled duct connecting the compressor to the turbine. This simple arrangement is impractical since the pressure loss incurred would be excessive [41]. The fundamental pressure loss because of combustion is proportional to the square of the air velocity and, for compressor outlet velocities of the order of 170 m/s, this loss could amount to almost one-third of the pressure rise achieved in the compressor [41]. Thus, to reduce this pressure loss to an acceptable level, a diffuser has to be used to lower the air velocity by a factor of about 5, as shown in Figure 2.6 b) [41].

Having fitted a diffuser, a flow reversal must then be created to provide a low-velocity region with the objective of anchor the flame. Figure 2.6 c) shows how this may be accomplished with a plain baffle [41]. The only remaining defect in this arrangement is that to produce the desired temperature rise, the overall air to fuel ratio in the chamber must normally be between 30 and 40, which is well outside the flammability limits for hydrocarbon–air mixtures. Ideally, the air to fuel ratio in the primary zone should be around 18 (for common fuels), although higher values (around 24) are sometimes preferred if low emissions of nitric oxides are a prime consideration [41]. To deal with this problem, combustion is sustained by a recirculatory flow of burned products that provide a continuous source of ignition for the incoming fuel-air mixture (this will be explained in section 2.3.4.1). The air not required for combustion is admitted downstream of the combustion zone, thereby reducing the temperature of the combustion products to an acceptable value to the turbine entry [41].

Figure 2.6 thus illustrates the logical development of the “conventional” gas turbine combustor in its most widely used form. As would be expected, there are many variations of the basic pattern shown in Figure 2.6 d), but, in general, all combustors incorporate an air casing, diffuser, combustion chamber (or liner), and fuel injector as key components [68].

2.3.3.2 Combustor design concepts for higher efficiency and lower pollutant emissions

The past decades have witnessed rapid changes both in the regulations for controlling gas turbine emissions and in the technologies used to meet these regulations. During this period and as mentioned in the chapter 1, the consumption of fuel by civil aviation has increased to the extent that air transport is today perceived as one of the world’s fastest growing energy-use sectors [41]. The continuing need to conserve fuel resources can only be met by raising the engine cycle efficiency. In practice, this traditionally calls for an increase in engine pressure ratio. This is an approach that usually reduces CO_2 emissions, but results in higher combustion temperatures and, thus, higher levels of NOx. So, the desire to burn less fuel, thereby generating less CO_2, is in direct conflict with the equally important need to reduce NOx emissions. According to Lefebvre and Ballal [41], for the foreseeable future, it seems likely that engine pressure ratios will rise to a maximum value of around 60 and yet designers of future combustors will be called on to reduce NOx emissions by another 50%, and virtually eliminate soot emissions and combustion instability.

Today, it might reasonably be argued that conventional combustors no longer pose any real technical challenge. Moreover, most of the knowledge of the key factors governing pollutant formation in continuous flow combustion systems, which is now being applied to the design and development of low-NOx combustors, was acquired from experience gained with that type of combustors [41]. According to Lefebvre and Ballal [41], the main factors controlling emissions from conventional combustors may be considered in terms of:

- Primary zone temperature and equivalence ratio;
- Degree of homogeneity of the primary zone combustion process;
- Residence time in the primary zone;
- Liner-wall quenching characteristics;
- Fuel spray characteristics (with liquid fuels).

Generally, low NOx levels can be readily achieved by eliminating zones of high temperature (hot spots) from the combustor. However, the challenge is broadly to keep flame temperatures down at high-power conditions without incurring unacceptable penalties on combustion performance when operating at low-power conditions. With this purpose, several solutions have already been presented. Some of them consist in ways to reduce the pollutant emissions in the conventional combustor designs through the application of variable geometries (mainly in the primary zone) or staged combustion techniques. The other ways consist in the utilization of new variants of the design with new operating modes of the combustor. The most promising concept designs known today are the Dry Low-Oxides of Nitrogen (DLN) or Dry Low-Emissions (DLE) (both already in service), or the Rich-Burn Quick-Quench Lean-Burn (known as RQL), Catalytic Combustion, Lean Premix Prevaporized Combustion (LPP) and Lean direct injection (LDI). All of these concepts shown good results in reducing the NOx emissions and a good overview about these conceptual designs was presented by Lefebvre and Ballal [41] and Reid Smith et al. [24].

Following Lefebvre and Ballal [41], for the immediate future, the development of various forms of staged combustion appears to be most promising, despite the attendant penalties for the engine in terms of more complex fuel scheduling and control strategy. Looking further ahead, these authors pointed that lean-premixed combustion appears to be the best technology available for achieving sub-10 ppmv NOx emissions in industrial combustors, but the problems of spontaneous ignition and flashback need to be fully addressed before lean-premixed combustion can be applied with confidence to aircraft engines. Problems of acoustic resonance may also be of great importance to the future development of lean-premixed combustors. Exactly for all these problems, Reid Smith et al. [24] concluded in their study, comparing numerous of combustion chamber concept designs applied in high pressure ratio aircraft gas turbine engines, that lean direct injection (LDI) in the form of lean multisource combustion is the better approach to be pursued.

2.3.3.3 Combustor Types

The choice of a particular combustor type and design is largely determined by the overall engine design and by the need to use the available space as effectively as possible [68]. In the present aeronautical engines, combustors may be classified as either subsonic or supersonic, depending on the velocity of combustion. Moreover, subsonic combustors may be subdivided into axial flow, reverse flow, and cyclone types. The last type is little used in the current gas turbine engines. Axial flow combustors may still be subdivided into three main types: can (or tubular), tubo-annular, and annular [68]. These three combustor types are illustrated in Figure 2.7.

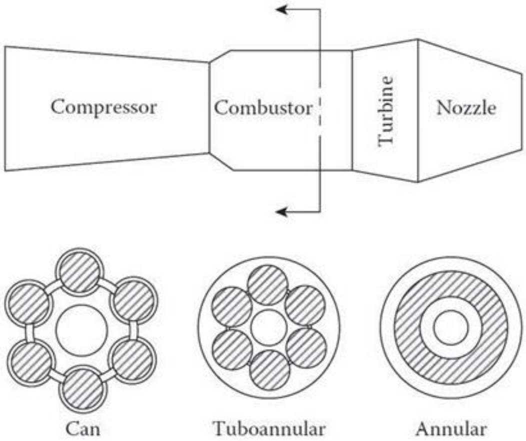

Figure 2.7: Illustration of the three main combustor types: Can; Tubo-annular; Annular [41].

Since the CFM56-3 has an annular combustor, only this type of combustor will be described here. A good overview about the other combustor types is made in the references [41, 62, 68].

2.3.3.4 Annular combustor design

The annular combustor configuration is used by most modern jet engines because of its lighter design. This type of combustor represents the ideal configuration for combustors, since its "clean" aerodynamic layout results in compact dimensions (and consequently in a small diameter engine). This configuration consists of an annular combustion chamber (or liner) that is mounted concentrically inside an annular casing [68]. This set is shown in Figure 2.8, where the annular casing and annular liner of the CFM56-3 are illustrated.

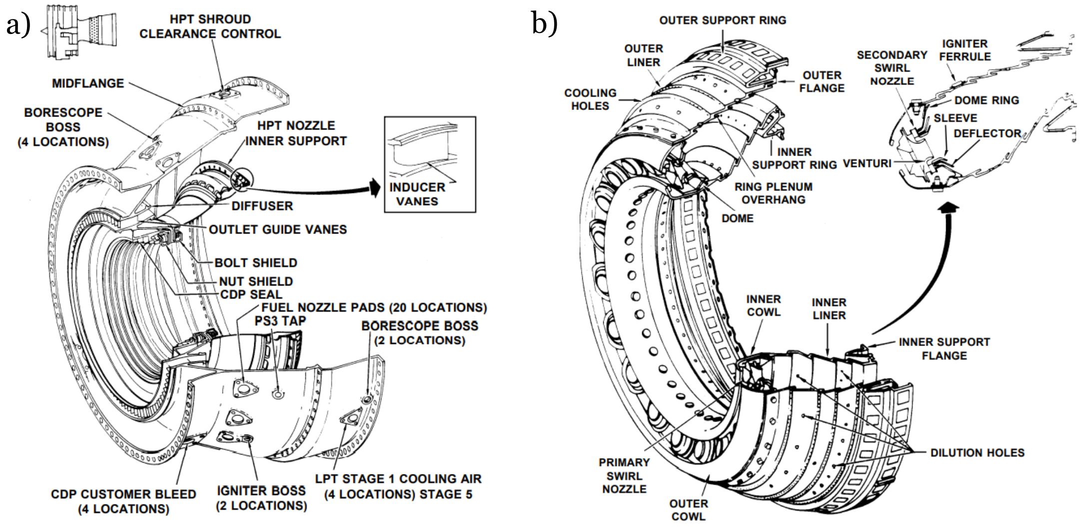

Figure 2.8: Arrangement of CFM56-3 combustor: a) annular combustion case; b) annular combustion chamber (or liner) [66].

As shows Figure 2.9, where a cut-view of the CFM56-3 annular combustor arrangement is illustrated, usually, enough space is left between the liner walls and the combustion chamber housing to allow the flow of the remaining air from the compressor for cooling purposes [68].

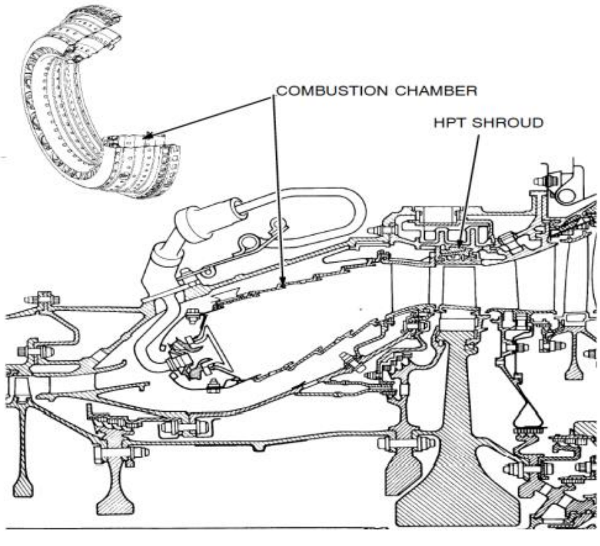

Figure 2.9: Cut-view of the CFM56-3 combustor [65].

When comparing with the other types, among the advantages, annular combustion chambers have a lower pressure drop due to larger volume per unit of surface area and are more efficient than can-type chambers. They also require about half of the diameter of can-type chambers for the same mass flow [62].

Their main drawback stems from the heavy buckling load on the outer liner [41]. Moreover, any change in the flow velocity profile can result in a significant change in the temperature distribution of the outlet gases, and distortion of inner annular chamber is critical because it can disrupt the flow of cooling air and also changes the temperature distribution of the outlet. This is because of the lower degree of curvature of the chamber surfaces [62]. Another drawback is related to the experimental tests of this type of combustion chamber. At full-power conditions, the tests of large annular combustion chambers supplying air at the levels of temperature, pressure and flow rate required are extremely difficult and expensive [41]. Moreover, there are very few facilities in the world that can provide air at these conditions [70].

2.3.4 Description of Combustion Chamber

As mentioned before, the combustor of an aero gas turbine engine includes all the combustion systems. However, in this subsection, the focus will be made on the combustion chamber, since in the combustion process the main objective is that the flame zone be limited to this component.

In brief, the combustion chamber of a "conventional" combustor can be subdivided in several zones, as shows Figure 2.10, being each one of them responsible for a set of functions and characterized by the phenomena that occurs there.

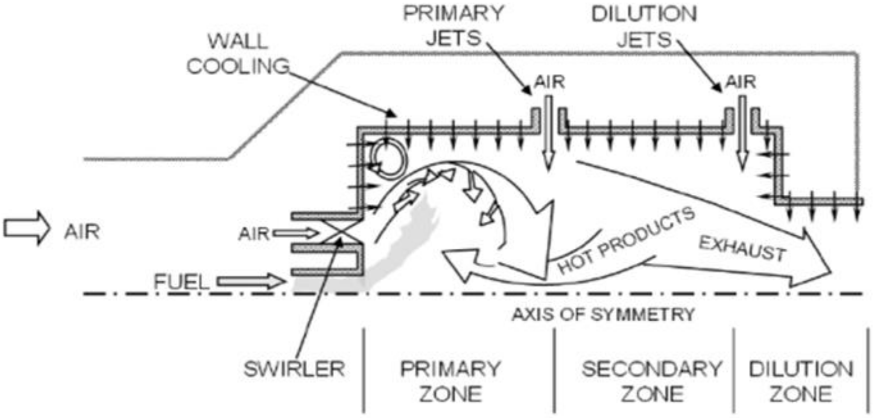

Figure 2.10: Description of the interior of a conventional combustor [72].

Looking at Figure 2.10, it is possible to conclude that the principal zones of a combustion chamber are the primary zone, secondary (or intermediate) zone and dilution zone. All of these zones will be described next.

It should be noted that the type of wall cooling used is of the greatest importance for the durability of the combustion chamber. For this reason, this phenomenon will also be analyzed in the end of this subsection.

2.3.4.1 Primary zone

The primary zone consists in the section of the combustion chamber that is closer to the swirler and its main functions are to anchor the flame and provide sufficient time (residence time), temperature, and turbulence to allow almost complete combustion of the incoming fuel–air mixture. The primary zone airflow pattern is of major importance to the attainment of these objectives. Many different types of flow patterns can be employed, but one feature that is common to all is the creation of a toroidal flow reversal that entrains and recirculates a portion of the hot combustion gases to provide continuous ignition to the incoming air and fuel [41].

In the primary zone, the air that comes from the compressor is injected through two injection points. These are the swirler and the primary air jets, which together have the function of control the structure of the flow as well as the mixing within the primary zone, as shows Figure 2.11.

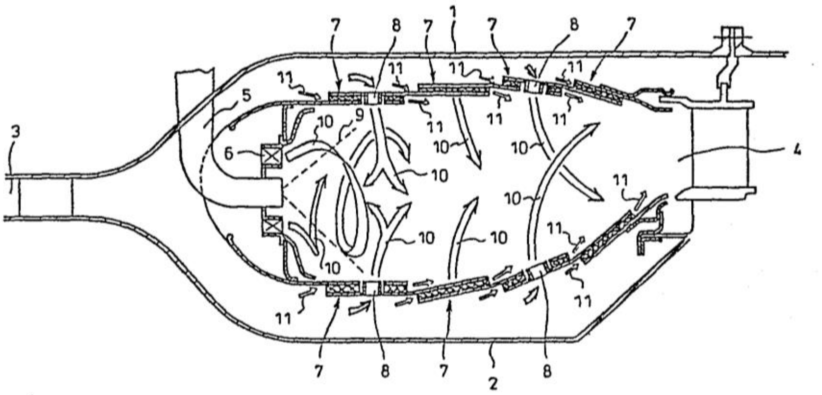

Figure 2.11: Combustion chamber with swirl vanes [129].

It is important to note that both, swirling air and primary air jets, are used to produce the desired flow reversal (or recirculation zone). Each one of these modes of air injection is capable of achieving flow recirculation on its own. However, if both are used, and if a proper swirl vane angle (for the swirlers) and the correct size, number, and axial location for the primary air holes are chosen, then, the two separate flow recirculation zones created by the two separate modes of air injection will merge and blend in such a manner that each one complements and strengthens the other. The result is a strong and stable primary zone airflow pattern that can provide wide stability limits, good ignition performance, and freedom from the type of flow instabilities that often give rise to combustion pulsations and noise [41]. In the following, a brief description of these two injection structures will be made.

2.3.4.2 *Swirler*

The swirl vanes, represented as an "X" in Figure 2.11, are located at the beginning of the combustion chamber, typically surrounding the fuel injection points, and are the first entry point for the air that comes from the compressor. These swirl vanes induce a circumferential velocity component to the air, which in turn creates a pressure void in the centre line and induces a backflow to fill the centre line pressure deficit. This creates a toroidal reversal flow that entrains and recirculates a portion of the hot combustion gases to provide continuous ignition to the incoming air-fuel mixture. The downstream extent of this recirculation zone defines the limit of the primary zone. The intended effect created by the swirl vanes is represented in Figure 2.12.

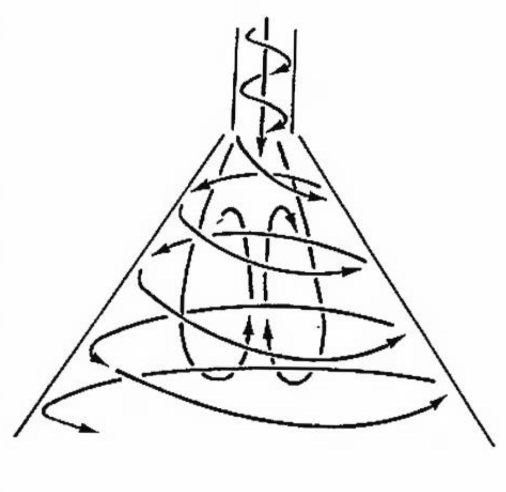

Figure 2.12: Recirculation induced by a strong swirl [71].

The efficiency of the recirculation zone, depends of the strength of the swirl, which is represented by Equation (2.1).

$$S_N = \frac{2G_m}{D_{sw}G_t} \tag{2.1}$$

Where, G_m is the axial flux of angular momentum, D_{sw} is outer swirler diameter and G_t is the axial thrust.

To induce a recirculation effect as shown in Figure 2.12, the swirl number (S_N) must exceed 0.6 (condition for strong swirl). For values of swirl number less than around 0.4, no flow recirculation is obtained, and the swirl is described as weak [41].

2.3.4.3 Primary air jets

In a “conventional” combustor, two sets of wall air jets are used in the end of primary and secondary zones, as shown in Figure 2.11 (structure numbered with 8). The air jets for the primary zone have two functions: the first is to force the toroidal flow staying within the limits of the primary zone, by providing a strong force against which this flow cannot easily penetrate; secondly, the primary air jets bifurcate with a substantial percentage of the flow directed upstream, in order to mix with the toroidal flow that contains the fuel-air mixture. The remaining air mixes downstream in the secondary zone to lower the temperature inside the chamber [69].

Throughout the primary zone, the fluid mixing and the chemical kinetics occurs in parallel with a range of scales [69]. In the recirculation zone (within the macro scale), a range of turbulent eddy scales exists and persists during a finite life time, before breaking up and mixing with adjacent eddies, forming a new eddy. Some of these eddies contain unreacted fuel and air that will ignite, however, others will not. These eddies will have to wait to mix with other eddies in order to acquire sufficient energetic species with the necessary mixture ratio required for ignition.

2.3.4.4 Secondary Zone

In the secondary zone, also known as intermediate zone, air is introduced gradually dropping the temperature to an intermediate level to encourage the complete combustion [62]. In the case of hydrocarbons, this means the burnout of soot, oxidation of the CO (both a pollutant and a source of combustion inefficiency) to CO_2, the combustion of any unburned hydrocarbons and the reduction of dissociation losses by allowing recombination of dissociated species remaining from the primary zone to proceed to completion before the flow reaches the dilution zone.

For these processes take place efficiently, besides the addiction of air, it is necessary to ensure that in the secondary zone exists an overall lean mixture ratio (provided by the primary air jets) and sufficient residence time is provided to promote the chemical reactions [60]. Ideally, the length of the secondary zone is dictated partly by the minimum length needed to mix the intermediate air with the gas flow and by the minimum residence time needed to complete combustion. The typical length is usually around a half of the total length of the combustion chamber [60].

2.3.4.5 Dilution Zone

The dilution zone is located at the end of the combustion chamber, as shown in Figure 2.10. The main functions of this zone consist in:

- Admit, to the combustion chamber, the air remaining from the compressor that was not used neither in the combustion process (in primary and secondary zones) nor to fulfil wall-cooling requirements;
- Provide an outlet stream with an acceptable temperature distribution to the turbine entry.

The amount of air available for dilution is usually between 20 and 40% of the total combustor airflow. This air is introduced into the hot gas stream through one or more rows of holes existing in the liner walls. The size and shape of these holes are selected to optimize the penetration of the air jets and the subsequent mixing of this air with the main stream [41].

The outlet temperature distribution is usually described in terms of “temperature traverse quality” (TTQ), which in turn is characterized by various indices, including the "Pattern Factor", the "Profile Factor" and the "Turbine Profile Factor". In theory, any given traverse quality can be achieved either using a long dilution zone or by tolerating a high liner pressure-loss factor. However, in practice, it is found that mixedness initially improves greatly with an increase in mixing length and thereafter at a progressively slower rate. This is why the length/diameter ratios of dilution zones all tend to lie in a narrow range between 1.5 and 1.8 [41].

Thus, the TTQ is one of the most important, and at the same time, most difficult problems in the design and development of gas turbine combustion chambers, because it is difficult to achieve satisfactory and consistent distributions of temperature from the hot gases that enter to the turbine. Moreover, generally, the actual exit temperature profile of a combustion chamber can deviate from the design profile, as shows Figure 2.13.

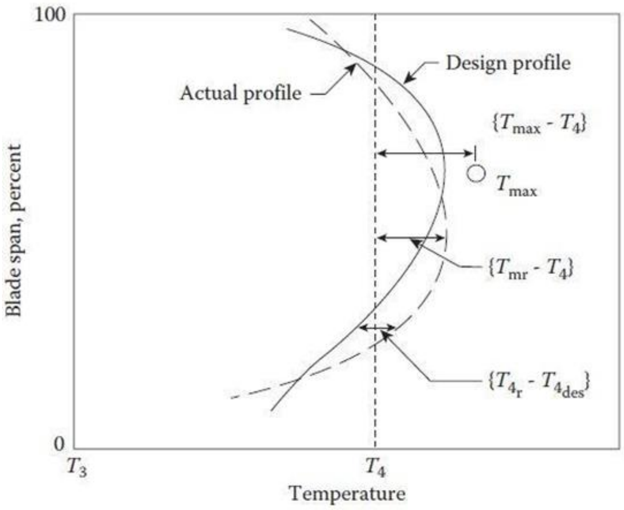

Figure 2.13: Explanation of terms in exit-temperature profile parameters [41].

The overall temperature distribution factor or "pattern factor" is the parameter of most relevance to the design of nozzle guide vanes, which highlights the maximum temperature. Based on the Figure 2.13, this parameter is defined by Equation (2.2).

$$Pattern\ Factor = \frac{T_{max} - T_4}{T_4 - T_3} \tag{2.2}$$

Where T_{max} is the maximum recorded temperature, T_3 is the inlet air temperature, and T_4 is the mean exit temperature.

The temperatures of most significance to the turbine blades are those that constitute the average radial profile. They are obtained by adding together the temperature measurements around each radius of the liner and then dividing by the number of locations at each radius. A typical radial temperature profile is shown in Figure 2.13. The expression used to describe the radial temperature distribution factor, also known as "profile factor", is:

$$Profile\ Factor = \frac{T_{mr} - T_4}{T_4 - T_3} \tag{2.3}$$

Where T_{mr} is the maximum circumferential mean temperature.

The pattern factor and profile factor are best suited for situations where a perfectly uniform exit temperature distribution would be considered ideal [41]. However, in modern high-performance engines, which employ high turbine entry temperatures and extensive air cooling of both nozzle guide vanes and turbine blades, the desired average radial distribution of temperature at the combustor exit plane is far from flat; instead, it usually has a profile that peaks above the midheight of the blade, as shown in the Figure 2.13. A parameter that takes the design profile into account is the "turbine profile factor", which is defined as shows Equation (2.4). The objective of this one is to provide lower temperatures at the turbine blade root, where mechanical stresses are highest, and at the tip of the blade (to protect seal materials), which is the most difficult to cool [41].

$$Turbine\ Profile\ Factor = \frac{\left(T_{4,r} - T_{4,des}\right)_{max}}{T_4 - T_3} \tag{2.4}$$

Where $\left(T_{4,r} - T_{4,des}\right)_{max}$ is the maximum temperature difference between the average temperature at any given radius around the circumference and the design temperature for that same radius.

2.3.4.6 *Wall Cooling*

To design a reliable combustion chamber, two of the major requirements are that the liner walls must have sufficient thermal resistance to withstand the continuous and cyclic high-temperature operation, and be also structurally strong to withstand the buckling load created by the pressure differential across the chamber walls. This is accomplished through the use of high-temperature, oxidant-resistant materials combined with the effective use of a constant supply of air in the form of film-cooling to maintain the liner surfaces adequately cooled.

In practice, the temperature of the liner walls is determined by the balance between the heat they receive via radiation and convection from the hot gas, and the heat transferred from them by convection to the annulus air (air present outside the chamber walls) and by radiation to the air casing [41].

On many combustors now in service, up to 20% of the total air mass flow of the combustor is employed in liner-wall cooling. This quantity should be the minimum possible, since the greater the amount of air required for cooling effect, the lesser the amount of air remaining for the emission control.

There are several wall protection techniques that can be used; however, in this subsection, the focus will be made only on the techniques applied in the CFM56-3 combustor, which, according to CFM [66, 116], are:

- Slots of machined rings;
- Thermal barrier coating (TBC).

Starting the analysis following the previous order, the "machined ring" approach basically consists in rows of holes that are accurately drilled in the combustion chamber's walls to allow the annulus air to enter the cooling slots by either total pressure feed, or static pressure differential, or a combination of both, as illustrated in Figure 2.14 [41].

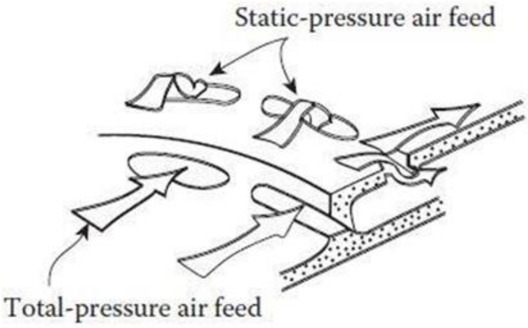

Figure 2.14: Machined rings: schematic illustration and working principle [41].

Thus, the air enters to the chamber axially or perpendicularly (depending on the type of pressure feed) and flows along the inner surface of the wall panels to provide a protective film of cooling air between the wall and the hot combustion gases [41].

In this case, the aft end of the previous wall panel, also known as lip or skirt, provides a plenum in which turbulence is dissipated and allows that the individual cooling air jets, which have passed through the holes, coalesce to form a single annular sheet of air. At the downstream end of each lip, the gaps between these structures and the liner walls are dimensioned to provide the required cooling air velocity for maximum cooling effectiveness, regardless the actual pressure along the combustion chamber. However, this cooling film is gradually destroyed by turbulent mixing with the hot gas stream. For this reason, the inner surface of the walls is coolest near each cooling slot and its temperature increases in a downstream direction until the next cooling slot. At the downstream end of the liner, the flow acceleration in the nozzle tends to suppress the hot stream turbulence and the cooling film can persist for greater distances [41].

It should be noted that, when using this technique, the total flow area of the cooling holes is calculated to meter the required amount of cooling air. In the case of the CFM56-3 combustor, it presents one slot of machined rings in each panel of the combustion chamber's walls. This can be seen in the Figure 2.15.

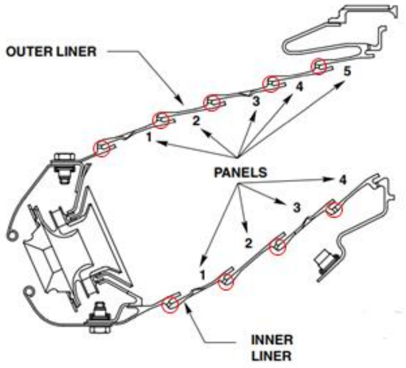

Figure 2.15: Position of the slots of machined rings in the CFM56-3 combustion chamber, adapted from [116].

Overall, the machined ring approach combines good mechanical strength with accurate airflow metering, which is particularly important for large annular combustors. Beyond that, the dimensional accuracy is also higher than other film-cooling devices, which reduces the variations in cooling airflow rate [41].

As referred before, the other type of protection that is also implemented in the CFM56-3 is the thermal barrier coating (TBC), which is applied to both the inner and outer walls of the combustion chamber [66]. This technique consists in spraying a protective coating (generally a ceramic coating) on the inner surface of the walls to increase the cooling efficiency, allowing to reduce the wall temperatures by up to 150K.

2.4 CFM56-3 Engine

2.4.1 Overview

The CFM56 engine series were developed and manufactured by CFM International SA. The project started in the 70's and the several produced versions were certified during the 70's and 80's [64]. The CFM56-3 is a derivative of the CFM56 family, whose engines can produce a thrust range from 18,500 to 34,000 pounds-force. The CFM56-3 series produces 20,000 to 23,500 pounds-force depending on whether it is mounted on the 737-300 or 737-400, respectively. The initial design of this engine first ran in 1974 and first flew in 1977 on the McDonnell Douglas YC-15 as a candidate in the United States Air Force's Advanced Medium STOL Transport competition [65]. The CFM56 won the competition and became the new engine for the KC-135 tanker fleet as well as the primary engine for the Boeing 737 and DC-8. Since then, the CFM56 has been extensively upgraded and it is now the most used high-bypass turbofan engine with over 800 million flight hours. Currently, the CFM56-3 is used by the Airbus A320, A340, the Boeing 737, and KC-135R Stratotanker [65].

2.4.2 General Specifications

The CFM56-3, illustrated in Figure 2.16, is a high-bypass, dual rotor (or dual-shaft), axial flow turbofan engine and this variant of CFM56-3 has a bypass ratio of 5.1:1 and a dry weight of 1966kg [64], [67]. Its dual-shaft design consists of a low-pressure compressor (fan and booster), high-pressure compressor, annular combustion chamber, and a high- and low-pressure turbine section. The two shafts connect the low- and high-pressure sections respectively using a five-bearing system (3 roller, and 2 ball bearings) [65].

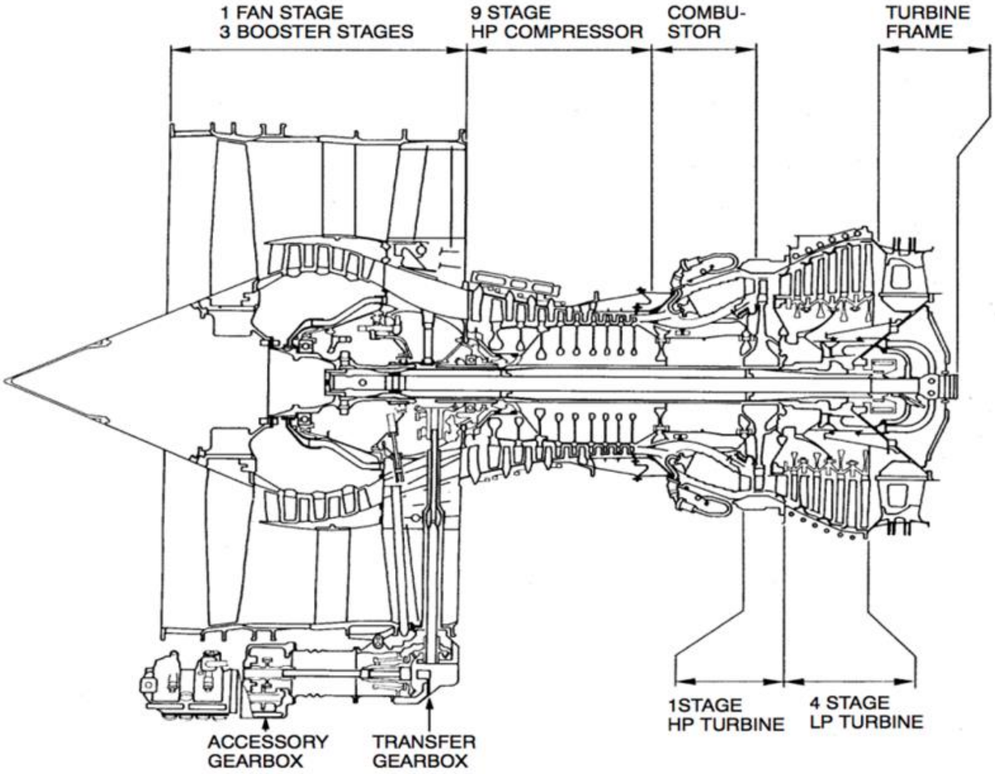

Figure 2.16: CFM56 schematic overview of engine components [65].

As it is possible to observe in Figure 2.16, the CFM56-3 is an engine that features [66]:

- A four-stage integrated fan and Low-Pressure Compressor (LPC) booster driven by a four stage Low-Pressure Turbine (LPT);
- A nine stage High-Pressure Compressor (HPC) driven by a single stage of High-Pressure Turbine (HPT);
- Compressor airflow controlled by Variable Bleed Valves (VBV) located at the booster and Variable Stator Vanes (VSV) within the HPC front stages;
- An annular combustion chamber increasing the HPC delivery air velocity to drive both turbines;
- An accessory drive system (consisting of three gearboxes) extracting energy from the high-pressure rotor to drive the engine mounted accessories;
- A pylon mounter thrust reverser that provides the capability of reducing aircraft speed on the ground.

It is worth noting that the high-pressure turbine (HPT) spins at 15,000 revolutions per minute (rpm) at 100% power and the low-pressure turbine maintains 5200 rpm at 100% power [65].

A more detailed description of the specifications of the engine and constitution of its several parts are summarized in Appendix A.

2.5 Combustion Fundamentals

Combustion can be described, in a simplified way, as an exothermic reaction of a fuel and an oxidant. However, this process is extremely complex as it depends on many factors. For example, this process can occur in many forms (or regimes), not all of which accompanied by flame or luminescence [41].

Thus, due to the difficulty in cover all that information and for a better understanding of the reader, in this section, the focus will be made in the combustion processes and parameters that are typically associated to the gas turbine engines.

2.5.1 Combustion Flames

In gas turbine combustors, all the flame processes occur in the regime of deflagration, which is characterized by the presence of a flame that propagates through the unburned mixture. In this context, a flame may be defined as a rapid chemical change occurring in a very thin fluid layer, involving steep gradients of temperature and species concentrations, accompanied by luminescence [41].

Although a flame can propagate through a static gas mixture, in a gas turbine combustion chamber it is usual to stabilize the flame at a fixed point and supply it with a continuous flow of combustible mixture. Under these conditions, flames can be classified in premixed flames, if the fuel and air are mixed before combustion, or diffusion flames, if the fuel and air are mixed by diffusion (turbulent and molecular) in the flame zone [41]. Depending on the prevailing flow velocities, both types of flame can still be classified as laminar or turbulent [41].

Regarding the combustible mixture, in gas turbine applications, the oxidant is always air, but the fuel may be gaseous or liquid [41]. Thus, if both the reactants are in the same physical state, the combustion process is described as homogeneous [41]. However, in the systems burning liquid fuels, if the fuel is not completely vaporized before entering the flame zone, heterogeneous spray combustion may take place, raising the production of pollutant emissions [41, 71].

In the study presented in this work, the combustion system is characterized by the diffusion flame type. For this type of flames, the rate of mixing between the fuel and the oxidant often limits the overall rate of combustion.

2.5.2 Laminar Flame Speed and Weaver Flame Speed

The speed of combustion of a gaseous fuel is largely determined by the flame velocity (or flame speed), which is defined as the velocity of the unburned gases through the combustion wave in the normal direction to the wave surface.

The flame speed has been reported to be influenced by many physical and chemical variables. Thermal diffusivity, specific heat, initial temperature, pressure, additives, fuel molecular structure, and so on have all been found to have varied effects on flame speeds. It was also reported that flame speed varies as the square of the absolute temperature and inversely as the fourth root of the pressure [76]. Usually, the mixture with the maximum flame temperature is also the mixture with the maximum flame speed [76].

The ratio between the laminar flame speeds of the gas of interest and hydrogen is called the weaver flame speed factor. This is used to define the propensity of the gas to react and it is greatly influenced by the amount of hydrogen in the mixture. [40]. Hydrogen has a weaver flame speed factor of 100 [40]. The lower the number, the lower is the flame speed. Inert gases, such as nitrogen, carbon dioxide and carbon monoxide reduce the flame speed and also the Wobbe number (this parameter will be explained later). Hydrogen does the reverse, by increasing both the flame speed and the Wobbe number. Hydrocarbons reduce the flame speed but increase the Wobbe number [40, 76].

2.5.3 Flammability limits

The ignition of a fuel (usually by a discrete ignition source) and the flame propagation require that the fuel vapour and the oxidant (normally air) produce a mixture whose composition falls within specific limits, known as flammability limits. These limits can be expressed as fuel to air ratios, equivalence ratios, vapour concentrations, or the temperatures at which these vapour concentrations are produced for a particular fuel [71].

In this work, the flammability limits will be presented and used as the limits for the concentration of fuel vapour in air that are flammable, expressed as percentage of fuel by volume. According to Mellor [71], these limits can be defined as:

- Lower (or lean, or weak) flammability (or explosive) limit: the minimum concentration of fuel vapor (or gas) in air that allows combustion, i.e., the point above which the mixture just becomes flammable and below which the mixture is too lean to support the combustion reaction.

- Upper (or rich) flammability (or explosive) limit: the maximum concentration of fuel vapor (or gas) in air that allows combustion and above which the mixture is too rich to support the combustion reaction.

These limits also correspond, in the case of the lower limit, to the critical flame speed (or critical pressure) below (or above, in the case of the upper limit) which flame propagation is not possible [40, 76].

The range of flammability limits can be influenced by some factors. For instance, an increase in pressure above atmospheric usually widens the range of limits for gases and vapours [41]. Moreover, the range of limits can be widened by an increase in temperature due to higher flame speeds and therefore the propagation of the flame through even more difficult compositions. However, this effect is usually less important than that of pressure [41, 76]. In the practically important range of pressures, from 10 kPa to 5 MPa, the weak flammability limit is not strongly pressure dependent [41].

2.5.4 Mixture Ratios

The mixture ratio represents the ratio in which the fuel and air are present in a system. In premixed combustion systems, there is only one mixture ratio throughout the entire combustion process. However, in the present non-premixed combustion case, there are an infinite range of ratios, which spread from pure air to pure fuel.

The mixture ratio can be defined through the FAR (or AFR), the equivalence ratio, or the mixture fraction. All of these parameters are important for a combustion system as they affect the combustor's performance, life span, efficiency and pollution characteristics. So, these parameters will be explained in the following.

The fuel to air ratio, represented as FAR (the inverse of the AFR), is commonly used in the gas turbine industry and refers to the ratio between the fuel mass flow rate, $\dot{m}_f$, and the air mass flow rate, $\dot{m}_a$, at any given moment. The fuel to air ratio can be expressed through Equation (2.5).

$$FAR = \frac{\dot{m}_f}{\dot{m}_a} = \frac{1}{AFR} \tag{2.5}$$

The equivalence ratio (ϕ) is widely used to indicate the ratio of the actual fuel to air ratio relative to the corresponding stoichiometric value. Through this parameter is possible to determine if the mixture is rich (have more fuel) or lean (have less fuel) and is represented by Equation (2.6).

$$\phi = \frac{FAR_{actual}}{FAR_{stoich}} = \frac{\left(\frac{\dot{m}_f}{\dot{m}_a}\right)_{actual}}{\left(\frac{\dot{m}_f}{\dot{m}_a}\right)_{stoich}} \tag{2.6}$$

Regardless of the fuel, a value of ϕ < 1 indicates a fuel-lean mixture; ϕ=1, a stoichiometric mixture and ϕ>1 a fuel-rich mixture [68, 71].

In some fields of application, it is the corresponding air to fuel ratio that is used and the symbol λ corresponds to the excess air coefficient. On this basis, ϕ is the inverse of λ [76].

The mixture fraction (ξ) is a very useful variable in combustion modelling, in particular for diffusion flames. In a two-feed system, where a fuel stream with mass flux $\dot{m}_f$ is mixed with an oxidizer stream with mass flux $\dot{m}_a$, the mixture fraction represents the mass fraction of the fuel stream in the mixture [75]. This parameter is represented by Equation (2.7):

$$\xi = \frac{\dot{m}_f}{\dot{m}_f + \dot{m}_a} = \frac{\frac{\dot{m}_f}{\dot{m}_f}}{\frac{\dot{m}_f}{\dot{m}_f} + \frac{\dot{m}_a}{\dot{m}_f}} = \frac{1}{1 + AFR} \tag{2.7}$$

As it is possible to verify with Equation (2.7), in the air stream (when the AFR → ∞), ξ=0, and in the fuel stream (when AFR = 0), ξ=1.

The parameters with more interest for this work will be the overall AFR and the AFR in the primary zone.

2.5.5 Combustion Stoichiometry

Physically, a stoichiometric reaction can be considered as a unique reaction in which the oxidizer is exactly the amount required to completely burn the quantity of fuel in the system. So, theoretically, it can be regarded as the most economic reaction [40].

Quite often, in the case of a hydrocarbon fuel, the stoichiometric reaction can be written in terms of 1 mole of hydrocarbon fuel in reaction with air, as shows Equation (2.8).

$$\mathrm{C}_x\mathrm{H}_y + n_{\mathrm{air}}\,(\mathrm{O}_2 + 3.762\mathrm{N}_2) \rightarrow x\mathrm{CO}_2 + \left(\frac{y}{2}\right)\mathrm{H}_2\mathrm{O} + 3.762 n_{\mathrm{air}}\,\mathrm{N}_2 \tag{2.8}$$

Where, $n_{air} = x + y/4$ and the constant 3.762 comes from the ratio of approximately 79% nitrogen to 21% oxygen by volume (or 77% nitrogen and 23% oxygen by mass) in the air [40], [41]. This means that for every mole of oxygen required for combustion, 3.762 mol of N_2 must also be introduced. The N_2 does not alter significantly the O_2 balance, however it has a major impact on thermodynamics, chemical kinetics, and formation of pollutants in combustion systems [77]. In this case, the small amounts of CO_2, argon and other traces of species present in the composition of the oxidizer (assuming it's air) can be disregarded.

For each fuel, the combustion reaction can be classified within two types, complete and incomplete reaction. The difference between these two types of combustion lies in the products of the reaction. In the complete combustion (of a hydrocarbon fuel) are released only completely oxidized products (such as CO_2 and H_2O), and energy while in the incomplete reaction are released completely oxidized products (CO_2 and H_2O), intermediate products (CO, unburned hydrocarbons, etc.), and energy.

Based on Equation (2.8), the stoichiometric air to fuel ratio can be determined through the Equation (2.9).

$$(AFR)_{\text{stoich}} = \left(\frac{m_{\text{air}}}{m_{\text{fuel}}}\right)_{\text{stoich}} = \frac{4.762 n_{\text{air}}}{1} \frac{M_{\text{air}}}{M_{\text{fuel}}} \tag{2.9}$$

In practice, however, there is no assurance that simply by providing the correct air to fuel ratio the combustion will be completed.

2.5.6 Enthalpy of formation, absolute enthalpy, and enthalpy of combustion

The enthalpy of formation (or heat of formation) of a substance, represented as $\Delta h_{f,i}^0$, is defined as the heat evolved when 1 mole of the substance is formed from its elements in the respective standard state [40]. The standard (or natural) state temperature and pressure are considered as T_{ref}=25°C (298.15K) and P_{ref}=P_o=1atm (101,325Pa), respectively, which are consistent with CHEMKIN and NASA thermodynamic databases [78]. For the elements that are in their natural state, the enthalpy of formation is conventionally adopted as zero and the values for the enthalpy of formation for other state than the reference are usually tabulated in the literature.

The sensible enthalpy change of a substance, represented as $\Delta h_{s,i}$, is defined as the heat evolved in the change between the standard state (T=298.15K, P=1atm) and the intended state (T, P).

The absolute enthalpy of a substance (reactant or a product of a reaction) can be found by adding the sensible enthalpy change ($\Delta h_{s,i}$) to the enthalpy of formation ($\Delta h_{f,i}^0$). The Equation (2.10) represents the absolute enthalpy for a substance i at a temperature T:

$$\bar{h}_i(T)[J/kmole] = \bar{h}_{f,i}^0(T_{ref}) + \Delta\bar{\mathrm{h}}_{\mathrm{s},i}(\mathrm{T}) \tag{2.10}$$

Where $\Delta\bar{h}_{s,i}(T) = \int_{T_{ref}}^{T} \bar{c}_{p,i}(T^*)dT^*$

The subscript *ref* represented in Equation (2.10) refers to the standard reference state. The subscript f indicates formation of the compound from elements, the index 0 refers to all products and reactants in their standard states and the subscript s indicates the term of the sensible enthalpy change.

Once expressed the absolute enthalpy for each substance, the absolute enthalpy for the reactants ($\mathrm{h}_{\mathrm{reac}}$) and products ($\mathrm{h}_{\mathrm{prod}}$) used in a reaction can be calculated by adding the absolute enthalpy values of all reactants and all products, respectively. Then, it is possible to define the enthalpy of reaction per mole of mixture, ΔH_R, or enthalpy of combustion, when it comes to combustion reactions.

The enthalpy of combustion consists in the heat released when a fuel (usually a hydrocarbon) reacts with an oxidant to yield the combustion products. This amount of heat can be calculated relating the absolute enthalpies of the reactants and products as given by Equation (2.11), or in terms of extensive properties, which is given by Equation (2.12).

$$\Delta H_R = h_{prod} - h_{reac} \tag{2.11}$$

$$\Delta H_R = H_{prod} - H_{reac} \tag{2.12}$$

2.5.7 Adiabatic Flame Temperature

Considering a combustion process that takes place adiabatically in a closed system with negligible changes in kinetic and potential energies, the temperature of the products is referred to as the adiabatic flame temperature, T_{ad}. This is the maximum temperature that can be achieved for the given reactants, since any heat transfer from the reacting substances and any incomplete combustion would tend to lower the temperature of the products.

The adiabatic flame temperature can be seen as a function of the temperature of the reactants and the equivalence ratio of the mixture, being possible to control this value with an excess amount of air or diluent. The maximum adiabatic flame temperature for a given fuel and oxidizer combination occurs always for a stoichiometric mixture [40].

In combustion studies, two types of adiabatic flame temperature can be used, depending on how the process is completed. These can be measured at constant volume or at constant pressure. However, in this work, only the combustion at constant pressure is relevant, as gas turbine combustors operate in this condition.

To determine the adiabatic flame temperature of a combustion reaction, it is necessary to consider the Equation (2.11) in which, if assuming an adiabatic process, the value of ΔH_R will be zero [40]. So, the adiabatic flame temperature can be calculated equating the absolute enthalpy of the products, $h_{prod}(T_{ad}, P_i)$, at adiabatic temperature ($T = T_{ad}$), to the absolute enthalpy of the reactants, $h_{reac}(T_i, P_i)$, at the temperature before be burnt ($T = T_i$), considering the same pressure ($P = P_i$) for both, as shows Equation (2.13).

$$h_{reac}(T_i, P_i) = h_{prod}(T_{ad}, P_i) \tag{2.13}$$

In practice, the temperature of the products resulting from the combustion is usually lower than the adiabatic flame temperature because of the heat losses induced by convection, conduction and radiation [41].

2.6 Combustion Chamber performance

A combustion chamber must be able to allow fuel to burn efficiently over a wide range of operating conditions without incurring neither in a large pressure loss, nor in any kind of penalty for the structural integrity of the engine components. So, to evaluate the combustion chamber performance, the following parameters/conditions can be used [68]:

- Pressure loss
- Combustion efficiency
- Combustion stability
- Combustion intensity

These parameters will be explained in detail next.

2.6.1 Pressure Loss (or drop)

To begin the analysis of this condition, it should be noted that for any flow process there is usually a pressure loss, greater or lesser, depending on the flow characteristics. However, since the occurrence of a pressure loss in a Joule-Brayton cycle means the reduction in the work output and cycle efficiency, the pressure loss in a combustor must be reduced to the minimum possible [80].

The sources of pressure loss (or drop) can be either cold or hot losses. Cold losses arise from sudden expansion, wall friction, turbulent dissipation and mixing. These losses can be measured by flowing air without fuel through all the slots, holes, orifices and so on. The hot losses (also known as fundamental losses) are due to temperature increase. Generally, the fundamental losses due to heat addition in an aero engine will be low compared with the losses due to friction and mixing [68].

Saravanamuttoo et al. [80] stated that, when the pressure loss is expressed non-dimensionally in terms of the dynamic head, it will not vary much over the range of the Reynolds numbers under which combustion system operates. Thus, the overall Pressure Loss Factor (PLF) can be expressed by Equation (2.14), in which the first member of the equation is used to calculate the cold losses and the second for the hot losses.

$$Pressure\ loss\ factor\ (PLF) = \frac{\Delta p_0}{\dot{m}^2/(2\rho_1 A_m^2)} = \overline{K_1} + \overline{K_2\left(\frac{T_{02}}{T_{01}} - 1\right)} \tag{2.14}$$

Where, $\dot{m}$ is the air mass flow rate, A_m is the maximum cross-sectional area of chamber, ρ_1 is the inlet density, K_1 and K_2 are determined by measurement of the performance of the combustion chamber on a test rig from a cold run and a hot run, respectively.

Table 1 represents the PLF in the various types of combustion chambers, representing the losses that arise from turbulence and friction that can be measured with accuracy from cold flow tests. For chambers of moderate temperature rise, the hot loss (resulting from burning conditions), ΔP_{hot}, usually lies between 0.5 and 1% of the inlet pressure [41]. Providing adequate turbulence and mixing is incurred a total pressure loss varying from about 3 to 8% of the air pressure at the entry of the chamber [60].

Table 1: Typical pressure loss factors in combustion chambers [41].

Type of chamber	PLF
Annular	20
Tubo-annular	28
Tubular	37

2.6.2 Combustion Efficiency

In a simplified way, the combustion efficiency can be seen as the capacity of the combustor to transfer the energy from the fuel, while burning it, to the gas stream. The objective is that the flow receives all the fuel energy. However, in practice, this will not occur for many reasons, one of them, for instance, is that some of the fuel may not find oxygen for combustion in the very short time available. Therefore, to ensure that the highest value for combustion efficiency is obtained from a combustor, the following conditions must be achieved [68]:

- The fuel should be completely vaporized and mixed with air before burning;
- Fuel and air must have adequate time and space to mix and react.

From a design point of view, an important requirement is the necessity of having a mean to relate combustion efficiency to the operating variables of air pressure, temperature, mass flow rate, and to the combustor dimensions [41].

Suitable parameters to relate the combustion performance to combustor dimensions and operating conditions can be derived using very simplified models to represent the combustion process [41]. One example of these models refers to the total time required to burn a liquid fuel, i.e., the sum of the times required for fuel evaporation, mixing of fuel vapor with air and combustion products, and chemical reaction. Thus, the combustion efficiency (η_b) can be expressed by Equation (2.15):

$$\eta_b = f(airflowrate)^{-1}\left(\frac{1}{evaporation\ rate}+\frac{1}{mixing\ rate}+\frac{1}{reaction\ rate}\right)^{-1} \quad (2.15)$$

In practical combustion systems, the maximum rate of heat release under any given operating condition may be governed by either evaporation, mixing, or chemical reaction, but rarely by all three at the same time [41]. However, when the combustion process is in transition from one regime to another, two of the three key rates will participate in determining the overall combustion efficiency (η_b).

Another definition for combustion efficiency introduces it in terms of the heat release during combustion as follows [68]:

$$\eta_b = \frac{(h_{02} - h_{01})_{\text{actual}}}{(h_{02} - h_{01})_{\text{ideal}}} = \frac{(T_{02} - T_{01})_{\text{actual}}}{(T_{02} - T_{01})_{\text{ideal}}} = \frac{\dot{m}_{f\ \text{ideal}}}{\dot{m}_{f\ \text{actual}}} \qquad (2.16)$$

In Equation (2.16), the subscript 02 refers to the combustor's exit conditions and the subscript 01 refers to the combustor's entry conditions.

Since the heat release from combustion arises from the formation of the combustion products (for instance, CO_2 and H_2O for a hydrocarbon), the combustion efficiency can also be determined by the quantity of these constituents in the exhaust gas relative to the maximum possible quantity.

In the case of a hydrocarbon fuel, before combustion is completed, the gas contains various molecules and radicals of hydrocarbon as well as carbon monoxide. These species represent unused chemical energy (in other words, wasting of fuel) and, if allowed to remain in the exhaust gases, constitute two of the major pollutants [68]. For these reasons, failure to achieve high levels of combustion efficiency is generally regarded as unacceptable and that is why current emission regulations call for combustion efficiencies in excess of 99% [41].

Currently, the combustion efficiency of most gas turbine engines at sea-level take-off conditions is almost 100%, reducing to 98% at altitude cruise conditions, as shown in Figure 2.17. To avoid the production of "white" smoke, efficiency must exceed 96% and at no point in the operating cycle it can be less than 90%. High combustion efficiency is also necessary at the "off design" point because, with the engine windmilling, the pressure and temperature of the air flowing through the combustor are close to ambient values [41].

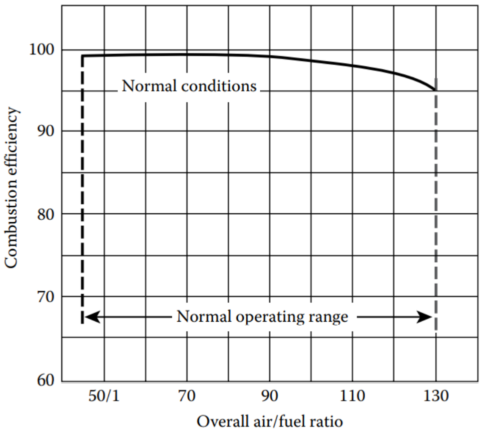

Figure 2.17: Combustion efficiency and air/fuel ratio [60].

2.6.3 Combustion Intensity

The combustion intensity is a parameter that evaluates the maximum possible conversion rate of reactants into products for a given volume of combustion chamber. A high combustion intensity is important for aero gas turbine engines due to their need of maximum size reduction [69]. Thus, to obtain the required high power output, a comparatively small and compact gas turbine combustion chamber must release heat at exceptionally high rates [60]. Moreover, if the intensity of combustion is kept within certain limiting values and the fuel is prepared adequately, it is possible to obtain combustion efficiencies of 98 to 100% at design conditions with conventionally designed combustion chambers [68].

According to Saravanamuttoo et al. [80], the combustion intensity, $f(\xi)$, is expressed in kW/m^3atm^{1-8} and is given by Equation (2.17):

$$f(\xi) = \frac{\dot{Q}}{Vp^n} \tag{2.17}$$

Where, $\dot{Q}$ is the heat release rate, V is the combustion volume and p is the pressure (where p^{1-8} can be employed).

From the above equation it is clear that the combustion intensity is an indication of the heat release rate in a given space, with a certain pressure, that takes into account the inlet conditions. So, high combustion intensity means a smaller space. Certainly, the lower the value of the $f(\xi)$ the easier it is to design a combustion system that will meet all the design requirements [80]. In aircraft systems, the combustion intensity usually lies between 2×10^4 and 5×10^4 kW/m^3atm.

2.6.4 Combustion Stability

The combustion stability is associated to smooth burning (or stable combustion) and to the ability of the flame to remain alight over a wide operating range. This combustion parameter is deeply related with the flammability limits of the fuel-air mixture used.

As discussed before for the flammability limits, also the range of stable operation, which consists in the range of possible operating conditions between the stability limits, will be influenced (increased or reduced) depending on several parameters.

According to EL-Sayed [68], the two main causes of combustion instability are:

- If the fuel–air mixture becomes too lean or too rich, the temperatures and reaction rates drop below the level necessary to effectively heat and vaporize the incoming fuel, and mixture it with the air;

- If the velocity of gas stream becomes higher than the flame speed, it causes the flame extinction. This is most likely to occur in flight during a glide or dive with the engine idling, while there is a higher air flow and a smaller fuel flow [41].

The stability loops provide these two basic types of information and Figure 2.18 shows a typical stability loop, where the limiting AFR is plotted against air mass flow [kg/s].

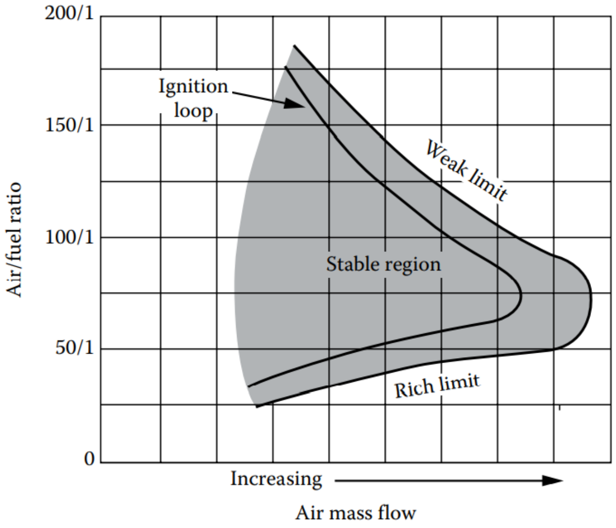

Figure 2.18: Combustion stability limits [60].

It is important to note that the stability loop is a function of the pressure in the combustion chamber, and a decrease in the pressure reduces the rate at which the chemical reactions proceed, which in turn narrows the stability limits. For aircraft gas turbine engines this is irrelevant because, when a new system is tested, it is important to check that the stability limits are sufficiently wide, with a combustion chamber pressure equal to the compressor delivery pressure which exists at the highest operating altitude [80]. Moreover, these stability limits will usually be well away from the normal operating point [68].

2.7 Ignition Process

When subjected to ambient conditions, common fuels and oxidisers usually combine at a slow rate. Thus, if an activation energy is not externally supplied, the acceleration of the reaction will not occur [69]. For that reason, most of the ignition theories are based on the idea that the transient ignition source, usually an electric spark, must supply enough energy to the combustible mixture to create a volume of hot gas that satisfies the necessary and sufficient condition for propagation that the rate of heat generation exceeds the rate of heat loss.

Regarding gas turbine engines, the ignition process occurs within 3 phases which can be described as follows:

- Phase 1: consists in the formation of a kernel of flame of enough size and temperature to be capable of propagation. This phase is affected by the effective fuel to air ratio adjacent to the plug, by the design of the igniter plug (*flush fire* or *sunken fire*), by its location and by the extent to which the plug tip protrudes through the liner wall. The survival of the kernel of flame depends entirely on whether or not the rate of heat release by combustion within the kernel exceeds the rate of heat loss to the surroundings by radiation and turbulent diffusion [41].
- Phase 2: consists in the subsequent propagation of flame from this kernel to all parts of the primary zone. The location of the ignition plug is important in this phase because it determines whether the hot kernel is entrained into the primary zone reversal or swept away downstream. This phase is also governed by all the factors that control flame stability. Thus, an increase in pressure and/or temperature, or a reduction in primary zone velocity, or any change in fuel to air ratio toward the stoichiometric value, will improve phase 2. All those factors are also beneficial to stability [41].
- Phase 3 (applied only to tubular and tubo-annular designs of chamber): consists in the spread of flame from a lighted liner to an adjacent unlighted liner. This phase is achieved using interconnectors, in which the flow area is made large to facilitate the passage of flame, and whose length is kept short to minimize heat loss by external convection to the annulus air [41].

A failure of any of the above steps will result in a failure to light up the combustor. If the ignition performance of a combustion chamber is unsatisfactory, the first step is to find out in which phase the ignition fails. This information can be obtained quite readily by examining the position of the ignition loop in relation to the stability limits as illustrated in Figure 2.19 [41]. Since the flow properties that control stability exercise a similar influence on ignition behaviour, it would be expected that ignition and stability limits should be coincident. However, the stability limits are related essentially to burning conditions and high metal temperatures, while ignition is inevitably associated to cold liner walls and comparatively high heat losses. For this reason, the two limits can never be the same, but the objective of ignition development is to ensure that they are separated only by the effects of heat loss [41].

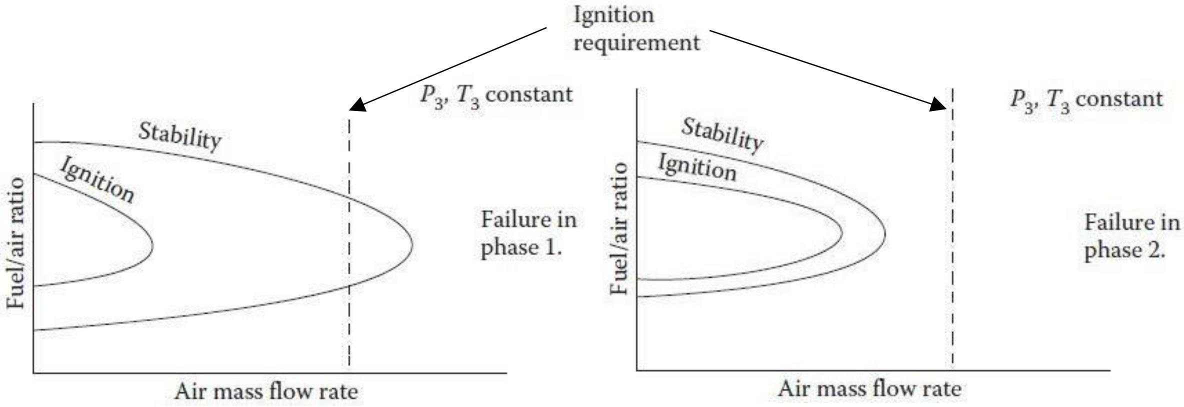

Figure 2.19: Curves illustrating the two main types of ignition failure, adapted from [41].

Looking at Figure 2.19, it is possible to conclude that if the ignition loop lies well inside the stability loop, this indicates that the limitation on ignition performance is arising in phase 1. This may be checked by changing the spark energy, which should produce a corresponding change in the ignition loop. If the ignition and stability loops lie in proximity, the bottleneck on performance is almost certainly in phase 2. Failure in phase 3 is indicated when the maximum relighting altitude is significantly less than the value predicted from rig tests carried out on a single liner [41].

2.8 Fuel Injection

Overall, in a gas turbine engine, the main objective of the injection system is to deliver the fuel to the combustor in such a way that allows it to be completely mixed with the air before combustion. Moreover, gas turbine combustors can be operated on liquid fuels as well as gaseous fuels. Thus, in the following, a brief overview will be made about the techniques and requirements used for the injection of liquid and gaseous fuels, with a greater focus in the last ones.

2.8.1 Liquid Fuel Injection

For liquid fuels there are two main methods through which fuel can be supplied to the air stream to form the fuel-air mixture: vaporizers and fuel spray nozzles. Both of these methods will be explained in the following.

2.8.1.1 *Vaporizers*

Generally, in vaporizers, the preparation of the liquid fuel for combustion is made by heating the fuel above the boiling point of its heaviest hydrocarbon ingredient so that it is entirely converted to vapor before combustion. However, this method is only applicable to high-grade fuels that can be completely vaporized, i.e., leaving no solid residue.

A much simpler alternative method of vaporization consists in inject the fuel, along with some air, into tubes that are immersed in the flame. So, the injected fuel–air mixture is heated by the tube walls and, under ideal conditions, emerges as a mixture of vaporized fuel and air. The remainder of the combustion air is admitted through inlets in the liner walls and reacts with the fuel–air mixture issuing from the tubes [41].

2.8.1.2 Fuel Spray Nozzles

In this case, the preparation of the liquid fuel is done by atomizing it and then mixing this fuel thoroughly with air before combustion. [62]. The atomization is the process in which a jet or sheet of liquid is disintegrated by the kinetic energy of the liquid itself or by exposure to high velocity air (or gas) [41]. This process represents a disruption of the consolidating influence of surface tension by the action of internal and external forces [41]. In the absence of such disruptive forces, surface tension tends to pull the liquid into the form of a sphere, which has the minimum surface energy. Liquid viscosity has an adverse effect on atomization because it opposes to any change in system geometry [41]. On the other hand, aerodynamic forces acting on the liquid surface promote the disruption process by applying an external distortion force to the bulk liquid. Breakup occurs when the magnitude of the disruptive force exceeds the surface tension force of consolidation.

The atomization process is generally regarded as comprising two separate processes; primary atomization, in which the fuel stream is broken into shreds and ligaments, and secondary atomization, in which the large drops and globules produced in primary atomization are further disintegrated into smaller droplets. These processes together determine the detailed characteristics of the fuel spray with respect to droplet velocities and drop-size distributions. In practice, these characteristics are markedly affected by the internal geometry of the atomizer, the properties of the gaseous medium into which the fuel stream is discharged, and the physical properties of the fuel. Once in this work the atomization model is not used, these processes will not be explained in detail here. However, the various mechanisms whereby a jet or sheet of fuel issuing from an atomizer is broken into drops (also known by jet disintegration) and the process of splitting the larger drops during the final stages of disintegration are very well explained by Lefebvre and Ballal [41].

The devices responsible to achieve the atomization process are the fuel spray nozzles, which can be distinguished through the operating mode in pressure atomizers, airblast atomizers and air-assist atomizers. There are other types, but they are less utilized [41].
In the original CFM56-3 engine, the injection method adopted was the utilization of fuel spray nozzles. However, in this work, since they cannot be used with gaseous fuels, greater importance will be given to the injection methods available for this type of fuels. For more information about the liquid fuel injection methods, please consult the references [41, 62].

2.8.2 Gaseous Fuel Injection

The use of gaseous fuels has some advantages over the use of liquid fuels. Among these advantages is the fact that, since the fuel is in the correct physical state for molecular mixing with the combustion air, generally, no special preparation is required before injecting the fuel into the combustor.

As with liquid fuels, the combustion is closely determined by the general flow characteristics in the primary zone of the combustor. Therefore, the gaseous fuel injector is simply a device to distribute the fuel into the combustor to promote uniform and rapid mixing with the primary air.

Many different methods have been used to inject gas into conventional combustion chambers, including plain orifices, slots, swirlers and venturi nozzles as described by Mellor [71]. However, due to proprietary considerations by the manufacturers and the relative simplicity of burning gaseous fuels, information on burner design and injection methods is relatively scarce. A good review of the principal works and studies in this field available until the 90's is made by Mellor [71]. Several methods of gas injection employed in modern low-emission combustors are also described by Lefebvre and Ballal [41]. Some other studies about the development and comparison of prototypes of gaseous fuel injectors to employ in modern and future combustors with the aim of reducing even more the pollutant emissions are presented in the works of J. Ziemann et al. [37], C. J. Marek et al. [38], Lei and Khandelwal [39] and Reid Smith et al [24]. The most relevant examples of gaseous fuel injectors presented in these works are shown in Appendix I.

To better understand which type of injector should be used in each application and since one of the objectives of this work is to adapt the injection parameters to improve the use of a gaseous fuel in the CFM56-3 combustor, this analysis should start to understand what are the basic performance requirements, influence of the fuel properties, and design principles of a gaseous fuel injector. Therefore, these parameters will be described next.

2.8.2.1 Performance Requirements of Gaseous Fuel Injectors

The performance of gaseous fuel injectors is measured by the effect of their design on the parameters of efficiency, stabilization, emissions, ignition, liner wall temperature, and temperature distribution quality, all of which are described below.

- Efficiency:
    - The design of the fuel injector can have a large effect on the combustion efficiency. According to some studies presented by Mellor [71], the efficiency is affected by all the factors that influence the fuel distribution and the fuel-air mixing, such as, injector type (axial, angled or radial), jet velocity, cone angle, axial position, and orifice size and shape to create the fuel jets and/or sheets. The fuel spreading is also a considerable factor that influences the efficiency. However, too much fuel spreading is undesirable for high efficiency. Some literature also suggests that further improvement in efficiency could be obtained by adding extra fuel injectors [24, 71]. The efficiency is also dependent on fuel properties. This is of concern particularly when burning low heating value gases. Under severe operating conditions, the differences in efficiency are more dramatic. For several fuels, the efficiency generally increases with increase in maximum burning velocity and flammability range, and decrease with minimum spark-ignition energy. It is therefore clear that the efficiency variation is such that injector/combustor design optimization is critical. Moreover, the efficiency of the injector should be high for all operating conditions.
- Stabilization:
    - Although flame stabilization depends mostly on the design of the stabilizer, it can also depend on injector design and on fuel properties. The fuel distribution near the injector significantly affects stabilization, and this parameter is determined by the jet velocity, angle and mixing rate. It must be noted that too much spreading of the fuel is undesirable for stabilization.
- Emissions:
    - Compared with liquid fuels, gaseous fuels with similar calorific value emit fewer pollutants, particularly NOx and soot. This occurs because the gas mixes intensively with the air, forming a homogeneous mixture, away from the stoichiometric one, which burns with low NOx production. In comparison, the unavoidable local stoichiometric burning in liquid sprays promotes high NOx production. Thus, the main requirement of the injector to achieve low NOx emissions consists in the ability to promote a

    lean and well mixed mixture [71]. To reach the limiting mixture and maintain good flame holding, it is necessary fuel staging. Generally, therefore, the overall combustor aerodynamics must be considered to minimize NOx emissions.

- Ignition:
    - The basic requirement for good ignition is the placement of a flammable fuel-air mixture in close proximity to an ignition source during an appropriate time. Therefore, the ignition problem is related with geometry of the chamber and the aerodynamics in the primary zone, which depends on the quality of the fuel injection and the fuel-air mixing. Also the fuel properties obviously affect ignition performance.
- Liner wall temperature:
    - The temperature of the combustion chamber walls can also be affected by the injector design. Often this is an aerodynamic problem that occurs when the fuel jet impinges directly on the liner causing hot streaks. However, it is typically found that, for the same liner, the use of a gaseous fuel results in lower wall temperatures than when using a liquid fuel.
- Temperature distribution quality:
    - The quality of the outlet temperature distribution largely depends on the fuel injector design, since it is closely linked to the overall aerodynamics of the combustor, which in turn is also affected by the combustor pressure drop. According to Mellor [71], variation in injection rate and limited change in jet angle had little effect on the temperature distribution quality.

2.8.2.2 Gaseous Fuel Property Effects on Injector Design

The fuel injector design may require considerable changes, particularly when alternative gaseous fuels are to be used. In this case, the most important property is the fuel heating value, since this property will decisively influence the required fuel mass flow rates, which in turn will influence the quality of the velocity profiles in the combustion chamber and the mixing intensity between the fuel and the air. Consequently, this property will affect the quality of the combustion and the quality of the exit temperature distribution. For instance, in case of burning low heating value fuels, the flow rates may be up to one-third of the total engine mass flow. This can result in poor mixing, causing unstable burning and high emissions. Moreover, if the mixture is too lean, the combustion is more susceptible to the occurrence of problems related with ignition and weak extinction. The turndown ratio also decreases due to the narrow burning range of fuels with low hydrogen content. Furthermore, the CO and unburned hydrocarbons emissions increase and the exit temperature distribution quality decreases. As a result, proper burner and swirler design is important for this type of fuels. For gases with very low heating values, both injector and combustor must be changed to handle the extra fuel volume [71].

For the present study, this problem is not posed, since the hydrogen fuel is a high heating value fuel. Furthermore, this fuel has been of some interest in the later decades as a replacement fuel as well as for studies of fuel property effects. For example, Nomura et al. [73] and Shum and Sampath [74] described a swirl injector and a multi-orifice type with angled jets for hydrogen fuel. General observations shown that the combustion efficiencies in all cases were nearly 100%. However, both references concluded that the design of the injector and the way it is adapted to the combustor are fundamental for good performance [71].

2.8.2.3 *Injector Design Principles*

In a simplified way, fuel injectors are actually orifices, which can be round or slotted, that control the flow of a fuel gas or a fuel-air mixture into the combustion zone.

According to Mellor [71], to fulfil the performance requirements described before, the following factors and their effects on performance must be considered:

1. Discharge coefficient and mass flow rate

Since the gas is injected through an orifice, the standard orifice equation can be used to determine the mass flow rate. This equation is given by:

$$A_{hole} = \frac{\dot{m}_{fuel}}{C_d\sqrt{2\rho\Delta P}} \qquad (2.18)$$

Where A_{hole} is the physical area of the hole (or orifice), $\dot{m}_{fuel}$ is the target fuel flow that will pass through the hole at the design point, ρ and ΔP are the design point density and pressure drop, respectively, and C_d is the hole discharge coefficient.

The injector's orifice(s) is(are) sized to provide the required heat input rate to the combustor. As with liquid fuel injectors, the state of the fuel holes is important and some care should be required in their manufacture to provide holes free of burrs, of equal diameter, and of uniform pitch and angle to ensure symmetrical flow.

2. Injector pressure drop

The fuel pressure drop over the injector orifice is an important consideration in the injector design, since sufficient pressure drop is required to produce an even fuel flow to provide stable and high-efficiency combustion. This produces a uniform turbine inlet temperature distribution and maximizes the operating life of the hot components. Such a pressure drop also improves fuel control, giving stable and repeatable operating conditions. If the pressure drop is too high it will result in unstable operation creating undue stress on hot sections.

3. Turndown ratio

The turndown ratio is a measure of the variability of the operating conditions for which stability and combustion efficiency are still acceptable. Therefore, this parameter is directly dependent on the orifice geometry and the fuel pressure drop. For most applications, this ratio should be quite large, requiring significant attention in the design.

4. Velocity of fuel jet(s)

For any particular fuel, the jet velocity is directly related to the orifice size and pressure drop. This velocity can have a significant effect on combustor performance, since the relative velocities of the air and the fuel jets determine their mixing rates in the combustion zone. Generally, a too little mixing rate generates rough combustion, while a too high mixing rate can cause a high lean blowout limit. The mixing rates must therefore be optimized.

For gas turbine engines, the literature shows the jet velocity varying widely up to sonic velocity. However, it is necessary to have some care when using high fuel jet velocities because they may cause the fuel jet to impinge on the combustor walls resulting in high liner temperatures. Furthermore, the exhaust temperature distribution can also be affected by the jet velocities.

As the effect of fuel jet velocity on combustion is critically related to the aerodynamics, no optimum value can be recommended for that parameter. Thus, the values have to be varied to give good combustor performance for all operating conditions [71].

5. Cone angle or direction of fuel jet(s)

As with the fuel jet velocity, the fuel jet direction can also have a significant effect on combustor performance through its effect on the mixing rate. Some specific research dealing with the effect of fuel cone angle on combustor performance through axial, angled and radial injection is reported in literature [71]. That literature suggests that no general recommendation could be given, since external influences such as the amount of swirl, overall combustor design and even the fuel properties critically affect the results.

6. Stabilizing devices

The utilization of stabilizing devices is essential in the combustion chamber design and must be considered. Stabilizing devices usually consist of bluff bodies or, more commonly, swirling devices placed in the annulus around the fuel injector, like those used in the case of CFM56-3 as described in the section 2.3.4.1.

The primary uses of swirl are to increase the angle of spread and the decay of the axial velocity of a jet. This will increase the rate of entrainment and rate of mixing of the air and fuel jets providing improved flame stabilization and giving a wide turndown ratio.

2.8.2.4 Final remarks

The main conclusion that can be drawn from all the previous information is that no single gas fuel injector design can be recommended for all applications. Moreover, the overall aerodynamics in the combustor (which is also affected by the combustor geometry and the fuel properties) can have a large effect on the performance. Therefore, each situation requires considerable care in the injector design process to obtain the best performance possible for the complete range of operating conditions.

2.9 Emission analysis

2.9.1 Regulation in Civil Aviation

The political organism responsible for the regulation of civil aviation is the International Civil Aviation Organization (ICAO). In the last decades, ICAO has enacted specific regulations, which have been updated over the years, for the emissions from aircraft engines for subsonic and supersonic speeds.

The study presented in this work considered the ICAO's standards and regulations required for emission control, more specifically, the landing and take-off (LTO) cycle (explained in the next subsection). The regulations in force during the elapse of this work are presented in [81].

For the regulation in gaseous emissions, the turbofan used in this work falls into the regulated category of the turbojet and turbofan engines intended for propulsion only at subsonic speeds with rated thrust above 26.7kN and date of manufacture after 1 January 1986. All of the regulatory levels are available in [81] and, for the engine used, the emissions shall not exceed the regulatory levels determined from the following equations:

- For hydrocarbons (HC):

$$\frac{D_p}{F_{00}} = 19.6 \tag{2.19}$$

- Carbon monoxide (CO):

$$\frac{D_p}{F_{00}} = 118 \tag{2.20}$$

- Oxides of nitrogen (NOx):

$$\frac{D_p}{F_{00}} = 40 + 2\pi_{00} \tag{2.21}$$

Where D_p is the mass of any gaseous pollutant emitted during the reference emissions landing and take-off cycle, F_{00}, the rated thrust, and π_{00}, the reference pressure ratio.

It should be noted that the regulatory levels for the NOx emissions change depending on the manufacture date of the first individual production model and for the more recent engine models (after 2004), the regulatory levels also depend on the maximum rated thrust. The Equation (2.21) represents the regulatory level "for engines of a type or model for which the date of manufacture of the first individual production model was before 1 January 1996 and for which the date of manufacture of the individual engine was before 1 January 2000" [81].

The engine in study has also to comply with the regulation for the smoke, since it is applied "to engines whose date of manufacture is on or after 1 January 1983 and before 1 January 2023". The Smoke Number at any of the four LTO operating mode thrust settings when measured and computed in accordance with the procedures presented in [81], or equivalent procedures as agreed by the certificating authority, shall not exceed the level determined from the Equation (2.22):

$$Regulatory\ Smoke\ Number\ (RSN) = 83.6(F_{00})^{-0.274} \tag{2.22}$$

Or a value of 50, whichever the RSN is lower.

2.9.2 Landing and take-off (LTO) cycle

The LTO cycle refers to all the operations the aircraft carry out below 3000 ft (914.4 m) above field elevation over a specific range of certifiable operating conditions. This cycle includes four stages characterized both in terms of engine power settings and typical time in each specific mode of operation (time-in-mode, TIM). According to ICAO [81], these four phases of the LTO cycle, illustrated in Figure 2.20, are defined as:

- Approach phase.: The operating phase defined by the time during which the engine is operated in the approach operating mode, i.e., average thrust setting from maximum altitude of 3000ft (above field elevation), until the end of the roll-out on the runway;

- Climb phase.: The operating phase defined by the time during which the engine is operated in the climb operating mode, i.e., average thrust setting from the point of throttle back to the maximum altitude of 3000 ft (above field elevation);
- Take-off phase.: The operating phase defined by the time during which the engine is operated at the rated thrust, i.e., the maximum take-off thrust approved by the certificating authority for use under normal operating conditions at ISA sea level static conditions, and without the use of water injection;
- Taxi/ground idle.: The operating phases involving taxi and idle between the initial starting of the propulsion engine(s) and the initiation of the take-off roll and between the time of runway turn-off and final shutdown of all propulsion engines.

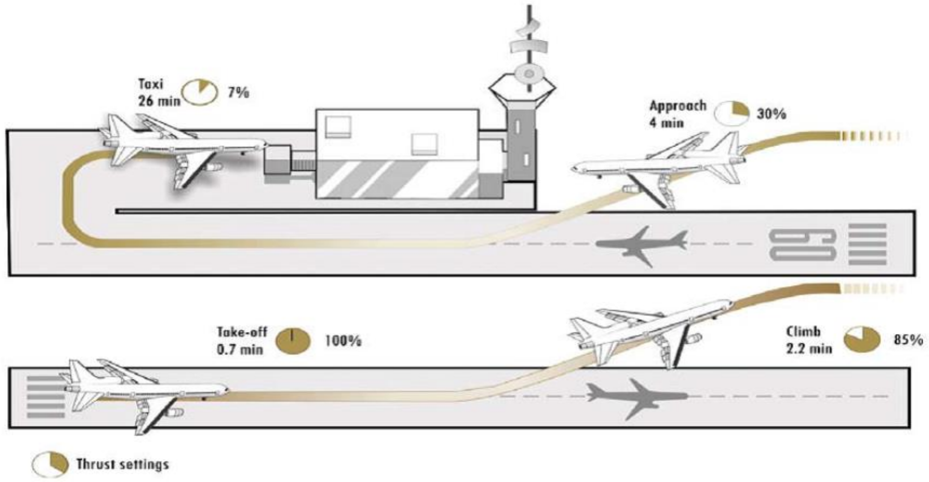

Figure 2.20: Illustration of ICAO emissions certification procedure representing the LTO cycle [126].

2.9.3 Regulatory Values for CFM56-3

Table 2 shows the regulatory data available for the CFM56-3 engine in the ICAO's engine exhaust emissions data bank [67] related to LTO cycle. In this case, the emissions are reported as emission indexes (EIs), expressed as mass of pollutant emitted per unit mass of fuel burned.

Table 2: LTO cycle measurements for CFM56-3, from ICAO's engine exhaust emissions data bank [67].

LTO operating mode	Thrust setting [%F_{00}]	Time in operating mode [minutes]	Fuel Flow [kg/s]	Emission index [g/kg]			Smoke number
				UHC	CO	NO_x	
Take-off	100	0.7	0.946	0.04	0.9	17.7	4
Climb	85	2.2	0.792	0.05	0.95	15.5	2.5
Approach	30	4.0	0.290	0.08	3.8	8	2.5
Taxi/ground idle	7	26.0	0.114	2.28	34.4	3.9	2.2

2.10 Turbofan engine performance

Considering the schematic representation of a turbofan engine in Figure 2.21, it is possible to define several equations that allow to analyze the design point performance of this type of engines.

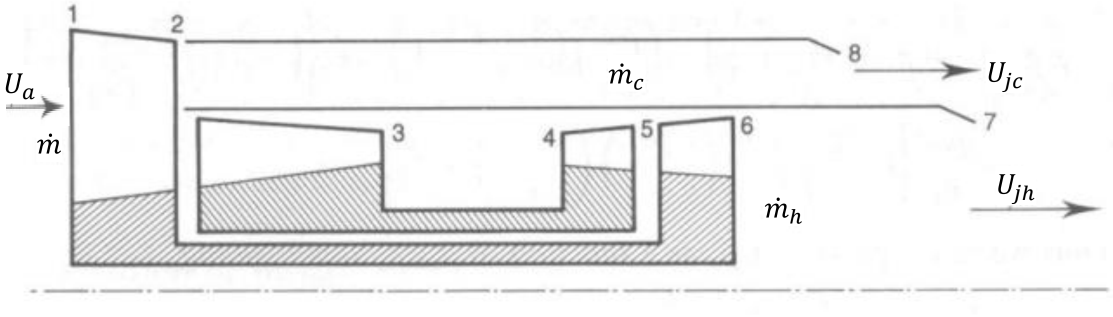

Figure 2.21: Schematic illustration of a turbofan engine (adapted from [80]).

So, to begin, considering Figure 2.21, the engine thrust, F, is proportional to the mass flow rate that goes through the engine, $\dot{m} = \dot{m}_c + \dot{m}_h$, the velocity of the gases in the nozzles over the flight velocity and the pressure differential in the nozzles. This way, the thrust produced by a turbofan engine can be calculated by:

$$F = \dot{m}_c(U_{jc} - U_a) + A_{jc}(p_{jc} - p_a) + \dot{m}_h(U_{jh} - U_a) + A_{jh}(p_{jh} - p_a) \tag{2.23}$$

Where U_{jc} is the jet velocity of the flow from the cold path, U_{jh} is the jet velocity of the flow from the hot path, U_a is the velocity with which the air enters in the inlet of the engine, A_{jc} is the area of the "cold nozzle", A_{jh} is the area of the "hot nozzle", p_a is the ambient pressure, p_{jc} is the pressure of the flow in the exit of the "cold nozzle", p_{jh} is the pressure of the flow in the exit of the "hot nozzle"; $\dot{m}_h$ is the mass flow rate from the hot path and $\dot{m}_c$ is the mass flow rate from the cold path [80].

The specific thrust is also an important engine design parameter for scaling the engine size with thrust, at a given flight condition. The specific thrust, F_S, is defined as the ratio between the engine thrust and the mass flow rate [80]. The Equation (2.24) represents this relation.

$$F_S = \frac{F}{\dot{m}} \tag{2.24}$$

Another important parameter is the thrust specific fuel consumption, $TSFC$, which represents the fuel efficiency of an engine design with respect to thrust output, in other words, the $TSFC$ is defined as the ratio between the fuel mass flow rate, $\dot{m}_f$, and the engine thrust, F, as shows Equation (2.25).

$$TSFC = \frac{\dot{m}_f}{F} \tag{2.25}$$

There are also several efficiency parameters that allow to analyze the performance of the engine in study [80]. For example, the efficiency of the air-standard Joule-Brayton cycle (η_{joule}), previously represented in Figure 2.2, is given by Equation (2.26):

$$\eta_{joule} = 1 - \frac{1}{r_p^{\frac{\gamma-1}{\gamma}}} \tag{2.26}$$

Where, r_p, is the pressure ratio and, γ, is the ratio of specific heats.

The propulsive efficiency, η_p, is a measure of the effectiveness with which the propulsive duct is being used to propel the aircraft [80]. This parameter can be defined as:

$$\eta_p = \frac{\dot{m}U_a(U_j - U_a)}{\dot{m}\left[U_a(U_j - U_a) + \left(U_j - U_a\right)^2/2\right]} = \frac{2}{1 + (U_j/U_a)} \tag{2.27}$$

The energy conversion efficiency, η_e, can also be defined as:

$$\eta_e = \frac{\dot{m}\left(U_j^2 - U_a^2\right)/2}{\dot{m}_f . LHV} \tag{2.28}$$

Finally, the overall efficiency (or thermal efficiency), η_0, can be defined as:

$$\eta_0 = \eta_p \eta_e = \frac{U_a}{TSFC . LHV} = \frac{TP}{Q_{in}} = \frac{FU_a}{Q_{in}} \tag{2.29}$$

Where TP is the thrust power, which is defined as the thrust, F, multiplied by the aircraft speed (or flight speed), U_a; Q_{in} is the thermal (or heat) input and it is equal to the fuel flow times the lower heating value of the fuel, $Q_{in} = \dot{m}_f \times LHV$.

Chapter 3 – Fuels

3.1 Background

Currently, the great majority of aviation fuel (more than 99%) used both in civil and military aircrafts is the jet fuel, which is extracted from the middle distillates of crude oil, i.e., kerosene fraction, which distils between the gasoline and the diesel fractions [70, 82]. Even so, in some smaller aircrafts, a small quantity of aviation gasoline is still used [82].

The kerosene type fuels most used worldwide in civil aviation are the Jet A and Jet A-1 grades, being the Jet A used in the USA, and Jet A-1 used in the majority of the rest of the world [83]. The main difference between these fuels is that while Jet A has a maximum freezing point of $-40^{o}C$, Jet A-1 has a lower freezing point (maximum of $-47^{o}C$) [84]. However, the minimum flash point is the same for both fuels and correspond to $38^{o}C$.

Other fuels can also be used as an alternative to Jet A/Jet A-1 [84]. For instance, Jet B is called wide cut fuel because it is a blend of gasoline and kerosene fractions and is used in very cold climates, e.g., in northern Canada where its thermodynamic characteristics are suitable for handling and cold starting [84, 85]. The TS-1 is the main jet fuel grade available in Russia and the Commonwealth of Independent States. This is a kerosene type fuel with slightly higher volatility and lower freeze point compared with Jet A-1 [86]. In China, the main fuel used is RP-3 (renamed No 3 Jet Fuel) and it is basically as Western Jet A-1 produced as an export grade [87].

The dependency on those oil products has been predominant in aeronautical sector due to their favorable weight to volume characteristics and low cost. However, the rise of the oil price combined with the growing concern of aircraft impact on climate change have led the aeronautical industry (and not only) to seek and develop alternatives for petroleum-derived fuel and new low-carbon propulsion technologies (advanced kerosene-propulsion systems) [69, 76]. As referred in Chapter 1, to mitigate the problem of the pollutant emissions, in the future there seem to be two viable solutions with regard to fuels, the use of SAFs or the use of hydrogen fuel (through hydrogen combustion engines or fuel cells). So, in this work, both types of fuel will be introduced, but the focus will be on hydrogen fuel associated to the combustion in gas turbine engines.

3.2 Sustainable Aviation Fuels (SAFS)

Nowadays, there are a wide variety of alternative fuels, and although they may present some challenges when compared to conventional jet fuel, most of the sustainable aviation fuels (SAFs) can be easily implemented in the present and future aircrafts (requiring little or no modification to current aircraft design), especially as blends optimized according to the local conditions, that generally reduce local emissions, especially particulates [76, 89].

In a simplified way, SAFs can be defined as combustible liquids and represent a renewable energy source that can be produced from a variety of feedstocks and manufacturing processes. To a certain extent, SAFs can also be considered carbon neutral as the combustion of them may not give any net contribution to the GHG emissions, since, for instance, for some biofuels an equivalent amount of CO_2 was absorbed by photosynthesis during the growth of new mass. There are, however, concerns over their sustained long-term use, which include, for example, first, the biodiversity, as large amounts of land may be required for the crops; second, the food versus fuel competition; and then, the fact of being carbon neutral only on the basis of life-cycle analysis [90]. Attending to these concerns, the SAFs can be described through three generations:

- Generation One: generally referred to as "biofuels", which are produced from biogenical sources, such as crops, which can be subject to additional sustainability concerns beyond carbon reduction, like competition with food and water, land-use changes, among others [6];
- Generation Two: refers to the alternative fuels produced with the current technology from non-biogenical sources, such as municipal wastes, used cooking oil, agricultural residues, or from other non-food biogenical sources, such as jatropha and algae, which raise fewer sustainability issues [6, 69];
- Generation Three: refers to alternative fuels, which sometimes are defined as "synfuels", that make use of new technologies to synthesize fuel from hydrogen (produced using electricity) and CO_2 taken from industrial, biomass (specially modified for biofuel purposes) or direct-air capture [88].

About the biofuels, they have the advantage of being "drop-in fuels" that do not require changes in aircraft or fuel infrastructure and are applicable across all aircraft segments. Moreover, the International Renewable Energy Agency (IRENA) projects biofuel availability to be around 100 to 150 exajoules (EJ), which would be sufficient to power a large proportion of aviation [88]. The two most representative biofuels are ethanol and biodiesel. For instance, ethanol or bioethanol at present are mostly produced from food crops (corn, starch, and sugarcane), but can also be produced from non-food-crop sources (miscanthus, switchgrass, cellulosic waste, and biomass) [76]. Similarly, biodiesels can be produced from a variety of feedstocks including vegetable oils, animal fat, and non-food crops, such as jatropha, karanja and algae [76].

In contrast to biofuels, the main source of synfuels is electricity, hence the designation of "power-to-liquid" of this type of fuels. This electricity is used to first produce hydrogen and then to capture carbon, combining the two into a kerosene-like fuel. Synfuel can also be used in current aircraft engines and fuel infrastructures, being suitable for all segments [88]. In the future, the generation three of SAFs should offer the required productivity, but since the technology is not mature yet, the production of second generation SAFs should be the focus for the next decades, once these alternative fuels use a sustainable resource to produce fuel that can replace conventional jet fuel, while not competing with food, land and water resources [91].

Overall, SAFs are expected to play an important role in the global energy supply, and could become a significant component of the sustainable energy paradigm, especially if non-food crops and marginal lands can be used to produce them in a significant manner [76].

3.3 Gaseous fuels

Gaseous fuels have distinct advantages over solid and liquid fuels. Overall, they are easy and convenient to handle, generally free of any mineral impurities, require low or negligible maintenance of burners and result in good combustion efficiencies. This type of fuels are composed mostly of one or a mixture of hydrogen, hydrocarbons (methane, propane, butane, or others) and carbon monoxide [76]. According to Lackner [76], gaseous fuels can be classified and grouped, based on their occurrence mode as follows:

1. Naturally occurring gases - the gases may be extracted directly, or obtained as a product of another process like refining;
2. Synthesized gases - which are manufactured from other sources such as solid/liquid fuels or water;
3. By-product gases - these gases are secondary products derived from a production process or chemical reaction, such as some gases obtained from coal processing.

From the classification made above, it is possible to conclude that the hydrogen fuel (at least the renewable component) belongs to the group of synthesized gases. Generally, the fuels of this group are characterized by having mainly carbon monoxide and/or hydrogen contributing to their calorific value. A good overview about these three groups is made by Lackner [76].

3.3.1 Hydrogen

Hydrogen is the simplest and most abundant of the chemical elements in the universe. On Earth, under standard conditions, it exists as diatomic gas (H_2), but its concentration is negligible (1 ppm by volume) as it escapes from Earth's gravity due to its low weight. However, in chemically combined form, it is the third most abundant element on Earth. Consequently, hydrogen can be considered an energy carrier, similar to electricity, since it can be produced from other compounds, mostly from hydrocarbons and water [76].
The main reasons why hydrogen can play an increasingly significant role in meeting the world's energy demands and addressing environmental concerns are that hydrogen meets three important criteria: a promising low-carbon alternative to reduce emissions of GHG, provide energy security, and the possibility of reducing local pollutants (NOx and particulates). For these reasons, hydrogen is today considered to be an attractive source for replacement of conventional fossil fuels [76].
In the following, a brief overview will be made about the properties and their influence in the use of hydrogen in converted gas turbine engines as well as the production methods and required infrastructure for the use of this fuel.

3.3.1.1 Hydrogen Fuel Properties and Challenges

Hydrogen has some distinct thermo-transport properties that make its combustion and emission characteristics notably different from those of hydrocarbons fuels. In Table 3 is provided a comparison between the main properties of hydrogen and Jet A [9, 76].

Table 3: Properties for hydrogen fuel and Jet A fuel [9], [76].

Properties	Units	H_2	Jet A
Molecular weight	---	2.016	~168
Liquid density	g cm^{-3}(at 283k)	0.071	~0.811
Freezing point	K	14.4	233
Boiling point	K (at 1atm)	20.27	440–539
Flash point	K	---	311.15
Heat of vaporization	J g^{-1} (at 1 atm)	446	360
Specific heat	J g^{-1}	9.69	1.98
Lower heating value	MJ kg^{-1}	119.96	43.15
Flammability limits in air	vol%	4.0-75.0	0.6-4.7
Burning vel. In NTP air	cm s^{-1}	265-325	18
Minimum ignition energy in air	mJ	0.019	0.25
Thermal energy radiated to surroundings	%	17-25	30-42
Diffusion vel. in NTP air	cm s^{-1}	≤2.00	<0.17
Flame temperature in air (stoichiometric)	K	2318	2200

Looking to the properties presented in Table 3, hydrogen is superior to conventional fuel in terms of power density by unit weight, since the hydrogen has a gravimetric energy density three times higher than Jet A [88, 104]. This is highly relevant for flight, in a weight-critical application, as it offers a Maximum Take-off Weight (MTOW) advantage over the other energy storage alternative. However, due to the hydrogen low volumetric density, it requires about four to five times the volume of conventional fuel to carry the same onboard energy [104]. Thus, effective storage solutions are essential to solve the issue of low volumetric energy density.

Currently, storage in the liquid state is the most promising option. However, with the actual technology, the cryogenic cooling (below -253 ºC), requires as much as 45 percent of the stored energy content and it is necessary the inclusion of cooling systems and significant insulation. All these factors lead to larger, complex and heavy tank designs that consequently reduce the effective gravimetric energy density of the fuel, which can significantly reduce economics for long-range aircrafts [88, 104].

Because of these considerations, the use of hydrogen fuel will require at least a partial redesign of the aircraft, being the major changes resulting from fuel delivery and storage (due to the additional fuel storage volume in the fuselage). However, to exploit the full benefits of hydrogen, the aircrafts must change substantially. This could amount to a redesign of almost all the components of the aircraft, from the propulsion system and the fuel storage to the form of the fuselage. The disadvantage of all radically new aircraft concepts is that they have a long and unpredictable commercialization process with extended development to ensure the aircraft's aerodynamic stability in all flight phases and to optimize cabin design, manufacturing processes and operations [88].

3.3.1.2 Considerations for Conversion of Conventional Gas Turbine Combustors to Hydrogen

In theory, to efficiently utilize hydrogen fuel in the current conventional gas turbine engines, the minimum modifications needed are the change of the injection system and the implementation of facilities to evaporate the hydrogen, which is usually stored in the tanks in a liquid (or cryogenic) state. This last process can be accomplished by an external heat source or a heat exchanger (HE) [28]. However, to take full advantage of the hydrogen's properties (mainly, high diffusivity, low ignition energy, wide flammability limits and the highest laminar flame speed), beyond the injection system, the combustion chamber must also be changed [76].

In both cases, when changing to hydrogen, either the combustor outlet temperature (COT) or the net thrust can be retained [28]. Generally, when the COT is preserved, the net thrust increases, resulting in a corresponding increased specific thrust. When is opted to retain the net thrust, this results in a lower COT [28]. It should be noted that, due to the considerably higher heating value of hydrogen, the fuel flow to achieve the same COT or net thrust is reduced by almost two-thirds.

According to Boggia and Jackson [33], the performance improvements could be explained by two fundamental changes when using hydrogen: reduced mass flow and changed composition of the gases expanding through the turbine(s). The performance is improved by the latter and deteriorated by the former.

Reduced mass flow through the turbine lowers the thrust output for two reasons. First, decreasing the fuel flow implies that the exhaust mass flow decreases accordingly; hence, without any variation in gas composition, the thrust output decreases. In second, a reduced mass flow through the turbine will result in a higher total temperature drop and, thereby, also a higher total pressure drop across the turbine to deliver the same amount of power to the compressor. As a consequence of the lower total temperature and pressure at the turbine exit, both the pressure thrust and momentum thrust decrease.

However, the loss in thrust due to reduced mass flow is offset by the increased thrust owing to changed properties of the combustion products [33]. With the use of hydrogen, the combustion products contain no CO_2 and a larger portion of H_2O, which has a higher c_p value than CO_2. This increased c_p value through the turbine will similarly, but in the opposite direction as reduced mass flow, affect the performance. For a fixed power output, it will cause smaller total temperature and pressure drops across the turbine. Provided that the core nozzle is not choked, a larger nozzle expansion ratio will result in a larger exhaust velocity, which, in turn, will increase the momentum thrust. In total, the positive effect of increased c_p value outweighs the effect of reduced mass flow and, hence, results in an increased net thrust when switching to hydrogen and retaining the COT.

Generally, if the COT is kept the same, the turbine entry temperature (TET) is also about the same, thus requiring the same cooling technology [33]. On the other hand, the option of lowering the COT to preserve the net thrust will lead to a decrease in TET. So, this option will require less advanced cooling technology as well as having a favorable effect on turbine blade life. Moreover, designing for a lower maximum cycle temperature will help to suppress the NOx emissions.

It should be pointed out that the energy consumption to attain a certain COT is highly dependent on the fuel injection temperature and the location of the heat exchanger (HE) used to evaporate the liquid hydrogen. In addition, by heating the fuel more, it is possible to achieve performance benefits. The effects on engine performance are quite small, but there are still some desired features that could be exploited [28].

3.3.1.3 Hydrogen production methods

On a commercial scale, despite the several production sources, most of the hydrogen is currently obtained by "gray" hydrogen processes, with 96 percent of hydrogen produced directly from CO_2 emitting processes such as steam reforming of methane (SRM) from natural gas, or direct dissociation of other hydrocarbons, and coal or biomass gasification (this process consist in heating organic materials so that they release hydrogen and carbon monoxide) [76, 92, 104].

The ultimate goal, though, is to produce hydrogen with little or no greenhouse gas emissions. Thus, to solve this problem, one option is to capture the carbon dioxide emitted when extracting hydrogen from fossil fuels and injecting (or storing) it deep underground or into the ocean. This process, named as Carbon Capture and Storage (CCS), could enable large-scale, clean production of hydrogen at relatively low cost, but it would be crucial to establish the technical feasibility and environmental safety of carbon sequestration.

Nowadays, hydrogen is increasingly being produced using other sources, which include, splitting of water using electric, renewable, or nuclear energy, and even through algae bioreactors [76]. However, considering the electrolysis of water using power generated by renewable energy sources such as wind turbines or solar cells, although this process faces no major technical hurdles, the current costs to produce hydrogen using these methods are high. Nuclear energy could also provide the power for electrolysis, although producing hydrogen this way would not be significantly cheaper than using renewable sources. In addition, nuclear plants could generate hydrogen without electrolysis, since the intense heat of the reactors can split water in a thermochemical reaction. This process might produce hydrogen more cheaply, but its feasibility has not yet been proved. Moreover, any option involving nuclear power has the same drawbacks that have dogged the nuclear electric power industry for decades: the problems of radioactive waste, proliferation and public acceptance [127].

In brief, the various hydrogen sources can be grouped into three types, namely: fossil fuels (coal, natural gas, petroleum, oil shale, etc.), renewable sources (biofuels, water, photovoltaic, algae, etc.) and nuclear (e.g., using thermal energy from nuclear reactions for water splitting, etc.). However, for hydrogen to be part of a sustainable future in aviation industry, renewable and nuclear sources need to play a more significant role in hydrogen production (for the "green" hydrogen), and cost-effective Carbon Capture and Storage (CCS) technologies (for "blue" hydrogen) need to be developed and upgraded to produce sufficient volumes [104].

About the cost, currently, hydrogen is more expensive than kerosene on a kWh basis. Excluding storage costs, average production costs are 0.14 USD/kWh for "green" hydrogen and 0.05 USD/kWh for "gray" hydrogen. The latter is on par with kerosene, but as "green" hydrogen would be necessary for "zero carbon" sustainable aviation, the price of these production methods must fall to compete on a cost basis [104].

According to a recent assessment by the National Research Council and the National Academy of Engineering, future technologies, and large-scale production and distribution could lower the price.

For more information about the hydrogen generation pathways, a really good overview, including the source of energy, hydrogen source, process, technology, reaction kinetics and temperature range, is made by Abdin et al. [128].

3.3.1.4 Infrastructure (production, transport, storage and conversion)

For the future, specially relatively to SAFs, hydrogen is more likely to penetrate into other industry sectors, which could speed up the development of the technology and storage systems, as well as the infrastructure. This would benefit the aviation industry, as the R&D and infrastructure development costs would be partially borne by other industry sectors pushing down the initial investment and production costs [104].

However, for hydrogen to become a viable alternative, it is necessary to find the optimal configuration for the infrastructure network (including production, transmission and distribution). This requires a detailed analysis considering the full range of impacting factors, i.e., including existing hydrogen production, transmission and distribution infrastructure, availability of resources for hydrogen production, distance between hydrogen production place and end-users, and demand of the refueling stations [128].

Logistically, hydrogen can be produced regionally in large plants and then stored and delivered as a liquified (or compressed) gas; or it can be produced locally in smaller stations from natural gas or electricity [127]. Generally, off-site, large-scale hydrogen generation suggests economies of scale, i.e., lower generation cost, but results in higher transmission and distribution costs. On the other hand, the on-site (smaller-scale/decentralized) hydrogen production usually results in lower transmission and distribution costs, but this imposes higher costs at the hydrogen generation stage.

Depending on the amount and distance, hydrogen can be transported from production facilities to the airports via various means. For example, for small quantities and short distances, delivery of gaseous hydrogen via tube trailers is usually the best option [128]. On the other hand, for long distances and average hydrogen amounts, liquid hydrogen can be transported by train or by liquid tankers, provided that appropriate railway lines and waterways, together with loading terminals are available. To transport large amounts of hydrogen over long distances, the pipelines are the best option [128].

When choosing which of the approaches best fits each case, there is a trade-off between the fixed capital investment and variable costs of hydrogen transmission and distribution options. Considering the three solutions mentioned, the first one presents a low fixed investment cost and high variable cost because of the lower transport capacity, whereas, in the case of pipeline transport, the fixed investment cost is high and the variable cost is low (considering that the pipeline network is fully utilized) [128].

About the hydrogen storage, the primary advantage over other energy storage alternatives such as batteries is its potential for seasonal and long-term storage. Energy can be stored in large quantities such as terawatt-hours, for a long time and in different forms. However, although the LHV of hydrogen is extremely favorable, the issue lies with its low volumetric energy density at ambient conditions (298K and atmospheric pressure). Therefore, improving its volumetric energy density is a necessary step to facilitate optimal hydrogen storage. Nowadays, the possible storage options are compression, liquefaction, or storing hydrogen in liquids and solid materials. All of these methods are briefly discussed by Abdin et al. [128].

About the refueling, the similarities in the process between hydrogen and kerosene could ease the transition between new and old processes: hydrogen would only require different piping and potentially different temperatures of fluid. However, at the airports, there could be an additional requirement to liquefy hydrogen on site, assuming that the infrastructure will be in place to deliver gaseous hydrogen. This will require local electricity generation or a reliable grid connection to ensure no network disruption.

3.4 Mechanisms of Pollutant Formation

The concentration level of pollutants in the gas turbine exhaust can be directly related to several factors that control the emissions in conventional combustors. As mentioned in section 2.3.3.2, these factors may be considered in terms of the temperature, equivalence ratio, degree of homogeneity and residence time in the primary zone, as well as the liner-wall quenching and the fuel spray characteristics [41]. These factors vary from one combustor to another and, for a given combustor, with changes in the power settings [41].

For the conventional fuels, like hydrocarbons (in this case Jet A) or even the SAFs, the pollutant emissions of most concern are CO, CO_2, UHC, NOx and PM (or smoke), since all these pollutants contribute to smog and also play an important role in acid rain and global warming [76].

The Figure 3.1 describes the characteristic trends of pollutant formation in a conventional gas turbine combustor for a conventional fuel as a relation with the throttle settings [41].

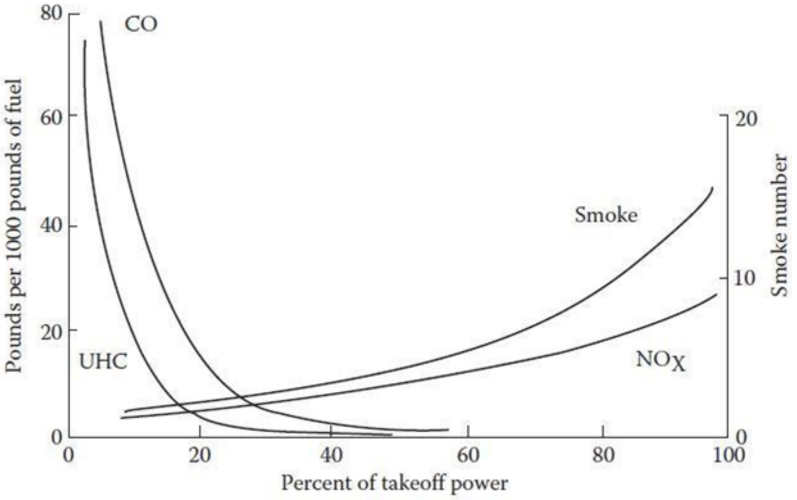

Figure 3.1: Emissions characteristics of conventional gas turbine engines [41].

From the Figure 3.1 it is possible to make some assumptions, that will be explained better in the following subsections.

Looking at low power conditions, where the combustor's inlet pressure and temperature are usually relatively low, the reaction rates for kerosene-type fuels are also expected to be low. As previously explained, to achieve the best combustion efficiency, i.e., total fuel conversion into completely oxidized products, the fuel (after being adequately prepared) must be burned with sufficient residence time at high enough temperatures. When this not occur and the flow field allows fuel vapor to exit the combustor without any reaction (or partially reacted), species of lower molecular weight, UHC and CO, will be formed and will be present along with the exhaust gases [69]. As shown in Figure 3.1, the presence of these species is more prone to happen at lower power conditions.

With the increase of engine power, the higher combustor's inlet pressures and temperatures lead to faster reactions, meaning that CO and UHC will be reduced to virtually zero. However, at these high temperatures, the formation of NOx and PM becomes prevalent, as shown in Figure 3.1.

This represents a problem for the conventional fuels, because efforts to reduce CO and UHC using parameters like temperature and pressure will lead to an inevitable increase in NOx and PM emissions [69].

3.4.1 Benefits of Using hydrogen

From the environmental standpoint, hydrogen is nearly a clean fuel that offers the possibility of reducing pollutant emissions when used in gas turbine engines [76, 104]. Generally, hydrogen propulsion is projected to be two to three times more effective than SAFs in reducing aviation's climate impact. According to the study made by Clean Sky and FCH[3] [88], the use of hydrogen combustion aircrafts has the ability to reduce climate impact in flight by an estimated 50 to 75 percent relative to conventional jet fuel. The same study refers that the use of SAFs (synfuels) using CO_2 from direct air capture can lead to a 30 to 60 percent reduction, while the reduction potential from SAFs (synfuels) using CO_2 from industrial processes depends a lot on the accounting of CO_2 emissions [88].

This higher reduction in the climate impact from the hydrogen is due to the fact that as a fuel, it does not contain carbon; thus, its combustion does not cause CO/CO_2 emissions in flight. SAFs (biofuels and synfuels), on the other hand, cause in-flight CO/CO_2 emissions that are similar to those of kerosene-powered aircrafts [88]. If, for the production of SAFs, carbon is directly extracted from the air, the overall result can be net carbon zero. However, if carbon is captured from an industrial or some similar process to produce the SAF, the resulting fuels are not carbon neutral.

As hydrogen combustion still produces NOx and water vapor emissions it will still contribute to global warming, since both NOx and water vapor have radiative forcing effects [104]. About the NOx emissions, initial studies of hydrogen powered aircrafts show that NOx emissions can be reduced by 50 to 80 percent with lean-mixture technology without large reductions in efficiency, while when kerosene aircrafts are switched to SAFs, NOx emissions are expected to remain largely unchanged [24, 38, 88]. About the water vapor, the emissions with SAFs are expected to be similar to those emitted by kerosene combustion. On the other hand, hydrogen combustion emits about two and a half times as much water vapor as kerosene, but does not emit soot at all. However, some initial simulations of hydrogen direct combustion show that the formed ice crystals of contrails are heavier, i.e., they precipitate faster, and the contrails are optically thinner, i.e., they are more "transparent". As such, these water molecules lead to a lesser, briefer global warming effect, resulting in a 30 to 50 percent reduction in impacts from contrail and cirrus formation compared to kerosene aircrafts [76, 104].

---

[3] It should be noted that the estimates include CO_2 emissions, non-CO_2 emissions and emission-related effects.

It should also be noted that, when compared to kerosene combustion, the local air quality is enhanced with the combustion of hydrogen, since the propulsion would significantly lower the emissions of NOx, particulate matter (PM) and non-methane volatile organic compounds (NMVOCs) [88].

Looking again at Figure 3.1, and considering the fact that in the case of using hydrogen fuel the emissions of CO, PM and UHC are not a problem, it is possible to conclude that the main objective when using this type of fuel will always be the reduction of the NOx emissions.

Considering all this and assuming that water vapor is not a major pollutant, in the following subsections, a greater importance will be given to the NOx emissions, since they will be used to compare the ability to reduce the pollutant emissions when using hydrogen instead of Jet A fuel in the same combustor. However, as in this work Jet A is used as fuel for the control simulations, a brief description of the parameters that influence the formation of CO, CO_2, PM and UHC will also be given.

3.4.2 Carbon oxides (CO and CO_2)

Hydrogen as a fuel does not contain carbon; thus, its combustion does not cause CO/CO_2 emissions in flight. Hydrocarbon fuels (and most of the SAFs), on the other hand, cause in-flight CO/CO_2 emissions as they contain carbon [88].

When a hydrocarbon fuel is burned, CO is formed as an intermediate specie in the oxidation process of the fuel to CO_2. Therefore, CO emissions arise from incomplete combustion of the fuel and this phenomenon is usually caused by one or more of the following reasons [41]:

- Inadequate burning rates in the primary zone, due to a fuel to air ratio that is too low and/or insufficient residence time;
- Inadequate mixing of fuel and air, which produces some regions in which the mixture strength is too weak to support combustion, and others in which over-rich combustion yields high local concentrations of CO;
- Quenching of the post-flame products by entrainment into the liner wall-cooling air, especially in the primary zone.

There are other factors that can influence combustion efficiency, and hence CO emissions, such as engine and combustor inlet temperatures, combustion pressure and, for liquid fuels, the mean drop size of the spray [41].

In brief, CO can only be completely oxidized to CO_2 when a sufficient amount of air is mixed with the hot gases within the right conditions. The extent of this process depends greatly on the kinetics of oxidation reactions and the method of cooling [93]. As the oxidation process of CO to CO_2 is not relevant to this work, this will only be presented in Appendix B. A good review of this process and the influence of the factors referred previously is also made by Kuo [40] and Lefebvre and Ballal [41].

3.4.3 Unburned Hydrocarbons (UHC)

The emissions of unburned hydrocarbons, UHC, include fuel that emerges from the combustor in the form of drops or vapor, as well as products of the thermal degradation of the parent fuel into species of lower molecular weight [41]. The occurrence of UHC is usually associated with poor atomization, inadequate burning rates, the chilling effects of film-cooling air, or any combination of these. The reaction kinetics of unburned hydrocarbon formation are more complex than those of carbon monoxide formation. However, it is generally found that those factors that influence CO emissions also influence UHC emissions and much in the same manner [41].

3.4.4 Particulate matter (Smoke or Soot)

For the hydrocarbon fuels, exhaust smoke is caused by the production of particulate matter (finely divided soot particles) in fuel-rich regions of the flame that, in conventional combustors, are always close to the fuel spray [41]. These are the regions in which recirculating burned products move upstream toward the fuel injector, and local pockets of fuel vapor become enveloped in oxygen-deficient gases at high temperature [41]. Thus, it is in these fuel-rich zones that soot is more likely to be produced in considerable quantities [41].

According to Lefebvre and Ballal [41], analysis of the soot found in exhaust gases shows that it consists mostly of carbon (96%) and a mixture of hydrogen, oxygen, and other elements. In practice, the rate of soot formation tends to be governed more by the physical processes of atomization and fuel–air mixing than by kinetics [41]. For this reason, CFD modelling of soot formation and oxidation is difficult because of the complexity of the physical/chemical processes involved, and the typical dimensions of the computational grids used for complex geometries (one of the greatest challenges to computational modelling of combustion products) [94].

Specifically for this work, the hydrogen fuel typically does not produce any type of particulate matter, since hydrogen fuel does not contain any carbon atoms. Thus, soot modelling isn't a priority for these simulations, nor for the control simulations where Jet A is used. For these reasons, this process will not be considered.

3.4.5 Oxides of Nitrogen (NO and NO_2)

According to Lefebvre and Ballal [41], in conventional gas turbine combustors, there are four main mechanisms responsible for the NOx (NO plus NO_2) formation: prompt NO, thermal NO, nitrous oxide (N_2O) mechanism, and fuel NO. The last one is usually of minor importance for normal fuels (there is no fuel-bond nitrogen). In the case of hydrogen burning, the NO formation through intermediate NO_2 must also be considered [76].

For hydrocarbon fuels, the two main mechanisms responsible for NOx formation are the thermal NO and prompt NO, while for hydrogen flames the two main mechanisms associated with NOx formation are the thermal NO and NO formation through intermediate NO_2. It should be noted that under specific conditions the nitrous oxide (N_2O) mechanism can also become relevant for the hydrocarbon fuels. So, in this subsection only these four mechanisms will be referred. For more information about the other, there are good reviews in Kenneth Kuo [40] and Lefebvre et Ballal [41].

The thermal NO is produced by the oxidation of atmospheric nitrogen (N_2) in high-temperature regions of the flame and in the post-flame gases [41]. This endothermic process is largely controlled by the flame temperature and it proceeds at a significant rate only at temperatures above around 1850K (it requires the breaking of the tight N_2 bond). For the typical conditions encountered in conventional gas turbine combustors (high temperatures for just a few milliseconds), NO increases linearly with residence time, but does not attain its equilibrium value [40, 41, 76].

The extended Zeldovich mechanism is utilized by most of the reaction schemes proposed for thermal NO. The principal reactions of this mechanism are represented in Equations (3.1) to (3.4).

$$O_2 \leftrightharpoons 2O \tag{3.1}$$

$$N_2 + O \leftrightharpoons NO + N \tag{3.2}$$

$$N + O_2 \leftrightharpoons NO + O \tag{3.3}$$

$$N + OH \leftrightharpoons NO + H \tag{3.4}$$

The rate at which NOx can be produced by Zeldovich mechanism can be estimated through the equilibrium concentration of O_2 in the post-flame zone through Equation (3.5).

$$\frac{d[NO]}{dt} = 6 \times 10^{16} T_{eq}^{-0.5} \exp\left(\frac{-69.090}{T_{eq}}\right) [O_2]_{eq}^{0.5} [N_2]_{eq} \tag{3.5}$$

Where the units are given in $\left[\frac{moles}{cm^3 sec}\right]$.

The prompt NO can be formed in a significant quantity in some combustion environments such as in low-temperature, fuel-rich conditions and when residence times are short. These conditions can be created in gas turbines [70].

In hydrocarbon flames, prompt NO occurs in the earliest stage of combustion and its formation is associated to the reaction of molecular N_2 with radicals, such as C, CH and CH_2, which are fragments derived from fuel, through a complex series of reactions and many possible intermediate species. Some of these reactions are represented in Equations (3.6) to (3.10).

$$CH + N_2 \rightleftharpoons HCN + N \tag{3.6}$$

$$N + O_2 \rightleftharpoons NO + O \tag{3.7}$$

$$HCN + OH \rightleftharpoons CN + H_2O \tag{3.8}$$

$$CN + O_2 \rightleftharpoons NO + CO \tag{3.9}$$

$$CH_2 + N_2 \leftrightharpoons HCN + NH \tag{3.10}$$

For hydrocarbon flames the major contribution is from CH and CH_2 species, as shown in Equation (3.6) and Equation (3.10). The products of these reactions can lead to the formation of amines and cyano compounds, which can subsequently react with species like N, O or OH to form NO by reactions such as those that occur in the oxidation of fuel nitrogen, as shown in Equation (3.11), or in the oxidation of other nitrogen species, such as Cyanonaphthalene (NCN), as shown in Equations (3.12) and (3.13):

$$HCN + N \rightleftharpoons N_2 + \cdots \tag{3.11}$$

$$NCN + OH \rightleftharpoons NO + HCN \tag{3.12}$$

$$NCN + O \rightleftharpoons NO + CN \tag{3.13}$$

Currently, the prompt NO contribution to total NOx from stationary combustors is small. However, as NOx emissions are reduced to very low levels by employing new strategies that tend to reduce the flame temperature (such as burner design or geometry modification), the relative importance of the prompt NO is expected to increase [70].

Regarding the intermediate N_2O mechanism, this mechanism is initiated by the reaction [76]:

$$N_2 + O \rightleftharpoons N_2O \tag{3.14}$$

and the nitrous oxide (N_2O) formed is then oxidized to NO mainly by the reaction:

$$N_2O + O \rightleftharpoons NO + NO \tag{3.15}$$

but also by the reactions:

$$N_2O + H \rightleftharpoons NO + NH \tag{3.16}$$

$$N_2O + CO \rightleftharpoons NO + NCO \tag{3.17}$$

For hydrogen flames the second relevant mechanism for the NOx emissions corresponds to the NO formation through intermediate NO_2. This mechanism may be represented by the Equations (3.18) and (3.19) [76]:

$$NO + HO_2 \rightarrow NO_2 + OH \tag{3.18}$$

$$NO_2 + H \rightarrow NO + OH \tag{3.19}$$

3.4.6 Influence of temperature and pressure in NOx formation with hydrogen fuel

Due to the high adiabatic flame temperature of hydrogen, its combustion produces significant NOx. Therefore, by increasing the strain rate (a_s), which is a pressure dependent parameter, the flame temperature can be reduced, lowering the emissions of NOx. Thus, the pressure can also be a controlling parameter for NOx formation with hydrogen flames.

So, the thermal NO mechanism is dominant at low pressures, whereas NO formation via intermediate NO_2 becomes important at moderate pressures, since, in that condition, the flame temperature decreases for a given strain rate, a_s, due to enhanced recombination by the reaction [76]:

$$H + O_2 + M \rightarrow HO_2 + M \tag{3.20}$$

Consequently, the maximum NO formation decreases for moderate pressures [76].

At higher pressures, the net effect of reactions (3.18) and (3.19) is to $H+HO_2 \rightarrow 2OH$, through which the radicals H, OH, and O are produced [76]. This enhances the formation of thermal NO. Some studies report that under specific conditions, the formation of NO can be dominant over NO_2.

Still considering the influence of pressure, but now for hydrocarbon fuels, the N_2O and prompt NO mechanisms are pressure independent and dominate at low temperatures, while the higher NOx levels associated with higher combustion temperatures are primarily due to thermal NO, which exhibits a square-root dependence on pressure [41].

3.5 Chemical kinetics

Chemical kinetics is a key point when modelling a combustion problem. In the present case, the fuel combustion kinetics is extremely important to develop a model that allows a good emission forecast from the engine. Without proper kinetics all the attempts will be in vain.

The development of detailed chemical kinetic models is extremely challenging, as typical fuels (such as gasoline, diesel and jet fuels) derived from different sources can be composed of hundreds to thousands of compounds [95]. Lu and Law [96] explained the importance of comprehensiveness of detailed chemistry. However, accommodating realistic fuel chemistry with current computational resources is quite difficult. Therefore, detailed kinetic models for such fuels cannot contain all the compounds [95, 96, 97]. These facts suggest that detailed chemistry has a restricted use in CFD.

As a mitigation measure, researchers have to put their emphasis on finding optimization techniques for mechanism reduction [96, 97]. Thus, a simplified mixture called surrogate mixture must be defined and used before attempting to develop a new kinetic model. The criteria and processes of developing a surrogate mixture are not unique. However, a proper surrogate fuel must have physical and chemical properties equivalent to those of the fuel it is representing. For instance, Violi et al [98] developed a JP-8 surrogate based on the following criteria:

- It was assumed that chemical kinetics for each candidate fuel was known.
- Simplicity must be maintained due to limited computational capabilities.
- The surrogate was required to match practical fuels in both physical and chemical properties:
  - volatility - boiling range and flash point;
  - sooting tendency - smoking point and luminous number;
  - combustion properties - heat of combustion, flammability, and reaction rates.

Furthermore, for kinetic model development, general procedures require data such as concentration profile versus time, concentration profile versus temperature, and concentration profile versus distance to the burner.

For the emission predictions, the kinetic model development can be even more difficult, since the NOx chemistry must be developed together with fuel chemistry, making realistic chemistry getting even more complicated [103].

In the following, the Jet A and hydrogen combustion kinetic models applied in this study will be introduced.

3.5.1 Jet A

Although jet fuel kinetic models are still under developed, significant progress has been made in this area in the recent decades. Jet fuels are kerosene-type cut of petroleum containing C-10 to C-18 hydrocarbons, including alkanes, cycloalkanes and aromatic compounds. Literature reviews show that there are several kinetic models available for jet fuel combustion and some of these models were listed (and briefly descripted) by Mostafa [99]. However, only a small number of them are suitable to satisfy the current needs of this work.

Based on the objective of predicting aircraft engine emissions (specifically NOx) using CFD simulation, it is necessary to find, at first, a jet fuel kinetic mechanism that allows to simulate the combustion process and then, one that fairly predicts the NOx formation in this combustion chamber. As CFD with kinetic models is computationally expensive, also the number of species in the kinetic scheme needs to be limited. Therefore, after evaluating the kinetic models available, there were found two mechanisms that meet "partially" the requirements for this work (Kundu et al. [100] and Wang [130]). However, as the main purpose of the kinetic scheme presented by Wang [130] for aviation kerosene (based on 10 species) is to predict soot formation in CFD computation, the option presented by Kundu et al. [100] ended up being chosen.

Kundu et al. [100] proposed a simplified kinetic mechanism with NOx chemistry based on 17 species and 26 reaction steps for Jet A (17 steps for Jet A reaction and 9 steps for the sub-mechanism for NOx prediction). This mechanism was developed specifically to predict the NOx formation during combustion of aviation kerosene. However, the mechanism does not cover the entire range of pollutant species, since to limit the number of species, the mechanism does not include NO_2. Despite the limitation of this kinetic model, it was used in this work. This was not a perfect option, but among the available ones it was the least bad.

3.5.2 Hydrogen

The hydrogen oxidation chemistry represents the most fundamental and important building block in the hierarchy of hydrocarbon chemistry. Consequently, its chemistry has been extensively investigated, and a large number of detailed mechanisms (which can be found in the literature), including H_2/O_2 kinetics, have been developed and validated using different combustion configurations [43, 76]. Some of these mechanisms have been optimized for the combustion of pure hydrogen, but most of them are dedicated to the combustion of hydrocarbons including sub-mechanisms for H_2/O_2 chemistry. However, the accuracy of the H_2/O_2 subset is fundamental for the overall performance of the hydrocarbon mechanism [43].

To choose the most suitable kinetic model for the present case, some reviews available in the literature [43, 101] were analyzed. For instance, Ströhl et al. [43] made an evaluation of detailed reaction mechanisms for hydrogen combustion under gas turbine conditions. This study shown that the mechanisms of Li et al. and Ó Conaire accurately represent the

H_2/O_2 kinetics under gas turbine conditions. According to the authors, the almost equally good performance of these two mechanisms at elevated pressures was not surprising, since they used the same experimental data for model development. However, the study suggests that the Li et al. mechanism is best suited for the prediction of H_2/O_2 chemistry as it includes more up-to date data for the range of interest [43].

Furthermore, the Li et al. mechanism has also been found to provide the best match with measurements over a wide range of equivalence ratio and pressure, using various targets, including shock tube ignition delay and laminar flame speed data [101].

Thus, after analyze those reviews, it was concluded that the Li et al. mechanism [63] should perform better than the others and for that reason it will be used in this work. For the NOx prediction (of hydrogen burn) was used the NOx sub-mechanism based on the study made by the Glarborg group [102], which is available in the database of ANSYS Fluent 2020R2 together with the mechanism of Li et al.

3.6 Fuel Properties

A number of properties both physical and chemical are used to define the composition and performance of a gas turbine fuel. Fuel characteristics such as density, heating value, boiling point, viscosity, ignitability and so on are essential to design combustion systems. These properties may be used to define operational parameters or to form part of a specification against which the fuel is produced.

Thus, in the following, firstly, the general properties of a fuel will be defined, and then, the properties related with the ignitability and interchangeability for liquid and gaseous fuels will also be presented.

3.6.1 Density

The expression of the mass/volume relationship for fuels that is used in accordance with standard metric practice is density (mass per unit volume), represented by ρ and expressed in kg/m^3 at 15°C [71].

For gases, the density of pure substances and gaseous mixtures can be calculated from several accurate equations of state, which relate density to temperature and pressure. Most equations of state are accurate only when density is substantially lower than the critical density of the substances, although several have been developed to maintain accuracy up to 2.5 times the critical density [40].

In general, the density of a fuel decreases with an increase in temperature [71]. For the liquid hydrocarbons, the density increases with an increase in the carbon chain length [76].

3.6.2 Relative Density

The mass/volume relationship is frequently expressed in terms of relative density, d_r, formerly called specific gravity. This parameter consists in the ratio between the fuel density and the density of water, and it is a dimensionless quantity normally referenced at 15.6°C (60°F) [71]. The relative density of a fuel is related to its average boiling point and chemical composition. This parameter, in addition of being easy to determine, provides a useful indication of hydrogen/carbon ratio, calorific value, and tendency toward carbon formation [41].

3.6.3 Calorific (or Heating) Value

The calorific (or heating) value, CV, of a fuel is a measure of the energy available in that fuel for conversion to mechanical work when it is burned to completion under standard conditions and it is equal to the symmetric of the enthalpy of reaction per mass of fuel [40, 71]. On a gravimetric basis, calorific value can be described as specific energy; and on a volumetric basis, as energy density. Heat of combustion (Δhc) is also a term that is synonymous with calorific value [40, 71]. The units for calorific value for hydrocarbon fuels, used in accordance with SI metric practice, is the megajoule (MJ), expressed on a mass basis in kilograms, MJ kg^{-1}, or volume basis in liters. Fuel specification requirements for calorific value are normally expressed on a mass basis [71]. It should be noted that the standard state calorific values (or heating values) for the large majority of fuels are presented in the literature.

For the fuels, it is possible to define two calorific values (or heating values):

- Higher Heating Value (HHV), which is the heat of combustion calculated, with the assumption that all the water in the products has condensed to the liquid state;
- Lower Heating Value (LHV), which is the heat of combustion calculated, with the assumption that all the water in the products is in the gaseous state.

The two heating values previously defined can be related by Equation (3.21):

$$\mathrm{HHV} = \mathrm{LHV} + \mathrm{h_v} \times \left(\frac{\mathrm{n_{H_2O,out}}}{\mathrm{n_{fuel,in}}} \right) \tag{3.21}$$

The amount of energy released in the combustion is larger when the water in the products is considered in liquid state than when the water is considered in the gaseous state.
For gas turbine fuels, the lower calorific value is more relevant than the higher calorific value, since the final products of complete combustion are mainly CO_2 and water vapor. For this reason, in this work, the LHVs of the fuels will be used.

3.6.4 Mixture Calorific Value (H_{mix})

The mixture calorific value (H_{mix}) is defined as the heat output upon combustion of a unit volume of a stoichiometric air–fuel mixture. In the case of a liquid fuel such as diesel, H_{mix} would be the calorific value of diesel burned in a mixture with air, since the volume occupied by the diesel is negligible in the volume of air–fuel mixture. However, when a gaseous fuel is used, the volume occupied will include the volume of air plus fuel [76]. Therefore, in the case of gaseous fuels, the mixture calorific value is given by Equation (3.22):

$$\mathrm{H_{mix}}\ [\mathrm{MJ\ m^{-3}}] = \frac{\mathrm{CV}\ [\mathrm{MJ\ m^{-3}}]}{1 + (\mathrm{air/fuel\ stoichiometric\ ratio})} \tag{3.22}$$

This property is of significance today because gaseous fuels are being more and more used in gas turbine engines and therefore the relative performance of the various available gaseous fuels needs to be predicted.

3.6.5 Volatility Point

The ease with which a fuel can be converted into the vapor state is defined by its volatility. This property may be assessed from the knowledge of its distillation range, vapor pressure and flash point (all explained in the following) [41].
It should be noted that, generally, increased volatility affects combustion performance by providing easier light up, improved stability, and higher combustion efficiency [41].

3.6.6 Distillation Range

The distillation range of a fuel largely determines the physical and combustion characteristics of that fuel. Since practical fuels are a mixture of many compounds, each having its own boiling point, these fuels have no single boiling point, but rather a distillation range, which is defined by a temperature versus percentage of fuel evaporated relationship and provide information on the boiling point distribution of its component fractions [71, 76]. The 10% and 20% distillation points of aviation fuels (temperatures at which 10% and 20% of the product has been recovered) are measures of volatility used to assess ease of starting, fuel "boil-off" at altitude and it is still related to its flammability and safety in handling [71]. The 90% distillation point is frequently used to control the quantity of higher boiling components that may be difficult to vaporize and whose presence may affect engine performance [71].

It should be noted that this fuel property has also a dominating influence on the availability, which is increased by widening the boiling range, or by lowering the initial boiling point, or both [41].

3.6.7 Vapor Pressure

The vapor pressure of a liquid is the pressure exerted by the vapor above its surface at a given temperature [41]. For a hydrocarbon mixture the vapor pressure will depend on the temperature (vapor pressure increases with it) and the boiling point distribution of its components [71].

A high vapor pressure ensures rapid evaporation of fuel in the primary combustion zone; on the other hand, low vapor pressure has advantages in terms of reduced pressure in unvented fuel tanks, lower fuel losses due to evaporation at high altitudes in vented fuel tanks, and reduced fire hazard [41].

3.6.8 Flash Point

The flash point of a fuel is the lowest temperature at which its vapor pressure is sufficient to form a flammable mixture (fuel vapor/air) at atmospheric pressure. The higher the vapor pressure, the lower the flash point [41]. Thus, the flash point in effect approximates to the lower flammability limit.

Generally, the flash point is used to provide an indication of the maximum temperature at which a fuel may be handled or stored in a normal manner without a serious fire hazard [71].

3.6.9 Viscosity

The viscosity of a fuel (or any fluid) is a physical property that consists in the measure of its internal resistance to flow caused by intermolecular forces. These forces appear as shear stresses between the moving layers of fuel [71].

The viscosity of a fuel is usually determined experimentally together with density, since the fuel flows through the viscometer under gravity. The viscosity so measured is called the kinematic viscosity, ν, and can be determined through Equation (3.23) [71]:

$$\nu = \mu . \rho \tag{3.23}$$

Where, ρ, is the density of fuel at the temperature of viscosity measurement, and, μ, is the coefficient of dynamic viscosity, which is defined as the ratio between the shear stress and the rate of shear.

In gases, cohesion is weak, but molecular transfer between molecules is significant. So, as in gases the molecular transfer increases with temperature, the gas viscosity also increases. However, for the liquids, the viscosity generally decreases as temperature increases due to weakened cohesion of the molecules [40].

For liquid fuels, the viscosity depends mainly on the chemical composition of the hydrocarbons contained in the fuel and increases with an increase in the carbon chain length [41].

It should be noted that viscosity has a marked effect on the formation of a well-atomized spray and hence on the rates of fuel evaporation and combustion. The higher the viscosity of a fuel, the poorer the quality of atomization for liquid fuels. This property also affects the power required to pump the fuel through the fuel system [41].

3.6.10 Freezing Point

The prime specification requirement covering the low temperature flow properties of aviation fuels is the freezing point. This one consists in the temperature at which a fuel first shows the presence of solid particles or wax crystals as its temperature is decreased. In other words, the freezing point of a fuel is defined as the temperature at which the last wax crystals melt when warming the solidified fuel [41]. This having into account that practical fuels are a mixture of many compounds.

3.6.11 Autoignition Temperature

The autoignition (or spontaneous ignition) temperature, AIT (or SIT), is defined in ASTM E 659 as the lowest temperature at which the fuel will produce hot-flame ignition in air at atmospheric pressure without the aid of an external source such as a spark or flame. It is the lowest temperature to which a combustible mixture must be raised so that the rate of heat released by the exothermic oxidation reaction exceeds the rate at which heat is lost to the surroundings, causing ignition. The autoignition temperature is not purely a function of the fuel consumption, but is also strongly dependent upon the environment in the ignition area [71].

3.6.12 Smoke point

The smoke point is probably the most widely used index of soot-forming tendency. This parameter is defined in ASTM D 1322, and it is determined experimentally by burning the fuel under test in a standardized wick lamp configuration and slowly increasing the height of the flame until it begins to smoke. The maximum height of smokeless flame in millimeters is the smoke point; the higher this value, the lower the tendency of the fuel to soot formation. For many aircraft fuels, the height of smokeless flame is specified to be not less than 25 mm [41, 71].

Although the smoke point is not a fundamental property of a fuel, it provides a very satisfactory indication of the propensity to form soot [41].

3.6.13 Luminometer Number (or Point)

The luminometer number is defined as being a measure of flame temperature at a fixed flame radiation level in the green—yellow band of the visible spectrum. This index is measured on a modified smoke lamp (ASTM D 1740) that includes thermocouples above and below the flame and a device for measuring flame radiation in the referred band of the visible spectrum. Through this, it is possible to obtain a curve of flame radiation against temperature rise across the burner [41, 71].

At a standardized level of radiation, the temperature rise, ΔT, across the flame is measured for the test fuel and compared with the corresponding values for isooctane (a paraffin) and tetralin (an aromatic), which are assigned values of 100 and 0, respectively. According to Lefebvre and Ballal [41], the luminometer number of the test fuel is then expressed as:

$$Luminometer\ number = 100\frac{\Delta T_{test\ fuel} - \Delta T_{tetralin}}{\Delta T_{isooctane} - \Delta T_{tetralin}} \tag{3.24}$$

The concept of luminometer number was introduced in the late 1950s in the hope that it would provide a more accurate description of the radiation signature of a fuel than is given by the smoke point. These early expectations were not fully realized in practice, and the apparatus and test method are no longer in common use. Luminometer number and smoke point are in effect measuring essentially the same property and the relationship between the two is shown in ASTM D 1740 [41, 71].

3.6.14 Ignitability and Interchangeability Properties for Liquid and Gaseous Fuels

To define the ignition tendency of different fuels in combustion engines, there are several technical parameters that can be used. Some of these parameters are the octane number and cetane number, which are applied to gasoline and diesel (or kerosene) engines, respectively. For the gaseous fuels, the methane number is usually the parameter used to define the ignition tendency.

About the interchangeability of fuels, this process is more likely to occur with gaseous fuels and the Wobbe Number is the parameter that helps to analyze that capacity.

In the following all these parameters will be briefly described.

3.6.14.1 Octane Number and Cetane Number

The octane number represents the knocking tendency of a gasoline fuel and it is critical in spark-ignited combustion engines [105]. This parameter is determined by comparing, under standard conditions, the knock tendency of the fuel in study with that of a blend of two reference fuels: iso-octane, which resists knocking, and heptane, which knocks readily. So, the octane number is the percentage by volume of iso-octane in the iso-octane–heptane mixture that matches the knocking tendency of the fuel being tested in a standard test engine.

The cetane number (CN) is an indicator of the ignitability of diesel (or kerosene) fuels. This parameter is determined by comparing, under standard conditions, the ignition quality of the fuel in test with that of a mixture of two reference fuels, the n-hexadecane (formerly cetane) and 1-methylnaphthalene. So, the cetane number describes the percentage of cetane found in the mixture of those reference fuels that corresponds to the same ignition quality of the fuel being tested in a standard test engine.

Generally, gasoline fuels have to exhibit a high resistance to ignitability expressed by the research octane number (RON) and diesel/kerosene fuels a good ignitability, expressed by the cetane number (CN) [106, 107].

It should be noted that the CN increases with the carbon number, also increasing the ignitability, and the effect of the molecule structure is as distinctive as that of the carbon number [106, 107].

3.6.14.2 Methane Number (MN)

With the use of alternative gaseous fuels, also their knocking tendency needs to be measured and represented. The knock measurement for these fuels was standardized in 1930 and the ASTM established a standard for gaseous fuel knock testing in terms of the motor octane number (MON) method. The MON method has an upper limit of 120 and therefore is suitable for gases such as LPG. However, since many alternative gaseous fuels were found to have MON values greater than 120, it was necessary to develop a new rating system extending the measurable range beyond MON.

The term Methane Number (MN) was then defined as the percentage by volume of methane blended with hydrogen that exactly matches the knock intensity of the gas mixture tested under specified operating conditions in a knock testing engine. For the range beyond 100 MN, methane–carbon dioxide mixtures were used as reference mixtures. In this case, in accordance with the definition, the MN is 100 + the % $\mathrm{CO_2}$ by volume in the reference methane–carbon dioxide mixture [105].

3.6.14.3 Wobbe Number (W_o)

The Wobbe number (W_o) is the parameter that determines if the interchangeability of two gaseous fuels in a burner is possible. This means that, for the same burner, pressure drop across the burner orifice and orifice area, when the heat release rates are similar for both fuels, then these fuels may be used interchangeably.

This parameter, which is derived from the calorific value and the specific gravity (in practice, the specific gravity with respect to air is used instead of density), is given by Equation (3.25).

$$W_o = \frac{\mathrm{CV}}{\sqrt{\mathrm{sp.\,gr.}}} \tag{3.25}$$

This is a dimensional number and depends on the units chosen [76].

Chapter 4 – Methodology, Modelling and Computation

To solve combustion problems there are three basic approaches that can be considered, consisting of theoretical, numerical and experimental approaches. Any combination of these methods can still be used [40].

To be economic and efficient, it is essential to apply correctly the basic principles of the phenomena that occur in combustion, and whenever possible, it is best to be able to tackle combustion problems both theoretically and experimentally to improve the results' credibility [40].

In the present case of study, the numerical approach will be used to model the combustion problem together with some experimental data obtained from previous works. However, for this approach, some caution is necessary regarding the results, since the experimental data for the hydrogen fuel are not available and the experimental infrastructure to obtain these values would be extremely expensive to build and operate. Thus, this section will first be used to explained the purposes of modelling combustion problems, and some of the techniques and models used to accurately represent the phenomena that occur inside the combustion chamber. Then, the methodology followed to accomplish the objectives purposed in Chapter 1 is explained. Finally, the computational methods and controls utilized to obtain the results and the techniques used for their verification are also presented.

4.1 General Objectives and Application of Combustion Modelling

According to Kuo [40], the typical objectives of combustion modelling are:

- Simulate certain combustion processes;
- Substitute difficult or expensive experiments, like the one in study;
- Develop predictive capability for combustion systems under various operating conditions;
- Determine the effect of individual parameters in combustion processes by conducting parametric studies;
- Guide the design of combustion experiments;

- Help in interpreting and understanding observed combustion phenomena, e.g., in experimental works.

Taking these objectives into account, it is possible to conclude that combustion modelling, especially when using Computational Fluid Dynamics (CFD), provides a virtual laboratory to perform the experiments in the early stages of the design phase without building the physical devices [109]. Moreover, CFD simulations can help to understand the mechanisms and phenomena that underlay flames (or explosions) and to determine their possible behavior when varying initial/operating conditions or geometric parameters. This is extremely helpful to select the key conditions and parameters at the design and operation stages, which is essential for effective and safe engineering practice [76].

In contrast to simple empirical or lumped-element models, CFD models take into account the interactions between chemical reactions, transport phenomena, flow field and geometry that occur in flames/explosions [76]. Thus, the correct use of CFD simulations usually helps to decrease the unit design costs and also the number of unsatisfactory experimental devices.

The CFD simulations can be performed using a commercial or own software with the same base. In this work, it was opted for the use of a commercial CFD software, the ANSYS Fluent 2020R2. ANSYS is a software package that spans the entire range of physics, providing access to lots of fields of engineering simulation that a design process requires. Fluent's models are focused on fluid flows and chemical reactions, including a very good model to run first-approach simulations of combustion systems [109].

Generally, the readiness of a numerical CFD study related to combustion in a gas turbine combustor can be assessed by the prediction capability of critical performance characteristics such as pollutant emissions, exit temperature profiles, wall temperatures, lean blowout (LBO), among others. Moreover, to ensure that CFD is a reliable tool in this type of application, there are four steps that must be taken into account [110]:

1. A study regarding the available turbulence models against standard benchmark cases. This is important because it helps to predict the capability of the solver and to choose the adequate turbulence model for CFD modelling.
2. An accurate prediction of the cold flow field that goes through and around the combustor, which includes the pressure, the velocity, the turbulence distribution, and the air flow that goes through the multiple inlet ports of the combustion chamber.
3. A state-of-art modelling of the fuel atomization process, which in turn results in an accurate estimation of the spray quality.

4. An appropriate choice of the chemistry model, along with a turbulence/chemistry interaction model, and a well-established process to use them. These aspects are very important to predict the characteristics of the chemical reacting flow within the combustor.

Although the fuel atomization is one of the most important aspects to be considered in this type of studies, since it directly affects combustion efficiency and emissions, this process was not considered due to the complexity of the present study.

It should be noted that except the fuel atomization model, all the other points mentioned were considered for this work.

4.2 Numerical Models

This subsection will be used to introduce some of the models and techniques that are usually applied in gas turbine combustion problems to accurately represent turbulence and heat transfer, and still to justify, theoretically, the reasons for using the models chosen in this work.

4.2.1 Turbulence Modelling

Turbulence is one of the principal unsolved problems in physics today and its modelling is one of the major issues that affect the precision of current numerical simulations in engineering applications, particularly for reacting flows. Turbulence is characterized by irregularity or randomness, diffusion, vortices, viscous dissipation and involves a wide range of time and length scales [57].

It is possible, in theory, to directly resolve the whole spectrum of turbulent scales using an approach known as direct numerical simulation (DNS), in which the Navier-Stokes equations are numerically solved without the need to use turbulence models [111, 112]. However, it is not feasible for practical engineering problems, since, due to the wide range of length scales and the complexity of phenomena involved in turbulence, this process is computationally expensive to simulate, especially in problems involving flows with high Reynolds numbers [111, 112].

For the current computational capacities, direct numerical simulations of turbulent flows remain practical only for very simple geometries, involving low Reynolds numbers [57, 59, 111, 112].

Instead of DNS, the exact governing equations can be time-averaged, ensemble-averaged, or otherwise manipulated to remove the resolution of small scales, resulting in a modified set of equations that are computationally less expensive to solve [111].

Simplifications such as those mentioned gave rise to two of the most commonly used numerical simulation methods today, the Reynolds Average Navier-Stokes (RANS) simulation and the Large Eddy Simulation (LES). A schematic comparison between all the referred models is represented in Figure 4.1.

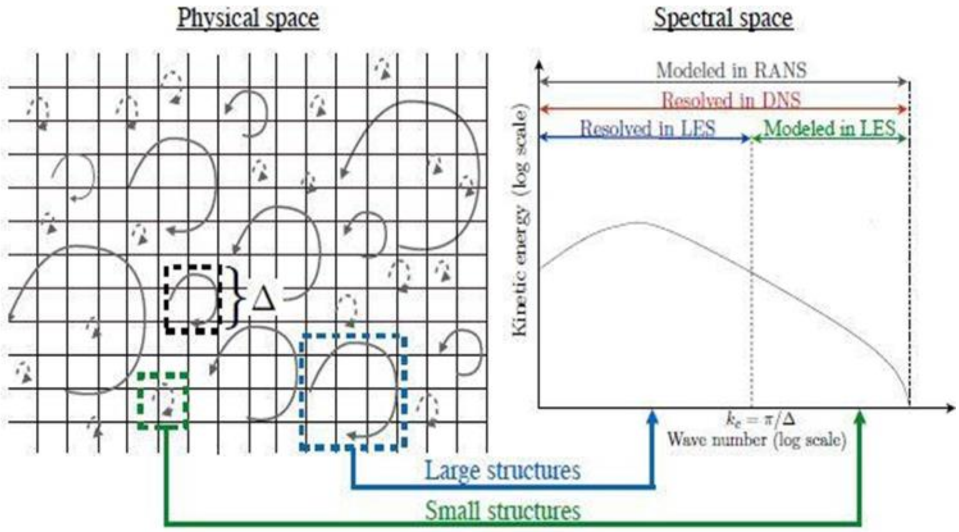

Figure 4.1: Comparison of DNS, LES and RANS simulation techniques on an idealized non-reacting homogeneous and isotropic turbulent flow [113].

Looking at Figure 4.1 and assuming that the symbol Δ stands for the LES filter size, it is possible to verify that only large turbulent structures are resolved in LES (solid line arrows) while structures smaller than the filter size Δ are modelled (dashed line arrows). Furthermore, all turbulent structures are modelled in RANS (solid and dashed arrows) and all turbulent structures are resolved in DNS (solid and dashed arrows).

According to Ansys [112], RANS models offer the most economic approach for computing complex turbulent industrial flows and usually provide the level of accuracy required. Typical examples of such models are the k-ε or the k-ω models in their different forms. These models simplify the problem to the solution of two additional transport equations and introduce an Eddy-Viscosity (turbulent viscosity) parameter to compute the Reynolds Stresses. The Reynolds Stress Model (RSM), which is a more complex RANS model, includes several effects that are not easily handled by Eddy-Viscosity models. For that, this model solves an individual equation for each of the six independent Reynolds Stresses directly plus a scale equation (ε-equation or ω-equation). The most important effect of this model is the stabilization of turbulence due to strong rotation and streamline curvature (as observed for example, in cyclone flows), improving the results especially for flows with strong swirl and rotation. However, RSM generally requires a significant increase in computation time, partly due to the additional equations, but mostly due to reduced convergence.

Excluding the DNS approach, the alternatives to RANS models are models that resolve at least a portion of the turbulence for at least a portion of the flow domain, generally termed 'Scale-Resolving' (SRS) models. The most widely known SRS modelling concept is Large Eddy Simulation (LES). This model is based on the approach of resolving large turbulent structures in space and time down to the grid limit everywhere in the flow. However, LES has very limited impact on industrial simulations because of the excessively high-resolution requirements for wall boundary layers. This happens due to the fact that, near the wall, the largest scales in the turbulent spectrum are, nevertheless, geometrically very small and require a small time step and a very fine grid, thus requiring a high computational cost. For this reason, the use of LES is only recommended by ANSYS for flows where wall boundary layers are not relevant and do not need to be resolved, or for flows where the boundary layers are laminar due to the low Reynolds number [112].

To avoid the high-resolution requirements of LES, numerous hybrid models have been developed in recent years. These are models that combine certain elements of RANS and LES approaches in a way that allows the simulation of high Reynolds number flows. With hybrid models, the attached wall boundary layers are typically covered by the RANS part of the model, while large detached regions are handled in LES mode, i.e., with a partial resolution of the turbulent spectrum in space and time. However, this models still require a considerable computing power.

4.2.1.1 Choosing the Turbulence Model

Despite the considerable progress in turbulence modelling, it is an unfortunate fact that no single turbulence model is universally accepted as being superior for all classes of problems. Generally, the choice of a turbulence model will depend on considerations such as the physics of the flow, the established practice for a specific class of problem, the level of accuracy required, the available computational resources and the amount of time available for the simulation. Therefore, it is important to understand the advantages and shortcomings of these models to make the most appropriate choice for each application [57, 112].

The ANSYS Fluent software, used in this study, provides a large set of options for turbulence modelling and a very detailed description of all these models is made in ANSYS Fluent Theory Guide [111].

To pick the best turbulence model for this work, an analysis was made of some reviews about the performance of the models available in Fluent when applied to reacting flows on a combustion chamber. There are several works in the literature where this type of assessment is done. For instance, A. Benedetto and V. Sarli [59] in their review affirm that for turbulent combustion problems, the improved representation of turbulence provided by LES implies a better description of the flame-turbulence interaction with respect to classical RANS methods. Moreover, LES grasps the inherently unsteady nature of turbulent flows and, thus, of transient combustion phenomena. On the other hand, when performing RANS, only the time dependence of statistical mean quantities is captured, and all the details about their unsteadiness are lost. So, LES can be seen as a truly predictive tool, whereas, RANS models are simply a posteriori descriptive tools, i.e., to reproduce flame speeds and pressure peaks, they need experimental data to compare and validate numerical results by an *ad hoc* tuning of model constants/parameters. Therefore, results cannot be extrapolated outside their range of validation.

In other study, G. Boudier et al. [58] studied some specific aspects of an aeronautical gas turbine combustion chamber (multiple inlets, multi-perforated plates and film cooling) using LES and comparing the results with predictions provided by Reynolds Averaged Navier–Stokes (RANS) simulations and experimental measurements. The authors concluded that the application of LES is of great interest for design purposes because of the capacity to predict unsteady turbulent reacting flows and yield information that is not accessible with conventional numerical approaches. Other conclusion is that the mean temperature fields within the chamber, provided by LES, were observed to be sharper and to reach larger values. The assessment of the predictions in terms of the profile of the mean exit temperature heterogeneities seen by the turbine proves LES to be very promising and out-performing RANS.

In both studies [58, 59], the authors concluded that LES is superior with respect to RANS, unfortunately, it is also much more computationally demanding. Moreover, the current computational capabilities continue to be favorable to RANS, especially in the industrial context. So, RANS turbulence models still remain the only viable methodology for modelling real-scale explosions/flames and for the development of advanced combustion systems in the foreseeable future. However, they must be used with the full awareness of their limitations.

In another review, L. Jiang [57] tested six of the most widely used RANS turbulence models in practical engineering, i.e., a second moment closure (RSM), and five two-equation eddy-viscosity models (standard k-ε, RNG k-ε, Rk-ε, standard k-ω and SST k-ω), to analyze their performance modelling the turbulence in a model combustor. According to the author, all six turbulence models can capture the flow features or patterns. However, for the quantitative predictions of velocity, temperature and species fields, different levels of performance were revealed. The RSM model gave the best performance, and it was the only one that could accurately predict the lengths of the recirculation zones and offer reasonable prediction on the turbulence kinetic energy distribution in the combustor. In addition, the performance of the Rk-ε model was better than the other four two-equation models, and for that case, it gave similar results to those of the RSM.

Considering all the information collected, and the available time and computational power, it was decided to use the RSM in this study after performing some initial tests with the RSM and the realizable k-ε turbulence models.

4.2.1.2 Governing Equations

For the fluid flows, the basic conservation principles are based in mass (continuity), momentum, energy and species [69, 111].

In Reynolds averaging, the solution variables in the instantaneous (exact) Navier-Stokes equations are decomposed into the mean (ensemble-averaged or time-averaged) and fluctuating components. Substituting expressions of this form for the flow variables into the instantaneous continuity and momentum (or energy, or species) equations and taking a time (or ensemble) average (and dropping the overbar on the mean velocity, $\bar{u}$) yields the ensemble-averaged momentum equations, also known as Reynolds Averaged Navier-Stokes (RANS) equations [111]. They can be written in cartesian tensor form as:

- Continuity:

$$\frac{\partial \bar{\rho}}{\partial t} + \frac{\partial}{\partial x_i}(\bar{\rho}\tilde{u}_i) = 0 \tag{4.1}$$

- Momentum:

$$\begin{aligned} &\frac{\partial}{\partial t}(\bar{\rho}\tilde{u}_i) + \frac{\partial}{\partial x_j}(\bar{\rho}\tilde{u}_i\tilde{u}_j) - \frac{\partial}{\partial x_j}\left(\overline{\rho u_i'' u_j''}\right) \\ &\qquad - \frac{\partial}{\partial x_j}\left[\mu\left(\frac{\partial \tilde{u}_i}{\partial x_j} + \frac{\partial \tilde{u}_j}{\partial x_i} - \frac{2}{3}\delta_{ij}\frac{\partial \tilde{u}_i}{\partial x_i}\right)\right] = -\frac{\partial \bar{p}}{\partial x_i} \end{aligned} \tag{4.2}$$

- Scalar transport:

$$\frac{\partial}{\partial t}(\bar{p}\widetilde{\Upsilon}_\alpha) + \frac{\partial}{\partial x_i}(\bar{p}\tilde{u}_i\widetilde{\Upsilon}_\alpha) + \frac{\partial}{\partial x_i}\left(\overline{p u_i'' \Upsilon_\alpha''}\right) - \frac{\partial}{\partial x_i}\left(\Gamma_\alpha \frac{\partial \widetilde{\Upsilon}_a}{\partial x_i}\right) = \widetilde{\omega}_\alpha \tag{4.3}$$

These equations have the same general form as the instantaneous Navier-Stokes equations, with the velocities and other solution variables now representing ensemble-averaged (or time-averaged) values.

In laminar flows, the fluid stress is proportional to the rate of strain with the viscosity being a constant of proportionality [69]. In turbulent flows, the turbulent stress is related to the mean rate of strain through turbulent viscosity (μ_T). This is the so called Boussinesq hypothesis, and is represented in Equation (4.4).

$$-\overline{\rho u_i'' u_j''} = \mu_T\left(\frac{\partial \widetilde{u_i}}{\partial x_j} + \frac{\partial \widetilde{u_j}}{\partial x_i}\right) - \frac{2}{3}\bar{\rho}k\delta_{ij} - \frac{2}{3}\mu_T\frac{\partial \tilde{u}_k}{\partial x_k}\delta_{ij} \tag{4.4}$$

The Boussinesq hypothesis is used in the Spalart-Allmaras model, the k-ε models, and the k-ω models. The advantage of this approach is the relatively low computational cost associated with the computation of the turbulent viscosity, μ_T. In the case of the Spalart-Allmaras model, only one additional transport equation (representing turbulent viscosity) is solved. In the case of the k-ε and k-ω models, two additional transport equations (for the turbulence kinetic energy, k, and either the turbulence dissipation rate, ε, or the specific dissipation rate, ω) are solved, and μ_T is computed as a function of k and ε or k and ω. The disadvantage of the Boussinesq hypothesis as presented is that it assumes that μ_T is an isotropic scalar quantity, which is not strictly true, but typically works well for shear flows dominated by only one of the turbulent shear stresses.

The alternative approach, embodied in the RSM, is to solve transport equations for each of the terms in the Reynolds stress tensor. An additional scale-determining equation (normally for ε or ω) is also required. This means that five additional transport equations are required in 2D flows and seven additional transport equations must be solved in 3D [111].

In many cases, models based on the Boussinesq hypothesis perform very well, however, the RSM is clearly superior in situations where the anisotropy of turbulence has a dominant effect on the mean flow, such cases include highly swirling flows and stress-driven secondary flows.

As mentioned above, the turbulent viscosity, μ_T, can be calculated from the turbulence kinetic energy, k, and from the turbulence dissipation rate, ε [69]. These parameters are related through Equation (4.5).

$$\mu_T = C_\mu \bar{\rho}\left(\frac{k^2}{\varepsilon}\right) \tag{4.5}$$

4.2.1.3 Regimes of Turbulent Combustion

To derive models for turbulent combustion, a physical approach is required. One possible approach can be based on the comparison of the various time scales present in turbulent combustion. The Damköhler number, represented in Equation (4.6), is important because it allows to compare the turbulent (τ_t) with the chemical (τ_c) time scales.

$$D_a = \frac{\tau_t}{\tau_c} \tag{4.6}$$

When the Damköhler number is very large ($D_a \gg 1$), the flame front is thin and its inner structure is not affected by turbulence, which at most can wrinkle the flame surface [114]. This occurs when the Kolmogorov scales, which are the smallest turbulence scales, have a τ_t greater than τ_c, which means that the turbulent motions are too slow to affect the flame structure [114].

4.2.2 Heat Transfer Modelling

The flow of thermal energy from matter occupying one region in space to matter occupying a different region in space is known as heat transfer. For simulation purposes, the representation of this process is of major importance, since the heat transfers influence the temperature distribution across the chamber [115].

Generally, the heat transfer processes can occur by three main methods: conduction, convection and radiation [111]. The physical models involving only conduction and/or convection are the simplest, while models involving radiation are more complex to simulate inside a combustion chamber. In some applications of this nature, the thermal radiation can be dominant and be responsible for 96% of the heat transfers [111, 115]. Still considering the radiation component, it should be noted that both the walls and hot gases absorb and reflect part of this combustion energy.

For the present study, due to the properties of the fuels, when burning hydrogen in a combustor, the thermal energy radiated to the surroundings is usually lower than that of kerosene, thereby beneficially affecting the liner durability and liner cooling requirements. The reason for this phenomenon was explained by Haglind and Singh [28]. According to these authors, in most gas turbine combustors, a sizeable proportion of the heat transferred from the hot gases contained within the combustor to the liner walls is by radiation. Moreover, the total emitted radiation by the combustion gases generated when burning a fuel (for instance, kerosene) comprises two components:

- "nonluminous" radiation, which emanates from certain heteropolar gases notably, CO_2 and H_2O;
- "luminous" radiation, which depends on the number and size of the solid particles (mainly soot) in the flame.

At high levels of pressure like those that are usually encountered in modern gas turbine combustors, the flame is characterized by a predominance of luminous radiation [28]. Since no particles are present in the combustion gases generated when burning hydrogen, there is no luminous radiation, thus essentially lowering the total heat transfer by radiation when compared to the combustion gases of kerosene combustion [28].

To model the radiation in a combustion chamber, the main available types of radiative transfer equation (RTE) solution methods are the Discrete Ordinates Method (DOM), Spherical Harmonics Method (SHM), and the Photon Monte Carlo (PMC) Method [115]. Depending on the problem, ANSYS Fluent can solve a variation of the energy equation that takes into account the specified heat transfer methods. For the P-1 model (one of the SHM methods), the RTE is a diffusion equation, which is easy to solve with little CPU demand. This model includes the effect of scattering, and for combustion applications where the optical thickness is large, the P-1 model works reasonably well. In addition, the P-1 model can easily be applied to complicated geometries with curvilinear coordinates. The DO model spans the entire range of optical thicknesses and allows to solve problems ranging from surface-to-surface radiation to participating radiation in combustion problems. It also allows the solution of radiation at semi-transparent walls. For this model, the computational cost is moderate for typical angular discretizations and the memory requirements are modest. The Monte Carlo (MC) model can solve problems ranging from optically thin (transparent) regions to optically thick (diffusion) regions, like combustion. This model allows to calculate quasi-exact solutions and, although it is more accurate when compared to other available models, it has a higher computational cost [111].

Taking into account all that has been mentioned, the fact that the geometry in study is really complex, and the objective of reduce the computational cost, it was decided to use the P-1 model, since for the combustion of hydrogen fuel the radiation modelling is less relevant than other flow characteristics.

4.3 Methodology

In this subsection, the methodology followed to accomplish all the objectives proposed in Chapter 1 will be presented and described. In brief, this work was made through three iterative and consecutive phases that consisted of:

- Phase 1- Related to geometry and mesh;
- Phase 2- Related to the definition of simulation parameters (models, methods, boundary conditions, etc.) and to the calculation of the final results. This phase was subdivided in three subphases:
    - Phase 2.1- Where the first step was taken to define the boundary conditions through the data collected from Ribeiro [120];
    - Phase 2.2- Where the final boundary conditions for the air inlets used in the simulations were defined and where the final results were obtained for the control simulations (with Jet A fuel) through the data collected from ICAO [67] and Ribeiro [120];
    - Phase 2.3- Where the final results were obtained for the simulations for hydrogen fuel with the final boundary conditions for the air inlets obtained in phase 2.2;
- Phase 3- Related to the comparison and analysis of the results obtained in phase 2.

For a better comprehension of the reader, the explanation of these phases will be made in three steps. First, the objectives of each phase and subphase will be presented. Then, the methodology followed in each phase will be described in a brief way through diagrams presenting the set of tasks performed and identifying the initial values used and the final values obtained. Finally, a more detailed explanation will be made for the processes and methods involved in those tasks.

4.4 Phase 1: Geometry and Mesh

4.4.1 Objectives

In phase 1, there were two main objectives. The first was to analyze the combustor's CAD model received and correct any problems detected in this geometry. As will be explained later, some of these problems were detected through the analysis of the available engine documentation and others were detected in the preliminary results obtained while running the first simulations. The second objective was to create an independent mesh with good quality, i.e., good orthogonal quality, aspect ratio and skewness, to allow the simulation of the desired operating conditions needed to realize this work.
The iterative process followed in this phase is represented, in a simplified way, in Figure 4.2.

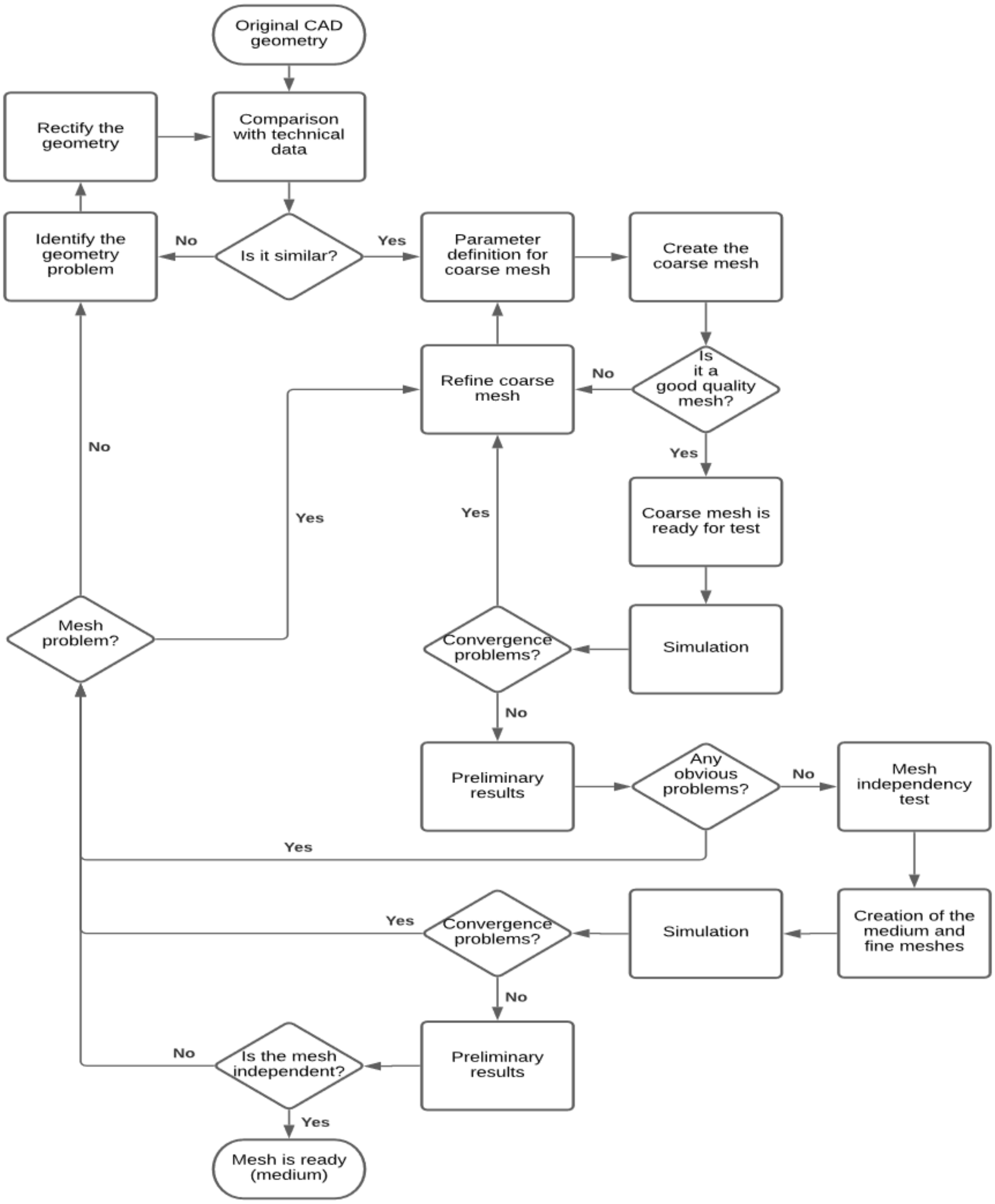

Figure 4.2: Diagram of the processes realized in phase 1.

In the end of this iterative process, three independent meshes were obtained. However, it was opted to use the mesh with medium refinement for the next phases.

It should be noted that the boundary conditions (temperature, pressure and mass flow rates for fuel and air) used in this phase were for the condition of 100% power and were different from those used in the next phases, but, since the final mesh obtained had an independent behavior for these values and the velocity inside the combustion chamber is approximately the same for all the power conditions - the average Mach number is approximately 0.2 (this is important for the analysis of Y^+) - the mesh should have an independent behavior for all the analysis. It should also be noted that the choice of the meshing software is not represented in this diagram, since the only one of the tested software that allowed the creation of an independent mesh through the process described before was the ANSYS Fluent Meshing software.

4.4.2 Combustor Model Geometry

For this study, the original combustor model received consisted in a CAD design of the CFM56-3 combustor developed and used in a previous master's thesis by Oliveira [69] based on a CFM56-3 combustor previously provided by TAP.

Thus, this subsection will start with a brief explanation of the CAD process developed by Oliveira. Then, the problems detected in the original CAD model during the course of this work will also be presented, as well as the modifications applied to try to fix these problems. Lastly, the final CAD model used in this work will be described.

4.4.2.1 Geometry Construction Process

It is known that is very difficult to obtain the blueprints for a specific part of a given engine due to the confidentiality that gas turbine engine manufacturing companies tend to maintain. According to Oliveira [69], the case of the CFM56-3 combustor was no exception and to obtain an accurate CAD model of the combustor geometry it was necessary to use reverse engineering, i.e., a 3D scan was performed followed by a CAD design.

As mentioned by Oliveira [69], for that task, the 3D scanning device used was the Artec Spider, which was provided by UBI. Moreover, the scanning process of the combustor was held at UBI while the scanning process of the dome and the fuel injectors was held at TAP facilities. According to Oliveira [69], the overall scanning process was a success. However, the internal structure of the swirlers could not be scanned properly nor the exit of the combustor due to the fact that the turbine support structure, which was attached to the combustor, was not removable, preventing the scanner from seeing that parts of the combustor. For that reason, the scan models of the swirlers and the combustor exit may have a slight difference from the original ones. Figure 4.3 represents the final 3D scan model of the combustor obtained by Oliveira [69].

Figure 4.3: 3D model combustor, obtained from the post-processing step, in Artec Studio 9.2 [69].

After obtaining the scanned 3D model of the CFM56-3 combustor, the CAD design was performed in CATIA V5R19. This process and the previous one are explained in detail in Oliveira's dissertation [69], where all the steps taken and the challenges overcome are identified. The final result of the CAD model developed by Oliveira is shown in Figure 4.4 and it represents a quarter section of the combustor, shaded with its base alloy material, Nickel.

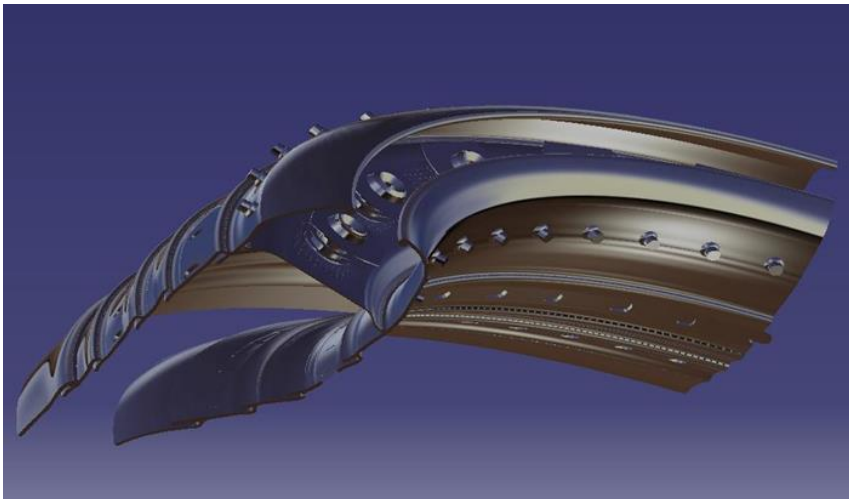

Figure 4.4: Quarter section of the combustor CAD model, shading with a Nickel alloy [69].

As in the previous works where this CAD model was used, to decrease the simulation time and effectively represent the four fuel injectors that supply a richer mixture, i.e., there is one fuel injector for every five fuel injectors present in each quarter section of the combustor model that supplies a richer mixture, only a quarter section of the combustor will be used for simulation purposes. This is possible due to the existing symmetry in the CFM56-3 combustor.

It should be noted that during the early phases of this work, it was concluded that even so, the simulation time for the quarter section was too long. So, to test new sets of modifications needed in the geometry, meshes or the models used, a new geometry was developed where only one injector was represented. Thereby, some sets of new configurations could be excluded without spend the total time of the simulation in the quarter section model.

4.4.2.2 *Relevant remarks about the CAD model*

For the present study, the most relevant information extracted from Oliveira's dissertation [69] about the combustor geometry model consisted of:

- All the details present in the real combustor were represented in the model, including the cooling lips and the bolts that attach the combustor walls to the dome;
- The dome and injectors are represented with their precise inclination in the final CAD model. The degree of inclination was accurately represented due to a document that TAP provided that indicated the degree of inclination that the dome should have after maintenance;
- The swirlers and the exit of the combustor have an approximate CAD representation. The exact geometry of these components was not achieved because, as mentioned before, the turbine support structure prevented the scanner from seeing these parts. In addition, there were some measures that were missing from the available documents.

4.4.2.3 *Geometry modifications and description*

The available CAD model of the CFM56-3 combustor was provided in the solid format. As reported by Oliveira [69], and mentioned earlier, there were some parts of the combustor such as the swirlers where the exact geometry was not achieved. Furthermore, after analyzing the few technical data available on the internet about this specific gas turbine engine [65, 66, 116] and running the preliminary simulations, some problems were found related to the position of the fuel injectors, the area of the inlets of the swirlers, the shape of the outlets of the secondary air swirlers, and the connection of these outlets to the cooling walls of the dome. All these issues were affecting the results.

For this reason, some changes were attempted to try to correct these small problems and to increase the similarity of the CAD model to the original combustor. In Figure 4.5 two cut-view images of the first swirler are presented, in which the Figure 4.5 a) shows the original CAD model received and the Figure 4.5 b) the final CAD model with the modifications made during this work.

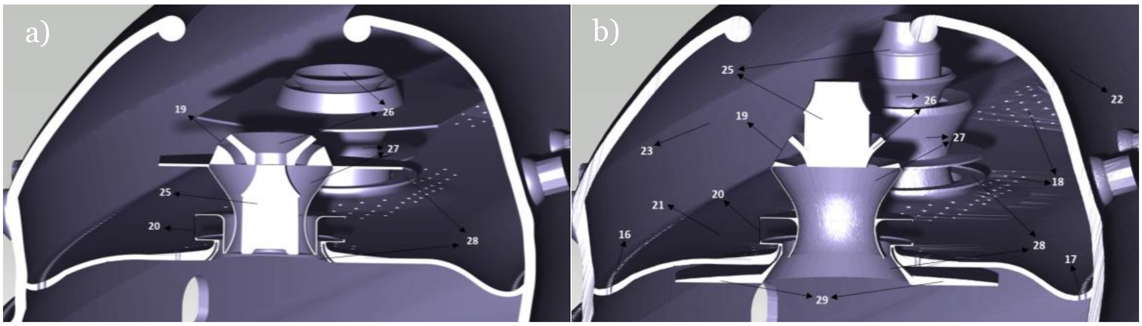

Figure 4.5: Cut-view of the first swirler of the geometry to highlight the modifications made: a) original geometry made by Oliveira [69]; b) final modified geometry used in this work.

It should be noted that all the changes made in the model were performed in CATIA V5 R20.

To make the modifications easier for the reader to understand, all the final changes made to the original CAD model are described and justified in Appendix H.

4.4.2.4 Final Geometry Description

The final geometry used in this work is represented in the Figure 4.5 b) and Figure 4.6. As explained before, due to the existing symmetry, only a quarter section of the combustor was used for the final simulations to reduce the computational cost.

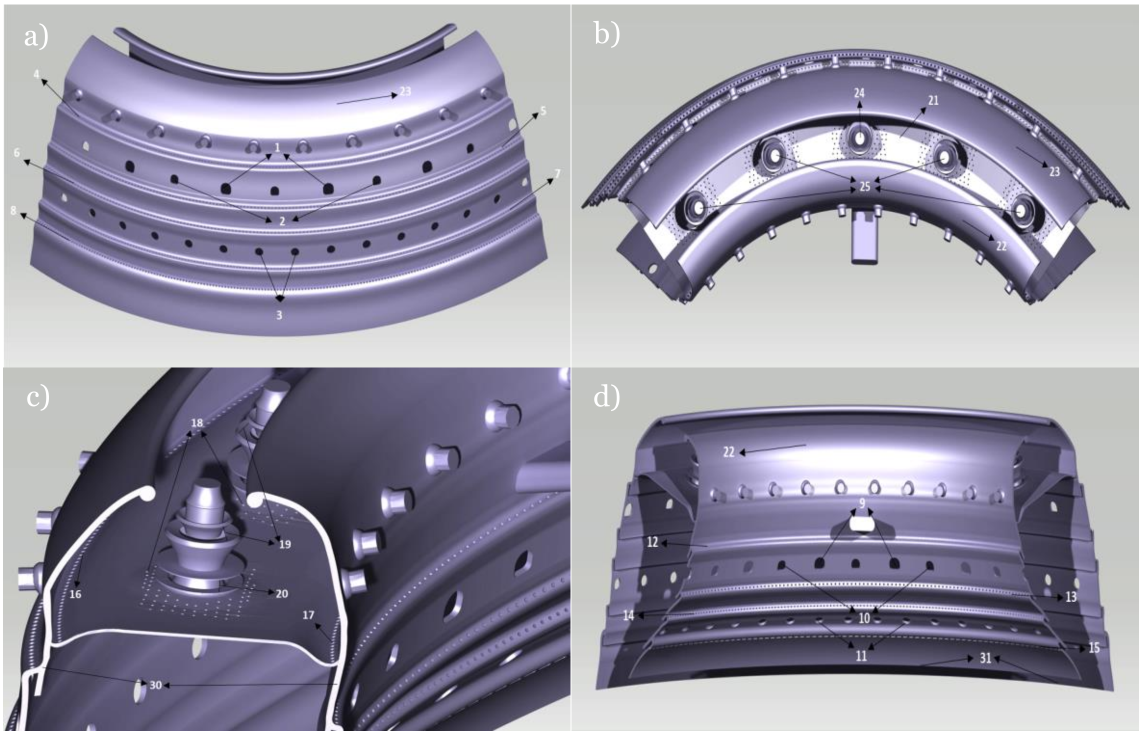

Figure 4.6: Views of the CAD combustor model section used in the simulations: a) outside view; b) top view; c) side view; d) inner view.

As can be seen in Figure 4.5 b) and Figure 4.6, all the components present in the combustor were represented in this model including the combustor walls, dome, dilution holes, fuel injectors and primary/secondary swirlers.

Table 4 presents a small description of all the relevant components/zones of the combustor and the type of boundary used in the simulations for each of these components/zones, which are numbered in Figure 4.5 and Figure 4.6.

Table 4: Combustor model boundary names/type.

Number	Location	Description	Boundary type
1	Exterior wall	Primary zone big mixers	Mass-flow inlet (air)
2	Exterior wall	Primary zone small mixers	Mass-flow inlet (air)
3	Exterior wall	Secondary zone mixers	Mass-flow inlet (air)
4	Exterior wall	First line dilution holes	Mass-flow inlet (air)
5	Exterior wall	Second line dilution holes	Mass-flow inlet (air)
6	Exterior wall	Third line dilution holes	Mass-flow inlet (air)
7	Exterior wall	Fourth line dilution holes	Mass-flow inlet (air)
8	Exterior wall	Fifth line dilution holes	Mass-flow inlet (air)
9	Inner wall	Primary zone big mixers	Mass-flow inlet (air)
10	Inner wall	Primary zone small mixers	Mass-flow inlet (air)
11	Inner wall	Secondary zone mixers	Mass-flow inlet (air)
12	Inner wall	First line dilution holes	Mass-flow inlet (air)
13	Inner wall	Second line dilution holes	Mass-flow inlet (air)
14	Inner wall	Third line dilution holes	Mass-flow inlet (air)
15	Inner wall	Fourth line dilution holes	Mass-flow inlet (air)
16	Dome wall	Exterior dilution holes	Mass-flow inlet (air)
17	Dome wall	Interior dilution holes	Mass-flow inlet (air)
18	Dome wall	Dilution holes swirler	Mass-flow inlet (air)
19	Swirler	Primary Inlet	Mass-flow inlet (air)
20	Swirler	Secondary Inlet	Mass-flow inlet (air)
21	Dome wall	Wall	Wall
22	Inner wall	Wall	Wall
23	Exterior wall	Wall	Wall
24	Injector	Rich mixture	Mass-flow inlet (fuel)
25	Injector	Poor mixture	Mass-flow inlet (fuel)
26	Swirler	Top	Wall
27	Swirler	Middle	Wall
28	Swirler	Bottom	Wall
29	Swirler	Cooling Wall	Wall
30	Symmetry	Plan	Symmetry
31	Outlet	Plan	Pressure outlet

Note: In the symmetry and outlet zones were previously created plans to use in the meshing software to define the limits of the fluid zone. These plans are not represented in the figures and the numbers refer to the respective limits of the combustor.

4.4.3 Generation of the Numerical Mesh

The aim of the numerical mesh is to provide a distribution of points where the solution can be calculated. For that reason, the generation of the model mesh is one of the most important steps in a CFD simulation.

In this subsection, a brief overview will be made about the basic fundamentals, the development process and the quality analysis of the numerical mesh. The reasons for the software choice will also be presented.

4.4.3.1 *Software Choice*

During this work, several meshing software were tried in order to get the best mesh possible with the computational resources available (mainly the quantity of RAM). At the beginning the HELIX-OS, which is based on *SnappyHexMesh,* was used to create the mesh for the geometry as it usually provides a quicker mesh generation time and it is a user-friendly software that allows the user to better refine any given part of the mesh [69]. However, after the modifications of the CAD model, none of the meshes created with this software could represent properly the area between the dome and the cooling walls that are closer to the swirlers. This happened due to a lack of RAM in the computer that was being used to the generate the mesh.

The second approach was to try to use *SnappyHexMesh* software directly. However, this approach was much more complex than the previous one, since this software is not as user-friendly as HELIX-OS. And again, due to a lack of RAM, the final mesh obtained was not good enough for this work and still had some of the problems presented with the previous approach.

Simscale, which is an online software, was also tried. However, due to the complexity of the uploaded geometry and the fact that the online solver must be used to simulate the flows, it was possible to conclude that this software was not suitable for the case in study.

Finally, after the update of the ANSYS version, the new version of the *Fluent Meshing* together with the set of tips provided by ANSYS in [117] about the best practices for gas turbine combustion meshing allowed to create a good enough mesh for the simulation, where all the features of the geometry were correctly represented with the available computational resources.

4.4.3.2 *Mesh independence analysis*

Overview

The examination of the spatial convergence of a simulation is a straight-forward method for determining the *ordered discretization error* in a CFD simulation.

One significant issue in numerical computations is to decide what level of grid resolution is more appropriate. This is a function of the flow conditions, type of analysis, geometry, among other variables [118].

Generally, a poorly refined mesh will compromise the results of the simulation, whereas a finer mesh will improve them. However, it is necessary to take into consideration that an increase in the number of elements of the grid will lead to an increase in simulation time and computational cost.

Thus, to assess what is the best balance between the grid resolution and the quality of the results, the analysis of the mesh should to start with a grid resolution and then perform a series of grid refinements to assess the effect of this new grid resolutions in the results. This is known as grid refinement study (or *grid convergence study).* Usually, to start this type of study, one might first consider a coarse grid spacing, perhaps the coarser mesh that can capture all the features of the geometry and then refine that mesh to get the finer meshes. It is hoped that as the grid is refined (grid cells become smaller and the number of cells in the flow domain increase) and resolution improves that the computed solution will not change much and approach to an asymptotic value, i.e., the true numerical solution. This happens as the spatial discretization errors also asymptotically approach zero, excluding computer round-off error. This results in a consistent numerical analysis. However, there still may be an error between this asymptotic value and the true physical solution to the equations [118].

In line with what was said and to optimize all aspects of the mesh to get a good relationship between mesh size, computational cost and the quality of the simulation results, there are some considerations that should be taken into account:

- First, it is necessary to make a selection of the zones of the model where a finer mesh is needed and the zones where a coarse mesh can be used without great changes in the results. This can only be done through a trial-and-error approach.
- Secondly, according to a NASA document [118], in the grid refinement study, it is not necessary to halve (or double) the number of grid points in each coordinate direction to obtain the coarser (or finer) grid. Non-integer grid refinement or coarsening can be used. In this process, the refinement (or coarsening) will require the generation of a new grid; however, it is important that the new grid maintain the same grid generation parameters as the original one. The number of grid points are then adjusted according to grid quality parameters (such as grid spacing ratio limits) in order to generate the new surface and volume grids. The grid refinement ratio, r, should be a minimum of $r \geq 1.1$ to allow the discretization error to be differentiated from other error sources (iterative

convergence errors, computer round-off, etc…). Generally, the higher this value, the better [118].

There are several methods for examining the spatial convergence of CFD simulations. Some of these methods were presented by Roache [119].

It must be noted that beyond the spatial discretization error, also the temporal discretization error is important. However, in the present study, the temporal discretization error is not relevant, since the simulations were steady-state.

In the following, it will be explained how the independence test was performed in this work.

Process followed

Considering all that was said before and the fact that the geometry was extremely complex, firstly, it was opted to create the coarser mesh possible that could represent all the features of the geometry and meet the requirements for Y^+. Then, this mesh was refined successively to get finer meshes until get closer results for two consecutive meshes. This iterative process is represented in the diagram of Figure 4.2.

After analyzing several meshes, the independence test was performed using three meshes, with coarse, medium and fine refinement, having 11,830,638 cells, 16,318,327 cells and 22,602,875 cells, respectively. The internal structure obtained for these three meshes (in the cut-view plane of the first swirler) is shown in the Figure A.E.2, in Appendix E, and the meshing process followed to obtain these meshes is described in Appendix C (the values presented in this appendix are for the intermediate mesh).

For the independence test, the information collected relative to numerical/experimental data for Jet A fuel (no experimental data relative to H_2 combustion in this gas turbine engine was available) was presented by Ribeiro [120] and ICAO [67], and these documents contain the outlet temperature of the combustion chamber (only for the operating condition of 100% power) and the NOx emissions of the engine, respectively. For that reason, the parameters used to analyze the independence of the mesh were:

- The average static temperature of the combustion chamber in the outlet;
- The average static temperature and velocity magnitude in a defined plane (cut-view of the first swirler), since the NOx emissions depend mainly of the temperature and residence time inside the combustion chamber.

All the independence tests were performed for the operating condition of 100% power, since it is the only operating condition where most of the boundary conditions were known.

Table 5: Values obtained in the mesh independence test for the power setting of 100%.

Plane	Outlet		Cut-view plane of swirler 1			
Parameter	Static Temperature [K]	Relative Error [%]	Static Temperature [K]	Relative error [%]	Velocity Magnitude [m/s]	Relative error [%]
Coarse	1755.009	0.018	1882.490	2.156	86.945	0.712
Intermediate	1755.329	0.008	1923.976	0.101	87.568	0.493
Fine	1755.188		1922.032		87.139	

Note: The presented values are not the final ones and they correspond to the first mass flow rates used in this work. However, this is not relevant, since the objective in the independence tests is just that the error between values has to be small and not exactly the values obtained.

It should be noted that the relative error for two consecutive meshes is obtained by dividing the absolute error of each parameter in study by the value obtained with the finer mesh of these two meshes, as shown in the Equation (4.7).

$$Relative\ error\ [\%] = \frac{|Value\ coarser\ mesh - Value\ finer\ mesh|}{Value\ finer\ mesh} \times 100 \qquad (4.7)$$

Looking at the Table 5, the maximum error occurred for the average static temperature in the plane of the cut-view of the swirler and it was in the order of 2.16% between the values of the coarse and the intermediate meshes; however, between the values of the intermediate and the fine meshes the difference was only 0.1%. The error between the values of the average static temperatures for the outlet was nearly 0% between the coarse and the intermediate meshes as well as between the intermediate and the fine meshes. For the velocity magnitude, in the cut-view plane, the relative errors between the values were approximately 0.71%, between the values of the coarse and intermediate meshes, and 0.49%, between the values of the intermediate and the fine meshes.

After analyzing these values, it was opted to use the intermediate mesh and it is possible to conclude that this mesh has an independent behavior.

Mesh Quality Analysis

According to ANSYS [117], the quality of the mesh plays a significant role in the accuracy and stability of the numerical computation. Therefore, Fluent allows to check the mesh quality to ensure metrics such as good orthogonal quality and low aspect ratio.

The cell orthogonal quality is computed using cell skewness, the vector from the cell centroid to each of its faces, the corresponding face area vector and the vector from the cell centroid to the centroids of each of the adjacent cells. This parameter has a range from 0 to 1, with 1 being perfect and 0 being poor, and it is usually recommended to achieve an orthogonal quality higher than 0.1. Having a high orthogonal quality ensures that the Fluent solution is robust [117]. Figure 4.7 presents a spectrum where the quality of the mesh can be related with the orthogonal quality of the cells [123].

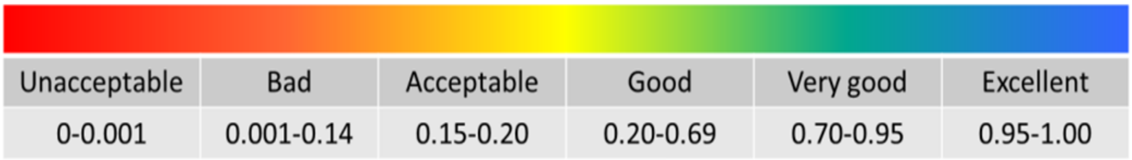

Unacceptable	Bad	Acceptable	Good	Very good	Excellent
0-0.001	0.001-0.14	0.15-0.20	0.20-0.69	0.70-0.95	0.95-1.00

Figure 4.7: Mesh orthogonal quality metrics spectrum [123].

The aspect ratio is a measure of the stretching of a cell. This parameter is computed as the ratio of the maximum value to the minimum value of any of the following distances: normal distances between the cell centroid and face centroids, and the distances between the cell centroid and nodes. It is best to avoid sudden and large changes in the cell aspect ratio in areas where the flow field exhibits large changes or strong gradients. When meshing a combustor using ANSYS the aspect ratio must be less than 100 [117].

In this work, in the end of the meshing process, a mesh quality report was provided by *Fluent Meshing* and the limit values obtained for the intermediate mesh (used in the simulations of this work) were:

- 0.1004 for the minimum orthogonal quality presented by the cell with the lowest value;
- 132 for the maximum aspect ratio presented by the cell with the highest value.

Although these reported values seem to be bad, they are only displayed in a small proportion of cells. Furthermore, the average orthogonal quality of the mesh is 0.96, which according to Figure 4.7 is considerably good, and the orthogonal quality of the cells is distributed as shown in Figure 4.8.

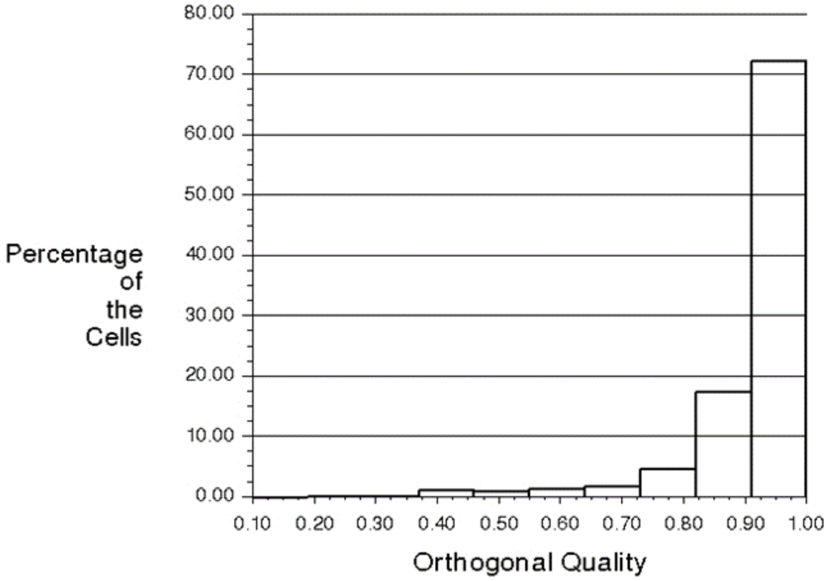

Figure 4.8: Histogram of mesh orthogonal quality by percentage of cells, obtained in the ANSYS Fluent software.

Moreover, through the Figure A.E.1 (Appendix E), which shows the orthogonal quality distribution of the cells (in the cut-view plane of the first swirler) for the intermediate mesh, it is possible to conclude that the zones where the orthogonal quality of the cells is lower are located far from the areas of greatest interest.

Finally, to ensure that there were no errors in the meshes, a Mesh Check was made in the end of the meshing process and no errors were encountered. So, that mesh was ready to use in the next phase. Figure 4.9 shows the final intermediate mesh obtained for a quarter of the combustor.

Figure 4.9: Intermediate mesh, obtained with Fluent Meshing software.

Figure 4.10 shows the internal structure of the mesh that was represented in the previous figure.

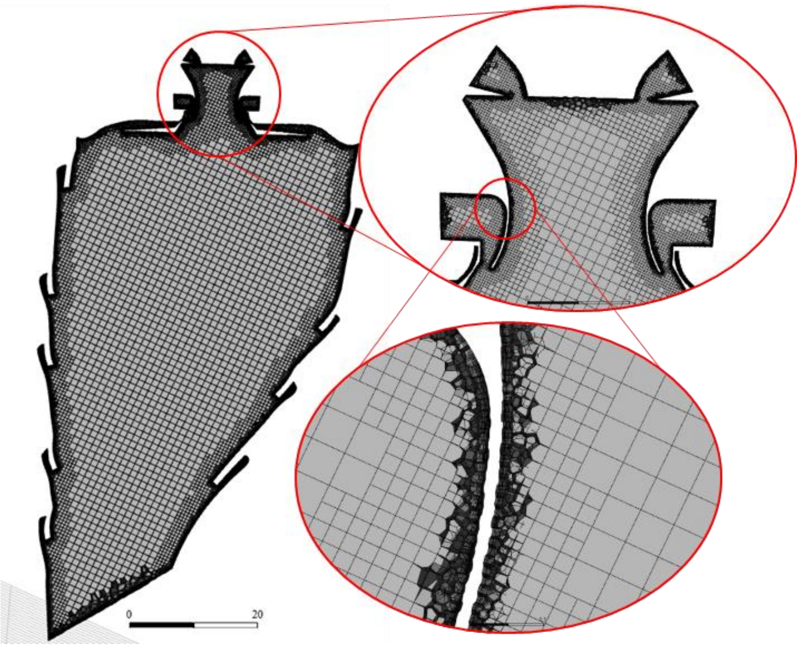

Figure 4.10: Mesh structure of the intermediate mesh in the cut-view plane of the first swirler, obtained with Fluent Meshing software.

It should be noted that in Figure 4.10 the scales shown in the smaller figures are 5mm for the first zoom and 0.5mm for the second zoom.

4.5 Phase 2: Boundary Conditions, Models, Methods and Results

Once the first phase was completed, it was possible to start phase number two. The main objective of this phase was to determine the final results of the control simulations (with Jet A) and the results of the simulations with hydrogen to use in the analysis made in phase 3. For that, it was first necessary to determine the boundary conditions, and then, with these values, calculate the results for the control and hydrogen combustion simulations. To achieve these objectives, this phase was divided in 3 subphases, which will be presented in the following.

At first, all the objectives of the subphases will be presented and then a detailed description of the processes involved in these subphases will be made as well as the identification of the experimental/numerical data used to accomplish the objectives.

After explaining all the three subphases, a detailed description will be made on the calculation of the boundary conditions and the simulation setup used. It should be noted that the subphases were developed and completed in the order in which they will be presented.

4.5.1 Phase 2.1

In this phase there were two main objectives. The first was to define the percentages of:

- Air mass flow rate that passes through the swirlers to the primary zone;
- Air mass flow rate that is used for cooling and dilution purposes;

The second objective was to choose the set of models (turbulence, radiation, species, etc.) that together allow a better agreement between the numerical results and the available experimental/numerical data.

The data used in this phase for validation purposes were obtained from Ribeiro [120] and correspond to the boundary conditions obtained in that work with *GasTurb* for the condition of full power. The relevant values for this phase are presented in Table 11 (Appendix D) and consist in:

- Air and fuel mass flow rates;
- Air temperature and pressure before entering the chamber;
- Fuel temperature before entering the chamber;
- Combustor's outlet temperature and pressure;
- Overall AFR inside the combustion chamber (can be calculated through the available data).

The iterative process followed in this phase is represented, in a simplified way, in Figure 4.11.

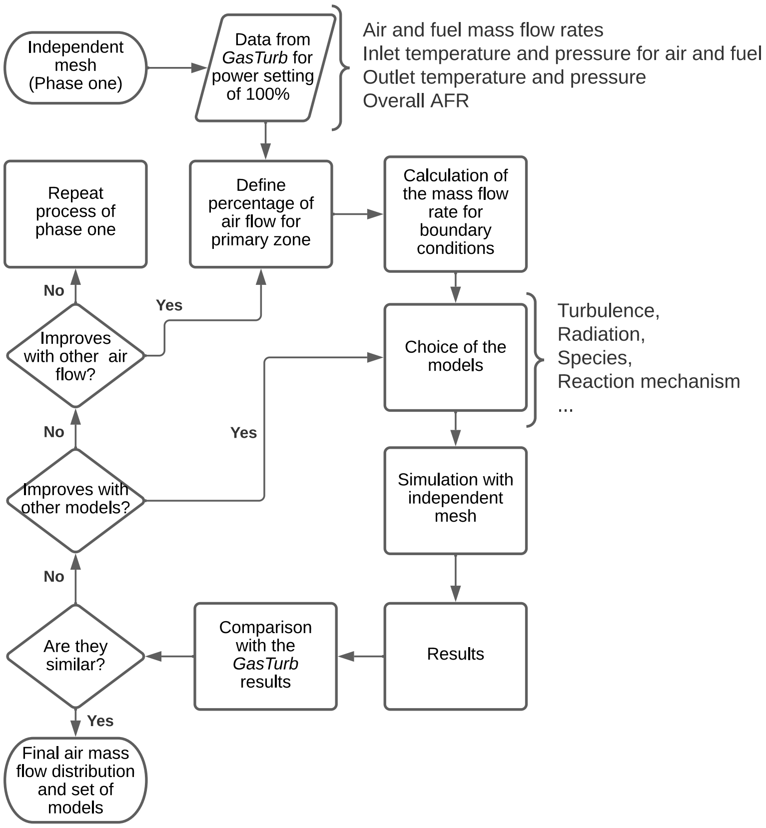

Figure 4.11: Diagram of the processes realized in phase 2.1.

In the end of this iterative process, the percentage of air that passes through the swirlers to the primary zone and through the other inlets for cooling and dilution purposes was obtained, as well as the set of models and methods that should be used as a reference for the next phases.

4.5.2 Phase 2.2

In this phase there were four main objectives and they consisted in:

- Define the final boundary conditions for each power setting (i.e., 7%, 30%, 85% and 100% power), mainly the outlet average static temperature and the air mass flow rate for each inlet to use in the next phase;
- Determine the operating conditions (air temperature and pressure) for the power settings of 7%, 30% and 85% power, once the operating temperature and pressure of the air for 100% power were defined in phase 2.1;

- Define which of the methods to determine the NOx emissions is in better agreement with the values of the ICAO database [67] to use the results of this method as control simulations when comparing with the results of phase 2.3;
- Verify if the set of models and methods defined in phase 2.1 works properly and can accurately predict the NOx emissions when compared with the reference values.

Beyond the results obtained in phase 2.1, the data used in this phase for validation purposes were also obtained from Ribeiro [120] and ICAO [67] and correspond to:

- Initial guesses for the values of temperature and pressure of the air in the inlets for the operating condition of 7% power. These data can be obtained through the charts of the experimental tests of the CFM56-3 engine on the testbed made by Ribeiro [120];
- The emission index of NOx for each operating condition presented in ICAO's database [67]. These values were presented in Table 2 (in section 2.9.3).

The iterative process followed to accomplish the objectives of this phase is represented in Figure 4.12.

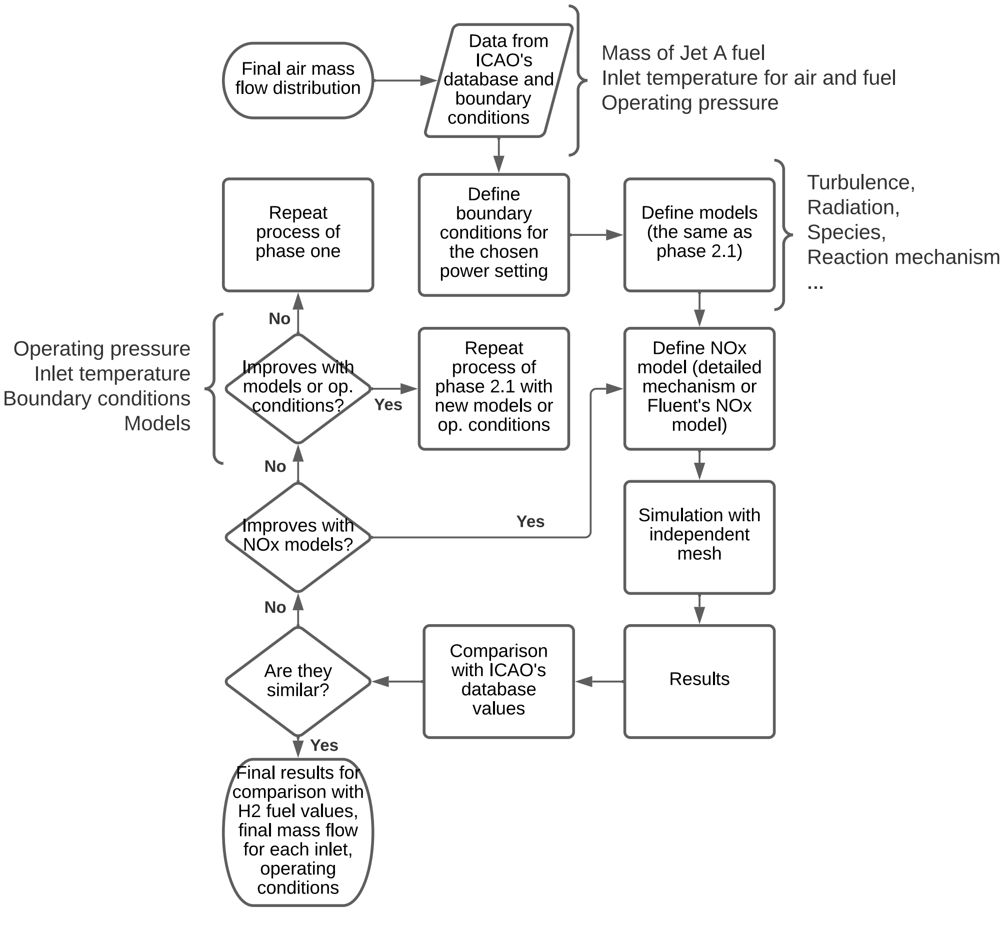

Figure 4.12: Diagram of the processes realized in phase 2.2.

In the end of this phase, the final set of models and methods to be tested in the phase 2.3 was obtained, as well as some relevant values for each power setting, which include the final boundary conditions (operating pressures, temperatures for air and fuel, air mass flow rates for each inlet), the outlet average static temperatures and the predicted NOx emissions for Jet A fuel to be used as standard controls in phase 3.

4.5.3 Phase 2.3

In this phase there were three main objectives and they consisted in:

- Define a method to determine the quantity of hydrogen that allows to obtain the same outlet average static temperatures of phase 2.2 for each power setting, using the same final models and methods defined in the previous phases;
- Determine the quantity of NOx emitted for each power setting through the NOx models available;
- Perform some sensibility tests by changing the swirl angle at the air inlets of the swirlers, and the fuel temperature and pressure, one at a time, to analyze the influence of these parameters in the quantity of NOx emitted for each power setting.

Since there were no experimental data available for the NOx emitted while burning hydrogen in this gas turbine engine, the only values used in this phase were the boundary conditions calculated in the previous phases for each power setting, mainly the air mass flow rate for each inlet, temperatures and pressures for air and fuel, etc.

The iterative process followed to accomplish the objectives of this phase is represented in Figure 4.13.

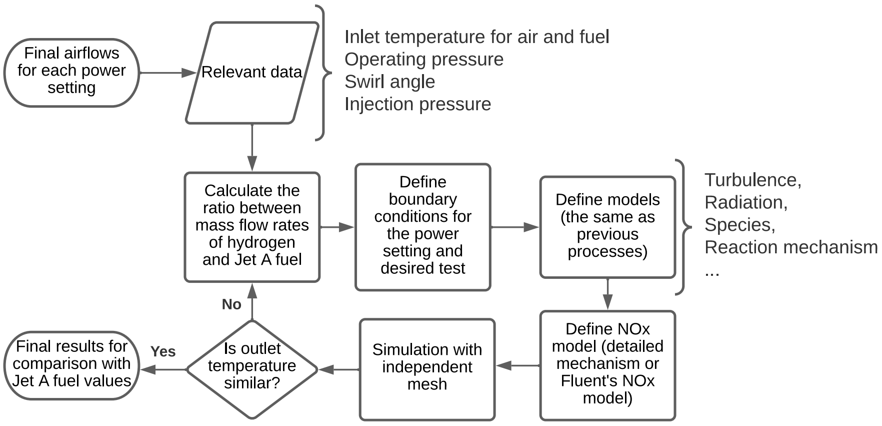

Figure 4.13: Diagram of the processes realized in phase 2.3.

In this process, it should be noted that the calculation of the ratio between the fuel mass flow rates was made only for one power setting and this ratio was used in all the simulations. Moreover, for the sensibility tests, the mass flow rate of hydrogen fuel was considered to be same for each power setting.

Once this phase is complete, all the results are ready for analysis and comparison in phase 3. It should be noted that, since there are no experimental data for NOx emissions for hydrogen fuel, there is no way to define which NOx model is the best to perform the analysis. So, in phase 3 all the results obtained in phase 2.3 will be compared with the control simulations.

4.5.4 Determination of the Boundary Conditions

The right definition of the boundary conditions is critical as this greatly affects the results and the convergence. Like was said in the section 4.4.2, the manufacturers maintain most of their technical information confidential. Thus, it is extremely difficult to obtain correct values for parameters such as the total air mass flow rate that is conducted through the compressor to the combustor entry, and practically no information is provided regarding the distribution of this air.

About this, Ribeiro [120] investigated the thermodynamic model of the CFM56-3 using *GasTurb*, which is a powerful cycle software used to simulate the most common types of gas turbine engines. Through that work, it was possible to obtain important aspects regarding each stage of the gas turbine engine in study, namely mass flow rates (of air and fuel) and some operating conditions (temperature and pressure) for the power setting of 100% power. The most relevant information of that work is presented in Table 11 (in Appendix D). Furthermore, in that work there are still represented some charts of relevant values such as temperature and pressure of the inlet of the combustion chamber obtained in the testbed analysis performed during that study for the several power settings.

Through all these available data, it was possible to obtain approximate values for the boundary conditions to be used in this work. The process followed to obtain these values was composed by several steps.

First, only a quarter of the combustor was studied. Thus, the process started by dividing the total mass flow rates of air and fuel that exist in the combustor entry (presented in Table 11) by four and calculating the overall AFR through Equation (2.5). These values are presented in Table 6.

Table 6: Reference values used for the calculation of the boundary conditions for the power setting of 100%.

	Reference Value
$\dot{m}_{fuel,1/4}$ [kg/s]	0.2818
$\dot{m}_{air,1/4}$ [kg/s]	10.3628
Overall AFR	36.777
Temperature Outlet [K]	1649.94
Temperature Inlet [K]	743.91
Inlet Pressure (air) [kPa]	2343.346
Pressure Outlet [kPa]	2226.179

Note: The $\dot{m}_{fuel,1/4}$ and $\dot{m}_{air,1/4}$ correspond to the total mass flow rates of fuel and air in the combustor's entry divided by four, respectively.

Typical values for the overall (or operating) AFR in gas turbine engines are stated by Bryn Jones [121] to be between 33 and 40 at 100% power, and approximately 100 at 7% power. As shown in Table 6, the overall AFR calculated in this work was 36.777 at full power, which represents a value within the stated values.

According to Bryn Jones [121], the next step is to ensure that the AFR in the primary zone is at stoichiometric conditions (or close) for all operating conditions and the overall AFR increases from 33-40 (at 100% power) until 100 (at 7% power). However, in this specific case, this would lead to different distributions (in percentage) of the air mass flow rate in the inlets. Hypothetically speaking, at 100% power, this would lead to a situation where approximately 30% of the air mass flow should enter in the primary zone through the swirlers; and at 7% power, this would lead to another situation where approximately 15% of the air mass flow should enter in the primary zone through the swirlers. Since the geometry is considered fixed, the percentage of the air mass flow that enters in the primary zone through the swirlers should be the same or have closer values regardless of the chosen power setting. Furthermore, these air mass flow rates led to malfunctions at the lower power settings for this combustion chamber. For this reason, the approach followed in the previous works by Oliveira [69] and Morão [70] was not adopted in the present work.

Instead, using the values of Table 6, based on the *GasTurb* values provided by Ribeiro [120] (presented in Table 11), it was possible to determine which percentage of the air mass flow should enter in the primary zone through the swirlers and which percentage should be used in the other inlets.

Since the combustion chamber design process was performed using a 3D scanning process, the area of the inlets represented in the chamber walls can be considered correct. So, assuming that the pressure and temperature on the outside of the chamber walls have constant values (for each operating condition), it is possible to assume that the air mass flow rate for each inlet depends only of its area.

In this case, only the areas of the inlets of the swirlers cannot be confirmed (as explained before). Therefore, through the iterative process represented in Figure 4.11, based on simulation and subsequent analysis of the results, and the values of Table 6, it was possible to determine an approximate value for the percentage of the air mass flow rate that should enter to the combustion chamber through the swirlers and the walls of the chamber, in order to obtain the desired outlet temperature for the combustion chamber. In this process, the $\dot{m}_{fuel,1/4}$ was divided by the 5 fuels injectors, with 10% more fuel being considered for the richest fuel injector than for the remaining four [69].

After realize this iterative process, it was concluded that the percentage of the air mass flow that should pass through the swirlers is approximately 21% of the available air mass flow. This value is in line with the work realized by Reid Smith et al. [24] with similar contemporary engines (V2500 engine) that use identical technology. Therefore, it can be concluded that the primary zone in this engine works with a rich mixture, instead of a stoichiometric one for the power setting of 100%.

As the fuel mass flow obtained by Ribeiro [120] is different from the value used by ICAO [67], this process had to be repeated for the operating condition of 100% power with the new mass of fuel, keeping the 21% of air passing through the swirlers and the same overall AFR, to test the NOx emissions value. This test was made through the iterative process represented in Figure 4.12, based on simulation and subsequent analysis of the results. After this, it was possible to define all the boundary conditions for 100% power.

Regarding the lower power settings, it was necessary to follow another path to define the boundary conditions, since no data was calculated in *GasTurb* by Ribeiro [120] for these conditions.

Looking again at the work of Reid Smith et al. [24], it was possible to verify that at the lowest power condition, the primary zone of this type of engines typically works in a stoichiometric or slightly rich condition. Furthermore, in Ribeiro's work [120], there is presented the experimental data collected in testbed from idle (assumed at 7% power) to full-throttle (assumed at 100% power) in the several probes across the engine. From these charts, utilizing the values of P_3 (corresponding to the pressure at the combustor entry) and T_3 (corresponding to the temperature at the combustor entry), it was possible to define good guesses for the values of temperature and pressure at the combustion chamber entry for the condition of 7% power. These values were considered approximately T=450K and P=3.5atm=354637.5Pa.

So, with these values, the percentage of air mass flow in the swirler (21%), the mass of fuel from the ICAO's database [67] and assuming that the primary zone operates in a stoichiometric condition, the overall AFR can be determined for 7% power through the process shown in the diagram of Figure 4.12. This method can be validated if, using these conditions, the simulated NOx emissions correspond to the ICAO's database value presented previously in Table 2. In the end of this process, all the boundary conditions are already determined for the condition of 7% power.

Finally, after defining the boundary conditions for the power settings of 7% and 100% power, it was possible to determine the operating conditions (pressure, oxidizer temperature, overall AFR, etc.) for the power settings of 30% and 85% power using a linear regression. Knowing the overall AFR and fuel flow for each one of these power settings, it was possible to determine the total air mass flow that enters to the combustion chamber. Then, through the primary zone AFR, it was possible to calculate the air mass flow that enters to the combustion chamber through the swirlers and the air mass flow that enters through the other entries (mixers and dilution holes).

After that, dividing these air mass flows proportionally by the areas of the inlets (presented in Table 15, in Appendix D), it was possible to determine the approximate air mass flow rate for each inlet.

Once these steps were concluded, all the operating parameters and boundary conditions for the air mass flow inlets were defined for each power setting of the LTO cycle. Table 7 presents all the values obtained for the mass flow rates in the inlets.

Table 7: Mass flow rate [kg/s] for each boundary, at its respective power setting.

	Mass flow rate [kg/s]					
Number-Description	*GasTurb*	ICAO's database				Air flow [%]
	100	100	85	30	7	
1-Primary zone big mixers	0.5334	0.4477	0.4059	0.2135	0.1027	5.147
2-Primary zone small mixers	0.3382	0.2839	0.2574	0.1354	0.0651	3.264
3-Secondary zone mixers	0.8862	0.7438	0.6744	0.3548	0.1706	8.552
4-First line dilution holes	0.5310	0.4456	0.4040	0.2125	0.1022	5.124
5-Second line dilution holes	0.3753	0.3150	0.2856	0.1502	0.0722	3.621
6-Third line dilution holes	0.4806	0.4034	0.3657	0.1924	0.0925	4.638
7-Forth line dilution holes	0.4147	0.3480	0.3155	0.1660	0.0798	4.002
8-Fifth line dilution holes	0.4581	0.3845	0.3486	0.1834	0.0882	4.421
9-Primary zone big mixers	0.5155	0.4326	0.3922	0.2063	0.0992	4.974
10-Primary zone small mixers	0.3404	0.2857	0.2590	0.1363	0.0655	3.285
11-Secondary zone mixers	1.0415	0.8742	0.7925	0.4169	0.2005	10.051
12-First line dilution holes	0.1274	0.1070	0.0970	0.0510	0.0245	1.230
13-Second line dilution holes	0.1659	0.1392	0.1262	0.0664	0.0319	1.601
14-Third line dilution holes	0.1560	0.1309	0.1187	0.0624	0.0300	1.505
15-Forth line dilution holes	0.8417	0.7064	0.6405	0.3369	0.1620	8.122
16-Exterior dilution holes	0.3302	0.2772	0.2513	0.1322	0.0636	3.187
17-Interior dilution holes	0.2472	0.2075	0.1881	0.0990	0.0476	2.386
18-Dilution holes swirler	0.4034	0.3386	0.3069	0.1615	0.0777	3.892
Total Cooling Flow	8.1866	6.8712	6.2295	3.2771	1.5760	79.000
19-Primary Swirlers	0.9994	0.8388	0.7605	0.4001	0.1924	9.644
20-Secondary Swirlers	1.1768	0.9877	0.8955	0.4711	0.2266	11.356
Total Swirler Flow	2.1762	1.8265	1.6560	0.8711	0.4190	21.0000
Total Air Mass Flow	10.3628	8.6977	7.8855	4.1482	1.9950	100.0000
Total Jet A fuel flow	0.28178	0.23650	0.19800	0.07250	0.02850	---
24-Rich Injector (1)	0.06078	0.05101	0.04271	0.01564	0.00615	---
25-Poor Injectors (4)	0.22100	0.18549	0.15529	0.05686	0.02235	---
Total hydrogen fuel flow	----	0.08507	0.07122	0.02608	0.01025	---
24-Rich Injector (1)	---	0.01835	0.01536	0.00562	0.00221	---
25-Poor Injectors (4)	---	0.06672	0.05586	0.02045	0.00804	---

Note: The numbering used in this table to describe the inlets is the same presented in Table 4.

4.5.5 Simulation Set Up

As mentioned before, the software chosen to perform the numerical simulations was ANSYS Fluent 2020R2.

In the present study, when starting ANSYS Fluent, it was necessary to ensure that 3D option was enabled, as well as the option of double precision. The double precision option was chosen due to the fact that a small error can largely influence the results of the models and, although this option makes the solution slower, it ensures that the results are more accurate.

Once ANSYS Fluent is launched, a mesh check must be done and the mesh quality should be checked again to ensure that no problems have appeared, since any problem with the mesh can greatly affect the solution's convergence and results [112]. As in *Fluent Meshing*, in the mesh check process, all the statistics and tests performed are displayed and, if the quality is checked again, also the maximum aspect ratio and minimum orthogonal quality of the mesh are displayed. In this case, as expected, no problems were encountered and the quality values were exactly the same. Figure A.E.3 (in Appendix E) shows the reports displayed for the Mesh Quality and the Mesh Check.

After these initial procedures, it was necessary to define the models to be used.

4.5.5.1 Defining the Models

ANSYS Fluent includes a wide variety of models that can be chosen according to the needs of each simulation. For the current setup, five models were used and they will be introduced in a simplified way below.

1- Energy model

This model must be activated, as it is the responsible for handling energy in any process related with heat transfer that occurs inside the chamber, such as the process related with the temperature changes due to combustion [69].

2- Viscous model

As discussed in section 4.2.1, the model chosen for all the final simulations was the RSM. The selected variant was *Linear Pressure-Strain* and all constants were kept at default values. The wall treatment chosen was the *Standard Wall Function* and the options "*Wall BC from k Equation*" and "*Wall Reflection Effects*" were also selected. It should be noted that the realizable k-ε model was also used to obtain the initial solutions for the simulations with hydrogen fuel.

3- Radiation model

As discussed in section 4.2.2, the P1 model was chosen to simulate the heat transfers by radiation for all simulations.

4- Species model

This model must be enabled so that ANSYS Fluent can model the mixing, transport and combustion of chemical species.

Due to the complexity of the simulations, two different species models were used in the step-by-step solution developed for this work. For the initial solutions, the models used were the *non-premixed combustion* for the initial guess of the Jet A combustion, and the *species transport* with a simple one-equation mechanism for the initial guess of the hydrogen combustion. After obtaining the initial solutions converged (or almost converged), the detailed mechanisms mentioned in section 3.5 (Kundu et al. for Jet A and Li et al. for hydrogen) were imported using the *species transport* and the simulations were resumed until obtaining completely converged solutions.

When *non-premixed combustion* is selected, the option *inlet diffusion* should be enabled, as this option allows to include the diffusion flux of species at the flow inlets. Then, it is necessary to create a PDF. In this case, on the *Chemistry* tab, *Chemical Equilibrium* was selected for *State Relation* and *Non-Adiabatic* was enabled in *Energy Treatment* so that the model considers any loss or gain due to chemical reactions. In *Model Settings*, the operating pressure values were selected according to Table 12 (Appendix D) and the *Fuel Stream Rich Flammability Limit* (FSRFL) was considered 1 (Ansys will calculate this value if the value 1 is chosen for this parameter) [112]. The specification of the names of the fuel and oxidizer species, and their mass fractions and temperatures must be made in the *Boundary* tab. In this case, the oxidizer was considered to be composed only by nitrogen and oxygen with mass fractions of 0.77 and 0.23, respectively. Regarding the fuel temperature, the same value that is assumed by the *GasTurb* software was used, which corresponds to 298.15K [122]. Just like the operating pressure, the oxidizer temperature varies with the gas turbine engine power setting and the values used for this parameter are also presented in Table 12 (Appendix D). In *Table* tab, *Automated Grid Refinement* was enabled. Finally, Fluent could calculate and display the PDF table, which could be checked under the Materials.

When *species transport* is selected, the option *Volumetric* must be enabled, as this option will activate the chemical equations. If the user intends to run some cold flow iterations to help the initial convergence, it is possible by disabling this option. Then, it is necessary to select the *Turbulence-Chemistry Interaction*. However, according to ANSYS [112], the encrypted CHEMKIN mechanisms can only be used with the *CHEMKIN-CFD solver* or the *Relax to Chemical Equilibrium* options. In this work, the *Eddy-Dissipation Concept* with *CHEMKIN-CFD solver* was tried, however, the extremely long computational time (approximately 3 weeks long per simulation) made this option unfeasible. Thus, it was necessary to use the option *Eddy-Dissipation* for the

Turbulence-Chemistry Interaction, with the option *Relax to Chemical Equilibrium* in *Chemistry Solver*. The options *Inlet Diffusion* and *Diffusion Energy Source* were also enabled. All the other options were left as default. Finally, and more important, it was necessary to import the CHEMKIN mechanisms through the files that contain the kinetics, thermal and transport data. The imported mechanisms can also be checked under the Materials.

5- NOx model

To assess the NOx emissions in this work, two approaches were followed. The first one was to use the sub-mechanisms provided in the detailed mechanisms. These sub-mechanisms, presented in section 3.5, may show some inaccuracy problems, since, for example, the sub-mechanism for the NOx produced by Jet A does not cover all the relevant pollutant species, such as the NO_2, which may affect the results.

The second approach was to use the NOx model provided in ANSYS Fluent. This model has to be enabled for ANSYS Fluent display information about NOx formation during the solution calculation or it can be calculated in post-processing (the approach chosen in this work). For this method, as the mechanisms of the Thermal NO and Prompt NO are the most important (explained in section 3.4), only they were selected. Then, the species that are present in the fuel must also be chosen. In the *Thermal* tab, the options *equilibrium* and *partial-equilibrium* were chosen for the [O] and [OH] models, respectively, as these options predict the *O* and *OH* radical concentrations required for thermal NOx prediction [112]. In the *Prompt* tab, the fuel carbon number and the overall equivalence ratio must be introduced (these values are in Table 16, in Appendix D). In the *Turbulence Interaction Mode* tab, it is important to select the *temperature* option in *PDF mode*, as this will enable the turbulence-chemistry interaction [112]. The other options selected in this tab were *beta* (for *PDF Type*), 30 (for *PDF points*), *transported* (for *Temperature Variance*) and *global-tmax* (for *Tmax Option*).

At the end, an assessment should be made to reveal which approach is in better agreement with the ICAO's database values (for Jet A) to be used in the work.

4.5.5.2 Defining the boundary settings

In the *Boundary Conditions* tab, there were four types of boundary condition applied, which consisted of:

- Mass-flow-inlets;
- Pressure-outlet;
- Symmetry;
- Walls.

The boundaries have already been distinguished in Table 4, in section 4.4.2.4. After identifying these boundaries, it was necessary to fill in all the parameters for each one of the them. In the present study, it was opted to start with the mass flow inlets.

In this case, the mass flow rate values from Table 7 are intended to be introduced in the *Momentum* tab for each of the mass flow inlets. Besides these values, there are still some other parameters that have to be configured for this type of inlets. Therefore, the direction of the flow was defined as *normal to boundary* for all the boundaries, except the swirlers. To simulate the swirl/counter-swirl effect, in the swirler inlets, the options *Direction Vector* and *Local Cylindrical* were selected and the directions were introduced according to Table 13 and Table 14 (Appendix D). These values simulate the entry of the air through the swirlers, with a 60° angle in the primary swirlers and -60° angle in the secondary swirlers (the effect of this swirl angle in the inlets can be seen in the Figure A.F.1 and Figure A.F.2, in Appendix F). The value of 60° was referred by Oliveira [69] and, in the current work, it was assumed as correct, since it is the only source that refers a value for this parameter. Then, the turbulent intensity and turbulent viscosity ratio can be introduced; however, it was opted to leave these parameters at their default values (5% and 10%, respectively). In the *thermal tab*, the *Total Temperature* must be introduced according to the type of inlet (air inlet or fuel inlet), the respective values are presented in Table 12 (in Appendix D). In the *species tab* (when using the *species transport*), for the fuel inlets, the *Species mass fraction* has to be set to 1 for the fuel specie; for the air inlets, the *Species mass fraction* of O2 has to be set to 0.23; and for both cases, the other parameters have to be left as 0 in that tab.

Regarding the *pressure-outlet* boundary, only the *gauge pressure* was set to zero, as this considers that the system pressure at the outlet is the *Operating Pressure*. All the other options were left at the default settings for this boundary.

About the other boundaries, both the *symmetry* and *wall* boundaries remained at the default settings.

The last step to take in this section was to set the operating pressure conditions. The easiest approach to set this value is to assume that there is no pressure loss inside the combustion chamber. In that case, it is only necessary to define the *Operating Pressure* in the *Operating Conditions* tab with the values displayed in the Table 12 (Appendix D) for the inlet pressure. On the other hand, the more realistic approach consists in set the pressure in the inlets and let the software calculate the pressure loss across the combustion chamber. This last option was tried, but the pressure loss was too high. So, it was opted by an intermediate approach.

In the *GasTurb* data collected from Ribeiro [120], the pressure loss in the combustion chamber was 5 percent of the inlet pressure, which means that the outlet pressure is 5 percent lower than the inlet pressure. So, it was decided to use this value as reference. Thus, to simulate this pressure loss, for each power setting, the pressure defined in *Operating Pressure* in the *Operating Conditions* tab was set as the outlet pressure values displayed in Table 12 (Appendix D). Furthermore, as in Fluent the pressure in the inlets is considered as the *Operating Pressure* plus the *gauge pressure* (defined in the *Momentum* tab), in the air mass flow inlets, the *gauge pressure* values were considered equal to the theoretical pressure variations, which are presented in Table 12 (Appendix D). Creating, this way, a better simulation of the pressure loss.

For the fuel mass flow inlets, according to Torenbeek [124], the pressure of the fuel should be twice the value of the operating pressure inside the chamber. Thus, the values used in the *gauge pressure* of the fuel mass flow inlets were always the same as the values defined for the *Operating Pressure* to simulate that the injection pressure is twice that value.

4.5.6 Solution Recommendations, Techniques, Methods, Controls and Convergence Analysis

In this subsection, the parameters used in the simulations for the solution methods (spatial discretization schemes), solution controls, convergence analysis and initialization method will be presented. All these parameters were chosen after analyzing some recommendations (related with this work) that will be presented in the following. Also the step-by-step approach developed and used in this work, based on these recommendations, will be described in this subsection.

4.5.6.1 Recommendations

Due to the complexity of this work and the number of models applied (turbulence, detailed kinetic mechanisms, radiation, etc.), it was really challenging to obtain completely converged solutions with a similar path for all the simulations using the desired models.

According to Ansys [112], using the RSM creates a high degree of coupling between the momentum equations and the turbulent stresses in the flow, and therefore the calculation can be more prone to stability and convergence difficulties than with the k-ε models. Thus, when the RSM is used, it may be necessary to adopt special solution strategies to obtain a converged solution. The following strategies are generally recommended by ANSYS when using RSM to model turbulence:

- The calculation should be started with a simpler model such as one of the k-ε models. The solution should be run until the flow field be reasonably converged.

The next step is to turn on the RSM and use the k-ε solution data as a starting point for the RSM calculation.

- For highly swirling flows or highly complex flows should be used low under-relaxation factors (0.2 to 0.3). In such cases, it may be necessary to reduce the under-relaxation factors both for the velocities and for all the stresses.

About the species models, according to ANSYS [112], for complex simulations involving chemical species (such as combusting flows), there are some solution techniques that may help to accelerate the convergence or improve the stability. Obtaining a converged solution in a reacting flow can be difficult for several reasons. First, although all reacting systems have some degree of coupling when the flow properties depend on the species concentrations, the impact of the chemical reactions on the basic flow pattern may be strong, leading to a model in which there is strong coupling between the mass/momentum balances and the species transport equations. This is especially true in combustion, where the reactions lead to a large heat release, subsequent density changes and large accelerations in the flow.

A second convergence issue in reacting flows involves the magnitude of the reaction source term. When the ANSYS Fluent model involves very rapid reaction rates (reaction time scales are much faster than convection and diffusion time scales), the solution of the species transport equations becomes numerically difficult.

For these reasons, for combusting flows that are difficult to converge and due to the high computational cost of chemical models, ANSYS [112] recommends that the following procedure be used to obtain a solution using the pressure-based solver:

1. Calculate an initial solution using the equilibrium Non-premixed or Partially-premixed model or even the Species Transport model with a reduced number of equations, i.e., 1 or 2 kinetic equations;
2. Import a CHEMKIN format reaction mechanism;
3. Enable the reaction calculations by turning on *Volumetric* in *Reactions* in the *Species Model* dialog box and select the mechanism imported as the *Mixture Material.*
4. Set the species boundary conditions.
5. Disable the flow and turbulence equations and solve for the species and temperature only.
6. Enable all equations and iterate to convergence.

4.5.6.2 Solution Techniques

After analysing the recommendations and try several combinations of the procedures previously mentioned, it was concluded that the best path to follow to obtain completely converged solutions was to use a step-by-step approach. Thus, the four-step solutions described in the Table 17 and Table 18 (both in Appendix D) were the approaches used in the simulations with hydrogen and Jet A, respectively. The Post-Processing step corresponds to the application of the NOx model provided in ANSYS Fluent.

In these approaches, to decide when to change from one step to the next, there were two possible scenarios, which consisted in:

- When the convergence criteria for the residuals were accomplished (the number of iterations is different for each simulation);
- When the chosen monitored variables (velocity, pressure, temperature, etc.) showed that the solution was converged or partially converged. This condition was only applied when the previous condition was not possible due to any convergence problem.

It should be noted that beyond the models and equations, also the solution methods and controls were changed. These changes will be described in the following subsections.

4.5.6.3 Solution Methods

In this study, the schemes selected in the *Solution Methods* task page for *Pressure-Velocity Coupling* and *Spatial Discretization* were the schemes recommended by ANSYS [111, 112] for the models used in each step of the simulations. Thus, the *Pressure-Velocity Coupling* scheme selected was *Coupled*. This solver is recommended by ANSYS [111, 112] when complex flows are simulated and, although it is slower than the others, it needs fewer iterations to converge. Furthermore, this solver provides better stability and improves accuracy [111, 112]. Then, the *Least Square Cell Based* gradient method was used because this scheme is known to be as accurate as the node-based gradient for irregular unstructured meshes (and both are much superior compared to the cell-based gradient), but less expensive to compute than the node-based gradient [111, 112]. The pressure discretization scheme selected was *PRESTO!*, since this scheme is recommended for flows with high swirl numbers, high-Rayleigh-number natural convections, high-speed rotating flows, flows involving porous media, and flows in strongly curved domains. For all the other equations, the *Second Order Upwind* scheme was selected to improve the accuracy of the simulations [111, 112].

The schemes used for each step of the simulations with Jet A and hydrogen are identified in Table 19 and Table 20 (presented in Appendix D), respectively.

It should be noted that, in this work, it was possible to solve the simulations directly with the schemes recommended by ANSYS. For this reason, there was no need to use simpler methods in the first steps to obtain the initial solutions.

4.5.6.4 Solution Controls

In the *Solution Controls* task page, it is possible to set common solution parameters for the *Coupled* solver. The first one consists in the *Flow Courant Number*, which can be used to stabilize the convergence behavior of the simulation.

Then, the *Explicit Relaxation Factors* (ERFs) for the *Coupled* scheme define the explicit relaxation of the variables between sub-iterations for momentum and pressure. Next, the *Under-Relaxation Factors* (URFs) section contains the under-relaxation factors for all equations that are being solved with the pressure-based solver [112]. The default values for these parameters generally work well. However, in the present case, those values were too aggressive for the type of combustion system in study, as they led to convergence problems. Thus, most of these values had to be initially reduced (as advised in the recommendations), some of them to very low numbers, namely the parameters of Flow Courant Number, density, energy, radiation, turbulence and viscosity.

After obtaining the initial solutions (step 1), to accelerate the calculation and increase the accuracy, the URFs for energy and radiation were increased. The final values used during the simulations for the several steps were obtained through an exhaustive try of several sets of values, until reaching the final converged solutions. The Table 21 and Table 22 (presented in Appendix D) present the values used for the several parameters in each step of the simulations for Jet A and hydrogen, respectively.

4.5.6.5 Monitors

During the solution calculation it is possible to monitor the convergence dynamically by checking residuals, statistics, specific values, and integrals. For this, Fluent allows to print reports or display plots of the variation of several variables of the flow (such as temperature, pressure, velocities, etc.), or even surface/volume integrations and residuals for the variables of interest. Running averages can also help to determine if a solution that is irregular or oscillating has reached convergence [112]. In brief, the purpose of the *monitors* is to display the value(s) of the relevant parameters in a simulation [112].

As will be explained in the following, in this work, several *monitors* were used to analyze the calculation processes and to monitor the convergence of each solution.

4.5.6.6 Convergence analysis

There are no universal metrics to judge convergence. For example, residual definitions that are usually useful for one class of problems are sometimes misleading for other classes of problems.

Generally, the default convergence criterion in ANSYS Fluent is sufficient. This criterion requires that the globally scaled residuals decrease to 10^{-3} for all equations except for the energy and P-1 equations, for which the criterion is 10^{-6} [112]. Sometimes, however, when using only the residual criterion, it is possible that if the initial guess is very bad, the initial residuals are so large that a three-order drop in the residual does not guarantee convergence. This is especially true for k and ε equations, where good initial guesses are difficult. So, it is wise to judge convergence not only by examining the residual levels, but also by monitoring relevant integrated or averaged quantities [112].

In this work, the convergence analysis was carried out using the globally scaled residuals together with the *absolute* convergence criterion and, to ensure that when the residuals are achieved, the solutions are converged, by monitoring several relevant quantities, such as:

- Average absolute pressure in the fluid volume;
- Average total temperature in the fluid volume;
- Average velocity magnitude in the fluid volume;
- Average static temperature in the outlet of the combustion chamber;
- Flow rate of NOx in the outlet of the combustion chamber;
- Mass imbalance.

The solutions were considered converged when:

- The residuals have decreased to a sufficient degree;
- The solution no longer changes with more iterations;
- The overall mass imbalance is obtained, i.e., the flow entering the system should be equal to the flow leaving the system. According to ANSYS [112], the net imbalance should be less than 0.5%.

4.5.6.7 Solution Initialization and Calculation

According to Ansys [112], the initial guess for the values used at the beginning of a simulation can influence the convergence velocity and stability. Thus, it is necessary to provide good and appropriate initial values to ensure that the solution converges as quickly as possible. In this case, the hybrid initialization option provided by ANSYS Fluent was selected because this option proved that the initial values were adequate, since the solutions generally converged smoothly and “relatively quickly”.

Regarding the calculation setup, it is a good practice to check the case first before starting the calculation process as this ensures that there are no errors within the case, mainly with mesh, models, boundaries, materials and solver. After that, the model is ready to be simulated and the solution calculation can be started. For this study, the calculations were performed until the convergence criteria defined in the previous subsection were reached.

4.6 Phase 3

In phase 3, an extensive comparison was made of the results obtained in the previous phases for the several power settings. For example, between the values of the control simulations with Jet A (from phase 2.2) and the values of the ICAO's database, or between the values of the control simulations and the resulting values of both NOx models tested in phase 2.3 for hydrogen, with the same conditions of swirl angle and temperature/pressure of fuel. Then, for each NOx model tested in phase 2.3, a comparison was made between the NOx emissions of the first simulation (with the original conditions of swirl and fuel pressure and temperature) and the values resulting from the sensibility tests performed.

All these results will be presented in the next Chapter.

Chapter 5 – Results and Discussion

In the present chapter, the results of the simulations for the combustion of Jet A and hydrogen in the CFM56-3 combustor (throughout ICAO's LTO cycle) are presented and analyzed. A total of 20 simulations followed by post-processing (for the NOx model) composes the final results. These simulations consist in four simulations with Jet A fuel and four simulations for hydrogen fuel for the standard parameters of the CFM56-3 engine and then, twelve simulations for the sensibility tests. All the results presented were obtained with an independent mesh, which was generated and verified as previously mentioned in section 4.4.3.

This chapter will start with an example of the convergence analysis made for all the results that will be presented to ensure the quality of the numerical solutions. Then, a comparison of results will be made to analyze the influence of changing the turbulence model in this case of study. In addition, an analysis will be performed on the influence of the use of fuels with different properties, as well as an analysis of the temperature distribution across the combustion chamber for both fuels for the several power settings. Next, to prove that the final results obtained are in accordance with the numerical/experimental data obtained from Ribeiro [120], there will be made an evaluation of the combustor's exit temperature.

Regarding the emissions, which are the main objective of this study, they are finally presented separately for each fuel, throughout the mentioned power cycle, for the different approaches followed. At first, a comparison will be made between the results obtained in this work for the control simulations (with Jet A) and the data available from ICAO [67]. Then, the best results of the control simulations will be compared with the results of the simulations with hydrogen fuel. In the end of this chapter, the results of the sensibility tests will be presented and analyzed.

During this work, two machines were used, one of them to create the several meshes and run the tests for the single injector geometry; the other (cluster) to run the independence tests and the several simulations done during the elapse of this work. The first machine was a workstation with 10 cores (20 logical processors) and 32GB of RAM. The cluster had 80 cores and 327.5GB RAM, but even so, each one of the solutions calculated in the cluster took an average time of almost 7 days (for the final geometry).

It should be noted that all the results presented in this chapter are only for a quarter of the CFM56-3 combustor. Moreover, all the results plotted in the present chapter were done with MS Excel and the contours displayed were obtained with ANSYS Fluent 2020R2.

5.1 Convergence Analysis

As mentioned before in section 4.5.6.6, several parameters were used to ensure that each solution obtained was completely converged. As an example, in this subsection, the analysis made for one of the 20 simulations will be presented, more specifically for the hydrogen simulation in the power setting of 7% power.

Starting by the analysis of the residuals, the first proof that the solution is converged is that the residuals have decreased to a sufficient degree. This criterion was met in the final step (step 4) of all the simulations. Figure 5.1 presents the plot of the behavior of the residuals in the final step of the simulation in analysis.

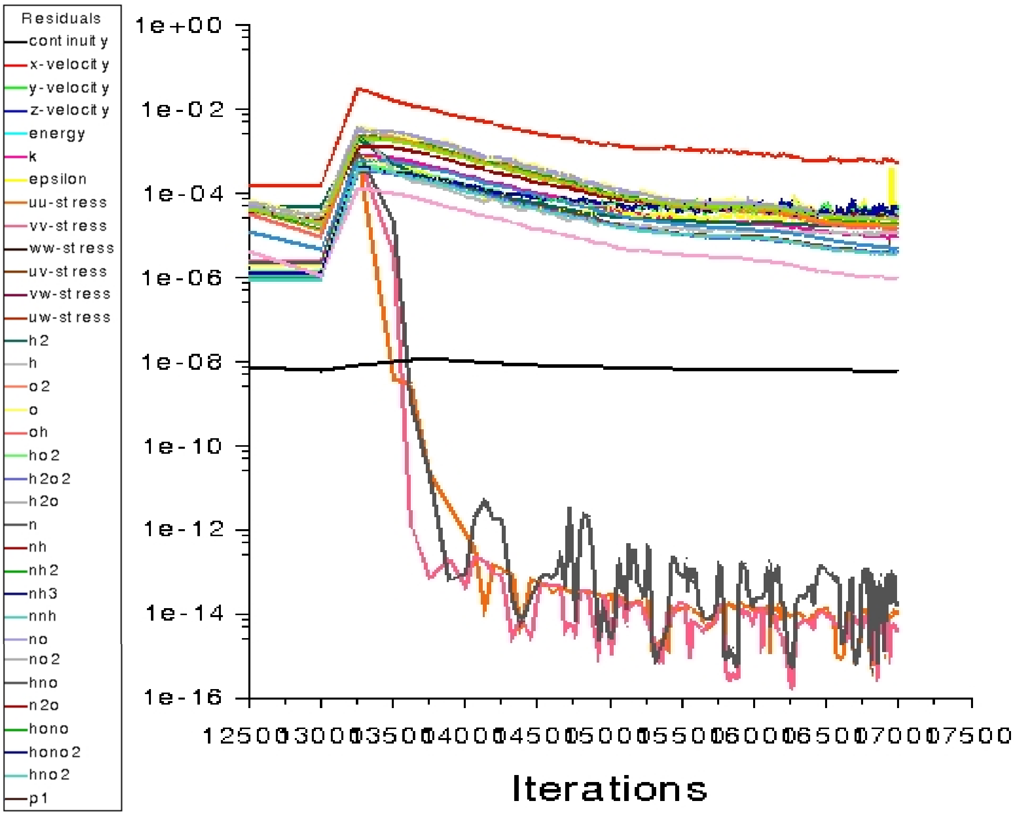

Figure 5.1: Residuals obtained in the fourth step of the simulation with hydrogen fuel at the power setting of 7%, obtained with Ansys Fluent software.

Looking at the Figure 5.1, it is possible to verify that all residuals were reduced to the intended values, i.e., 10^{-6} for the energy and P-1 equations and 10^{-3} for all the other equations.

It should be noted that, in this case, it was not possible to show the entire range of residuals for all the steps of the simulation, since the ANSYS Fluent does not save the values of the residuals for a range of iterations as large as the one needed in this simulation.

The second proof that the solution is completely converged is that the relevant quantities monitored converge to a value. In Figure 5.2, there are plotted the average absolute pressure and the average total temperature in the fluid volume for the same simulation as the residuals previously plotted.

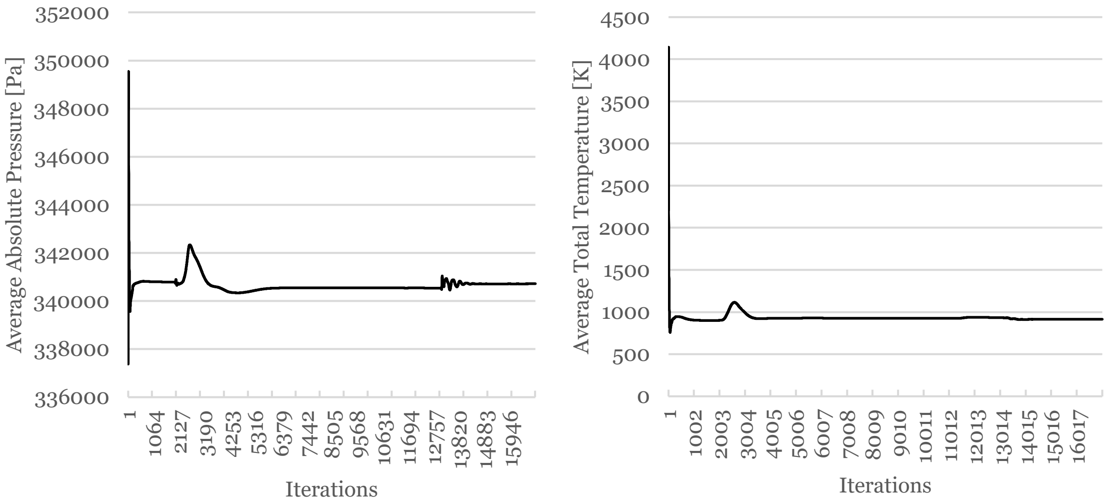

Figure 5.2: Plots of the average absolute pressure (left) and average total temperature (right) obtained for the complete simulation with hydrogen fuel at the power setting of 7%.

Looking at these plots, it is possible to identify regions where the values of the studied parameters were constant and regions where the values were fluctuating. As previously explained, when a solution is converged, all the relevant parameters have a constant value. So, the iterations where the values are constant (in both plots) can be associated to converged solutions for the steps of the simulation. Looking at the end of the plots, the presence of constant values in the last step is a strong proof that the solution obtained is converged. It should be noted that the iterations where the values change from a constant value to a range of floating values correspond to the iterations where the step change occurred.

Finally, the mass imbalance in this case was 4.88 E^{-7} (≈0), which is another proof that the solution is completely converged and therefore correct for the problem setup.

It should be noted that although the plots are not represented in this work, the convergence analysis for each of the other 19 simulations was performed exactly in the same way as for this example.

5.2 Influence of the Turbulence Model Inside the Chamber

During the initial simulations, the influence of the turbulence model was tested. As explained in section 4.2.1.1, it was known from the beginning that the RSM should perform better in determining the position and the effects in the recirculation zone than the other RANS models. However, it was also referred that the realizable k-ε turbulence model could provide good results.

As mentioned in the section 4.5.6.2, a step-by-step approach had to be used to obtain the final solutions for the simulations with RSM. During this process, it was possible to visualize the influence of the use of both turbulence models in the phenomena that occur in the combustion chamber. To make this comparison, Figure 5.3 presents the velocity magnitude vectors in the cut-view plane of the first swirler for both models, the realizable k-ε and the RSM.

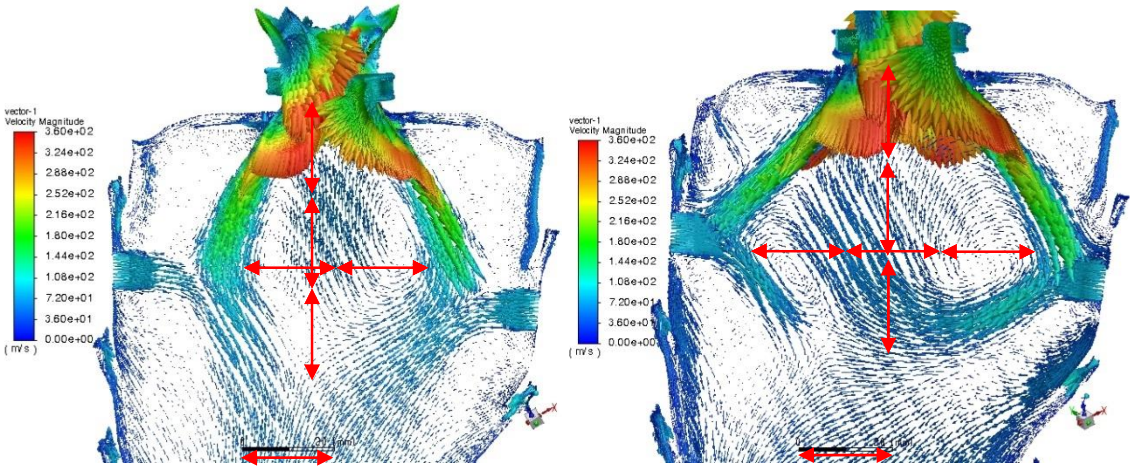

Figure 5.3: Velocity magnitude vectors in the cut-view plane of the first swirler, while burning hydrogen fuel at the power setting of 100%, for realizable k-ε (left) and RSM (right) turbulence models, obtained with ANSYS Fluent software.

Through Figure 5.3, it is possible to conclude that:

- Both turbulence models can identify the presence of the recirculation zone;
- For the realizable k-ε turbulence model, the inner zone of the recirculation zone has a length of approximately 60mm and a width of approximately 40mm;
- For the RSM turbulence model, the inner zone of the recirculation zone has a length of approximately 60mm and a width of approximately 60mm;
- According to the two previous points, the use of RSM causes a larger recirculation zone than the realizable k-ε for the same operating conditions;
- The recirculation zone created with the RSM model (shown in the image on the right side of Figure 5.3) seems to present some instability and does not have a shape as good as the one obtained with the realizable k-ε model (image on the left side of Figure 5.3).

One detail that can be observed through the Figure 5.3 is that the primary air jets (or primary mixers) seem to have a different influence on the flow pattern developed by each of the turbulence models. This may be the reason why the shapes and behaviors of the flow patterns inside the chamber are different in the two approaches.

To better analyze this issue, in Appendix G, the contours of the velocity magnitude for both the approaches are presented in Figure A.G.1. Through this figure, it is possible to conclude that the primary air jets influence the flow in different ways for these turbulence models. While with the RSM the primary air jets seem to penetrate into the flame zone, with the realizable k-ε this phenomenon does not seem to happen. However, to be sure about this conclusion, the static temperature contours were also analyzed in the same cut-view plane through Figure 5.4.

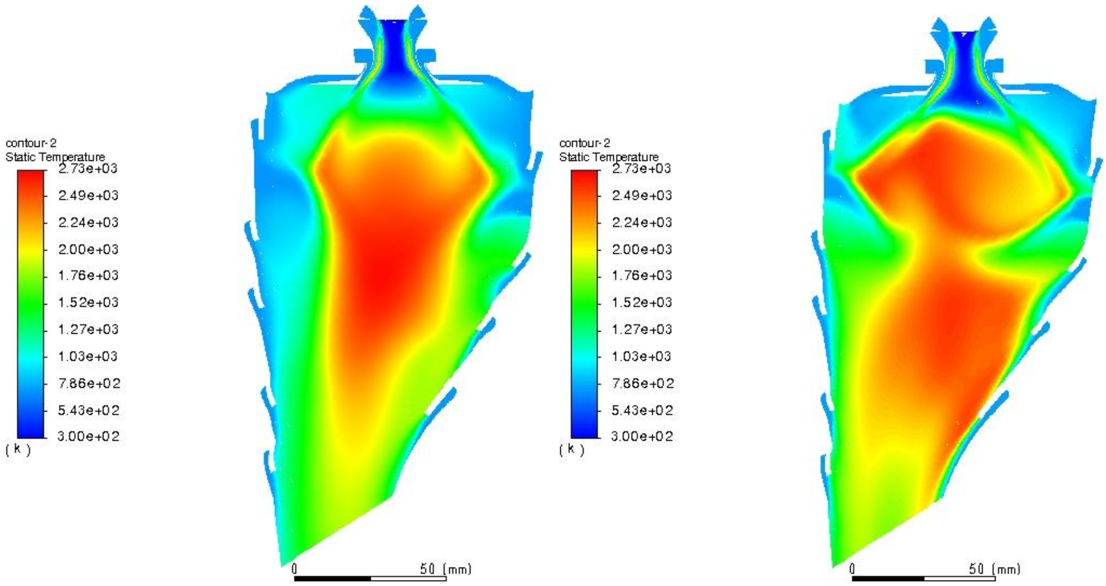

Figure 5.4: Contours of static temperature in the cut-view plane of the first swirler, while burning hydrogen fuel at the power setting of 100%, for realizable k-ε (left) and RSM (right) turbulence models, obtained with ANSYS Fluent software.

Looking at Figure 5.4, it is possible to conclude that:

- About the figure in the left side, one the one hand, the use of the realizable k-ε model generates a stable flame zone, which extends from the primary zone until a little beyond the end of the secondary zone. One the other hand, the presence of the primary air jets does not seem to be influencing the temperature in the flame zone as it should, since the purpose of this cold air should be to mix with the hot gases in the primary zone to reduce the flame temperature and this is not happening.
- About the figure in the right side, due to the instabilities created in the recirculation zone by the primary air jets and the swirl effect, the shape presented by the flame zone generated with the RSM does not seem as good as intended and it extends almost until the outlet of the chamber. However, it is possible to verify that the primary air jets are able to penetrate inside the hot gases in the primary zone to help reducing the flame temperature.

It should be noted that, although this cannot be noticed by the images in Figure 5.4, the temperature at the center of the flame zone generated with the realizable k-ε model is almost 40K higher than that of the flame zone generated with the RSM.

Considering that one of the primary objectives of this work is to identify all the parameters that can lead to malfunctions in the chamber, since the realizable k-ε model cannot properly represent the flow and tends to stabilize the instabilities, this model does not allow to accomplish the referred objective. Moreover, as the NOx emissions are deeply related to the temperature across the combustion chamber and the production of this pollutant is particularly sensitive to the presence of higher temperatures, it is expected that the influence of that higher temperature for the realizable k-ε lead to greater production of NOx, negatively influencing another of the main objectives of the work, which is highly undesirable. Thus, after analyzing all the considerations that were presented in this subsection, the RSM was definitely chosen to model the turbulence in this work.

5.3 Influence of the Fuel Change in the Combustion Chamber

As referred in section 2.3.3.2, the main factors controlling the emissions in conventional combustors are strictly related with the characteristics of the flow in the primary zone, mainly with the temperature, equivalence ratio, degree of homogeneity and residence time.

Changing the fuel will influence some of these factors throughout the combustion chamber, but having a particular impact on the primary zone. This can cause the new fuel to perform better or worse than the original one in terms of efficiency, pollutant emissions, etc.

Generally, when switching from Jet A to hydrogen, the biggest challenge to achieve low NOx emissions is to eliminate the zones of high temperature in the flame zone (mainly in primary zone), since the flame temperature is usually higher for hydrogen than for Jet A. Another major challenge is the fact that the flame speed of hydrogen is much higher than that of Jet A (up to 7 times), which makes flashback and blowout phenomena more likely to occur when using hydrogen, mainly in the higher power settings. Among many others, the difference in the density of the fuels can also be seen as a major challenge.

Thus, to analyze the influence of the fuel change in this study, the comparison will start with Figure 5.5, which shows the contours of the static temperature across the chamber for both fuels (for the power setting of 100%).

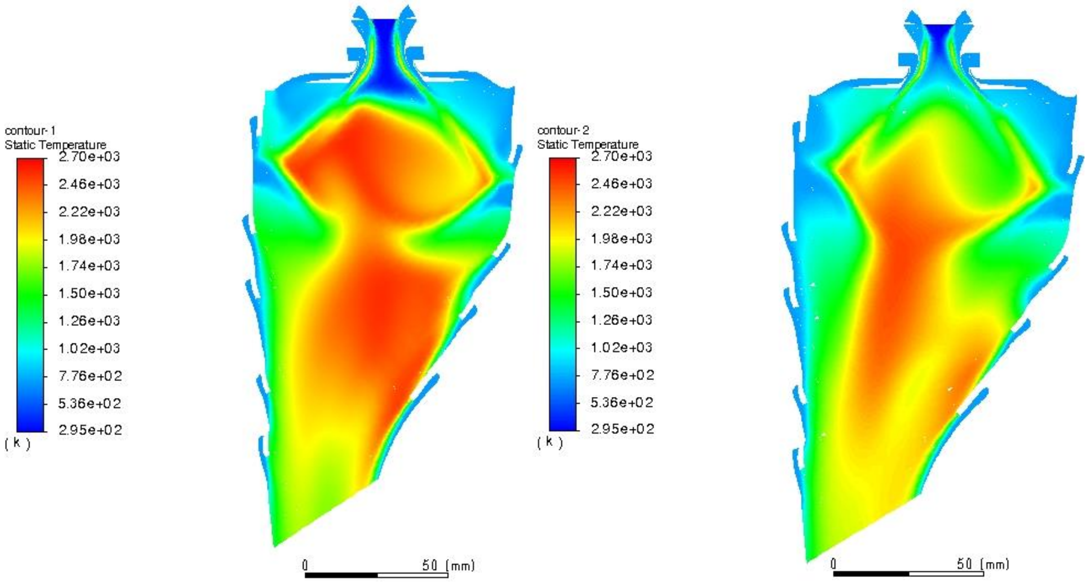

Figure 5.5: Contours of static temperature in the cut-view plane of the first swirler, while burning hydrogen fuel (left) and Jet A fuel (right) at the power setting of 100%, obtained with ANSYS Fluent software.

Through the Figure 5.5 it is possible to identify some of the main influences of this fuel change. First, it is possible to conclude that the main change is related to the temperature across the chamber. As can be noticed, for the hydrogen fuel, the temperature across the chamber is clearly superior than for the Jet A fuel. This phenomenon indicates that, probably, switching for hydrogen will cause more NOx emissions. Looking now at the position where the flame begins, it is possible to conclude that for the hydrogen fuel the flame begins closer to the swirler outlet than for the Jet A fuel. This phenomenon can cause an efficiency problem. As the flame begins earlier, this will probably cause the hydrogen fuel to start burning in a position where the mixture is richer, since the fuel has not yet had enough time to properly mix with the air in the recirculation zone to form a completely homogeneous mixture, thus reducing the combustion efficiency and making the combustor more prone to flashback occurrence at the higher power settings.

The fact that the flame begins earlier for hydrogen fuel can be explained due to the fact that the flame speed of the hydrogen fuel is much higher than that of the Jet A and the velocities of the air flows in the combustion chamber have similar values for both cases. This can be observed in Figure 5.6, which shows the contours of the velocity magnitude across the chamber for both fuels (for the same power setting as the previous contours).

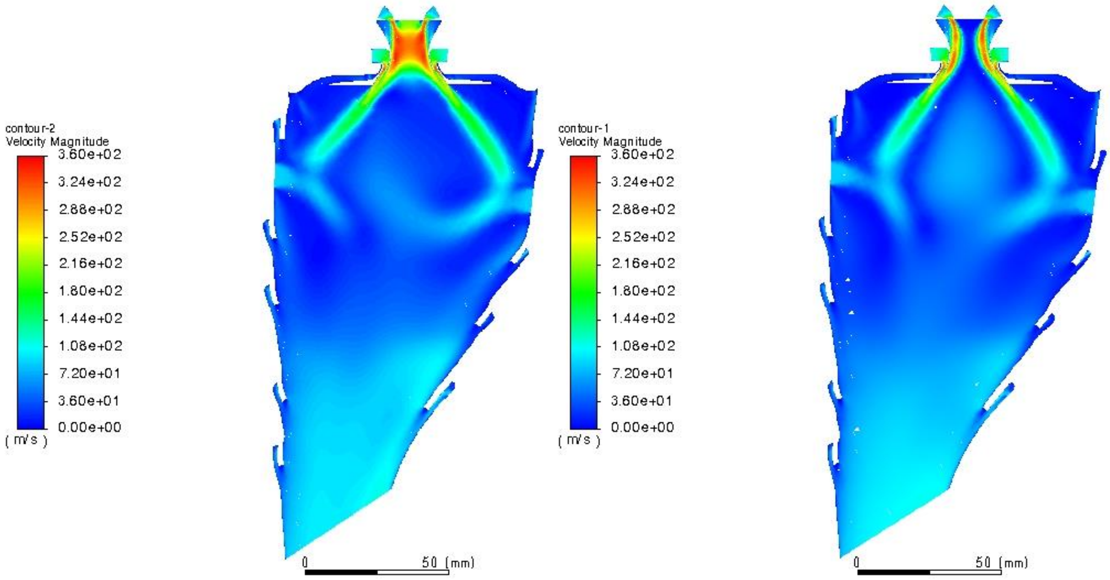

Figure 5.6: Contours of velocity magnitude in the cut-view plane of the first swirler, while burning hydrogen fuel (left) and Jet A fuel (right) at the power setting of 100%, obtained with ANSYS Fluent software.

Through the Figure 5.6, another great difference that can be noticed consists in the fact that the velocity of the hydrogen fuel flow is much higher than the velocity of the Jet A fuel flow inside the swirler. This can be explained by the fact that the density of the hydrogen is much lower than the density of the Jet A. So, the volume of hydrogen needed is much higher than the equivalent volume of Jet A, even considering the fact that the mass flow rate of hydrogen is almost one third of the mass flow rate of Jet A.

Another detail that can be identified in this figure is that the recirculation zone obtained when burning hydrogen seems to be slightly larger than when burning Jet A for the same operating condition. This phenomenon can also be justified due to the higher volume of hydrogen.

5.4 Temperature Distribution Across the Combustion Chamber

To analyze the differences in the temperature distribution across the combustion chamber when burning hydrogen and Jet A, the following figures show the contours of the static temperature in the cut-view plane of the first swirler for each power setting for both Jet A fuel (in the left) and hydrogen fuel (in the right), considering the same temperature scale in all images.

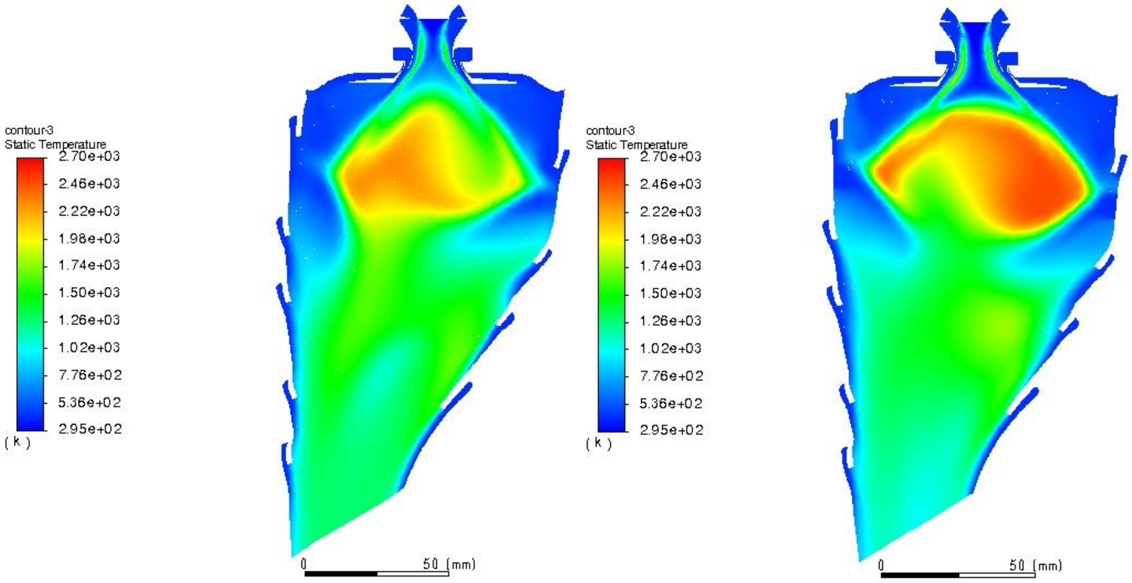

Figure 5.7: Contours of static temperature in the cut-view plane of the first swirler, while burning Jet A (left) and hydrogen fuel (right) at the power setting of 7%, obtained with ANSYS Fluent software.

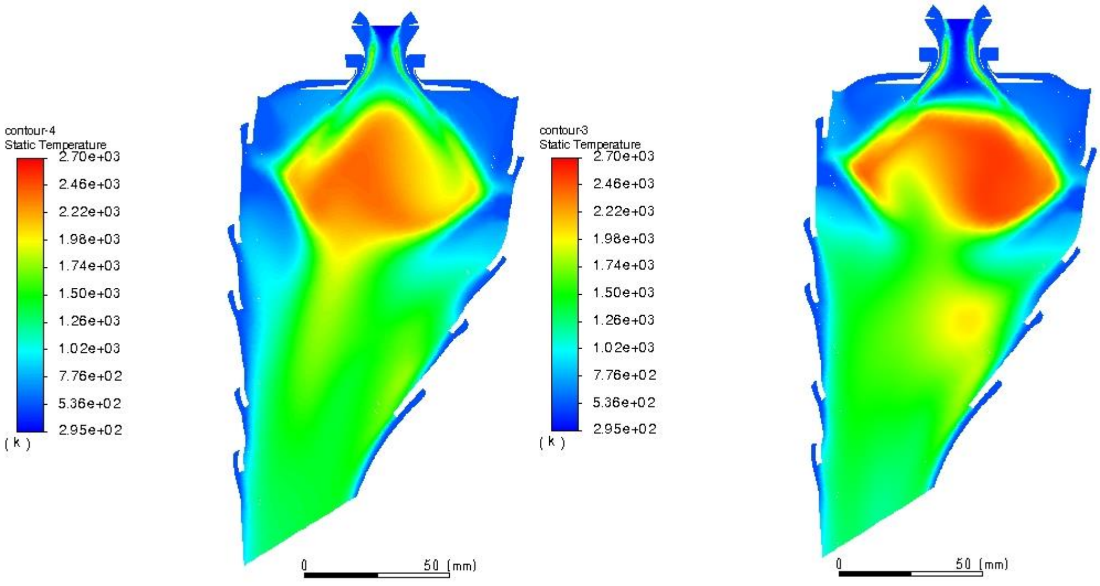

Figure 5.8: Contours of static temperature in the cut-view plane of the first swirler, while burning Jet A (left) and hydrogen fuel (right) at the power setting of 30%, obtained with ANSYS Fluent software.

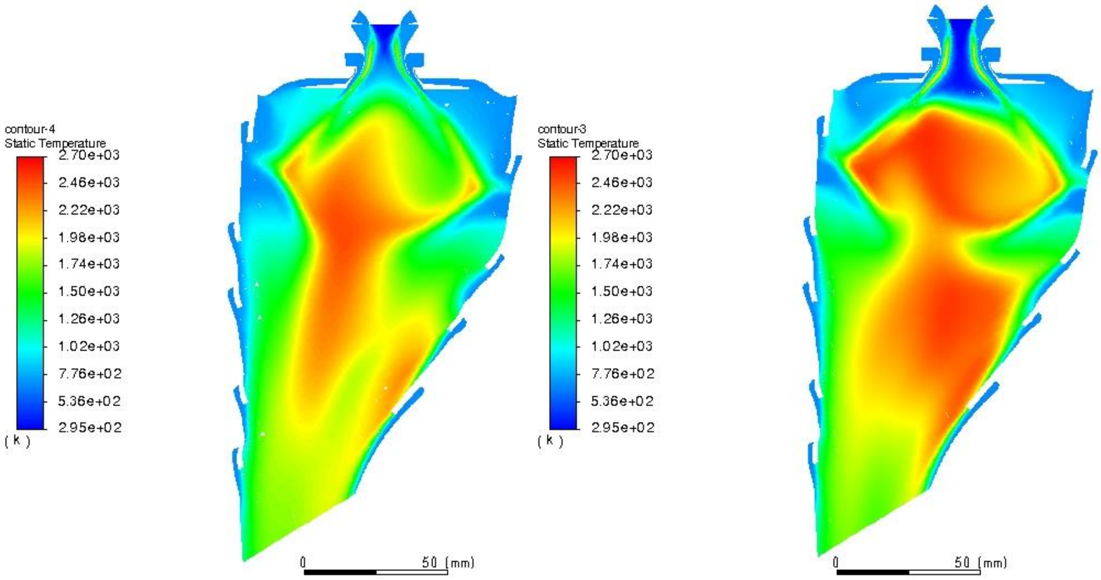

Figure 5.9: Contours of static temperature in the cut-view plane of the first swirler, while burning Jet A (left) and hydrogen fuel (right) at the power setting of 85%, obtained with ANSYS Fluent software.

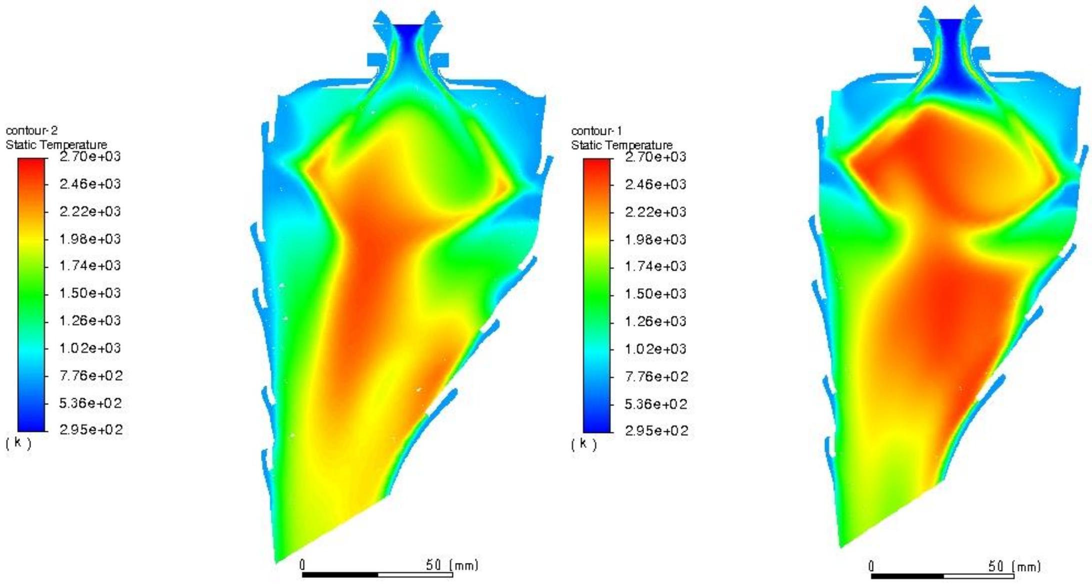

Figure 5.10: Contours of static temperature in the cut-view plane of the first swirler, while burning Jet A (left) and hydrogen fuel (right) at the power setting of 100%, obtained with ANSYS Fluent software.

Through the analysis of the previous figures, it is possible to conclude that:

- For both fuels, as the power setting increases, the temperature inside the chamber also increases. This would be expected, since more fuel is being burned;
- For each power setting, the hottest areas occur mainly in the recirculation zone (primary zone). However, it should be noted that for the 85% and 100% power settings, the flame extends to the secondary zone for both fuels;
- For each power setting, the temperature across the combustion chamber is always higher when burning hydrogen than when burning Jet A;

- For all the power settings, the flame begins always closer to the outlet of the swirler when burning hydrogen than when burning Jet A. As explained in the previous subsection, this phenomenon occurs due to the higher flame speed of the hydrogen fuel.

5.5 Combustor Exit Temperature

This set of results was obtained during the process of determining the boundary conditions where the outlet average static temperatures were calculated for the simulations with Jet A fuel, as shown in Figure 5.11. These values are important because they are needed, firstly, to compare with the reference temperature of 1649.94K obtained by Ribeiro [120] to the condition of 100% power, and then, to obtain reference values for the outlet temperature to allow the calculation of the mass flow of hydrogen fuel for each power setting.

The quantity of fuel for the simulations with hydrogen was calculated through the mass of Jet A fuel for each power setting and the ratio between the lower heating values, LHVs, of the fuels, as shown in Equation (5.1) and Equation (5.2).

$$\dot{m}_{Hydrogen} = \dot{m}_{Jet\ A} \times \frac{LHV_{Jet\ A}}{LHV_{Hydrogen}} \tag{5.1}$$

$$\dot{m}_{Hydrogen} = \dot{m}_{Jet\ A} \times 0{,}3597 \tag{5.2}$$

As the LHVs change from author to author, the ratio between these values was calculated and then adjusted to the condition of 7% power to obtain the same value for the outlet average static temperature for the simulations with Jet A and hydrogen.

Figure 5.11 shows the most relevant outlet average static temperatures obtained in this work. The values for the sensibility tests are not represented here.

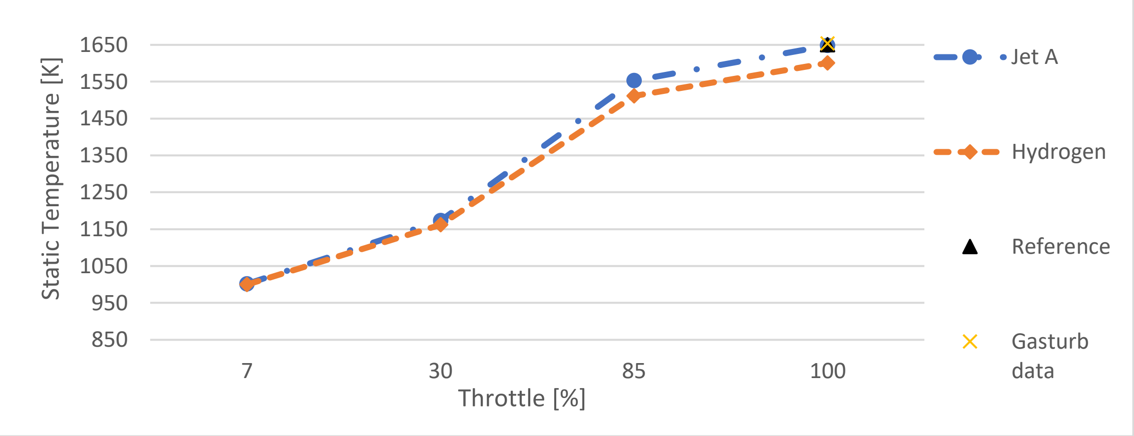

Figure 5.11: Combustor outlet average static temperature throughout ICAO's LTO cycle, while burning Jet A and hydrogen fuel; and the reference values for 100% throttle.

Considering Figure 5.11, it is possible to conclude that the values of outlet average static temperature obtained through the simulations with the input data from ICAO and *GasTurb* (blue line and yellow x, respectively) are quite similar to the reference value (triangle) for the full power condition (for Jet A).

Still considering the same figure, but looking now to the simulations with hydrogen, it is possible to conclude that the values of outlet average static temperature for the power settings of 7% and 30% power are similar to those of Jet A, which indicates that the ratios between the amount of hydrogen and Jet A should be correct. However, for the power settings of 85% and 100% power, the lower outlet average static temperatures for hydrogen fuel indicate that the quantity of hydrogen should be higher in these cases.

In this study, it was opted to fix only one value for the ratio, but according to these values, the best approach seems to be to calculate the specific ratio between the fuels to get exactly the same outlet average static temperatures for each power setting.

Another parameter that should be analyzed in this subsection is the temperature profile in the combustor outlet. For this, the Figure 5.12, which shows the contours of the static temperature at the outlet while burning Jet A and hydrogen fuel at 7% power, will be used, since the outlet average static temperatures are the same for both fuels.

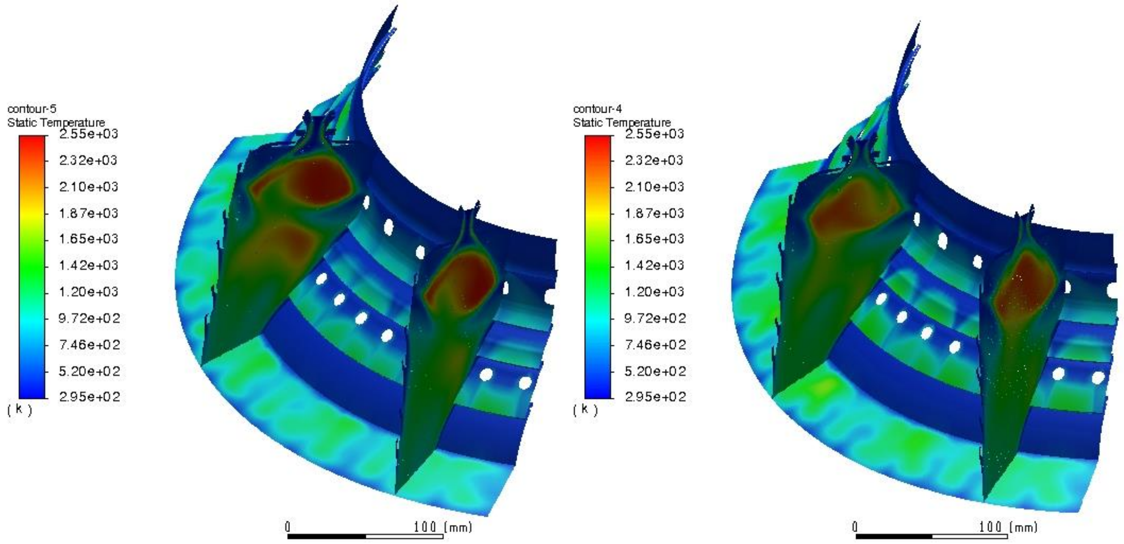

Figure 5.12: Contours of static temperature in the cut-view plane of the first and third swirlers and in the outlet, while burning hydrogen (left) and Jet A fuel (right) at the power setting of 7%, obtained with ANSYS Fluent software.

Looking at Figure 5.12, it can be noticed that, for both cases, the static temperature of the combustor outlet does not present a completely uniform temperature profile pattern, allowing the identification of the presence of some hot-spots. The presence of this phenomenon is more evident in the section under the influence of the richest injector (the middle one), and it is extremely undesirable, since these hot-spots will lead to a higher degradation of the turbine nozzle guide vanes, as well as the turbine blades, and will negatively influence the overall performance of the engine.

In Figure A.G.2 (Appendix G), which represents the same contours as in Figure 5.12, but for the power setting of 100%, the presence of the hot-spots is more evident. However, the comparative analysis cannot be performed in the same way, since the outlet average static temperatures are different for each of the fuels.

5.6 Emission analysis - NOx

In the emission analysis, it is possible to study the emissions of all the pollutants, mainly CO, CO_2, UHC and NOx. However, as in this work the only objective related to the pollutants is to compare the pollutant emissions between the Jet A fuel and hydrogen fuel, the only emissions analyzed were the NOx, since H_2O is not assumed as a pollutant.

In the first analysis (reference standard), regarding to Jet A fuel simulations, the emission index, EI, is used for comparison purposes, since the quantity of fuel burned is the same used in ICAO's data for each power setting and it can be easily interpreted by the reader. This value can be calculated using Equation (5.3):

$$EI[g/kg] = \frac{\text{Emission flow rate [kg/s]} \times 1000}{\text{Inlet } \dot{m}_{fuel} \text{ [kg/s]}} \tag{5.3}$$

In Equation (5.3), the emission flow rate was obtained by reporting the *Flow rate* of the desired pollutant in the outlet plane of the combustor in Ansys Fluent. This value is given in kg/s. The values used for the $\dot{m}_{fuel}$ at the inlets (obtained from ICAO [67]) are given in kg/s. Thus, the results are presented in the form $g[Emissions]/\mathrm{k}g[fuel]$, which allows the comparison with the ICAO's reference data.

However, when comparing the pollutant emissions from Jet A fuel and hydrogen fuel, as the quantities of fuel are very different (the mass flow rate of hydrogen is almost a third of the mass flow rate of Jet A), the use of the EI may give a wrong perception of the difference in emissions to the reader. So, to simplify the analysis of the simulations with hydrogen, it was opted to use of the flow rate of NOx, in grams per second, for a quarter of the chamber.

5.6.1 Control Simulation

The results of the control simulations are presented in the Figure 5.13 and show the EI(NOx) in the outlet of a quarter of the combustion chamber for the Jet A fuel.

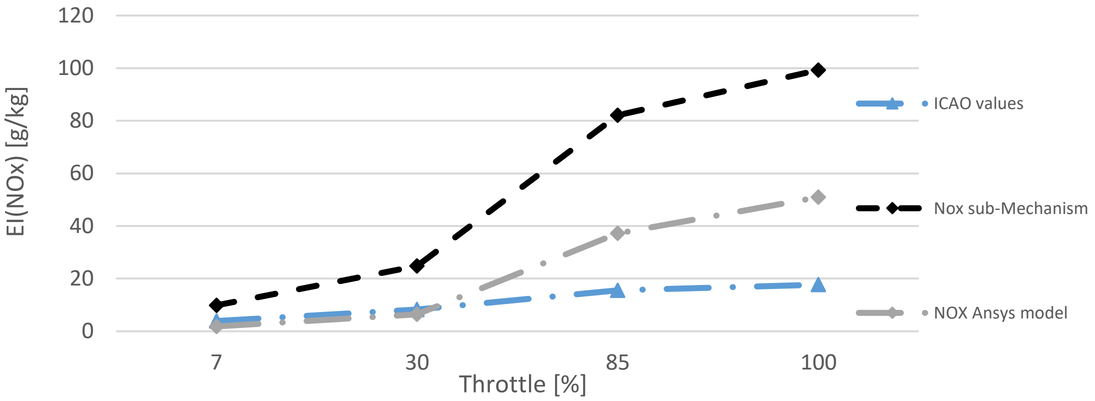

Figure 5.13: EI results for the NOx emissions for the combustion of Jet A obtained through the use of two approaches, NOx sub-Mechanism and Ansys NOx model, for one fourth of the combustion chamber throughout ICAO's LTO cycle.

As expected, and previously referred, for both approaches, the NOx emissions are lower at low power settings and attain maximum values at the highest power condition, where the temperatures are higher.

Considering the two approaches used for NOx prediction, presented in Figure 5.13, it is possible to conclude that the NOx sub-mechanism clearly overpredicts the NOx quantity in relation to the reference values (ICAO's database). Regarding the NOx model available in ANSYS Fluent, it can be concluded that, for the lower power conditions (7% and 30% power), the model can predict values for the NOx quantity close to the ones of ICAO's database. However, for the higher power conditions (85% and 100% power), this model also overpredicts the NOx emissions in relation to the reference values (ICAO's database), approximately 2.4 times more for 85% power and 2.9 times more for 100% power. Despite this condition, it is possible to conclude that this model can predict the NOx emissions better than the other approach, and these values will be used in the next step.

To better analyze the difference between these two approaches, Figure 5.14 is shown in the following. This figure presents the contours that allow a comparison of the mass fractions of NOx predicted for Jet A fuel in the cut-view plane of the first swirler with the NOx sub-mechanism and the NOx model from Ansys, for the power setting of 100%. To offer another perspective, in the Appendix G, the Figure A.G.6 and the Figure A.G.7 show the same contour, but for the outlet plane of the combustion chamber.

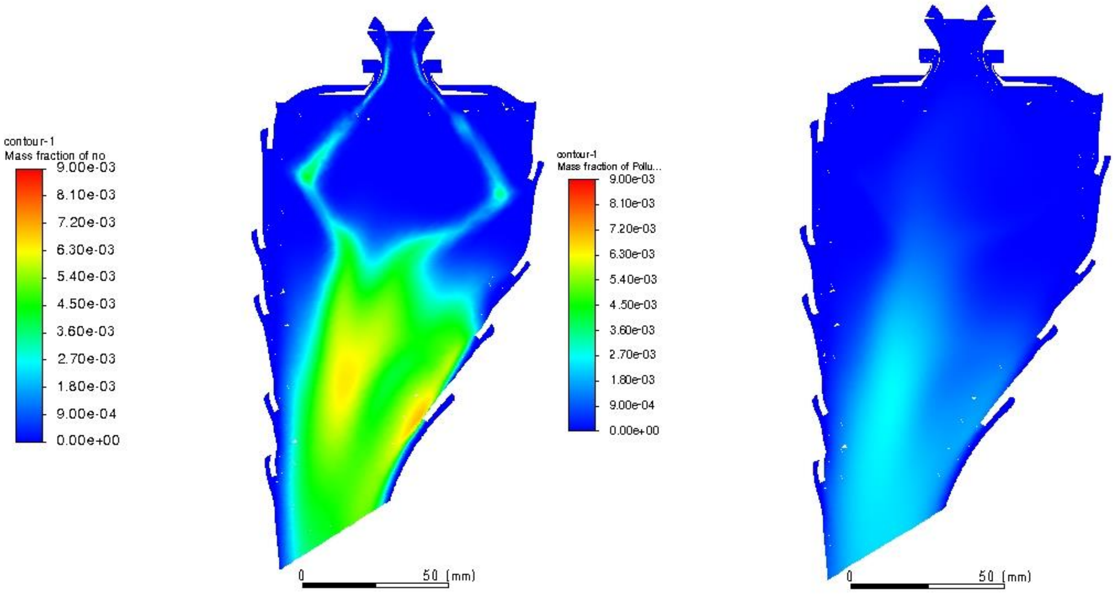

Figure 5.14: Contours of the mass fraction of NO in the cut-view plane of the first swirler, while burning Jet A at the power setting of 100%, obtained with ANSYS Fluent software: in the left, with the NOx sub-mechanism and, in the right, with the ANSYS NOx model.

Through the previous figure, it is possible to understand why the NOx forecast with the NOx sub-mechanism gave a higher value for the NOx emissions in relation to the NOx model available in Fluent. As can be seen in the figures mentioned, the sub-mechanism predicted a much higher mass fraction of NOx. Furthermore, the mass fraction of NOx predicted by the ANSYS model is so low that it is barely detected in the contours with the scale used.

5.6.2 Comparison of Emissions Between Jet A and Hydrogen Fuel

As previously explained in the methodology, the results used in this comparison were obtained through simulations using the same boundary conditions (air mass flow rates, temperatures, pressures, etc.) as the control simulations for each power setting, but now burning hydrogen, instead of Jet A.

The Figure 5.15 shows the comparison between the reference values (from ICAO and from the better model of the previous results for Jet A fuel) and the NOx emission analysis made through two different approaches for hydrogen fuel, the NOx sub-mechanism and the NOx model from ANSYS Fluent.

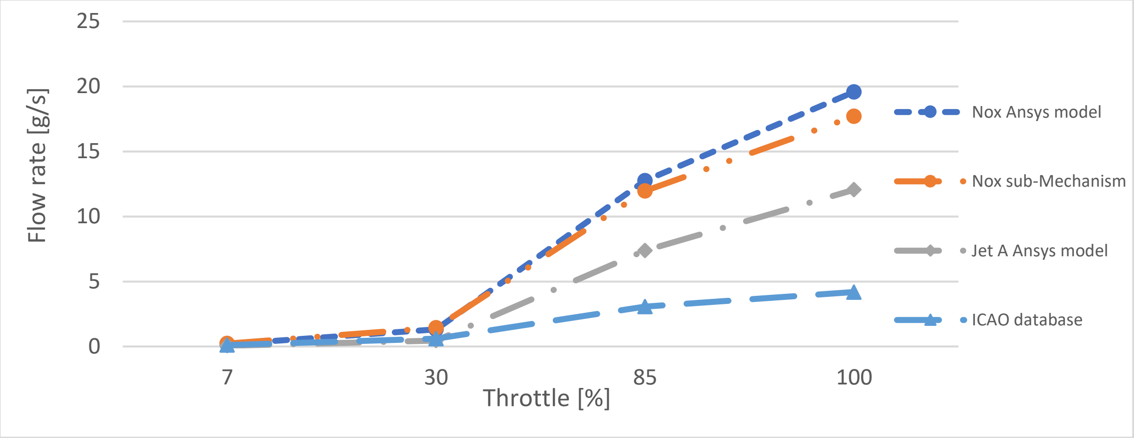

Figure 5.15: Comparison of the flow rates of NOx for the combustion of Jet A and hydrogen fuel obtained through the use of two approaches, NOx sub-Mechanism (only for hydrogen) and Ansys NOx model (for both fuels), for one fourth of the combustion chamber throughout ICAO's LTO cycle.

As referred before, these analyzes were performed in terms flow rate, with the units of grams per second.

Looking at Figure 5.15, considering the models used for NOx forecast, it is possible to draw two main conclusions. Regarding the models used for NOx forecast, it is possible to observe that the forecasts made by the ANSYS NOx model provide higher values than those made with the NOx sub-mechanism for all the operating conditions; however, the error between these values is relatively small (up to ten percent). Then, comparing the quantity of NOx produced by the hydrogen fuel with the quantity of NOx produced by the Jet A for each power setting, it is possible to conclude that for the lower power settings, the quantities of NOx emitted are nearly the double of the quantities for the Jet A (both for ICAO's database and for the prediction with the model); and, for the higher power settings, the quantities of NOx emitted continue to be nearly the double of the quantities predicted for the Jet A fuel simulations with the NOx model and the emissions are predicted to be nearly four to five times higher than the reference data from ICAO. Since the same swirlers and injector geometry (single hole) are being used for both fuels, these results are in agreement with the results of C. J. Marek et al. [38], who concluded in their work that, using similar injection geometries, the minimum NOx levels for hydrogen fuel were twice as high as for Jet A fuel.

In the following, the Figure 5.16 and Figure 5.17 will be presented to analyze the difference between the two approaches used to predict the NOx emissions for the hydrogen simulations.

The Figure 5.16 presents the contours of the mass fractions of NO and NO_2 produced while burning hydrogen in the cut-view plane of the first swirler for the power setting of 100%, obtained through the NOx sub-mechanism.

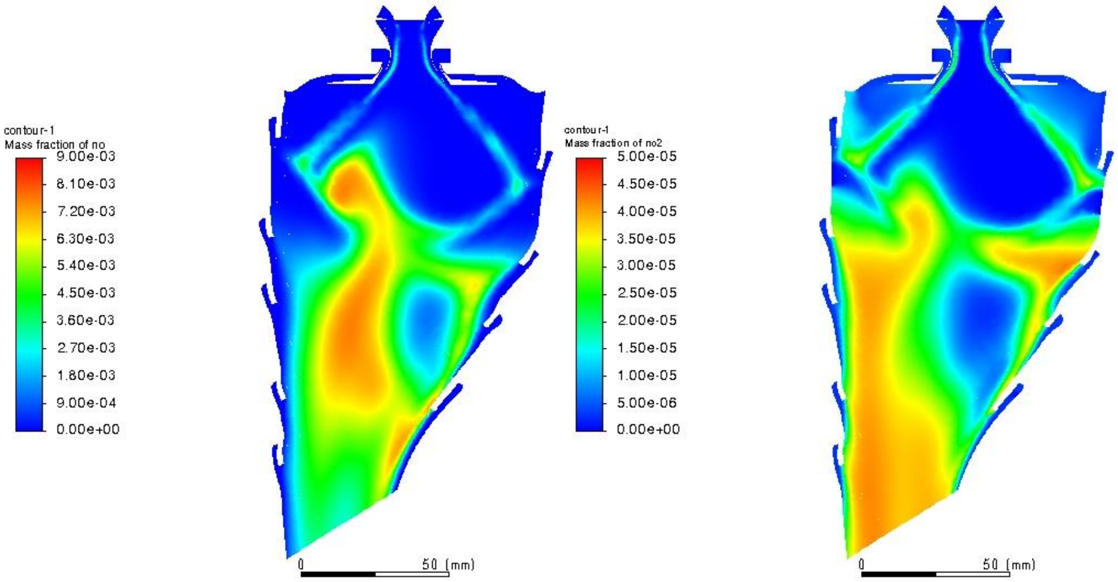

Figure 5.16: Contours of the mass fraction of NO (left) and NO_2 (right) in the cut-view plane of the first swirler, while burning hydrogen fuel at the power setting of 100%, obtained with the NOx sub-mechanism through ANSYS Fluent software.

It should be noted that the scale used in the two images is not the same due to the fact that if the scale for the contour of the NO_2 mass fraction was the same as the one used for the contour of the NO mass fraction, this contour would not bring any useful information to the work because the values of the NO_2 mass fraction are residual when compared with the values of the NO mass fraction.

The Figure 5.17 presents the contours of the NOx mass fraction produced while burning hydrogen in the same plane used in the previous figure for the power setting of 100%, obtained through the NOx model from ANSYS Fluent.

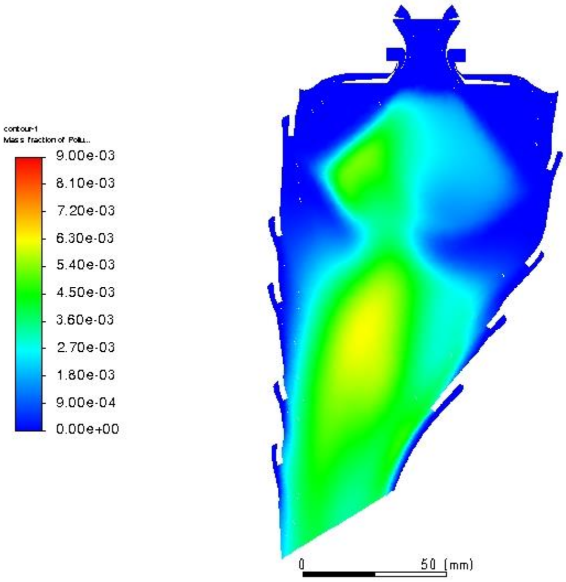

Figure 5.17: Contour of the mass fraction of NO in the cut-view plane of the first swirler, while burning hydrogen fuel at the power setting of 100%, obtained with the Ansys NOx model through ANSYS Fluent software.

As can be observed through the Figure 5.16 and Figure 5.17, it seems that the mass fractions of NOx predicted across the combustion chamber by the ANSYS model are lower than the mass fractions of NOx predicted by the NOx sub-mechanism. However, as shown in Figure 5.15, the flow rate of NOx predicted at the outlet of the combustor by the ANSYS model is higher than the value predicted by the sub-mechanism. A possible explanation for this phenomenon may be the existence of a high chemical recombination in the dilution zone of the chamber promoted when using the sub-mechanism, which does not occur with the ANSYS NOx model, as it predicts the quantity of NOx only through local temperatures.

Another conclusion that can be drawn from the previous figures is that, for both approaches, the zones where the higher quantities of NOx are produced correspond to the zones where the temperatures are higher (shown in Figure 5.10).

In Figure A.G.3 (Appendix G), the same contours (only for the mass fractions of NO) are presented, but for the power setting of 30%, and, for this case, the conclusions are identical to the previous ones.

5.6.3 Sensibility Tests

In this work, several sensibility tests were carried out, namely, the presence of the swirl effect on the swirlers' inlets and the influence of the fuel injection pressure and temperature. The most relevant results of these tests are presented in Figure 5.18 and Figure 5.19.

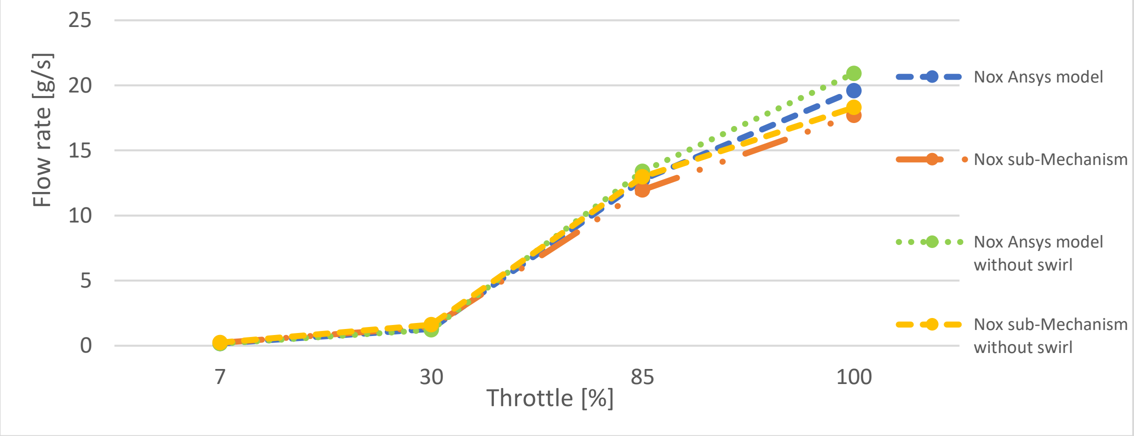

Figure 5.18: Flow rates of NOx emissions in the analysis of the influence of swirl effect, while burning hydrogen, through the use of two approaches, NOx sub-Mechanism and Ansys NOx model, for one fourth of the combustion chamber throughout ICAO's LTO cycle.

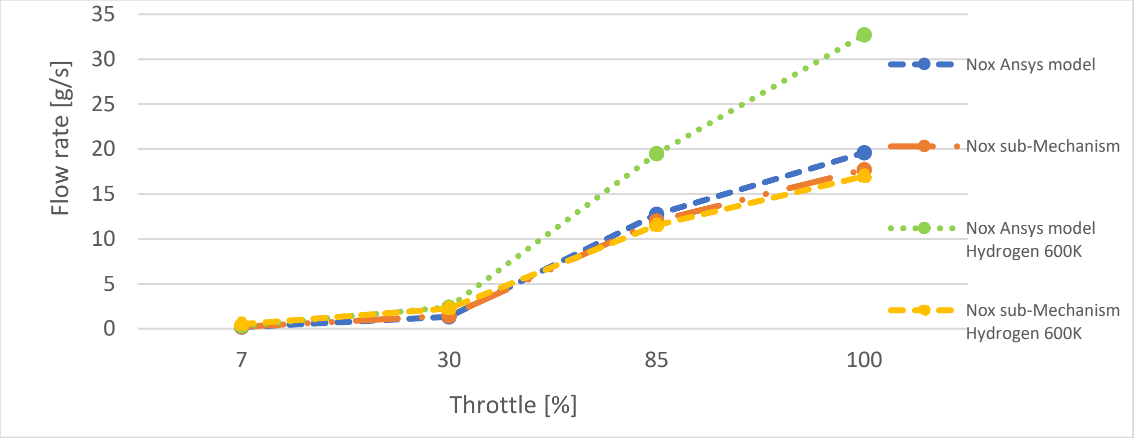

Figure 5.19: Flow rates of NOx emissions in the analysis of the influence of the hydrogen fuel temperature through the use of two approaches, NOx sub-Mechanism and Ansys NOx model, for one fourth of the combustion chamber throughout ICAO's LTO cycle.

As the values represented in Figure 5.18 and Figure 5.19 are quite similar, it was decided to present these values also in Table 8.

Table 8: NOx flow rates in [g/s] obtained for hydrogen fuel (as in Figure 5.18 and Figure 5.19).

Op. Cond.	Standard Reference		Without swirl		Fuel 600K	
	Sub-Mechanism	*Ansys model*	*Sub-Mechanism*	*Ansys model*	*Sub-Mechanism*	*Ansys model*
100	17.70	19.58	18.30	20.91	16.97	32.70
85	11.97	12.75	12.98	13.40	11.51	19.49
30	1.44	1.30	1.61	1.22	2.26	2.38
7	0.22	0.17	0.24	0.16	0.51	0.32

Regarding the injection pressure tests, the modification of these values did not cause any relevant change in the results. For this reason, the results are not previously presented neither in graph nor in the table, since they do not allow to analyze the influence of this parameter.

Generally, in practice, in gas turbine engines, the fuel injection pressure is used to control the quantity of fuel injected. In this study, the geometry of the injectors was always considered the same (the area of the inlets did not change) and the fuel mass flow rate was also considered the same for each power setting. Thus, for these tests, where injection pressure increases of 1.5 and 2 times were applied, an increase in fuel density would be expected and, consequently, a reduction in the fuel jet velocity, which, however, proved to be irrelevant for all the power settings, not significantly influencing the results.

Regarding the influence of the swirl effect, whose results for the NOx emissions are presented in Figure 5.18, if one considers the same forecast approach (only the values of ANSYS model, or the values of the sub-mechanism) it is possible to conclude that for this specific case, the presence of this phenomenon helps to reduce slightly the quantity of

NOx emissions for the higher power settings, while for the lower power settings the NOx values remain quite close.

To assist in the analysis of the influence of the swirl effect, the Figure 5.20 shows the contours of static temperature (in the cut-view plane of a swirler for the power setting of 85%) for the simulations with and without the swirl effect.

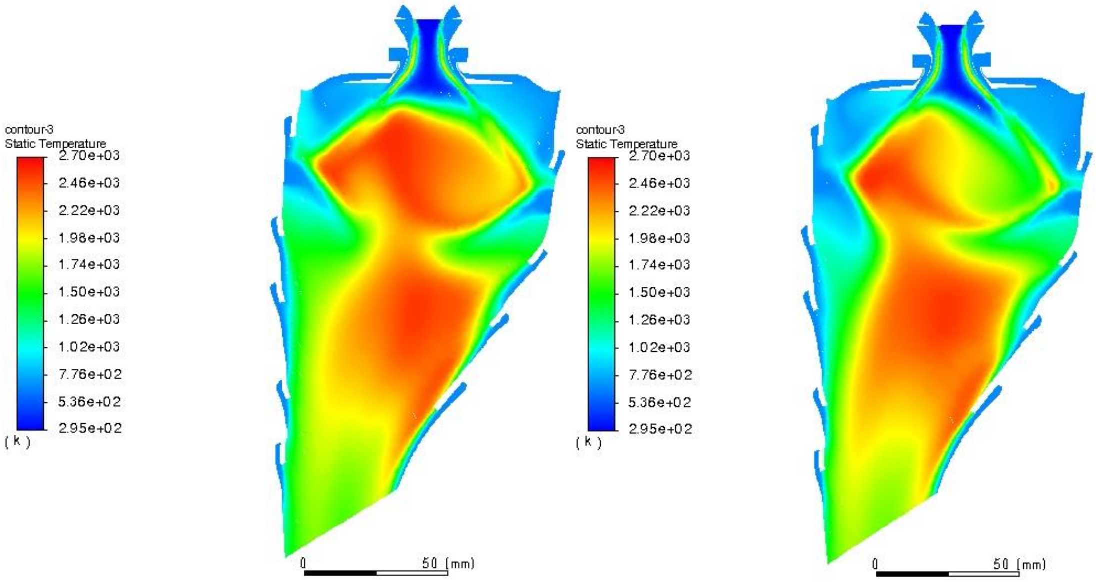

Figure 5.20: Contours of static temperature in the cut-view plane of the first swirler, while burning hydrogen fuel with the swirl effect (left) and without the swirl effect (right) at the power setting of 85%, obtained with ANSYS Fluent software.

Looking at the image for the simulation without the swirl effect (in Figure 5.20), it is possible to identify a low temperature region inside the recirculation zone (in primary zone) where apparently the combustion intensity is lower. After analyzing this recirculation zone (species, shape, etc.), it was concluded that this phenomenon probably occurred due to the existence of some difficulties in properly mixing the fuel and air in this zone because of the decrease in the airflow rotation, caused by the removal of the swirl effect. This decrease in the airflow rotation due to the absence of the swirl effect can be observed through Figure A.G.4 (Appendix G), where the velocity magnitude vectors are represented (cut-view of the same swirler for the power setting of 85%) for the simulations with and without the swirl effect.

To analyze the influence of the inlet fuel temperature, the sensibility tests were made with the hydrogen fuel at 600K and the results for the NOx emissions are presented in Figure 5.19. From this figure it is possible to conclude that, contrary to the previous results, for the analysis with the hydrogen temperature of 600K, the error between the two approaches used to forecast the NOx emissions is considerable for the higher power settings (85% and 100% power), i.e., looking to the values obtained, the predicted emissions with the NOx model of ANSYS are almost twice the predicted values with the NOx sub-mechanism. Furthermore, for the higher power settings (85% and 100% power), the approaches showed different behavior. For the sub-mechanism, the NOx emissions are lower for the fuel temperature of 600K, while for the NOx model of ANSYS, the emissions keep higher than for the reference temperature (298.15K). However, in the lower power settings (7% and 30% power) the quantities of NOx emitted are higher for the fuel temperature of 600K than for the reference temperature (298.15K) for both approaches.

To assist in the analysis of the influence of the hydrogen fuel temperature, the Figure 5.21 shows the contours of static temperature (in the cut-view plane of a swirler for the power setting of 85%) for the simulations with the hydrogen fuel at 298.15K and 600K.

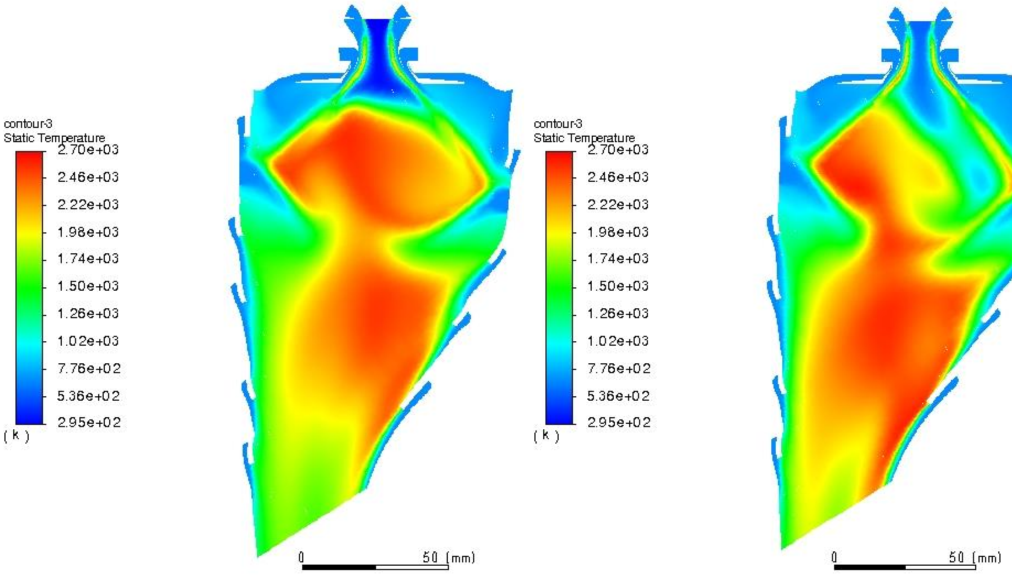

Figure 5.21: Contours of static temperature in the cut-view plane of the first swirler, while burning hydrogen fuel at 298.15K (left) and at 600K (right) at the power setting of 85%, obtained with ANSYS Fluent software.

Looking at the image for the simulation with the hydrogen fuel temperature of 600K (in Figure 5.21), it is possible to identify the appearance of at the least three problems that can lead to the malfunction of the chamber. At first, like in the analysis with the swirl effect, it is possible to identify a low temperature region inside the recirculation zone (in the primary zone) where apparently the combustion intensity is lower (or the combustion does not even occur). Moreover, it is still possible to detect the formation of higher temperature regions in the primary zone and in the zones closer to the inner wall.

The appearance of these two problems can be justified through the Figure 5.22, which shows the contours of the velocity magnitude (in the same plane and power setting as in the previous figure) for the simulations with the hydrogen fuel at 298.15K and 600K.

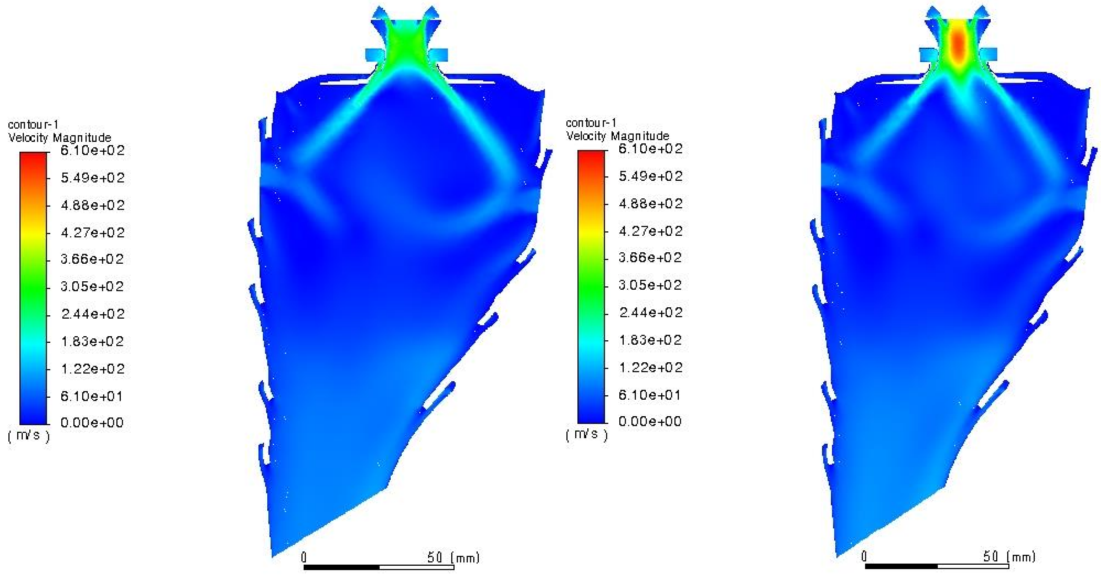

Figure 5.22: Contours of velocity magnitude in the cut-view plane of the first swirler, while burning hydrogen fuel at 298.15K (left) and at 600K (right) at the power setting of 85%, obtained with ANSYS Fluent software.

Through this figure, it is possible to observe that the velocity of the hydrogen fuel jet almost doubled when the fuel temperature was increased to 600K. This phenomenon is probably the responsible for the deterioration of the quality of the velocity profiles in the recirculation zone, impairing the mixing intensity between the fuel and the air and, consequently, reducing the quality of the combustion. The most plausible reason for the occurrence of this phenomenon is the decrease in the fuel density due to the increase in temperature, which in turn causes an increase in the velocity of the fuel jet, since the injection area and the fuel mass flow rate are constant parameters.

The last of the three problems mentioned before can be identified in Figure 5.21 (image for the fuel temperature of 600K). In this figure, it is possible to identify two regions where the flame starts very early (almost inside the swirler), in what seems to be the occurrence of autoignition. This is an unwanted phenomenon that should always be avoided.

For the lower power settings, the same problems continue to be detected. As can be observed in Figure A.G.5 (in Appendix G), which represents the contours of static temperature (in the cut-view plane of a swirler for the power setting of 7%) for the simulation with the fuel temperature of 600K, it is possible to conclude that there are regions where the flame is also initiated before the recirculation zone (autoignition), and it is still possible to detect the presence of hot-spots across the chamber, as well as a low temperature region inside the recirculation zone (in primary zone).

In brief, the use of higher temperatures for the hydrogen fuel is not advisable in this case, as this change will lead to malfunctions and, consequently, to the presence of unwanted phenomena (hot-spots, autoignition, etc.), which will probably lead to a higher production of NOx.

Chapter 6 – Conclusion

This work presents an overview of the use of hydrogen in the aeronautical sector, a brief description of the components of the current gas turbine engines, the modifications needed to adapt these engines to use hydrogen as a fuel, and an introduction to the mechanisms of pollutant formation, focusing on the species that are more likely to be produced in these engines when burning the fuels considered in this study.

Still in this work, the evaluation of the feasibility of converting existing gas turbine engines, from Jet A to hydrogen, from the combustion point of view, was also carried out using an analysis of the emissions produced when burning these fuels through the specific power settings represented in the ICAO's LTO cycle. For that, a CFD simulation study was performed on a model of a CFM56-3 combustor while burning hydrogen and Jet A (as a reference standard).

The main objectives of this study were, first of all, to adapt the injection system for hydrogen fuel and then to determine the correct boundary conditions for the air and fuel. The second main objective was to analyze the pollutant emissions resulting from the combustion of hydrogen fuel, i.e., the NOx emissions. The last primary objective was to compare these results with the pollutant emissions obtained for the Jet A fuel. In the end, all these objectives were accomplished and it was demonstrated that, theoretically, the CFM56-3 can work with hydrogen fuel with minor changes (related only to the injection system).

As in all works with this complexity, several problems appeared throughout this study to correctly predict results that are in agreement with the available experimental/measured data. These problems were mainly related to the geometry, mesh and boundary conditions. However, after several improvements in all of these parameters (explained during the work), there were obtained satisfactory results.

During this work, it was possible to deepen knowledge on several topics including thermodynamics (mainly on the combustion process and pollutant formation in annular chambers), turbulence, radiation and chemistry models used in this type of works. It was also needed to learn how to properly use the ANSYS software (Fluent and Fluent Meshing).

Regarding the results, starting the analysis with the control simulations (reference standard), although for this case the results obtained through the numerical study are acceptable when compared with those of ICAO, there is still a little margin of error for some of the conditions studied (more evident for the higher power settings). However, there are several possible reasons that can be pointed out for the differences between the values of the simulations and the values of the ICAO's database. For instance, the fact that the Jet A fuel was considered to be in the gaseous state when injected into the combustion chamber simulates "perfect" atomization, increasing the combustion efficiency and creating a higher temperature inside the combustion chamber. Another reason can be the fact that the chosen mechanism/sub-mechanism does not represent in the best way the combustion of the Jet A fuel or the NOx production, respectively. The choice of the radiation model can also influence this result, since the radiation representation is more important when simulating the burning of hydrocarbon fuels than when simulating the burning of hydrogen. Another possible reason could be the chemical model used. However, due to the limited computational resources, it was not possible to use more complex models.

Regarding the results obtained for hydrogen, it was demonstrated that with the increase of the accelerator percentage, a higher mass of NOx per mass of hydrogen is produced, due to the increase in the temperature inside the chamber. Moreover, when comparing the NOx emissions obtained for the simulations with both fuels (Jet A and hydrogen) for the standard operating conditions of the engine, it was shown that for this geometry of combustor and injector, the quantity of NOx produced when burning hydrogen is almost twice as high as the NOx emissions for Jet A for each power setting. As previously mentioned, this behavior is in line with other works available in the literature. However, it is necessary some caution when making this comparison, since the results obtained for hydrogen fuel could not be confirmed due to the lack of experimental data.

Finally, regarding the sensibility tests (changing the swirl effect, fuel injection pressure and fuel temperature), only the changes in swirl effect and fuel temperature produced relevant changes in the results. The fact that the changes in fuel injection pressure have not influenced the results can be explained as a consequence of the fuel mass flow rates and the injector geometry being fixed for each power setting and the fact that the changes in the fuel density, due to the modification of the injection pressure, have been irrelevant. Thus, it was possible to conclude that the pressure changes did not affect the behavior of the fuel jet nor the velocity profiles inside the chamber in a significant manner. Consequently, the effect on NOx emissions was also irrelevant. Even so, for this specific test, it should be noted that this behavior may still have occurred due to any problem related to the values chosen for the tests, or the way they were introduced in Fluent.

Through the results obtained for the tests with the changes in the swirl effect, it was shown that in the tests without the presence of this effect, the quality of the recirculation zone was reduced, and the temperature across the combustion chamber was slightly increased. Consequently, the NOx emissions also increased. Thus, it was concluded that the presence of the swirl effect increases the airflow rotation, improving the mixing intensity between the fuel and the air, stabilizing and retaining the flame in the primary zone, which in turn helps to reduce the chamber's peak temperature and, consequently, the NOx emissions.

About the influence of the fuel temperature, it was expected that an exponential raise in this value could largely affect the temperature in the outlet of the chamber, due to increased combustion efficiency. However, that did not happen, and not only the outlet temperature changed just a small percentage (1% to 2%) for the double of the initial fuel temperature, but it also caused malfunctions across the chamber, with greater evidence in the higher power settings, where the analysis of the flame (obtained in the numerical study) shows a great deterioration of the recirculation zone and the presence of a phenomenon that seems to be the occurrence of autoignition or flashback inside the swirlers. These malfunctions were associated with the velocity of the hydrogen fuel flow, which almost doubled when the temperature was raised. The most credible reason for this behavior consists in the density reduction of the hydrogen fuel due to that change in temperature.

6.1 Future Works

As stated during this work, the combustion is an extremely complex process involving several processes that are complex enough by themselves (thermodynamics, turbulence, radiation, etc.). So, there are several parameters that could not be considered throughout this work with which the results could be improved. Thus, in the future, this study can be continued and complemented involving the following items:

- The study of the influence of the fuel injection angle (inside the swirler) on the amount of NOx emitted;
- The analysis of the influence of the fuel pressure through another approach, to identify the true effect of this parameter on the combustion process;
- Repeat the study with a transient approach like URANS, or through more expensive computational models like SBES, LES or DNS, and try to understand if these approaches could give better results for the pollutant emissions;
- The improvement of the geometry of the swirler, mainly in the zone between the cooling wall and the outlet of the secondary swirler. Although in this work the flow produced by the swirlers has been improved, this factor should be further investigated;
- An experimental study about the pollutant formation (mainly NOx emissions) in this combustor for the tested fuels. One of the biggest limitations in this work was exactly the lack of experimental data to compare with the numerical results,

mainly the behaviour of the flame inside the combustion chamber. These data could help to better choose the models to use in order to reduce the computational cost. However, the prohibitive costs of this type of study may turn it unfeasible. Alternatively, a numerical study in a software like the *GasTurb* for at the least one of the lower power conditions could also help to improve this work, since, for instance, the operating conditions for the lower power settings were obtained through a trial error approach.

Many more examples can be mentioned such as improving the mesh near the walls to allow the correct study of the heat transfer, or test some other gaseous fuels and compare the results obtained with those of this work, etc.

Most of the items in the previous list prove once again the potential that CFD can provide for problems that are difficult to carry out experimentally.

Bibliography

[1] ICAO (International Civil Aviation Organization). ICAO GLOBAL ENVIRONMENTAL TRENDS – PRESENT AND FUTURE AIRCRAFT NOISE AND EMISSIONS. Working Paper, reference A40-WP/54 EX/21, 5/7/19

[2] ICAO (International Civil Aviation Organization). PERSPECTIVES ON SUSTAINABLE AVIATION. Working Paper, reference A40-WP/102 EX/40, 24/07/19

[3] ICAO (International Civil Aviation Organization). Aviation and the Environment: Outlook. Chapter one in: ICAO 2019 Environmental Report, 2019

[4] European Commission. Revision of the EU Emission Trading System Directive 2003/87/EC concerning aviation [Internet]. Ref. Ares (2020) 3515933. 03/07/2020. Available from: https://ec.europa.eu/clima/eu-action/transport-emissions/reducing-emissions-aviation_en [Accessed: March 17, 2022]

[5] ATAG (AIR TRANSORT ACTION GROUP). Waypoint 2050 report. Second Edition, September 2021

[6] ICAO (International Civil Aviation Organization). SUSTAINABLE AVIATION FUELS GUIDE, version 2. 2018

[7] ICAO (International Civil Aviation Organization). (2019). *Innovative Fuels* [Internet]. Available from: https://www.icao.int/environmental-protection/Pages/innovative-fuels.aspx [Accessed: May 8, 2022]

[8] ICAO (International Civil Organization). (2019). *CAEP Fuels Task Group* [Internet]. Available from: https://www.icao.int/environmental-protection/Pages/CAEP-FTG.aspx [Accessed: May 9, 2022]

[9] Brewer, GD. Hydrogen Aircraft Technology. Vol. 33431. Boca Raton, Florida: CRC Press; 1991. ISBN: 0-8493-5838-8

[10] Mulready, RC. Liquid hydrogen engines. Chapter 5 in: Technology and Uses of Liquid Hydrogen, Scott, R. B., Denton, W. H., and Nicholls, C. M., Eds., Macmillan, New York, 1964

[11] Silverstein A, Hall EW. Liquid Hydrogen as a Jet Fuel for High-Altitude Aircraft. NACA RM E55C28a, National Advisory Committee for Aeronautics-Lewis Flight Propulsion Laboratory, Cleveland, OH, 1955

[12] Seeckt K. Conceptual Design and Investigation of Hydrogen-Fueled Regional Freighter Aircraft, [Licentiate Thesis], Sweden: Stockholm; 2010

[13] Westenberger A. HYDROGEN FUELLED AIRCRAFT. LAirbus Deutschland GmbH 21129 Hamburg, Germany, 22/05/2003, In: AIAA 2003-2880

[14] BOEING. (2010, July 12). *Boeing Unveils Unmanned Phantom Eye Demonstrator* [Internet]. Available from: https://boeing.mediaroom.com/2010-07-12-Boeing-Unveils-Unmanned-Phantom-Eye-Demonstrator/ [Accessed: April 17, 2022]

[15] AIRBUS. ZEROe [Internet]. Available from: https://www.airbus.com/en/innovation/zero-emission/hydrogen/zeroe [Accessed: April 23, 2022]

[16] BBC. (2021, April 8). The hydrogen revolution in the skies [Internet]. Available from: https://www.bbc.com/future/article/20210401-the-worlds-first-commercial-hydrogen-plane [Accessed: May 20, 2022]

[17] Center, D. G. (2009, July 7). DLR motor glider Antares takes off in Hamburg – powered by a fuel cell [Internet]. Available from: https://www.dlr.de/content/en/downloads/news-archive/2009/20090707_dlr-motor-glider-antares-takes-off-in-hamburg-powered-by-a-fuel-cell_18278.pdf;jsessionid=55CD132BCF3D0E9308F052DF6FF43DE6.delivery-replication1?__blob=publicationFile&v=11 [Accessed: May 4, 2022]

[18] BOEING. (2008, April 3). Boeing Successfully Flies Fuel Cell-Powered Airplane [Internet]. Available from: https://web.archive.org/web/20080406204719if_/http://www.boeing.com:80/news/releases/2008/q2/080403a_nr.html [Accessed: May 16, 2022]

[19] ENFICA-FC. ENvironmentally Friendly Inter City Aircraft powered by Fuel Cells *(ENFICA-FC)* [Internet]. Available from: http://www.enfica-fc.polito.it/ [Accessed: April 28, 2022]

[20] ENGINEER, T. (2016, September 30). Fuel cell aircraft HY4 makes maiden flight [Internet]. Available from: https://www.theengineer.co.uk/fuel-cell-aircraft-hy4-makes-maiden-flight/ [Accessed: April 29, 2022]

[21] CORDIS, E. C. (2021, February 3). ENABLing cryogEnic Hydrogen based CO2 free air transport (ENABLEH2) [Internet]. Available from: https://cordis.europa.eu/article/id/428900-lh2-powered-aircraft-are-coming-but-when [Accessed: April 30, 2022]

[22] ENABLEH2 [Internet]. Cranfield University; 2022. Available from: https://www.enableh2.eu/ [Accessed: April 25, 2022]

[23] Airbus Deutschland GmbH. Liquid Hydrogen Fuelled Aircraft – System Analysis. FINAL TECHNICAL REPORT (PUBLISHABLE VERSION), September 2003.

[24] Reid Smith, et al. Advanced Low Emissions Subsonic Combustor Study. Final Report. NASA/CR-1998-207931, PWA-6420-28, Lewis Research Center; December 1998

[25] Robinson AE, Funke HH-W, Hendrick P, Wagemakers R. Design and Testing of a Micromix Combustor with Recuperative Wall Cooling for a Hydrogen Fueled μ-Scale Gas Turbine. Journal of Engineering for Gas Turbines and Power. 2010; 133. DOI:10.1115/GT2010-23453

[26] Boggia S, Jackson A, Singh R. Unconventional Cycles for Aero Gas Turbine Engines Burning Hydrogen. 15th Symposium on Air Breathing Engines, ISABE, Bangalore, India; September 3–7, 2001.

[27] Payzer RJ, Renninger SW. (1979). Hydrogen Fueled High Bypass Turbofans in Subsonic Aircraft. Hydrogen in Air Transportation, International DGLR/DFVLR Symposium, September 11–14, Germany.

[28] Haglind F, Singh R. Design of Aero Gas Turbines Using Hydrogen. Journal of Engineering for Gas Turbines and Power. 2004; 128: 754–764

[29] Lee MC, Bin Seo S, Chung JH, Kim SM, Joo YJ, Ahn DH. Gas turbine combustion performance test of hydrogen and carbon monoxide synthetic gas. Fuel. 2010; 89: 1485–1491.

[30] Svensson F, Hasselrot A, Moldanova J. Reduced environmental impact by lowered cruise altitude for liquid hydrogen-fuelled aircraft. Aerosp. Sci. Technol. 2004; 8: 307–320.

[31] Koç Y, Yaglı H, Görgülü A, Koç A. Analysing the performance, fuel cost and emission parameters of the 50 MW simple and recuperative gas turbine cycles using natural gas and hydrogen as fuel. Int. J. Hydrog. Energy. 2020; 45: 22138–22147.

[32] Osigwe EO, Gad-Briggs A, Nikolaidis T, Jafari S, Sethi B, Pilidis P. Thermodynamic Performance and Creep Life Assessment Comparing Hydrogen and Jet-Fueled Turbofan Aero Engine. Appl. Sci. 2021; 11 (9), 3873. DOI: https://doi.org/10.3390/app11093873

[33] Boggia S, Jackson A. Some Unconventional Aero Gas Turbines Using Hydrogen Fuel. In: Proceedings of ASME Turbo Expo 2002, Amsterdam. Vol. 2B. New York: ASME; 2002. pp. 683–690.

[34] Jackson AJ. Optimisation of Aero and Industrial Gas Turbine Design for the Environment [Ph.D. Thesis]. Cranfield, UK: Cranfield University; 2009

[35] Gunasekar P, Manigandan S, Venkatesh S, Gokulnath R, Vimal R, Boomadevi P. Effect of hydrogen addition on exergetic performance of gas turbine engine. Aircr. Eng. Aerosp. Technol. 2019; 92: 180–185.

[36] Dahl G, Suttrop F. ENGINE CONTROL AND LOW-NOx COMBUSTION FOR HYDROGEN FUELLED AIRCRAFT GAS TURBINES, Int.J. Hydrogen Energy. 1998; Vol. 23, No. 8, pp. 695-704

[37] Ziemann J, Shum F, Moore M, Kluyskens D, Thomaier D, Zarzalis N, Eberius H. LOW-NOx COMBUSTORS FOR HYDROGEN FUELED AERO ENGINE. ht. J. Hydrogen Energy. 1998; Vol. 23, No. 4, pp. 281-288

[38] Marek CJ, Smith TD, Kundu K. Low Emission Hydrogen Combustors for Gas Turbines Using Lean Direct Injection. In: 41st AIAA/ASME/SAE/ASEE Joint Propulsion Conference and Exhibit. Tucson, Arizona, USA. July 10–13, 2005

[39] Lei H, Khandelwal B. Investigation of Novel Configuration of Hydrogen Micromix Combustor for Low NOx Emission. In: Proceedings of the AIAA Scitech 2020 Forum, Orlando, FL, USA, 6–10 January 2020; American Institute of Aeronautics and Astronautics: Reston, VA, USA. 2020; p. 11.

[40] Kuo KK. PRINCIPLES OF COMBUSTION. Second Edition. Hoboken, New Jersey: John Wiley & Sons, Inc.; 2005. ISBN 0-471-04689-2

[41] Lefebvre AH, Ballal DR. Gas turbine combustion. Third Edition. Boca Raton, FL: CRC Press; 2010. ISBN: 978-1-4200-8605-8

[42] Ziemann J, Mayr A, Anagnostou A, Suttrop F, Lowe M, Bagheri S A, Nitsche Th. (1998). Potential Use of Hydrogen in Air Propulsion. EQHHPP, Phase III.0-3, Final Report, submitted to the European Union.

[43] Ströhle J, Myhrvold T. An evaluation of detailed reaction mechanisms for hydrogen combustion under gas turbine conditions. In: International Journal of Hydrogen Energy. 2007; 32: 125 – 135. DOI: 10.1016/j.ijhydene.2006.04.005.

[44] Ströhle J, Jørgen H, Seljeskog M, Ditaranto M, Langørgen Ø, Jakobsen J, Rønnekleiv M. (2006). Experimental and numerical investigation of NOx emission characteristics of swirled hydrogen rich flames. In: 8th International Conference on Greenhouse Gas Control Technologies (GHGT-8). Trondheim, Norway: Elsevier.

[45] Todd DM, Battista RA. (2000). Demonstrated applicability of hydrogen fuel for gas turbines. In: Proceedings of the IchemE Gasification 4Conference

[46] Cocchi S, Pandey GN, Provenzale M, Zucca A, Romano C, Ceccherini G. (2008). A simple model for NOx formation in diffusion gas turbine combustors:

rig test validation with a wide range of fuel gases. In: 31st Meeting on Combustion, I.S.o.t.C. Institute, Editor.

[47] Murthy P, Khandelwal B, Sethi V, Singh R. Hydrogen as a Fuel for Gas Turbine Engines with Novel Micromix Type Combustors. In: Proceedings of the 47th AIAA/ASME/SAE/ASEE Joint Propulsion Conference & Exhibit, San Diego, CA, USA. 31 July–3 August 2011; pp. 1–7.

[48] Funke H.-W, Beckmann N, Abanteriba S. An overview on dry low NOx micromix combustor development for hydrogen-rich gas turbine applications. Int. J. Hydrog. Energy. 2019; 44: 6978–6990.

[49] Agarwal P, Sun X, Gauthier PQ, Sethi V. Injector Design Space Exploration for an Ultra-Low NOx Hydrogen Micromix Combustion System. In: Proceedings of the Turbo Expo: Power for Land, Sea and Air. Phoenix, AZ, USA. 17–21 June 2019.

[50] Karakurt A, Khandelwal B, Sethi V, Singh R. Study of Novel Micromix Combustors to be used in Gas Turbines; using Hydrogen, Hydrogen-Methane, Methane and Kerosene as a fuel. In: Proceedings of the 48th AIAA/ASME/SAE/ASEE Joint Propulsion Conference & Exhibit. Atlanta, GA, USA. 30 July–1 August 2012.

[51] Cerutti M, Cocchi S, Modi R, Sigali S, Bruti G. Hydrogen Fueled Dry Low NOx Gas Turbine Combustor Conceptual Design. In: Proceedings of the ASME Turbo Expo 2014: Turbine Technical Conference and Exposition, Düsseldorf, Germany, 16–20 June 2014.

[52] Agbadede R, Nkoi B, Kainga B. Performance Analysis of Industrial Gas Turbines Fueled with Hydrogen. Niger. Res. J. Eng. Environ. Sci. 2020; 5: 178–189.

[53] Najjar YS, Zahed A, Bashir M, Alp T. Feasibility of Hydrogen Utilization in Gas Turbine Engines. Energy Environ. 1990; 1: 240–251.

[54] Eshati S, Ghafir MFA, Laskaridis P, Li YG. Impact of operating conditions and design parameters on gas turbine hot section creep life. In: Proceedings of the Turbo Expo: Power for Land, Sea and Air. Glasgow, UK. 14–18 June 2010.

[55] Eshati S, Abu A, Laskaridis P, Haslam A. Investigation into the Effects of Operating Conditions and Design Parameters on the Creep Life of High Pressure Turbine Blades in a Stationary Gas Turbine Engine. Mech. Mech. Eng. 2011; 15: 237–247.

[56] ETN Global. HYDROGEN GAS TURBINES-THE PATH TOWARDS A ZERO-CARBON GAS TURBINE [Internet]. January 2020. Available from:

https://etn.global/wp-content/uploads/2020/02/ETN-Hydrogen-Gas-Turbines-report.pdf [Accessed: March 21, 2022]

[57] Jiang L-Y. RANS Modelling of Turbulence in Combustors. Journal of Engineering for Gas Turbines and Power. 2017. DOI: 10.5772/intechopen.68361

[58] Boudier G, Gicquel LYM, Poinsot T, Bissières D, Bérat C. Comparison of LES, RANS and experiments in an aeronautical gas turbine combustion chamber. In: Proceedings of the Combustion Institute. 2007; 31: 3075–3082. DOI: 10.1016/j.proci.2006.07.067

[59] Benedetto AD, Sarli VD. (2005). Theory, Modeling and Computation of Gas Explosion Phenomena. Chapter 3 in Handbook of Combustion Vol.3: Gaseous and Liquid Fuels, 2010. ISBN: 978-3-527-32449-1

[60] Rolls-Royce. (1996). The Jet Engine. 5th Edition. Derby, England: The Technical Publications Department, Rolls- Royce plc.

[61] Jansohn P. (2013). Modern gas turbine systems - High efficiency, low emission, fuel flexible power generation. 80 High Street, Sawston, Cambridge CB22 3HJ, UK: Woodhead Publishing Limited. ISBN: N 978-1-84569-728-0

[62] Mathur ML, Sharma RP. (2007). GAS TURBINES AND JET AND ROCKET PROPULSION. Second Edition. Nem Chand Jain, Delhi-110006. ISBN: 81-8014-062-8

[63] Li J, Zhao Z, Kazakov A, Dryer F. An updated comprehensive kinetic model of hydrogen combustion. International Journal of Chemical Kinetics. 2004; Vol. 36, No. 10, pp. 566-575. DOI: https://doi.org/10.1002/kin.20026

[64] EASA (European Aviation Safety Agency). EASA TYPE-CERTIFICATE DATA SHEET -CFM56-2 & CFM56-3 Series Engines. TCDS: E.066. November, 2008

[65] Aubuchon D, Campbell J. CFM56–3 Turbofan Engine Description. Toronto, Canada: Seneca College; 03/2016

[66] CFMI. CFM56-3 TRAINING MANUAL-GENERAL ENGINE DATA. October 1995

[67] ICAO (International Civil Aviation Organization). ICAO engine exhaust emissions data bank “CFM56-3-B1” Tech. Rep.; January, 2015

[68] El-Sayed AF. Aircraft Propulsion and Gas Turbine Engines. Second Edition. Boca Raton, FL 33487-2742: CRC Press; 2017. ISBN: 978-1-4665-9516-3

[69] Oliveira J. (2016). CFD Analysis of the Combustion of Bio-Derived Fuels in the CFM56-3 Combustor [Master's Thesis]. Covilhã, Portugal: University of Beira Interior.

[70] Morão I. (2019). The influence of jet fuels on the emission of pollutants [Master's Thesis]. Covilhã, Portugal: University of Beira Interior.

[71] Mellor A M. (1990). Design of Modern Turbine Combustors. San Diego, CA 92101: ACADEMIC PRESS INC. ISBN: 0-12-490055-0

[72] Samuelsen S. (2006). Conventional type combustion. Gas Turbine Handb.

[73] Nomura M, Tamaki H, Morishita T, Ikeda H, Hatori K. (1981). Hydrogen combustion test in a small gas turbine. Int. J. Hydrogen Energy 6, 397-412.

[74] Shum F, Sampath P. (1984). Hydrogen combustion research. Final report by Pratt and Whitney Canada Inc. for National Research Council, Dept. of National Defence, Transport and Dept. of Supply and Services Canada.

[75] Peters N. (2010). Combustion Theory. CEFRC Summer School, Princeton,RWTH Aachen University.

[76] Lackner M, Winter F, Agarwal AK. Handbook of Combustion: Gaseous and Liquid Fuels. Vol.3. KGaA, Weinheim: WILEY-VCH Verlag GmbH & Co.; 2010. ISBN: 978-3-527-32449-1

[77] Flagan RC, Seinfeld JH. Fundamentals of air pollution engineering. NY, USA: Courier Corporation. 2013.

[78] Turns SR. An Introduction to combustion. Vol. 287. New York: McGraw-hill. 1996.

[79] Waitz IA, Gauba G, Tzeng Y-S. Combustors for micro-gas turbine engines. Journal of Fluids Engineering. 1998; Vol. 120, No. 1, pp. 109-117.

[80] Saravanamuttoo HIH, Rogers GFC, Cohen H. Gas turbine theory. Fifth Edition. Pearson Education, 2009.

[81] ICAO (International Civil Organization). Annex 16: Environmental Protection: Volume II-Aircraft Engine Emissions Fourth Edition. July 2017. ISBN 978-92-9258-314-9

[82] Taylor WF. (2022, August 02). Aviation Fuel. In: Macmillan Encyclopedia of Energy [Online]. Available from: https://www.encyclopedia.com/environment/encyclopediasalmanacs-transcripts-and-maps/aviation-fuel. [Accessed: August 9, 2022]

[83] Bering R, Buskov K. (2012). Numerical Investigation of the Soot Initiated Formation of Ultra Fine Particles in a Jet Turbine Engine Using Conventional Jet Fuel [Master's Thesis]. Aalborg, Copenhagen, Denmark: Alborg University.

[84] Masiol M, Harrison RM. Aircraft engine exhaust emissions and other airport related contributions to ambient air pollution: A review. Atmospheric Environment. Vol. 95, pp. 409-455; May 2014.

[85] Nehru College of Aeronautics & Applied Sciences Kuniyamuthur. (2022, June 1). Turbine Engine Fuel [Online]. India. Available from: https://sites.google.com/site/ncaaslecturenotes/gas-turbine-engine/unit-iv---fuelsystems/types-of-jet-fuel-its-characteristics. [Accessed: June 14, 2022]

[86] Shell Global. (2022, June 12). Shell Aviation Fuels [Online]. Available from: https://web.archive.org/web/20141219050306/http://www.shell.com/content/dam/shell/static/aviation/downloads/AeroShell-Book/aeroshell-book-2fuels.pdf. [Accessed: June 27, 2022]

[87] Shell Global. (2022, June 12). *CIVIL JET FUEL* [Online]. Available from: https://www.shell.com/business-customers/aviation/aviation-fuel/civil-jet-fuelgrades.html. [Accessed: June 27, 2022]

[88] Clean Sky 2 JU, FCH 2 JU, Hydrogen-powered aviation: A fact-based study of hydrogen technology, economics, and climate impact by 2050. May 2020. ISBN 978-92-9246-341-0.

[89] ATAG (Air Transport Action Group). Beginner's guide to aviation biofuels. Brochure; May 2009.

[90] Seungdo K, Dale BE. (2005). Life cycle assessment of various cropping systems utilized for producing biofuels: bioethanol and biodiesel. Biomass and Bioenergy. Vol.29 No. 6, 426–439.

[91] Daggett D, Hadaller O, Hendricks R, Walther R. Alternative fuels and their potential impact on aviation. National Aeronautics and Space Administration, NASA/TM. 2006; Vol. 214365, No. 6.

[92] Nazim ZM, Veziroglu TN. (2008). "Green" path from fossil-fuel to hydrogen economy: an overview of carbon-neutral technologies. International Journal of Hydrogen Energy, Vol. 33, 6804–6839.

[93] Flagan RC, Seinfeld JH. Fundamentals of air pollution engineering. NY, USA: Courier Corporation, 2013.

[94] Lieuwen T, Yang V. (2013). Gas Turbine Emissions (Cambridge Aerospace Series). Cambridge: Cambridge University Press. doi:10.1017/CBO9781139015462

[95] Pitz W, Mueller C. (2011). Recent progress in the development of diesel surrogate fuels. Progress in Energy and Combustion Science. Vol. 37, 330-350

[96] Lu T, Law C. (2009). Toward accommodating realistic fuel chemistry in large-scale computations. Progress in Energy and Combustion Science. Vol. 35, 192–215.

[97] Elliott L, Ingham D, Kyne A, Mera N. (2006). A novel approach to mechanism reduction optimization for an aviation fuel/air reaction mechanism using a genetic algorithm. Journal of Engineering for Gas Turbines and Power. Vol. 128, 255-263.

[98] Violi A, Yan S, Eddings E, Granata S. (2002). Experimental Formulation and Kinetic model for JP-8 surrogate mixtures. Combustion Science and Technology. Vol.174 (11&12), 399-417.

[99] Mostafa, Mohammad Golam, 3D Simulation Of Jet-A Combustion In A Model Aircraft Engine Combustion Chamber. 2012. Theses 90. Available from: https://digital.library.ncat.edu/theses/90 [Accessed: April 7, 2022]

[100] Kundu K, Penko P, Yang S. Simplified Jet-A/air combustion mechanisms for calculation of Nox emissions. In: Proceedings of the 34th AIAA/ASME/SAE/ASEE Joint Propulsion Conference and Exhibit, Cleveland, Ohio, USA. 1998

[101] Briones AM, Aggarwal SK. A numerical study of H2–air partially premixed flames. International Journal of Hydrogen Energy. 2005; 30: 327-339.

[102] Rasmussen CL, Rasmussen AE. Sensitizing Effects of NOx on CH4 Oxidation at High Pressure. Comb. Flame. 2008; 154: 529-545.

[103] Hoekman S, Robbins C. Review of the effects of biodiesel on NOx emissions. Fuel Processing Technology. 2012; 96: 237–249.

[104] Thomson R. Hydrogen: A future fuel for aviation?. Sederanger 1, 80538 Munich, Germany: ROLAND BERGER GMBH. 2020

[105] Malenshek M, Olsen DB. (2009). Methane number testing of alternative gaseous fuels. Fuel. Vol. 88, 650–656.

[106] Pischinger S. (2002). Verbrennungsmotoren – Band I. Vol.23. Auflage, RWTH-Aachen, Aachen.

[107] Nagy G. (2009). Key factors of the production of modern diesel fuels. Presented at the 6th International Colloquium of Fuels, Esslingen 2009

[108] Nascimento D. (2015). Desenvolvimento de uma Câmara de Combustão para uma Turbina a Gás [Master's Thesis]. Lisboa, Portugal: Instituto Superior Técnico.

[109] Fernández JMI. (2015). Study of Combustion Using a Computational Fluid Dynamics Software (ANSYS). Barcelona, Spain: Universitat de Barcelona.

[110] Mongia H. (2007). Comprehensive gas turbine combustion modelling methodology. International Aerospace CFD conference.

[111] ANSYS, Inc., ANSYS Fluent Theory Guide. Release 2020 R2, July 2020

[112] ANSYS, Inc., ANSYS Fluent User's Guide. Release 2020 R2, July 2020

[113] Mercier R. (2015). Turbulent combustion modeling for Large Eddy Simulation of non-adiabatic stratified flames [Master's Thesis]. Paris, France: École Centrale Paris.

[114] Chatterjee P. (2004). A computational fluid dynamics investigation of thermoacoustic instabilities in premixed laminar and turbulent combustion systems [Ph.D. dissertation]. Blacksburg, Virginia: Virginia Polytechnic Institute and State University.

[115] Gamil AAA, Nikolaidis T, Lelaj I, Laskaridis P. (2020). Assessment of numerical radiation models on the heat transfer of an aero-engine combustion chamber. Case Studies in Thermal Engineering. Vol.22, 100772. DOI: https://doi.org/10.1016/j.csite.2020.100772

[116] CFMI. TRAINING MANUAL CFM56-ALL BOROSCOPE INSPECTION. September 2003.

[117] ANSYS, Inc. 5 Best Practices for Gas Turbine Combustion Meshing Using Ansys Fluent. White Paper; 2020.

[118] Slater JW. (2021, February 10). Examining Spatial (Grid) Convergence [Online]. Available from: https://www.grc.nasa.gov/WWW/wind/valid/tutorial/spatconv.html [Accessed: May 24, 2022]

[119] Roache PJ. (1998). Verification and Validation in Computational Science and Engineering. Albuquerque, New Mexico: Hermosa Publishers.

[120] Ribeiro P. (2012). Análise de performance da Família de Motores de Avião CFM56. [Master´s Thesis]. Lisboa, Portugal: Instituto Superior de Engenharia de Lisboa.

[121] Jones B. Gas turbine combustor, design and development. Gas Turbine Combustion, Cranfield University, short course, 2015.

[122] Kurzke J. (2021). GasTurb Details 6. Germany: GasTurb GmbH. Available from: https://www.gasturb.de/Downloads/Manuals/GasTurbDetails6.pdf [Accessed: April 26, 2022]

[123] ANSYS, Inc. Lecture 7: Mesh Quality & Advanced Topics. Release 15.0. Germany. February 12, 2015.

[124] Torenbeek E. Advance aircraft Design: CONCEPTUAL DESIGN, ANALYSIS AND OPTIMIZATION OF SUBSONIC CIVIL AIRPLANES; 2013. ISBN 978-1-118-56811-8

[125] Funke H.-W, Beckmann N, Abanteriba S. An overview on dry low NOx micromix combustor development for hydrogen-rich gas turbine applications. Int. J. Hydrog. Energy. 2019; 44: 6978–6990

[126] ICAO (International Civil Aviation Organization). (2022, May 29). *Local Air Quality Technology Standards* [Online]. Available from: https://www.icao.int/environmental-protection/Pages/LAQ_TechnologyStandards.aspx [Accessed: April 30, 2022]

[127] Ogden J. High Hopes for Hydrogen. In: A HYDROGEN ECONOMY, SCIENTIFIC AMERICAN, September 2006

[128] Abdin Z, Zafaranloo A, Rafiee A, Mérida W, Lipinski W, Khalilpour KR. (2019). Hydrogen as an energy vector. Renewable and Sustainable Energy Reviews. 2020; Vol.120 109620, DOI: https://doi.org/10.1016/j.rser.2019.109620

[129] European Patent Office. (1986, October 29). *EUROPEAN PATENT APPLICATION, EP 0 199 534 A1* [Online]. Available from: https://data.epo.org/publication-server/document?iDocId=285984&iFormat=2 [Accessed: May 27, 2022]

[130] Wang T-S. Thermophysics characterization of kerosene combustion. Journal of Thermophysics and Heat Transfer. 2001; 15: 140–147

Appendix A – Description of the CFM56-3

According to CFM [66], the dual rotor design of the CFM56-3 engine consists of:

Engine Zone	Components
Low-Pressure System:	-A single stage fan, connected to a three-stage booster rotor assembly; -Four stage booster stator assembly in the primary airflow; -A single stage fan Outlet Guide Vane (OGV) assembly in the secondary airflow to guide the Fan discharge air; - Twelve fully controlled Variable Bleed Valves (VBV), located in the fan frame between booster and HPC for engine air cycle matching throughout the operating range; - Four stage Low Pressure Turbine (LPT) to drive fan and booster;
High-Pressure System:	-Nine stage High Pressure Compressor (HPC) rotor; -One variable Inlet Guide Vane (IGV) assembly to guide the incoming air to the HPC. -Three Variable Stator Vane (VSV) assemblies, together they make the variable stator system of the HPC. -Five HPC stator assemblies; -One Outlet Guide Vane (OGV) assembly used to make the air enter the combustion chamber axially (HPC stator stage 9); -Short machined ring construction annular combustor with 20 fuel nozzles; -A single stage High Pressure Turbine (HPT) nozzle and rotor assembly to drive the HPC.
Accessory Drive System:	-Inlet Gear Box (IGB). -Radial drive shaft; -Transfer Gearbox (TGB); -Horizontal drive shaft; -Accessory Gearbox (AGB).

The Figure A.A.1 helps to identify those components as well as their location in the engine.

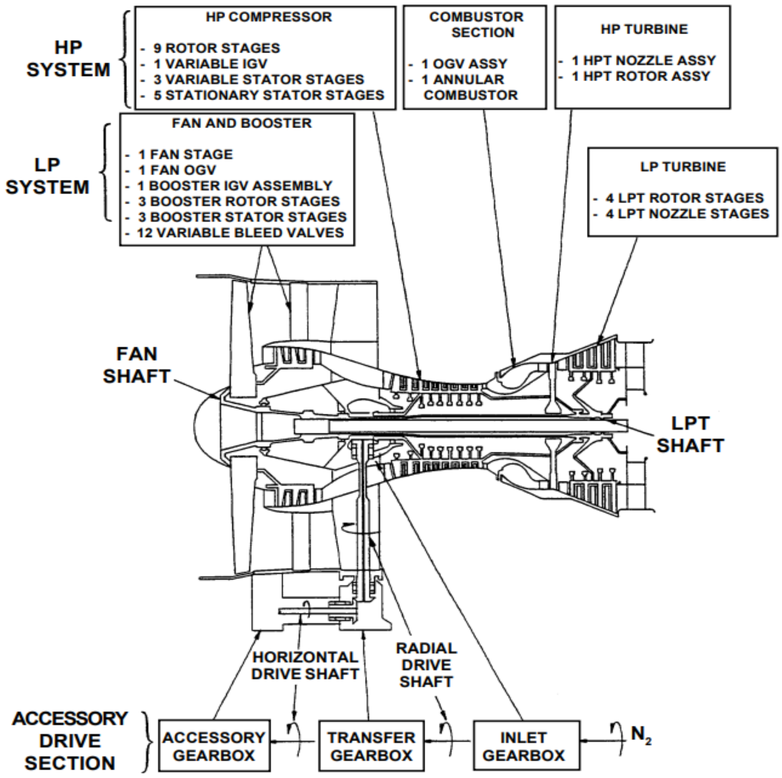

Figure A.A.1: Scheme of CFM56 engine construction [66].

The Figure A.A.2 shows the organization of the engine's core components.

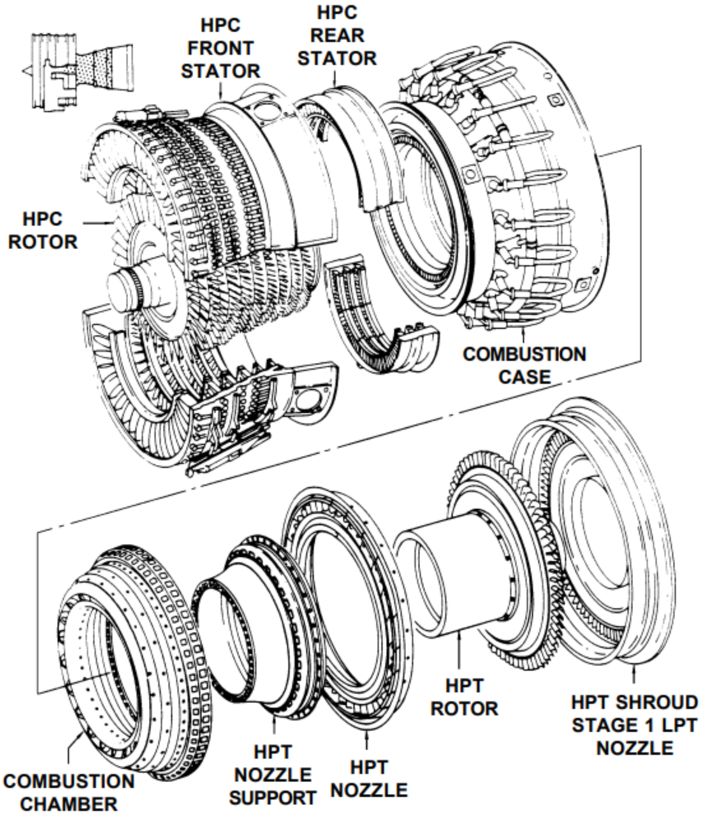

Figure A.A.2: CFM56 schematic overview of core engine components [66].

Appendix B – Oxidation of CO to CO_2

Once formed, CO is relatively resistant to oxidation and, in many practical systems, its oxidation is crucial to achieve complete combustion [41]. In the absence of an atmosphere with radicals H, the main reactions involved in the oxidation of CO are represented by Equations (B-1) and (B-2):

$$\mathrm{CO + O + M \rightarrow CO_2 + M} \tag{B-1}$$

$$\mathrm{CO + O_2 \rightarrow CO_2 + O} \tag{B-2}$$

However, Equation (B-1) and Equation (B-2) do not contribute significantly to CO_2 formation, due to the fact that these are slow reactions and present low weight at high temperatures [108].

During a combustion process, the CO oxidation process is dependent on the chemical equilibrium of the radicals CO, OH and H. The main reactions involved in the chemical equilibrium between these radicals and the molecules O_2, H_2O and H_2 are represented by Equations (B-3) to (B-6).

$$\mathrm{H + O_2 \rightleftharpoons OH + O} \tag{B-3}$$

$$\mathrm{O + H_2O \rightleftharpoons OH + OH} \tag{B-4}$$

$$\mathrm{H_2 + OH \rightleftharpoons H + H_2O} \tag{B-5}$$

$$\mathrm{H + O_2 + M \rightleftharpoons HO_2 + M} \tag{B-6}$$

At high temperatures, the main reaction removing CO is given by:

$$\mathrm{CO + OH \rightarrow CO_2 + H} \tag{B-7}$$

This is a fast reaction over a broad temperature range [41]. Equation (B-7) is also an initiation chain sequence, as it produces H atoms that react with O_2 to form OH and O through Equation (B-3). These radicals react with CO and H_2O, through Equation (B-7) and Equation (B-4), respectively.

At lower temperatures, the reaction of Equation (B-8) is more important as a means of removing CO [41].

$$\mathrm{CO + OH \rightarrow CO_2 + H} \tag{B-8}$$

In addition to the reactions reported for the oxidation of CO, the reaction represented by Equation (B-9) also presents a possible route to this process [108].

$$\mathrm{CO + HO_2 \rightarrow CO_2 + OH} \tag{B-9}$$

It is important to note that there are other possible (but less important) oxidation reactions for CO. All the reactions presented can always occur in the several operating conditions studied; however, the conversion rates are highly dependent on the combustion chamber conditions.

Appendix C – Mesh Refinement Parameters

This appendix will be used to describe the process followed in this work to generate the meshes obtained.

So, before setting the parameters for generating the mesh, each of the boundaries/surfaces of the CAD model was converted to *STL* format in CATIA V5R20. After all the *STL* files have been created, everything was ready to begin the mesh generation setup in the ANSYS *Fluent Meshing* software.

In this software, the first step is to choose the *Workflow type* desired to create the mesh. In this case, the *Fault-tolerant Meshing* option was chosen because the files were in *STL* format and that option require no special treatment for the geometry.

After the workflow has been chosen, a series of tasks appear to be completed. In the first task, it is necessary to import the geometries. For that, the files are uploaded to the software, and then, after click *load,* if the geometry is imported correctly, it is just click in the *Creating Meshing Objects* option. In this task, it was necessary to make sure that one zone was created per object imported to prevent troubles in the following tasks.

In the second task, the flow type must be chosen. Here, the option *Internal flow through the object* was chosen and all the other options available in that task were selected as *No*. In this task, it is possible to define the inlets and outlets. However, this description was only made in a later phase of the process as it is easier for the software to generate the mesh if all the objects are considered as walls.

The third task is to identify the fluid regions to mesh. The main purpose of this task is to select a material point inside the volume of the combustion chamber where is supposed to create the mesh. This step will then define a mesh volume within the closed boundaries of the model combustion chamber. To accomplish this, in the option *Define Location Using* was chosen the option *Centroid of Objects* and in the parts listed were chosen two objects, the *STL* file where is included the rich injector and the *STL* file that correspond to the outlet.

In the task *Define Leakage Threshold*, the option chosen was *No*, since the set of *STL* files uploaded was already completely closed.

Then, in *Update Region Settings*, for the fluid region, the options *fluid, wrap* and *poly-hexcore* were chosen in the *Type, Extraction Method* and *Volume Fill* sections, respectively. Choosing these options is advised by ANSYS in [117] for complex geometries. In this task, all the other options were left with the default options.

The next step is to choose the refinement level for each *STL* uploaded. This is one of the sections where it is possible to make the refinement or coarsening of the mesh closer to the walls of the geometries imported, through the option *Add Local Sizing*. In this option, it is necessary to choose the refinement method in *Size Functions*. For the final meshes created, two refinement methods were used, the *Curvature* and *Proximity*. For instance, the parameters used in these two methods to create the intermediate mesh are presented in Table 9 and Table 10 (presented in the following).

Table 9: Mesh refinement parameters used in the intermediate mesh through the "Add Local Sizing" option with the "Size Functions" of "Curvature".

Refinement Group	Objects Refined	Minimum Size	Maximum Size	Growth Rate	Curvature Normal Angle
1	1, 2, 3, 9, 10, 11	1.3	2.5	1.2	18
2	4, 5, 6, 7, 8, 12, 13, 14	0.2	0.3	1.2	18
3	15	0.3	0.5	1.2	18
4	16, 17	0.15	0.25	1.2	18
5	18	0.1	0.25	1.2	18
6	19, 20	0.5	2.5	1.2	18
7	22, 23	0.4	1.2	1.2	18
8	21	0.7	1.5	1.2	18
9	24, 25	1.3	2.5	1.2	18
10	26, 27	1	2	1.2	18
11	29	0.6	1	1.2	18
12	30, 31	1.3	2.5	1.2	18
13	28	1	2	1.2	18

Note: The options *Size Functions* and *Scope To* were defined as *Curvature* and *faces-and-edges*, respectively, for all the refinement groups. The numbering of the "Objects Refined" is the same defined in Table 4.

Table 10: Mesh refinement parameters used in the intermediate mesh through the "Add Local Sizing" option with the "Size Functions" of "Proximity".

Refinement Group	Objects Refined	Minimum Size	Maximum Size	Growth Rate	Cells Per Gap
1	1, 2, 3, 9, 10, 11	0.5	2.5	1.2	3
2	4, 5, 6, 7, 8, 12, 13, 14	0.2	0.3	1.2	3
3	15	0.3	0.5	1.2	3
4	16, 17	0.15	0.25	1.2	3
5	18	0.1	0.25	1.2	3
6	19, 20	0.5	2.5	1.2	3
7	22, 23	0.33	0.58	1.2	3
8	21	0.7	1.3	1.2	3
9	24, 25	0.5	2.5	1.2	3
10	26, 27	0.13	0.17	1.2	3
11	29	0.6	1	1.2	3
12	30, 31	1.3	2.5	1.2	3
13	28	0.12	0.15	1.2	3

Note: The options *Size Functions* and *Scope To* were defined as *Proximity* and *faces-and-edges*, respectively, for all the refinement groups. The numbering of the "Objects Refined" is the same defined in Table 4.

In this task, it is really important to make sure that the refinement level is enough to cover all the features of the geometry and it is not too much to increase the computational cost unnecessarily. In this specific case, it was also necessary to ensure that the mesh met the requirements for Y^+ closer to the walls in the simulations.

In the *Generate the Surface Mesh* task, it is necessary to select the target skewness for the cells that are closer to the walls. In this case, the value selected was 0.7.

In the *Add Boundary Layers* task*,* as referred by ANSYS [117], it is advised the use of 3 layers. In this work, the *Offset Method Type* used was the *aspect-ratio*, the *First Aspect Ratio* used was 10, the *Growth Rate* was 1.2, and the option *only-walls* was chosen in *Grow on*. The two values used in these options were obtained after several attempts to achieve the desired Y^+ range.

The final step is to create the volume mesh. In this step, it is possible to choose the target skewness for the volume mesh and if the option *Enable Region Settings* is enabled*,* it is possible to change the base mesh spacing. This option allows the user to refine or coarsen the mesh, decreasing or increasing the base mesh spacing (in the option *Max Cell Length*), respectively. For the three meshes referred in the previous section, the values used were 5, 2.5 and 1.5, for the coarse, intermediate and fine meshes, respectively.

After completing all these tasks, the software will generate the volume mesh through an iterative process, to obtain the best possible mesh quality with all the defined parameters. A much more detailed explanation of the tasks and options of this process is available in the ANSYS Fluent User's Guide [112].

Appendix D – Problem Set up Inputs

Table 11: Relevant data from GasTurb for the power setting of 100%, obtained by Ribeiro [120].

Station	$\dot{m}_{air\ total}$ [kg/s]	Temperature [K]	Pressure [kPa]	$\dot{m}_{fuel\ total}$ [kg/s]
Fan	314.82	288.15	101.325	---
HPC exit	51.42	743.91	2343.346	---
Combustor entry	41.451	743.91	2343.346	1.1271
Combustor exit	42.58	1649.94	2226.179	---
HPT entry	45.73	1593.23	2226.179	---

Table 12: Operating pressures and temperatures considered in the inlets for the several power settings.

Parameter	Power Setting [%]			
	100	85	30	7
Inlet Pressure (Oxidizer) [Pa]	2343346	2022587	846468.6	354637.5
Theoretical Pressure Variation [Pa]	117167.3	101129.3	42323.43	17731.88
Outlet Pressure (Oxidizer) [Pa]	2226179	1921457	804145.2	336905.6
Oxidizer Temperature [K]	743.91	696.5052	522.6874	450
Fuel Pressure [Pa]	4452357	3842914	1608290	673811.3
Fuel Temperature [K]	298.15	298.15	298.15	298.15

Table 13: Origins and directions used to define the vectors in the inlets of the swirlers to create the counter swirl effect.

Coordinates		Swirler				
		1	2	3	4	5
Origin	x	-159.022	-133.017	-84.847	-19.225	57.424
	y	22.284	77.018	120.129	147.398	156.156
	z	177.003	122.508	72.883	32.986	6.72
Direction	x	0.46195	0.43209	0.37663	0.30098	0.21256
	y	0.5467	0.48346	0.4336	0.40201	0.39177
	z	0.69838	0.76129	0.81862	0.86475	0.89517

Table 14: Components used to define the vectors in the inlets of the swirlers to create the counter swirl effect.

Inlet	Component of flow direction		
	Radial	Tangencial	Axial
Primary Swirlers	-0.24913	0.431506	-0.498261
Secondary Swirler	-0.5	-0.866	0

Table 15: Total areas calculated for each boundary to determine the air mass flow rates.

Number-Description	Area of Each Inlet [mm^2]	Number of Inlets	Total Area [mm^2]
1-Primary zone big mixers	97.789	5	488.945
2-Primary zone small mixers	62.001	5	310.005
3-Secondary zone mixers	54.155	15	812.325
4-First line dilution holes	3.181	153	486.693
5-Second line dilution holes	2.278	151	343.978
6-Third line dilution holes	2.937	150	440.55
7-Forth line dilution holes	2.172	175	380.1
8-Fifth line dilution holes	2.333	180	419.94
9-Primary zone big mixers	94.497	5	472.485
10-Primary zone small mixers	62.402	5	312.01
11-Secondary zone mixers	63.647	15	954.705
12-First line dilution holes	1.168	100	116.8
13-Second line dilution holes	1.584	96	152.064
14-Third line dilution holes	1.144	125	143
15-Forth line dilution holes	10.287	75	771.525
16-Exterior dilution holes	1.857	163	302.691
17-Interior dilution holes	1.813	125	226.625
18-Dilution holes swirler	0.785	471	369.735
Total Area of mixers and dilution holes			7504.176
19-Primary Swirlers	301.718	5	1508.59
20-Secondary Swirlers	355.29	5	1776.45
Total Area of the Swirlers			3285.04
Note: The numbering used in this table to describe the inlets is the same presented in Table 4.			

Table 16: Relevant inputs and statistics for fuel and fuel-air mixture used in the NOx model of ANSYS.

Throttle	ICAO's database			
	100	85	30	7
Jet A Stoichiometric AFR	14.7	14.7	14.7	14.7
Jet A Carbon Number	12	12	12	12
Overall AFR	36.7772	39.8258	57.2166	70.0000
Overall Equivalence Ratio	0.3997	0.3691	0.2569	0.2100
Primary Zone AFR	7.7230	8.3636	12.0156	14.7000
Primary Zone Equivalence Ratio	1.9034	1.7576	1.2234	1.0000
Hydrogen Stoichiometric AFR	34.0595	34.0595	34.0595	34.0595
Hydrogen Carbon Number	0	0	0	0
Overall AFR	102.2429	110.7187	159.0689	194.5962
Overall Equivalence Ratio	0.3331	0.3076	0.2141	0.1750
Primary Zone AFR	21.4706	23.2516	33.4048	40.8652
Primary Zone Equivalence Ratio	1.5863	1.4648	1.0196	0.8335

Table 17: Models used in the four-step solution technique, while burning hydrogen fuel.

Step	Viscous Model	Species model	Solution equations
1	Realizable k-ε	Species transport 1 eq. (H_2/O_2)	All
2	RSM	Detailed Mechanism	Energy, Species (all), Radiation
3	RSM	Detailed Mechanism	Energy, Species (all), Radiation
4	RSM	Detailed Mechanism	All
Post-Processing	RSM	---	Pollutant NO, Temperature Variance, NO, NO_2

Table 18: Models used in the four-step solution technique, while burning Jet A fuel.

Step	Viscous Model	Species model	Solution equations
1	RSM	Non-premixed combustion ($Jet\ A/O_2$)	All
2	RSM	Detailed Mechanism	Energy, species, radiation
3	RSM	Detailed Mechanism	Energy, species, radiation
4	RSM	Detailed Mechanism	All
Post-Processing	RSM	---	Pollutant NO, Temperature Variance, NO

Table 19: Schemes selected in Solution Methods Task Page in the simulations with Jet A.

	Step		
Parameters	1	2, 3, 4	Post-Processing
Pressure-Velocity Coupling	Coupled	Coupled	Coupled
Gradient	Least Squares Cell Based	Least Squares Cell Based	Least Squares Cell Based
Pressure	Presto!	Presto!	Presto!
Momentum	Second order Upwind	Second order Upwind	Second order Upwind
Turbulent Kinetic Energy	Second order Upwind	Second order Upwind	Second order Upwind
Turbulent Dissipation Rate	Second order Upwind	Second order Upwind	Second order Upwind
Reynolds Stresses	Second order Upwind	Second order Upwind	Second order Upwind
Energy	Second order Upwind	Second order Upwind	Second order Upwind
Mean Mixture Fraction	Second order Upwind	---	---
Mixture Fraction Variance	Second order Upwind	---	---
Species	---	Second order Upwind	Second order Upwind
Pollutant no	---	---	Second order Upwind
Temperature Variance	---	---	Second order Upwind

Table 20: Schemes selected in Solution Methods Task Page in the simulations with hydrogen.

	Step		
Parameters	1	2, 3, 4	Post-Proc.
Pressure-Velocity Coupling	Coupled	Coupled	Coupled
Gradient	Least Squares Cell Based	Least Squares Cell Based	Least Squares Cell Based
Pressure	Presto!	Presto!	Presto!
Momentum	Second order Upwind	Second order Upwind	Second order Upwind
Turbulent Kinetic Energy	Second order Upwind	Second order Upwind	Second order Upwind
Turbulent Dissipation Rate	Second order Upwind	Second order Upwind	Second order Upwind
Reynolds Stresses	---	Second order Upwind	Second order Upwind
Species	Second order Upwind	Second order Upwind	Second order Upwind
Energy	Second order Upwind	Second order Upwind	Second order Upwind
Pollutant no	---	---	Second order Upwind
Temperature Variance	---	---	Second order Upwind

Table 21: Solution control parameters for flow Courant Number, explicit relaxation factors (ERF) and under-relaxation factors (URF), used in the several steps of the simulation with Jet A.

	Step				
Parameters	1	2	3	4	Post-Proc.
Flow Courant Number	2	2	2	2	2
	Explicit Relaxation Factors (ERF)				
Momentum	0.25	0.25	0.25	0.25	0.25
Pressure	0.25	0.25	0.25	0.25	0.25
	Under Relaxation Factors (URF)				
Density	0.2	0.2	0.2	0.2	0.2
Body Forces	0.5	0.5	0.5	0.5	0.5
Turbulent Kinetic Energy	0.2	0.2	0.2	0.2	0.2
Turbulent Dissipation rate	0.4	0.4	0.4	0.4	0.4
Turbulent Viscosity	0.4	0.4	0.4	0.4	0.4
Reynolds Stresses	0.2	0.2	0.2	0.2	0.2
Energy	0.4	0.4	0.8	0.8	0.8
Temperature	0.4	---	---	---	---
P1	0.7	0.7	0.8	0.8	1.8
Mean Mixture Fraction	0.3	---	---	---	---
Mixture Fraction Variance	0.3	---	---	---	---
Species	---	0.35*	0.35*	0.35*	0.35*
Pollutant no	---	---	---	---	1
Temperature Variance	---	---	---	---	0.9

*This value was applied to all the species

Table 22: Solution control parameters for flow Courant Number, explicit relaxation factors (ERF) and under-relaxation factors (URF), used in the several steps of the simulation with hydrogen.

	Step				
Parameters	1	2	3	4	Post-Proc
Flow Courant Number	2	2	2	2	2
	Explicit Relaxation Factors (ERF)				
Momentum	0.25	0.25	0.25	0.25	0.25
Pressure	0.25	0.25	0.25	0.25	0.25
	Under Relaxation Factors (URF)				
Density	0.2	0.2	0.2	0.2	0.2
Body Forces	0.5	0.5	0.5	0.5	0.5
Turbulent Kinetic Energy	0.2	0.2	0.2	0.2	0.2
Turbulent Dissipation rate	0.4	0.4	0.4	0.4	0.4
Turbulent Viscosity	0.4	0.4	0.4	0.4	0.4
Reynolds Stresses	---	0.2	0.2	0.2	0.2
Species	H_2-0.2; O_2-0.35; H_2O-0.35	H_2-0.2; 0.35*	H_2-0.2; 0.35*	H_2-0.2; 0.35*	H_2-0.2; 0.35*
Energy	0.4	0.4	0.8	0.8	0.8
P1	0.3	0.7	0.8	0.8	0.8
Pollutant no	---	---	---	---	1
Temperature Variance	---	---	---	---	0.9

*This value was applied to all the other species

Appendix E – Mesh quality analysis and independence test

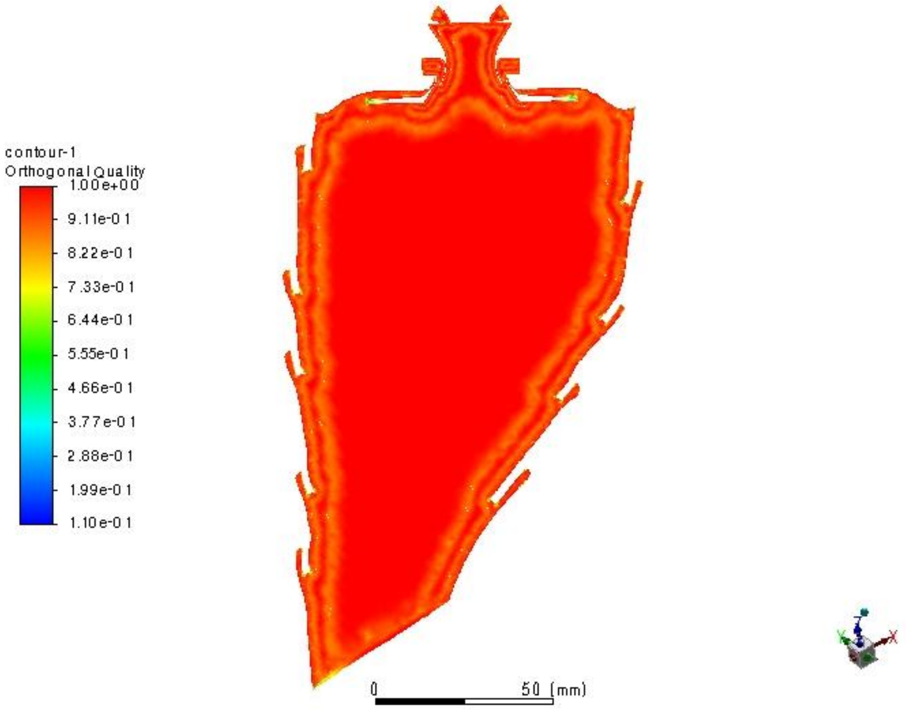

Figure A.E.1: Contours of orthogonal quality in the cells in the cut-view plane of the first swirler, obtained with ANSYS Fluent software.

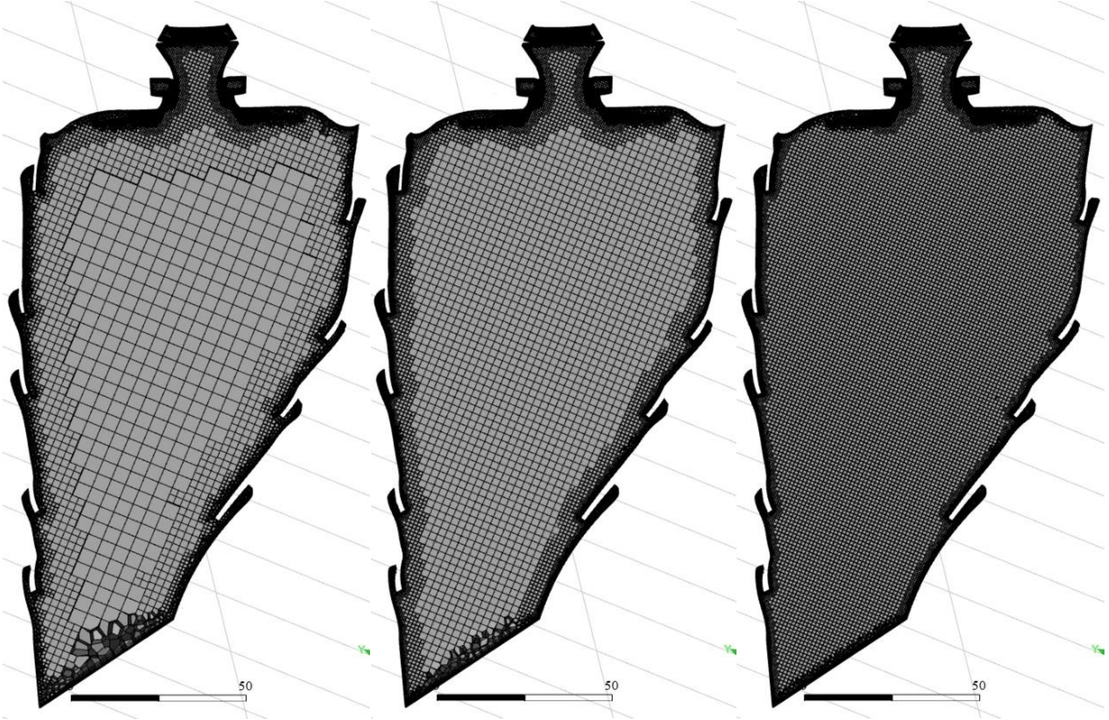

Figure A.E.2: Structure of the meshes in the cut-view plane of the first swirler used in the independence test: in the left, the coarse mesh; in the middle, the intermediate mesh (used in this work); and in the right, the refined mesh, obtained with the Fluent Meshing software.

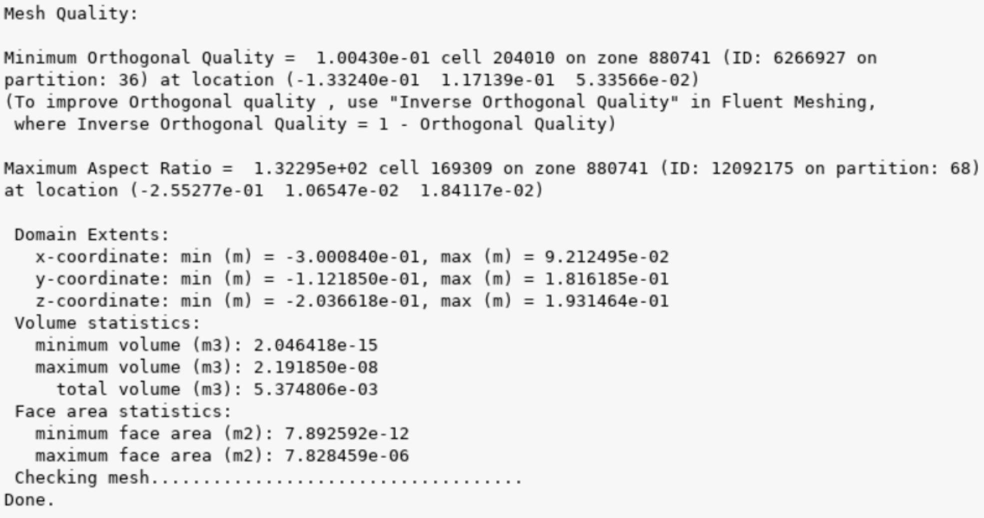

```
Mesh Quality:

Minimum Orthogonal Quality =  1.00430e-01 cell 204010 on zone 880741 (ID: 6266927 on
partition: 36) at location (-1.33240e-01  1.17139e-01  5.33566e-02)
(To improve Orthogonal quality , use "Inverse Orthogonal Quality" in Fluent Meshing,
 where Inverse Orthogonal Quality = 1 - Orthogonal Quality)

Maximum Aspect Ratio =  1.32295e+02 cell 169309 on zone 880741 (ID: 12092175 on partition: 68)
at location (-2.55277e-01  1.06547e-02  1.84117e-02)

 Domain Extents:
   x-coordinate: min (m) = -3.000840e-01, max (m) = 9.212495e-02
   y-coordinate: min (m) = -1.121850e-01, max (m) = 1.816185e-01
   z-coordinate: min (m) = -2.036618e-01, max (m) = 1.931464e-01
 Volume statistics:
   minimum volume (m3): 2.046418e-15
   maximum volume (m3): 2.191850e-08
     total volume (m3): 5.374806e-03
 Face area statistics:
   minimum face area (m2): 7.892592e-12
   maximum face area (m2): 7.828459e-06
 Checking mesh...................................
Done.
```

Figure A.E.3:Command window of ANSYS Fluent with the reports of Mesh Quality and Mesh Check.

Appendix F – Swirl effect

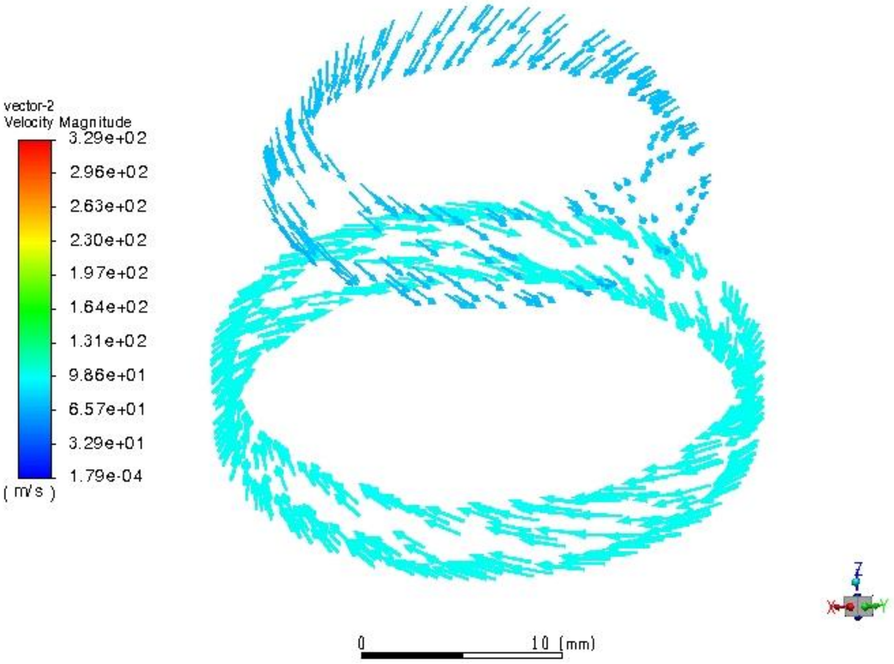

Figure A.F.1: Counter swirl effect obtained with the inputs of Table 13 and Table 14, side view, obtained with the ANSYS Fluent software.

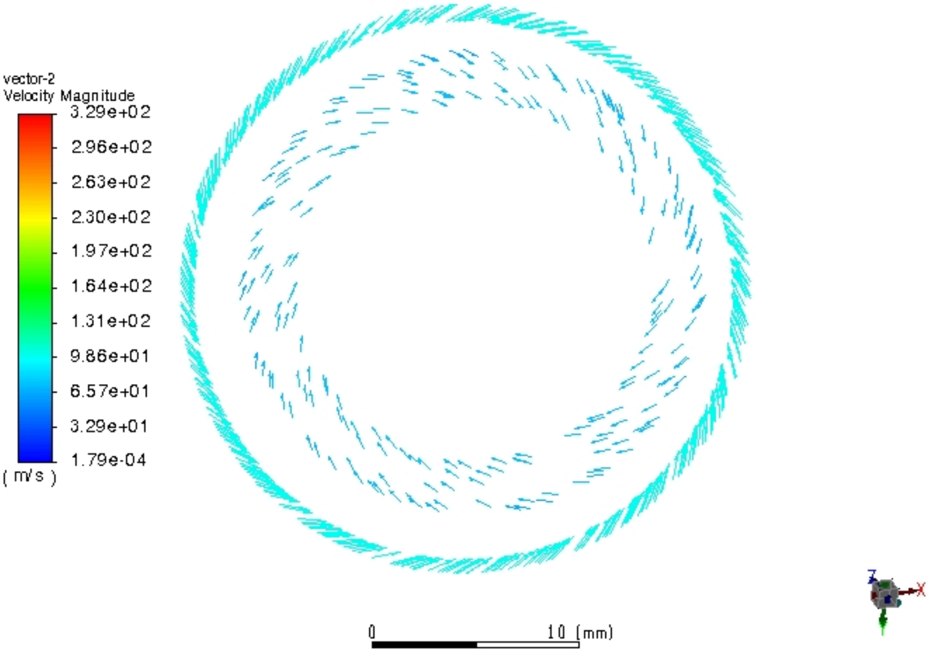

Figure A.F.2: Counter swirl effect obtained with the inputs of Table 13 and Table 14, top view, obtained with the ANSYS Fluent software.

Appendix G – Results

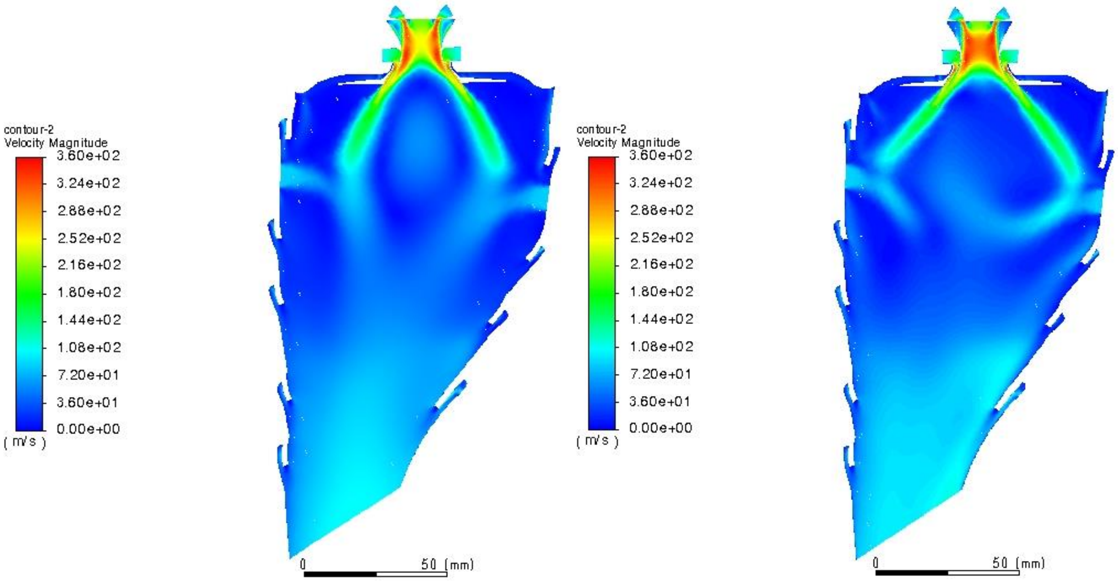

Figure A.G.1: Contours of velocity magnitude in the cut-view plane of the first swirler, while burning hydrogen fuel at the power setting of 100%, for realizable k-ε (left) and RSM (right) turbulence models, obtained with ANSYS Fluent software.

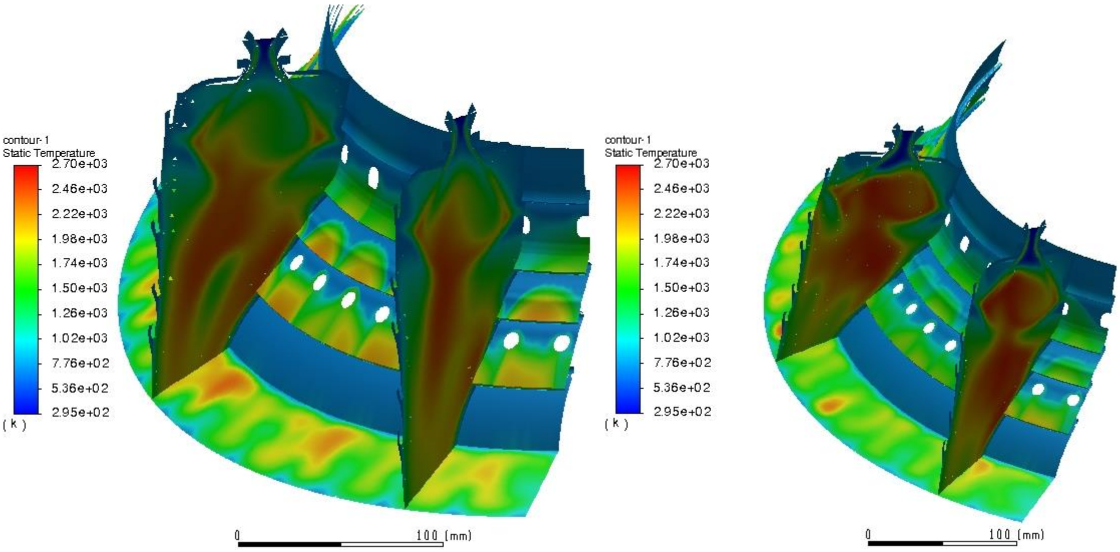

Figure A.G.2: Contours of static temperature in the cut-view plane of the first and third swirlers and in the outlet, while burning Jet A (left) and hydrogen fuel (right) at the power setting of 100%, obtained with ANSYS Fluent software.

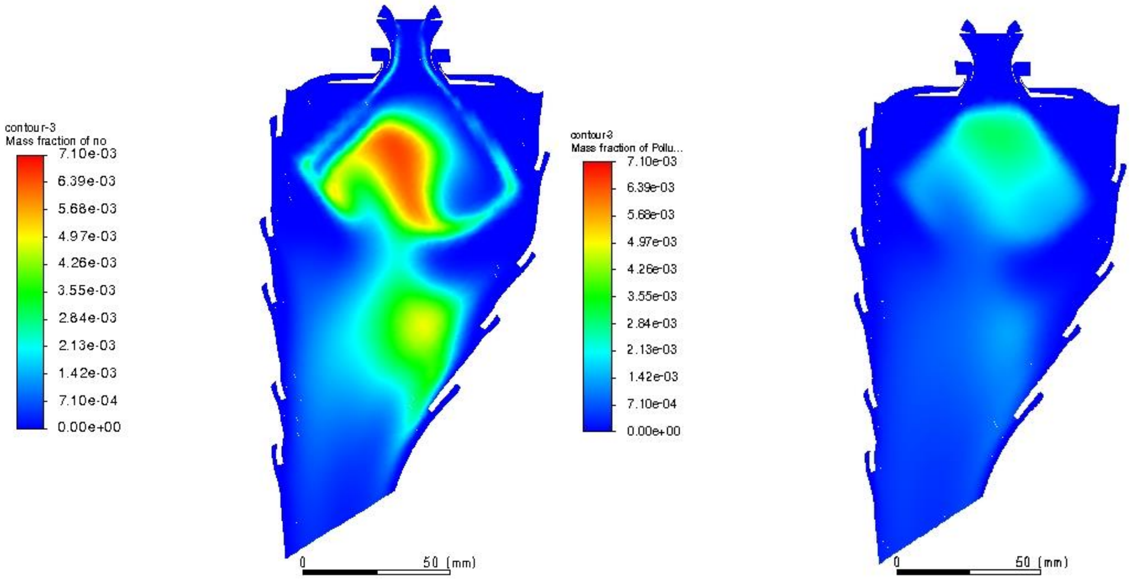

Figure A.G.3: Contours of the mass fraction of NO in the cut-view plane of the first swirler, while burning hydrogen at the power setting of 30%, obtained with ANSYS Fluent software: in the left, with the NOx sub-mechanism and, in the right, with the ANSYS NOx model.

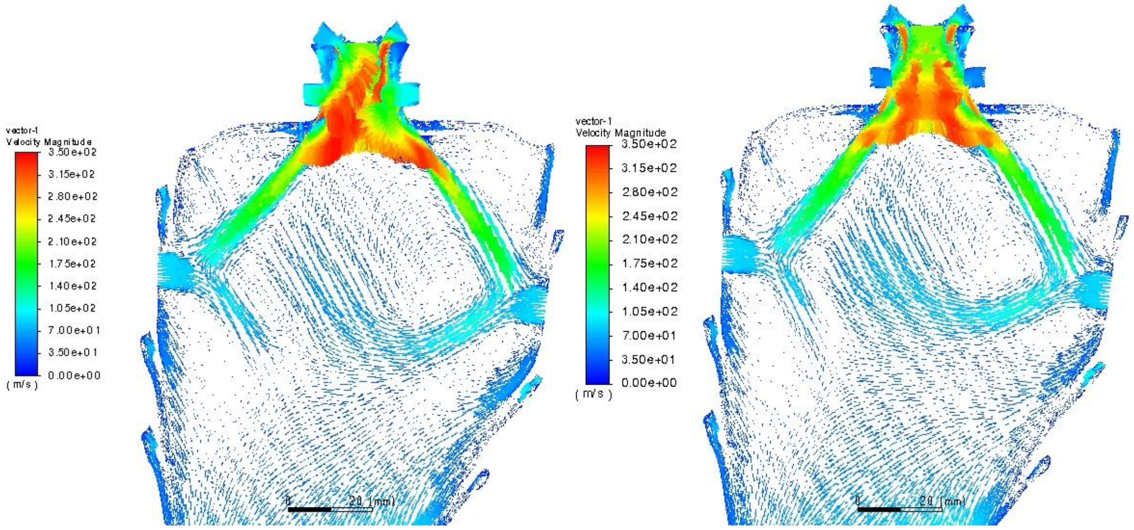

Figure A.G.4: Velocity magnitude vectors in the cut-view plane of the first swirler, while burning hydrogen fuel with the swirl effect (left) and without the swirl effect (right) at the power setting of 85%, obtained with ANSYS Fluent software.

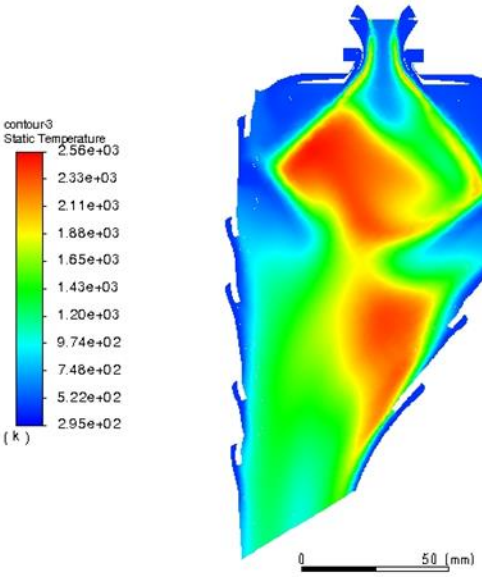

Figure A.G.5: Contours of static temperature in the cut-view plane of the first swirler, while burning hydrogen fuel at 600K at the power setting of 7%, obtained with ANSYS Fluent software.

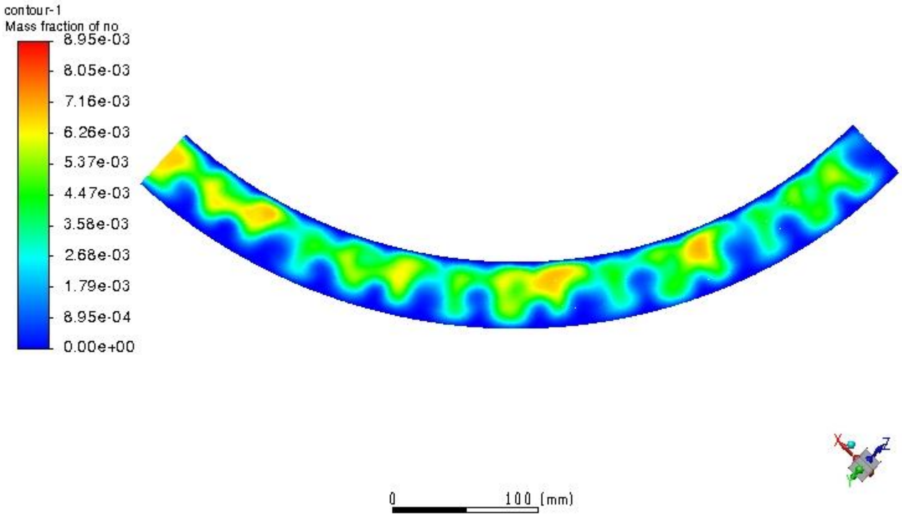

Figure A.G.6: Contours of the mass fraction of NO in the outlet plane, while burning Jet A at the power setting of 100% using the NOx sub-mechanism, obtained with ANSYS Fluent software.

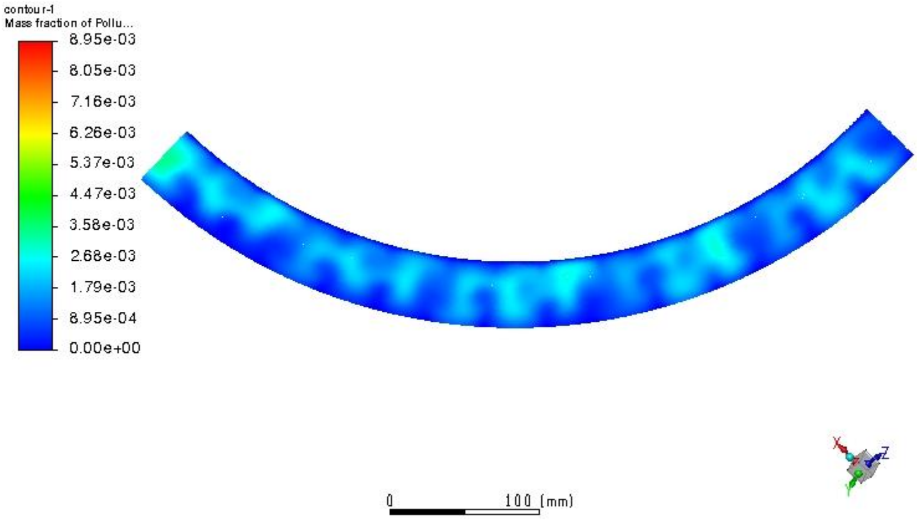

Figure A.G.7: Contours of the mass fraction of NO in the outlet plane, while burning Jet A at the power setting of 100% using the ANSYS NOx model, obtained with ANSYS Fluent software.

Appendix H – Modifications in the CFM56-3 Combustor CAD Model

As mentioned in section 4.4.2.3, after analyzing the few technical data available on the internet about this specific gas turbine engine [65, 66, 116] and running the preliminary simulations, there were detected some problems that were affecting the results.
Thus, the following modifications were applied to try to correct these small problems and to increase the similarity of the CAD model to the original combustor:

1. Positioning of the Injectors

As mentioned in section 4.4.2.2, the inclination of the injectors was correct. However, the tip of the injectors was positioned too far ahead of the correct position. This conclusion was drawn when the diagram presented in Figure A.1 in Annex 1, from the documentation [116], was compared with the original CAD model, represented in Figure 4.5 a). For this reason, the position of the injectors was pulled back, as shown in the Figure 4.5 b).

2. Secondary Swirler Outlet

The second modification carried out was related with the geometry of the inner wall of the outlet of the secondary swirlers. As in the initial simulations, an overpressure was detected right after the inlet of the secondary swirlers, showing that the flow was too much choked in the narrowest area of the flow passage, the distance between the two walls had to be enlarged to reduce this overpressure to an acceptable value. This modification can be noticed in the Figure 4.5 b).

3. Inlet of the Primary Swirlers

As mentioned in section 4.5.4, in the previous works [69, 70], the air mass flow for each inlet was calculated, dividing the available air for each zone of the combustor (primary, secondary and dilution zones) considering only the AFR needed according to B. Jones [121]. In the present work, one of the objectives was that the air mass flow was correctly divided by the inlets in an attempt to recreate the correct flow pattern inside the chamber. However, during the initial simulations, this approach gave raise to some problems with the flow pattern inside the chamber, mainly in the recirculation zone. So, it was necessary to follow another approach, as mentioned earlier.

As, for each power setting, the air pressure and temperature in the combustor was assumed to be the same in all inlets (swirlers, mixers, dilution holes and cooling holes), the mass flow rate entering to the combustion chamber through each inlet must be, in a simplified way, proportional to the area of each one of these inlets. Thus, during the calculation of the boundary conditions, it was necessary to increase the inlet area of the primary swirlers so that this area could meet the air mass flow determined to pass through these inlets to the primary zone.

In this work, it was opted to change only the areas of the inlets of the primary swirlers, since the areas of the other inlets represented on the combustor walls (film cooling, dilution and mixers) could be easily determined through the scanner, and increasing the inlets of the secondary swirlers would increase the existing problem with the overpressure. Moreover, it was noticed by Oliveira that the exact geometry of the swirlers was not achieved.

4. Dome Cooling Walls

The last modification of the model was the addition of the cooling walls, in front of each of the swirlers, that had been removed in the previous works to try to reduce the computational costs. Once these walls were added, it was necessary to extend the outlet of the secondary swirlers to obtain a final geometry of the connection between the swirler outlets and the cooling walls of the dome similar to the one shown in Figure A.2, presented in Annex 1. It should be noted that there may be some inaccuracy in the representation of these connections, since this zone was not perceptibly represented in the available documentation.

Appendix I – Examples of Gaseous Fuel Injector Designs

This appendix will be used to present several examples of gaseous fuel injectors tested and applied in gas turbine engines.

According to Mellor [71], the earliest reported work in this topic was performed for the National Advisory Committee for Aeronautics (NACA) as early as 1950. A series of reports describe the results of gaseous fuel combustion in various combustors for aeronautical applications. Some of these earliest tests were carried out by McCafferty, in 1950, using liquid propane injected through single port and multiport injectors, as shown in Figure A.I.1.

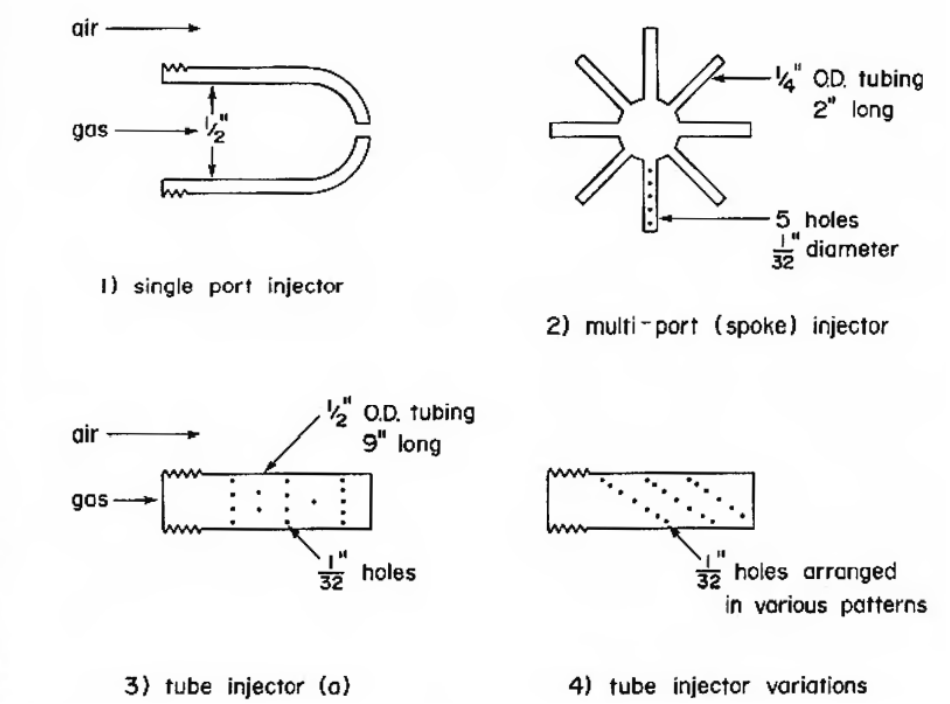

Figure A.I.1: Injector designs of McCafferty [71].

In 1953, Norgren and Childs also made some tests using eleven injectors distributing the fuel in axial and radial jets and fans with and without swirl. The objective of these tests was to distribute the gaseous fuel quickly in the primary zone, aided by the higher diffusion coefficient and the elimination of vaporization time, improving the combustion efficiency over that of liquid fuel [71]. Some of these injectors are shown in Figure A.I.2.

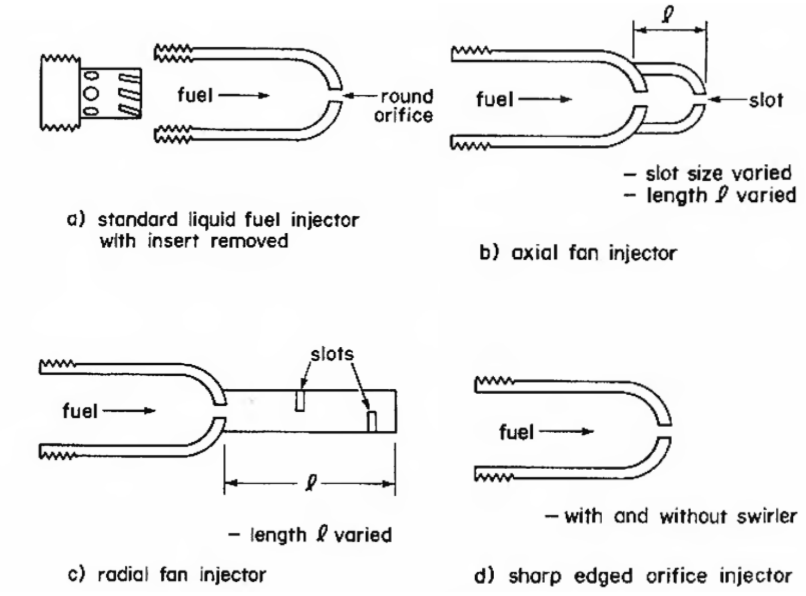

Figure A.I.2: Injector designs of Norgren and Childs [71].

In 1956, Smith and Wear studied the effects of the fuel properties using five gaseous fuels. In these tests, the injection was done through simple pepper-pot injectors with six holes, each varying in size from 0.0625" (1.4mm) to 0.125” (28 mm) at included angles of 114° and 90° from the axis [71]. The basic design of this injector is shown in the left image of Figure A.I.3.

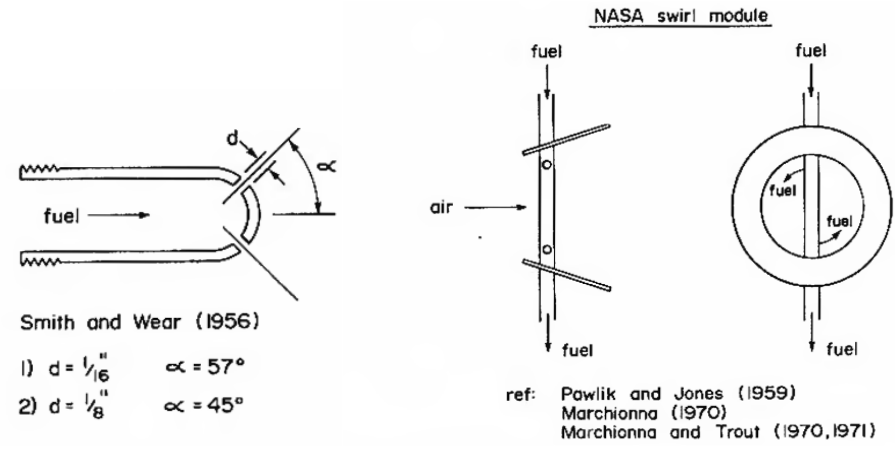

Figure A.I.3: Other early gas injectors, adapted from [71].

The work on the use of gaseous fuels continued in NASA laboratories from 1959 to about 1975. Of particular interest was the use of liquefied natural gas in supersonic flight. Pawlik and Jones (1959), Fear and Tacina (1970), Marchionna (1970) and Marchionna and Trout (1970b) used experimental swirl-can elements to reduce the overall combustor length [71]. The fuel was injected tangentially at sonic velocity in each element, as shown in the right image of Figure A.I.3.

The most extensive tests with gaseous fuels were performed by Wear and Schultz using 13 injectors varying injection velocities, axial position, jet or sheet injection from axial, angled and radial designs, as shown in Figure A.I.4 [71].

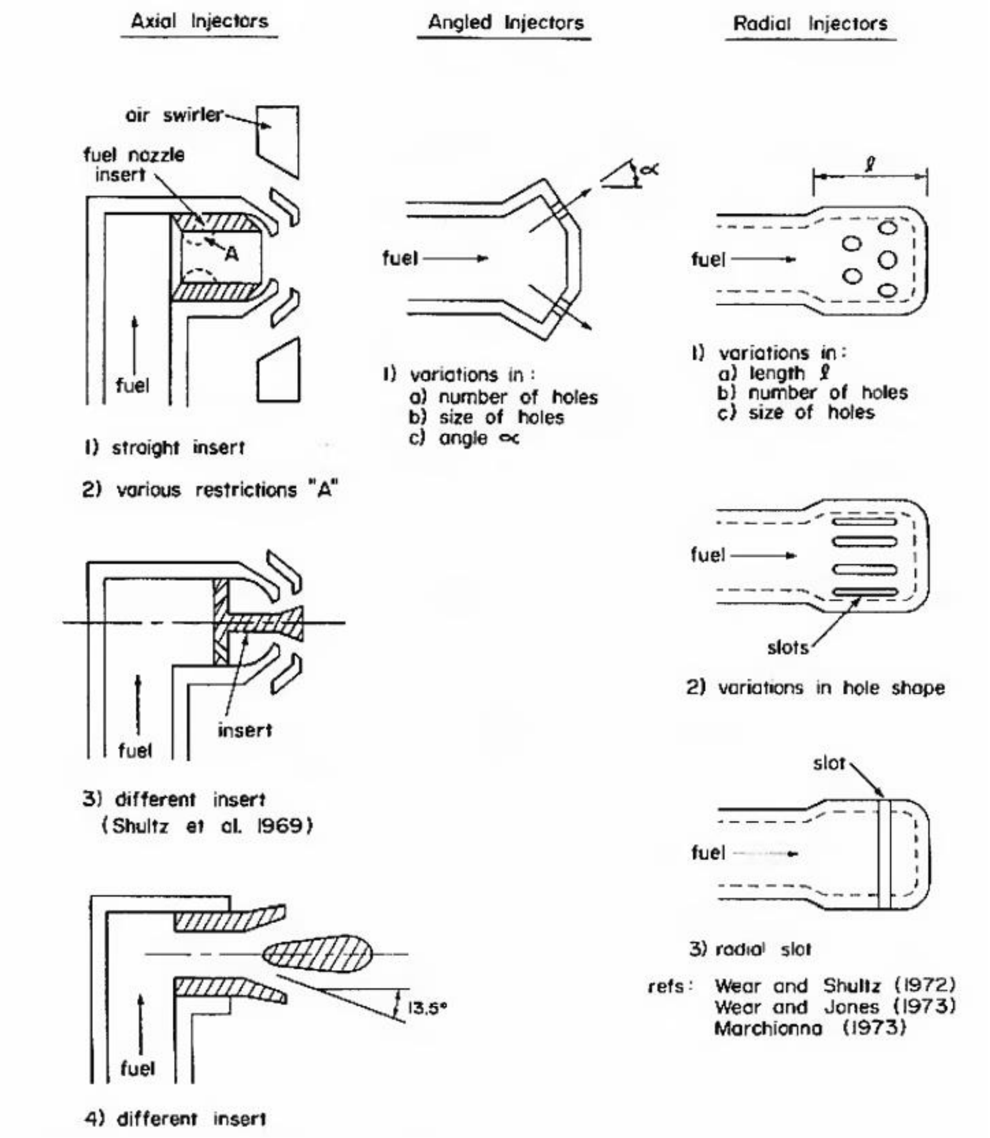

Figure A.I.4: NASA injector variations [71].

For more information about the injector designs presented please consult the reference [71].

In 1998, J. Ziemann et al. [37] presented a report of a study where six different fuel injector concepts were evaluated through steady and transient tests. In these tests, the nozzle designs followed two different strategies, being that two of the injectors tested fall into the category of the lean premix combustion, and the remaining four of the injectors tested fall into the category of lean combustion without premixing. From these six injector concepts, the concepts of the “premixed perforated plate” and the “high shear swirl injector” were identified as the most promising systems in each of the premix and non-premix categories. These two concepts are shown in Figure A.I.5.

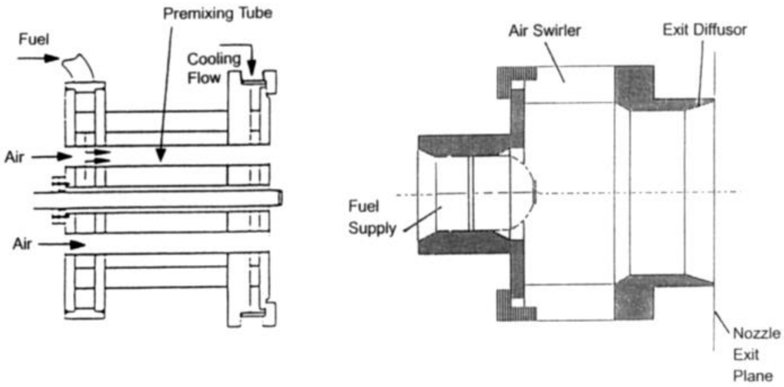

Figure A.I.5: Fuel injection concepts [37]: Premixed Perforated Plate (in the left); High Shear Swirl Concept (in the right).

In general, the authors concluded that the NOx emissions improve when the degree of premixing increases. Based on the test results of this program, practical low-NOx hydrogen gas turbine combustors can be achieved [37].

In 2005, C. J. Marek et al. [38] also presented a report of a study where a total of five fuel injector configurations were tested to investigate the combustion performance of gaseous hydrogen using lean direct injection. In their work, one of the designs used was generated inhouse at NASA Glenn (used as reference), while the four remaining designs were generated by major fuel injector manufacturers. All of the tested configurations (shown in Figure A.I.6) use some variation or combination of lean direct injection (LDI) and lean premixed prevaporized (LPP) schemes. The specifications of each configuration used in that study were described by C. J. Marek et al. in [38].

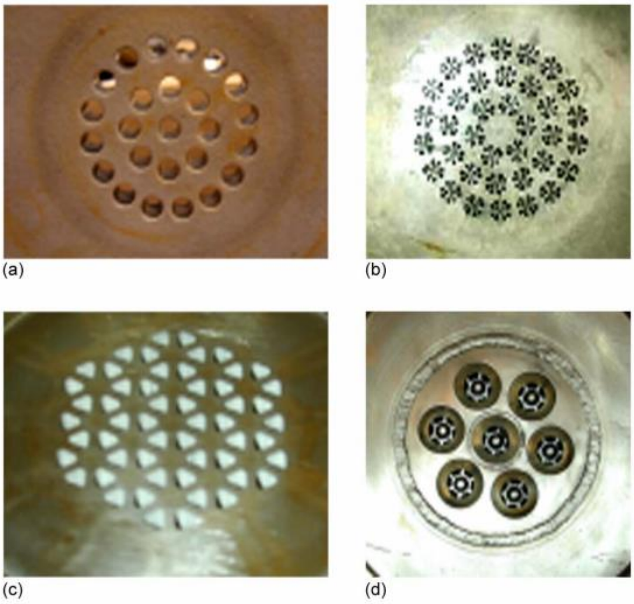

Figure A.I.6: Four injectors tested [38]: (a) NASA N1 injector; (b) Configuration C1; (c) Configuration C2; (d) Configuration C3 and Mod C4.

In the end, the authors concluded that all the LDI configurations performed well and were very stable. Moreover, all the lean direct injection configurations did result in low levels of NOx and compare well with the LDI Jet A combustors.

Nowadays, various manufacturers are following their efforts to achieve low pollutant emissions, in particular low NOx, without having to resort to the injection of water or steam [41]. Combustors of this type are usually named as “dry low-NOx” (DLN) or “dry low-emissions” (DLE) combustors. Thus, in the following, some of the injection systems used by these manufacturers will be presented.

The first example consists in the gaseous fuel injetor developed by Solar Turbines for the DLE combustors used in industrial gas turbines. This fuel injector is presented in Figure A.I.7, which shows a cross-sectional view of a fuel injector designed for installation in multiple-can combustion systems for the Mars and Centaur engines.

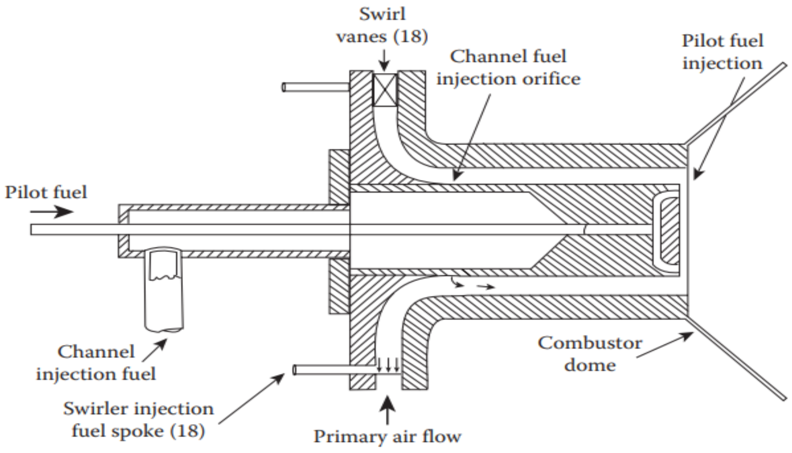

Figure A.I.7: Solar low-NOx fuel injector for natural gas [41].

As indicated in Figure A.I.7, the fuel injector/air swirler assembly permits three different modes of fuel injection. The combustion tests carried out with this fuel injector assembly attached to a cylindrical combustion liner showed that the concept is capable of achieving NOx emissions below 10 ppmv when burning natural gas at pressures up to 1.1 MPa, along with low values of CO and UHC.

Another example of an injection system for gaseous fuels was developed by the ABB company and it consists in a conical premix burner module, called the EV-burner, which has demonstrated good performance in a wide range of DLN combustion applications. A cross-sectional view of the burner is shown in Figure A.I.8 to illustrate the operating principles. Each burner is formed by two offset half cones, which are shifted to form two diametrically opposed air inlet slots of constant width [41].

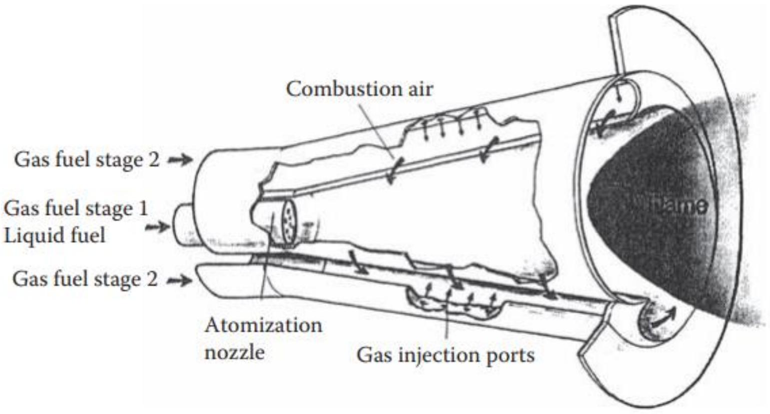

Figure A.I.8: Operating principle of ABB EV conical premix burner [41].

In this burner, the gaseous fuels are injected into the combustion air flowing into the slots through two fuel distribution tubes containing rows of small holes that inject the fuel across the airstream. Fairly complete mixing of fuel and air is obtained shortly after injection and the swirling mixture flows out of the cone and into the flame zone. A unique feature of this burner is that the flame stabilization is achieved in free space near the burner outlet because of the sudden breakdown of a swirling flow. It should be noted that the device can operate satisfactorily on both gaseous and liquid fuels [41].

For more information and examples of injectors that can be used for gaseous fuel injection, please consult the references [41, 71].

Annex 1 – CFM56-3 Technical Data

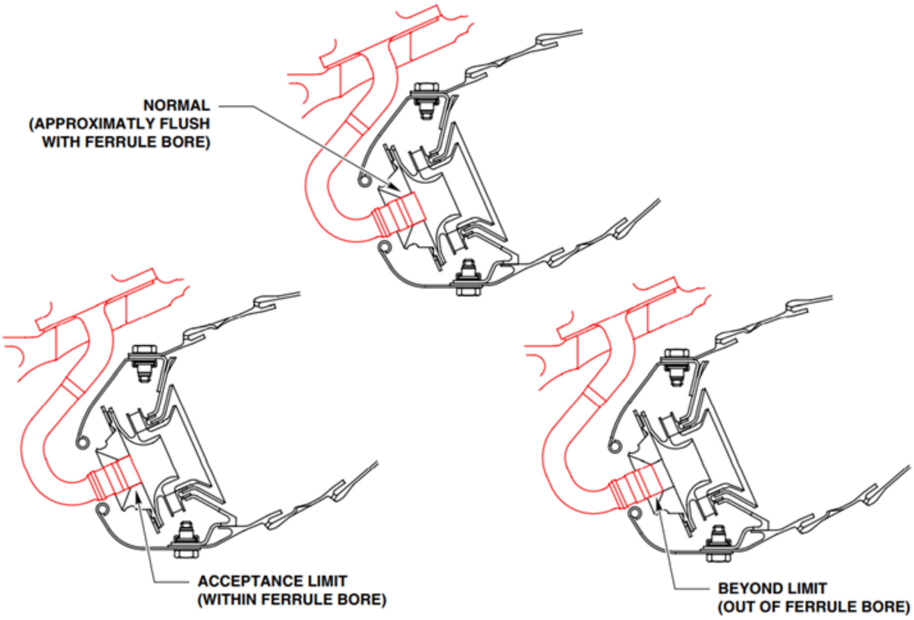

Figure A.1: Correct positions for the injectors according to the maintenance manual [116].

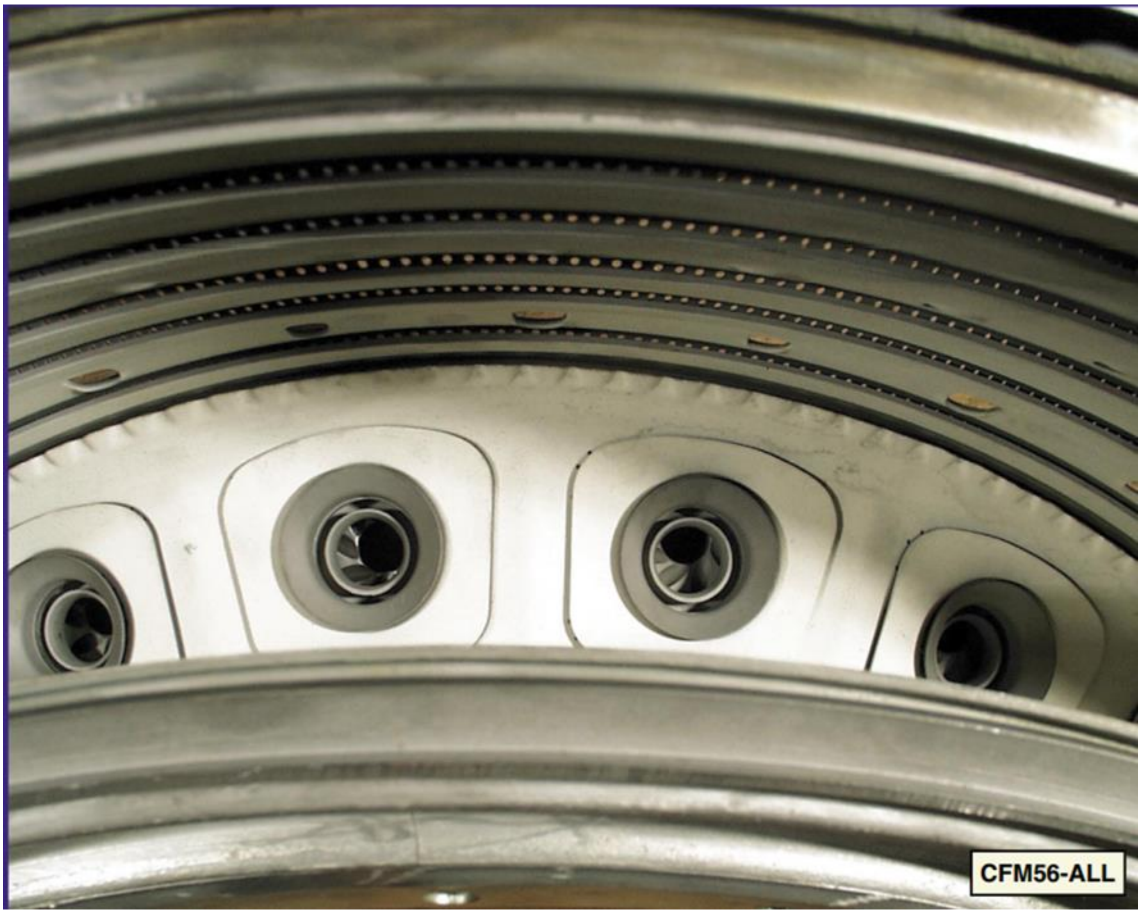

Figure A.2: Image of the bottom view of the swirlers [116].